BEHAVIOR OF STEEL REINFORCED CONCRETE PANELS SUBJECTED TO DIRECT TENSION

NABIL FARAH A. DAWOOD

BEHAVIOR OF STEEL REINFORCED CONCRETE PANELS SUBJECTED TO DIRECT TENSION

By

Nabil Farah A. Dawood, B.Sc., M.Sc.

A thesis submitted to the
School of Graduate Studies
In partial fulfillment of the requirements for the degree of
Doctor of Philosophy

FACULTY OF ENGINEERING AND APPLIED SCIENCE

MEMORIAL UNIVERSUTY OF NEWFOUNDLAND

April 2010

St. John's Newfoundland Canada

Abstract

Cracking of massive concrete structures like offshore and nuclear power plants structures is an important issue in designing and maintaining such structures. The low tensile strength of concrete can destroy the structural aesthetics and expose steel reinforcements to severe environmental conditions, leading to corrosion of reinforcement and other deterioration.

The present research investigation ultimately aims to investigate the general behavior of steel-reinforced normal- and high-strength concrete panels subjected to uniaxial and biaxial direct tension loading taking into consideration the effect of the set of parameters that have the most significant effect on the cracking response. This investigation includes experimental, theoretical, and numerical modeling phases for the cracking response.

The experimental study incorporates the effect of some important parameters such as the concrete strength, bar diameter, bar spacing, concrete cover, and reinforcement ratio on the cracking response of concrete panels. To conduct the current experimental investigation, a special test setup was designed and fabricated. The loading system was equipped to make it possible to simultaneously apply loads in both directions. Results of the experimental work will be presented in terms of cracking behavior (cracking load, crack spacing, crack width, and crack pattern and the mode of failure), stresses and strains in concrete and steel reinforcement before and after cracking.

Compared with NSC panels, HSC panels showed lower strains and greater tension stiffening response at a given load level thanks to the corresponding improvement of the bond between the reinforcing steel bars and the high strength concrete matrix. The panels

tested under biaxial loading conditions showed lower concrete tensile strength and tension stiffening response, compared with the panels subjected to uniaxial loading conditions. This reduction in the tensile strength of concrete panels subjected to biaxial loading was found to be equal to 5% – 15%. The reduction of the tension stiffening contribution of concrete between cracks due to applying the axial into biaxial direction became more significant as the reinforcing bar diameter was increased.

An analytical study was conducted to study the bond characteristics between concrete and steel reinforcing bars. Also, a practical and new analytical model, which is capable of predicting the crack spacing of orthogonally reinforced concrete plate panels, was developed. Afterwards, this study developed a model for evaluating crack widths for thick reinforced concrete plates subjected to in-plane axial loading. The calculation procedure was supported by an evaluation of existing test data.

Finally, the nonlinear analysis of reinforced concrete plates using the damage plasticity model was performed. The tension stiffening model developed in this study was implemented to simulate the cracking response of the concrete. The numerical results show reasonable accuracy in predicting the behavior of steel-reinforced concrete panels.

Acknowledgements

I am greatly indebted to Prof. Dr. H. Marzouk, Professor of Civil Engineering, under whose guidance and supervision the project was carried out. His guidance, support, and patience helped a lot me to complete this thesis.

My special thanks to Drs. A. Hussien and S. Bruneau, for their support and encouragement, and also for serving on the supervisory committee.

Special gratitude is extended to Drs. R. Seshadri, S. Adluri, and L. Lye for their kind encouragement during my study period at MUN.

I am grateful to the fellow graduate students for their encouragement and company. I would like to thank my friend E. Rizk for his true friendship and his moral support to me throughout the course of my thesis. Also, I am also thankful to my fellow students S. Alam and Y. Ebrahim for their help during the experimental program.

This thesis was completed at Memorial University of Newfoundland as part of a project funded by the Natural Science and Engineering Research Council of Canada (NSERC). Funding in the form of graduate fellowship and graduate supplement from Memorial University is gratefully acknowledged.

I would like to take this chance to express my profound gratitude to all my family members for their continuing encouragement and affection.

St. John's, Newfoundland — Nabil Dawood

April, 2010

Contents

List of Figures

List of Tables

Acronyms

ACI	:	American Concrete Institute
ASTM	:	American Society for Testing and Materials
CSA	:	Canadian Standards Association
CEB-FIP	:	Comité Euro-Internationale du Béton et Fédération Internationale de la Précontrainte model code
E	:	East
E-W	:	East-West Direction
EC2	:	European Committee for Standardization Eurocode 2
F.E.A.	:	Finite Element Analysis
FEM	:	Finite Element Model
HSC	:	High Strength Concrete
LPDT	:	Linear Potential Differential Transducer
MUN	:	Memorial University of Newfoundland
N	:	North
N-S	:	North-South Direction
NS	:	Norwegain Council for Building Standardization
NSC	:	Normal Strength Concrete
S	:	South
W	:	West
3D	:	Three Dimensional

Notations

A_c	:	Cross-section area of concrete
A_{ct}	:	Effective tensile area of concrete
A_{st}	:	Reinforcing steel area
A_b	:	Bond surface area of the reinforcement;
A_{sp}	:	Area that provides confinement for the splitting stresses
ΣA_{trans}	:	Total area of the of transverse reinforcement normal to the splitting cracks
α	:	h-C ratio ($1.0 < \alpha \leq 2.0$)
α_{trans}	:	Factor reflects the influence of the transverse bar on the steel stress distribution.
β_1	:	Factor characterizing the bond quality of the steel (β_1 is 0.5 for smooth bars, otherwise is 1.0)
β_2	:	Factor representing the effect of load type (β_2 is 0.5 for cyclic load or long term, otherwise is 1.0).
C	:	Concrete Cover
C_c	:	Clear Concrete cover
C_s	:	Side concrete cover
d_b	:	Bar diameter of the outer layer of the bars
d_b/ρ_{eff}	:	Bar diameter-reinforcment ratio
Δ_i	:	The individual reading from LPDTs
E_c	:	Young's modulus for concrete
E_s	:	Young's modulus for Steel
ε_{sm}	:	Average increase in strain of reinforcement relative to the adjacent concrete.
ε_{s2}	:	Calculated strain in the steel calculated for a transformed section
$\varepsilon_{t,}$	:	The average measured strain for the concrete panel
ε_t	:	The elastic strain in concrete at cracking.
ξ_x	:	Factor to define the influence of longitudinal bar Reinforcement on the local value of the crack width
ζ	:	Strain reduction factor to allow for the tension stiffening effect of the concrete.
f_{scr}	:	Steel stress at cracking load
$f_{t,}$	:	Tensile strength of concrete
f_c'	:	Concrete cylinder compressive strength
f_y	:	Yield stress of reinforcing bars
f_{bb}	:	The bearing stress
F_{spT}	:	Total splitting force
F_{sp}	:	Radial component of the inclined compressive force
F_b	:	Bond force which causes primary cracks
$Ø_1$	:	The longitudinal bar diameter
$Ø_2$	:	The transverse bar diameter

h	:	Effective height of the concrete around the reinforcing bars
h_t	:	Total thickness of the concrete section
k_1	:	Coefficient that characterizes bond properties
k_2	:	Coefficient to account for strain gradient
l_g	:	The gage length of the LPDTs
L_t	:	The transfer length
λ	:	Factor represents the ratio between the stabilized crack spacing at high steel stress and the maximum crack spacing at the primary cracks stage
n	:	Modular ratio (E_s/E_c);
$\sum o$	:	The surface area per unit length of the reinforcement
P_c	:	Load sustained by concrete
P_{cr}	:	Cracking load
P_s	:	Load sustained reinforcement
ρ_{eff}	:	The effective reinforcement ratio
S_1	:	The longitudinal bar spacing
S_2	:	The transverse bar spacing
S_b	:	Reinforcing bar spacing
S_{max}	:	Maximum crack spacing
S_m	:	Average crack spacing
σ_{s2}	:	Steel stresses in a cracked section under the applied load
σ_{sr}	:	Steel stresses in a cracked section at initial crack formation
$\sigma_{s_{all}}$	:	Allowable steel stress for the crack control
σ_{trans}	:	Average stress induced in the transverse reinforcement due to splitting stresses
θ	:	Angle to specify various sections location from longitudinal bar [$\tan\theta = (S_b-2x)/2C$]
τ_b	:	The bond stress at steel-concrete interface
τ_{sp}	:	Splitting bond stress of concrete
u	:	Perimeter of the reinforcement
w_{max}	:	Maximum value of the crack width
w_{min}	:	Minimum value of the crack width
$w_{ave} = w_m$	:	Average crack width
w_x	:	Local crack width at any location along the crack Length between the longitudinal bars
w_{lim}	:	Limiting value of crack width according to Crack-control recommendations proposed in the ACI 224R- 01; CEB-FIP 1990; and Euro EC2 2004, with respect to appearance and safety.

Chapter 1

Introduction

1.1 General

Reinforced concrete structure can crack easily due to its low tensile strength. Cracks may not only destroy the aesthetics of the structure, but also expose steel reinforcement to corrosion. Steel reinforcement is used to carry tensile forces across the cracks once the concrete has exceeded its tension capacity; it can restrain the crack opening and it can prevent a premature and brittle failure in structural members subjected to tensile stresses. However, there are certain types of structures, such as pcontainment structures, offshore platforms, tanks, silos, and nuclear reactor structures where tensile cracks can cause very serious problems. Cracks can cause loss of load-bearing capacity or increase in permeability of the concrete so that it can cause an unacceptable flow of liquid through the structure. Loss of load-bearing capacity can occur due to deterioration of the concrete and the attendant loss in strength, or corrosion of the reinforcement. Corrosion damage can be in the form of reduction in cross-sectional area of the reinforcing bars or in loss of the bond between the reinforcement and the surrounding concrete due to surface spalling of concrete. Corrosion can cause volume expansion that is mainly responsible for exerting an expansive radial pressure at the steel-concrete interface. The development of hoop tensile stresses in the surrounding concrete will result ultimately in the cracking of the cover concrete.

Loss of bond means that reinforcing bars are not able to develop their useable strength. Increased permeability can occur because of degradation mechanisms that affect the overall integrity of the concrete, such as sulfate attack or alkali-aggregate reactivity, or it can occur due to the formation of discrete structural cracks. In order to be able to predict the effects of structural cracks on structural performance, it is necessary to understand the causes and mechanisms of discrete crack formation in reinforced concrete structures.

Cracking in a reinforced concrete member can also cause a significant increase in deflection. This is a result of the reduction of flexure stiffness of the cracked sections when the effect of tensile concrete below the neutral axis diminishes. However, some tensile stress is retained in the concrete between the consecutive cracks around steel bars due to the bond action. The effect of the steel reinforcement on concrete under tension is known as "tension stiffening" effect. Ignoring the effect of tension stiffening of concrete between cracks can lead to overestimated values for the displacement and crack openings by a large amount. This relationship allows concrete to retain some tensile stress beyond the cracking strain.

1.2 Research Objectives and Scope

The present investigation aims to investigate the general behavior of steel-reinforced normal and high strength concrete panels subjected to uniaxial and biaxial direct tension loading taking into consideration the effect of the set of parameters that have the most significant effect on the cracking response of these panels. This investigation includes

experimental, theoretical and numerical modeling phases for the cracking behavior of steel-reinforced concrete panels under uniaxial and biaxial direct tension loading.

In the experimental phase, the research aims to study the effect of using different levels of compressive strength, as the high-strength concrete panels are used in parallel with normal-strength concrete as reference panels. The experimental study incorporates the effects of some important parameters such as bar diameter, bar spacing, concrete cover, and reinforcement ratio on the cracking response of concrete panels.

A theoretical investigation is conducted to develop constitutive relationships to describe the tensile response of the steel-reinforced concrete panels taking into consideration the tension stiffening response of the steel reinforced concrete for normal and high strength concrete panels. In addation, an analytical model that is capable of predicting the crack spacing and width of orthogonally reinforced concrete plate elements is also developed. In such a model, the reinforced concrete plate element is studied using equilibrium and compatibility equations to formulate the average stresses in steel and concrete. This model can account for the influence of the transverse reinforcement on the cracking behavior. The major parameters influencing the cracking behavior of reinforced concrete members, such as the tensile strength of concrete, bond characteristics, reinforcement ratio, bar diameter and spacing in both longitudinal and transverse directions, are also considered. Furthermore, the effect of splitting stresses on the cracking behavior of concrete plates is studied as the concrete splits parallel to the bars and the resulting cracks propagate out to the surface of the reinforced concrete panels.

In the final part of the thesis, the tension stiffening model developed in the present study is used in the nonlinear analysis to predict the tensile response of thick normal and high strength concrete plates subjected in-plane loading condition.

1.3 Research Rationale

Cracking of reinforced concrete structures is unavoidable due to the low tensile strength of the concrete; these cracks may cause serious problems in some structures such as the offshore structures where the steel reinforcement is exposed to severe environmental condition leading to corrosion. Nuclear power concrete walls must be maintained free of cracking, since these walls are the final defensive shield against unexpected accidents that prevents radioactive leakage.

Existing research related to this study mostly corresponds to reinforced concrete panels under uniaxial tension. So there is a need to obtain experimental and analytical results for biaxial tension reinforced concrete structures, reflecting their characteristics and behavior. For the purpose of experimental convenience, the effect of significant parameters such as concrete strength, reinforcement ratio, reinforcement arrangement in the concrete section, and concrete cover are considered in studying the cracking behavior of reinforced concrete panels subjected to axial loading.

At the same time, there is a great need to develop theoretical models suitable for normal and high strength thick concrete plates in order to reflect properly their structural behavior. The transfer of forces across the interface between concrete and steel reinforcing bars is investigated as it is of fundamental importance in analysis of the

behavior of reinforced concrete structures. Proper simulation of the post-cracking behavior of concrete has a significant effect on the accuracy of the nonlinear finite element modeling of RC members, as the tension-stiffening effect is crucial for any nonlinear analysis. Moreover, theoretical models for crack spacing and crack width of thick reinforced concrete plates are developed. The validity of such models is checked by comparing the measured experimental data with the corresponding predicted results based on the proposed models.

Finally, numerical modeling is carried out to provide an accurate prediction of crack response of thick plates used for offshore structures and containment structures for nuclear power plants. The developed tension stiffening model is implemented in a nonlinear finite element analysis.

1.4 Thesis Layout

Following this introduction chapter, Chapter 2 reviews the earlier investigations carried out by various researchers to study concrete tensile response and the interaction between concrete and reinforcement. A review on the different tension stiffening models used to simulate the pre- and post-cracking response is presented. A review on different codes approaches to evaluate the crack width and spacing is also carried out.

Chapters 3 and 4 present the experimental program carried out in this study to investigate the behavior of thick steel-reinforced concrete plates. This program is focused on investigating the cracking response of panels subjected to uniaxial and biaxial direct tension loading. The cracking behavior including the cracking load, crack patterns, crack

spacing, and crack width of these panels under applying direct tension loads, is analyzed. The tension stiffening effects is examined taking into consideration the effect of variables such as concrete compressive strength, reinforcement ratio, loading ratio in the two directions, and concrete cover.

Chapter 5 describes the transfer of forces across the interface between concrete and steel reinforcing bars as it is of essential significance to investigate the cracking response of the reinforced concrete structures. In this chapter, an analytical model is developed for predicting the complete distribution of the slip, bond stress, concrete and steel stress at different loading stages.

Chapter 6 analyzes the relationship between the bond and the splitting stresses, resulting from the bearing of lugs of the reinforcing steel bars on concrete. A model to predict the effect of the splitting stresses, caused by bond action between the uncracked concrete and deformed bars, on the cracking behavior of orthogonally reinforced concrete panels subjected to in-plane axial stresses, is developed.

Chapter 7 provides theoretical models for calculating the crack spacing and width of thick reinforced concrete plates subjected to in-plane axial loading. This model enables the estimation of the variations in crack width at any section along the crack length. As well, a crack width model is developed that considers the significant effect of the reinforcement distribution, concrete cover, and the level of the strain of the reinforcement. Recommendations for control of cracking for thick reinforced concrete panels are achieved based on the measured data from the experimental results and proposed models.

A nonlinear finite element analysis for reinforced concrete plates is conducted in chapter 8, to predict the tensile response of thick plates under axial loading condition. The tension stiffening model developed in chapter 4 is implemented in 3D (three dimensional) concrete damaged plasticity model.

Finally, conclusions from the experimental, theoretical and numerical simulation are summarized in chapter 9.

Chapter 2

Review of Literature

2.1 General Remarks

This chapter includes relevant literature on cracking behavior and tension stiffening response of steel reinforced concrete members subjected to axial loading. The first section deals with previous research aiming to study the response of concrete under axial loading conditions with methods of incorporating the tension stiffening effects in steel reinforced concrete members. Literature on various models for predicting crack spacing of reinforced concrete structures subjected to axial loading is also discussed later in this chapter. Current code provisions used for estimating and controlling the crack width in reinforced concrete members are also briefly discussed.

2.2 Concrete Tensile Behavior

The uniaxial tensile test is the most direct experimental method for obtaining the stress-deformation relationship and it reflects the uniaxial mechanical behavior more directly rather than bending tests. However, such tests are difficult to conduct. To capture the strain-softening branch, a stiff testing set up with the test controlled by a feedback from the deformation of the specimen is required. The test specimen geometry must also ensure that a crack initiates in the desired part of the specimen. This is frequently achieved by notching the specimen.

Several studies have examined the effect of various parameters on basic mechanical and fracture mechanics properties such as initial Young's modulus E_0, tensile strength f_t', fracture energy G_f, the shape of the descending branch, brittleness, etc. Macro-crack formation is closely associated with the structure of the composite material and the relative strength and stiffness of the aggregates and cement matrix, and the bonding between all of these elements. Consequently, the type size and volume content of aggregate, the water-cement ratio, and age at loading, all significantly influence behavior of the macro-crack zone, which develops through the concrete.

The complete measure of the stress-deformation characteristics can be useful to determine other properties such as fracture energy G_f. The fracture energy is a material property, and it is defined as the total energy dissipated on a unit crack surface and is equal to the area under the stress-crack width curve, as shown in Fig. 2.1 as reported by Hillerborg et al. [1], 1983; Bazant and Oh, 1983[2]; Phillips and Zhang, 1993 [3]; and Etse and Willam, 1994[4].

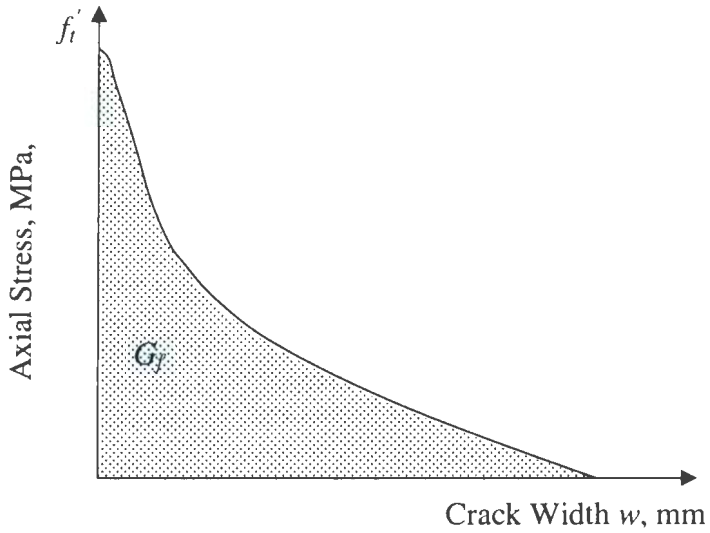

Fig. 2.1 Stress-Elongation Curve for Cracked Section

The fracture energy of the concrete can be expressed as presented in the following equation:

$$G_f = \int_0^{w_c} \sigma(w)dw \tag{2.1}$$

The energy of fracture G_f increases as the strength increases, even for high strength concrete. However, as with tensile strength, the increment in $G_f^{'}$ decreases as the strength level increases; thus the relative toughness ($G_f/f_c^{'}$) decreases. The fracture energy value for normal strength concrete (35 MPa) is around 110 N/m, while for high-strength concrete (75 MPa) its value is in the range of 160 N/m reported by Marzouk and Chen, 1995 [5].

2.2.1 Uniaxial Tensile Behavior

In recent years, testing techniques have been improved by the use of electro-hydraulically controlled testing machines. It is now possible to perform tests through which the complete stress-deformation behavior of concrete specimen under direct uniaxial tension may be obtained (Gapalaratnam and Shah, 1985; Guo and Zhang, 1987 [6, 7]).

The general mechanical behavior of concrete under uniaxial tensile loading shows many similarities to the behavior observed in uniaxial compression. Typical stress-strain curve for concrete in uniaxial tension are shown in Fig. 2.2. The curve is nearly linear up to a relatively high stress level. However, these curves have a markedly lower tensile strength, $f_t^{'}$, compared to the corresponding strength in compression, $f_c^{'}$. For stresses less than about 60% of the uniaxial tensile strength $f_t^{'}$, the creation of new microcracks is negligible. A reasonable value for "onset of unstable crack propagation" is about 75% of

f_t' recommended by Welch, 1966 [8]; and Evans and Marathe, 1968 [9]. The ratio between uniaxial direct tensile strength f_t' and compressive strength f_c' may vary considerably but usually ranges from 0.05 to 0.1. The modulus of elasticity under uniaxial tension is somewhat higher and the Poisson's ratio somewhat lower than in uniaxial compression.

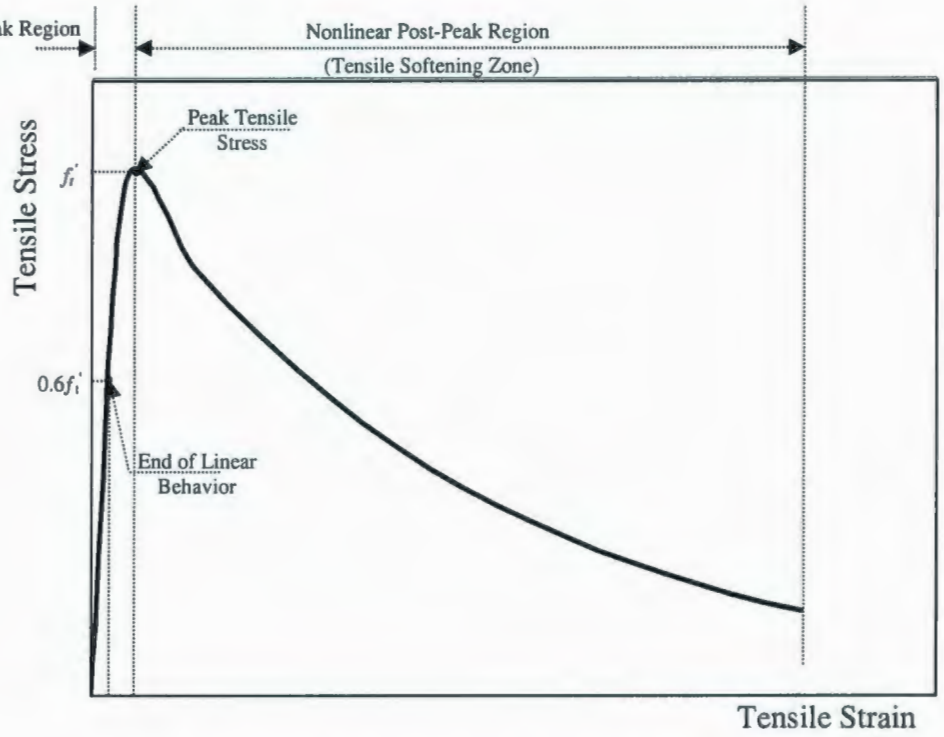

Fig 2.2 Tensile Stress-Strain Curve of Concrete

Regarding high strength concrete, test results reported by H. Marzouk and Z. W. Chen, 1995 [5] revealed that high-strength concrete exhibits a more brittle and stiffer behavior with a large initial modulus of elasticity and more sharply descending branch of the stress-deformation curve beyond the peak load. It was observed from statistical analysis of the test results that the direct tensile strength was only recorded as about 4.8% of the

compressive strength (f_c') compared to 8.0% of (f_c') for normal strength concrete. The splitting tensile strength was about 7.2% of (f_c'), whereas the modulus of rupture was about 9.4% of (f_c').

2.2.2 Biaxial Tensile Behavior

Several studies have been done on the mechanical properties of concrete in biaxial loading. Advanced methods for the design of concrete structures have placed increasing emphasis on the stress-strain behavior of concrete subject to biaxial stress. Expressions were developed by Kupfer et al., 1969[10]; Buyukozturk et al., 1971 [11]; Liu et al., 1972 [12]; Tasuji et al., 1979 [13], to account for non-linear stress-strain behavior, which can be applied to concrete under biaxial loading in the form:

$$\sigma = \frac{\varepsilon E}{1 + \left(\frac{E}{E_s} - 2\right)\left(\frac{\varepsilon}{\varepsilon_p}\right) + \left(\frac{\varepsilon}{\varepsilon_p}\right)^2} \tag{2.2}$$

where σ is the principal stress; ε is principal strain; E is the uniaxial elastic modulus; E_s is the secant modulus at ultimate load (σ_p/ε_p); σ_p is the ultimate stress, ε_p is the strain at ultimate stress.

In Fig. 2.3 the relationship between the principal stresses at failure, σ_1/β, and σ_2/β is given for the three types of concrete investigated by Kupfer et al., 1969 [10]. According to this figure, the strength of concrete under biaxial compression is larger than under uniaxial compression. In the range of compression-tension and biaxial tension, however, the relative strength decreases as the uniaxial strength increases. The strength of concrete under biaxial tension is almost independent of the stress

ratio σ_1/σ_2, and equal to the uniaxial tensile strength as reported by (Bresler and Pister, 1958 [14]; Bellamy, 1961 [15]; Henry and Karni, 1958[16]). In biaxial compression-tension region, there is a significant difference in the behavior between high-strength and normal-strength concrete, where introducing a small amount of tension decreases the compressive capacity more radically for high-strength concrete than for normal-strength concrete as explained by Su and Hsu, 1988 [17]; Yin et al., 1989 [18]; Hussein and Marzouk, 2000 [19].

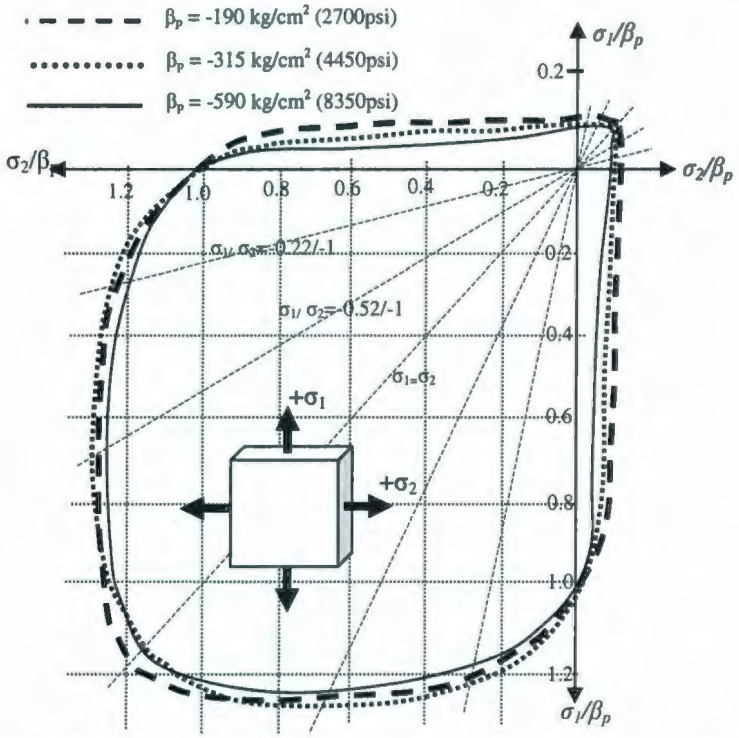

Fig. 2.3 Biaxial Strength Envelope of Concrete, Kupfer et al. [22]

Several studies have been conducted to investigate the behavior of high-strength concrete under uniaxial and biaxial loading (Hussein and Marzouk, 2000 [19]; Ren et al., 2008 [20]). Test results confirmed the ultimate strength of concrete under biaxial

compression to be higher than that uniaxial compression. The maximum biaxial strength occurred at a biaxial stress ratio of 0.5 for all specimens tested. At this stress ratio, a strength increase of about 31% for the NSC specimens, 32, 35, and 38% for HSC, UHSC, and HSLEC specimens, respectively, reported by Hussein and Marzouk, 2000 [19], as shown in Fig. 2.4.

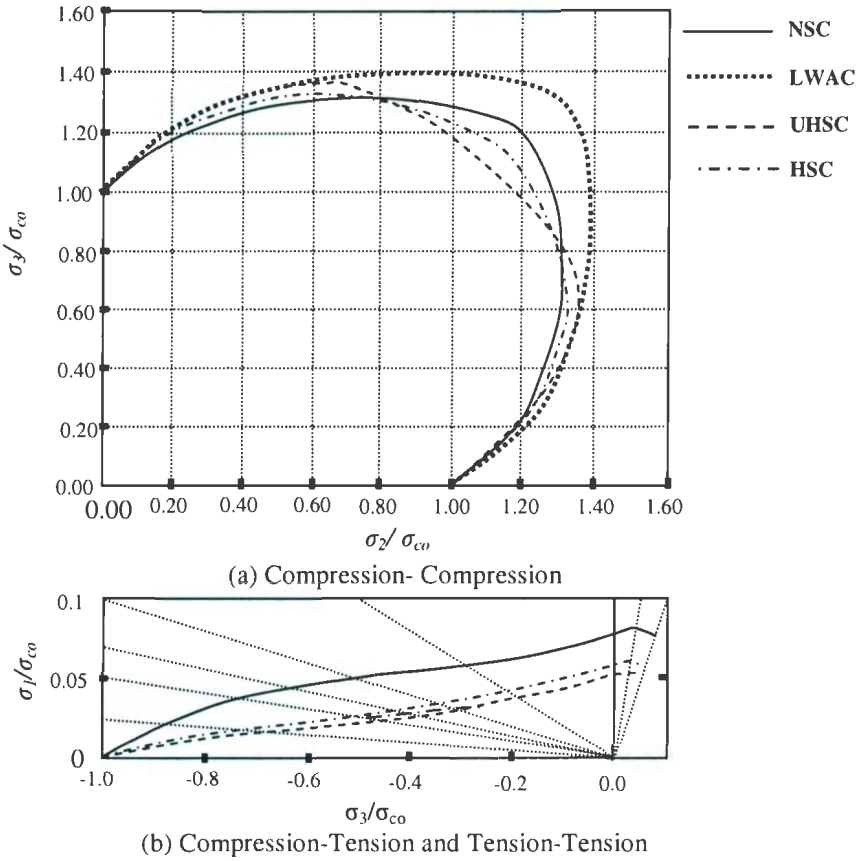

Fig. 2.4 Biaxial Strength Envelopes for Four Different Types of Concrete under Combined Tension and Compression, Biaxial Tension, and Biaxial Compression [19]

2.3 Interaction between Concrete and Reinforcement

Reinforcement in concrete structures enhances the strength of a section in tension but the structural behavior depends on the composite action of the concrete and steel in resisting

the external load. If the reinforcing bar undergoes the same strain or deformation as the surrounding concrete, no slip occurs between the two materials under load and a perfect bond exists. In reality, some slip does occur between the steel and concrete after cracking and reliable estimates of cracking, including the prediction of crack width and crack spacing, require accurate modeling of the bond stress versus slip relationship. After the initial cracking of a reinforced structural member, three interdependent steel-concrete load transfer mechanisms are activated: steel-concrete bond; aggregate interlock or interface shear; transfer dowel action.

In the cases of flexural cracking in beams or slabs, or direct-tension cracking in longitudinally restrained members, the steel-concrete bond is of paramount importance. Bond can be thought as the shear stress or force between a reinforcing bar and the surrounding concrete. The force in the bar is transmitted to the concrete by bond; bond stress must be present wherever the stress or force in a reinforcing bar changes from point to point along its length. In the absence of bond stress, the bar will pull out of the concrete. Bond comprises three components: chemical adhesion, friction, and mechanical interaction between concrete and steel.

Lutz et al., 1966; 1967 [21, 22] conducted an experimental program to examine the bond force action and the associated slip, and cracking of reinforced concrete to explain some basic aspects of the bond-slip and cracking behavior. The cracking behavior of axially loaded tensile specimens with a single deformed reinforcing bar encased concentrically in a long concrete prism was investigated by Goto, 1971 [23]. Shah et al., 1981; 1984 [24, 25] studied the cracking response and transfer of the forces by bond in tension members,

assuming exponential function for bond stress versus slip relationship. A technique for the determination of complete bond versus slip responses was experimentally calibrated by Abrishami and Mitchell, 1992 [26], this technique enables investigating of both pull out and splitting failure. The bond characteristics of high strength concrete under monotonic and cyclic pull out loading were studied by Alavi-Fard and Marzouk, 2002; 2004 [27, 28], considering the load history, confining reinforcement, bar diameter, concrete strength, and the rate of pull out loading. Yang and Chen, 1988 [29] studied the cracking behavior of tension members and developed a model to represent the distribution of bond-slip relationship.

Although friction and adhesion are present in deformed bars, when they are loaded for the first time, the bond mostly is transferred by bearing of the deformations of the bar, as shown in Figure 2.5-a. Equal and opposite bearing stresses act on the concrete and these stresses on the concrete have a longitudinal and a radial component (see Figs. 2.5-b and 2.5-c). The radial component causes circumferential tensile stress in the concrete around the bar (see Fig. 2.5-d), such that eventually, the concrete splits parallel to the bar and the resulting crack propagates out to the surface (MacGregor, 1992) [30].

In a simplified approach, the complex mechanism of force transfer between concrete and reinforcement is substituted by an average bond shear stress uniformly distributed over the nominal perimeter of the reinforcing bar

$$\tau_b = \frac{F}{d_b \pi l_b} \tag{2.3}$$

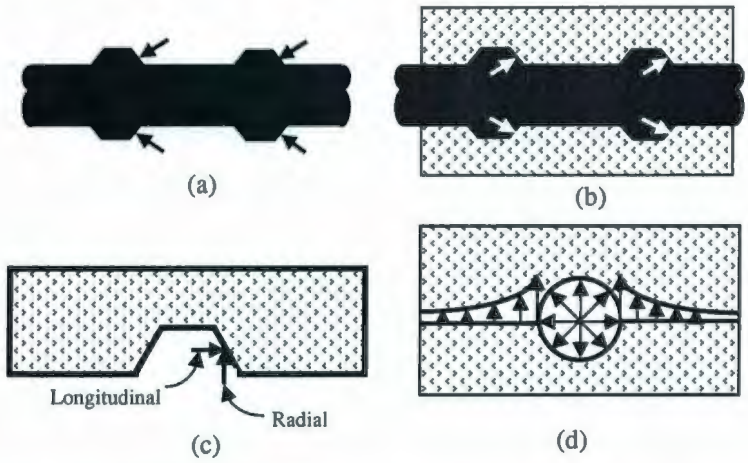

Fig. 2.5 Mechanism of Bond Transfer (a) Forces on Bar (b) Forces on Concrete (c) Components of Forces on Concrete (d) Radial Forces on Concrete and Splitting Stress (MacGregor, 1992 [30])

where, d_b is the nominal diameter of reinforcing bar; and F is the force in the reinforcing bar (Sezen and Moehle, 2003) [31]. Bond behavior is a combination of adhesion, bearing of deformations on the bar against the concrete (mechanical interlock), and friction. Interaction between concrete and a bar subjected to pull-out force generally has four different stages (FIP, 2000) [32], as shown in Fig. 2.6.

The bond stress–slip curve of high-strength concrete is characterized by a sharp drop of the stress at the beginning of the descending portion of the bond stress–slip curve as shown in Figure 2.7 [27]. The area under the curve of the bond stress–slip curve can be defined as bond energy. The influence of extra confinement on bond is significant on improving the ductility and the bond energy, especially after reaching the maximum bond strength.

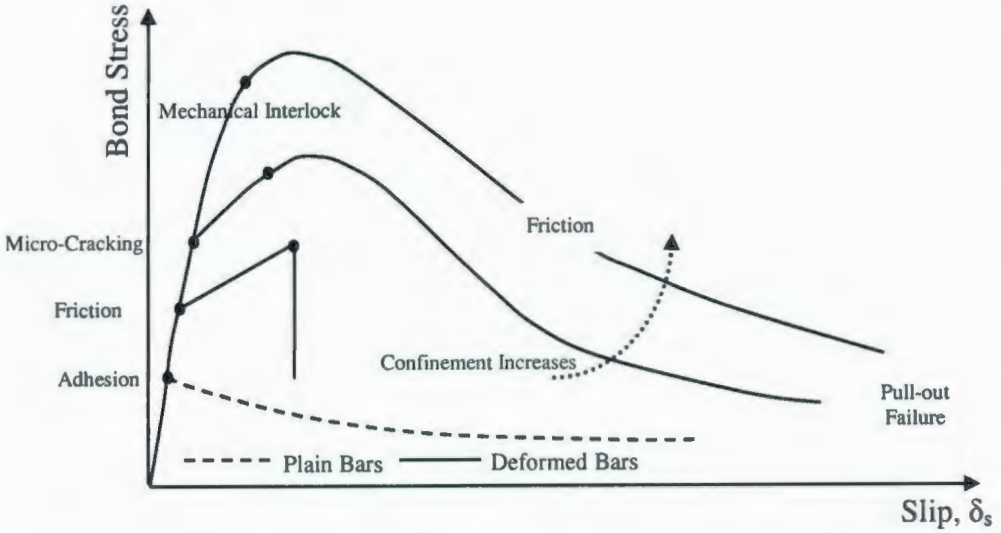

Fig. 2.6 Schematic Representation of Bond Stress versus Slip Relationship and Different Phases of Bond Behavior (FIP, 2000 [32])

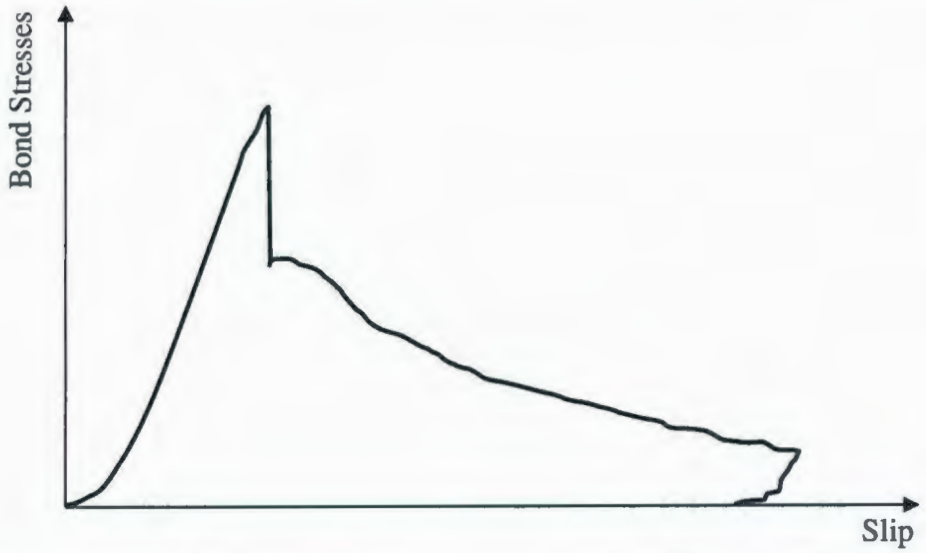

Fig. 2.7 Typical Bond Stress- Displacement for High-Strength Concrete (Alavi-Fard and Marzouk, 2004 [27])

2.4 Tension Stiffening of Steel-Reinforced Concrete

One of the main factors affecting the stiffness of a cracked reinforced concrete member is the bond between the reinforcement and concrete. This phenomenon is

called "tension stiffening" that allows tensile stresses to transfer between the reinforcement and the uncracked concrete between the cracks. Tension stiffening results from crack formation and bond slip between the reinforcing bars and surrounding concrete and is influenced mainly by the tensile strength of concrete, the magnitude of bond stresses, the reinforcement ratio, and the load history. The response of concrete of post-cracking or post-crushing is illustrated in Fig. 2.8 (Reinhardt and Cornelli, 1984) [33].

The bond between the reinforcing bar and the concrete will enable some tension to be transferred from the bar to the concrete. Forces are transferred from the bar to the concrete by inclined compressive forces radiating out from the bar (Goto, 1971) [34], as shown in Fig. 2.9.

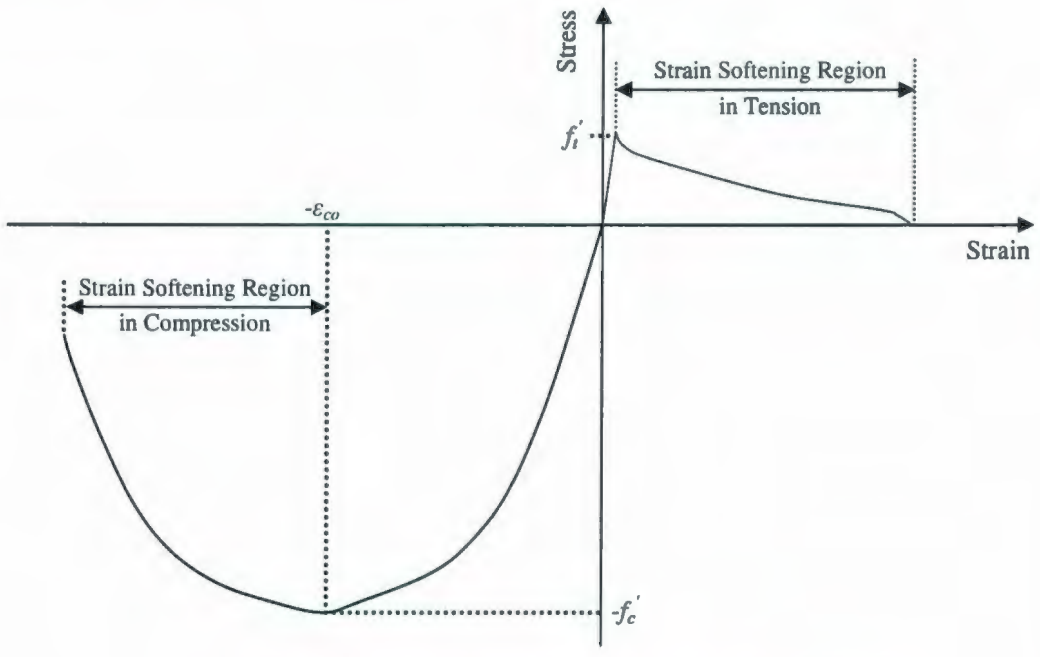

Fig. 2.8 Complete Stress-Strain Curve for Concrete

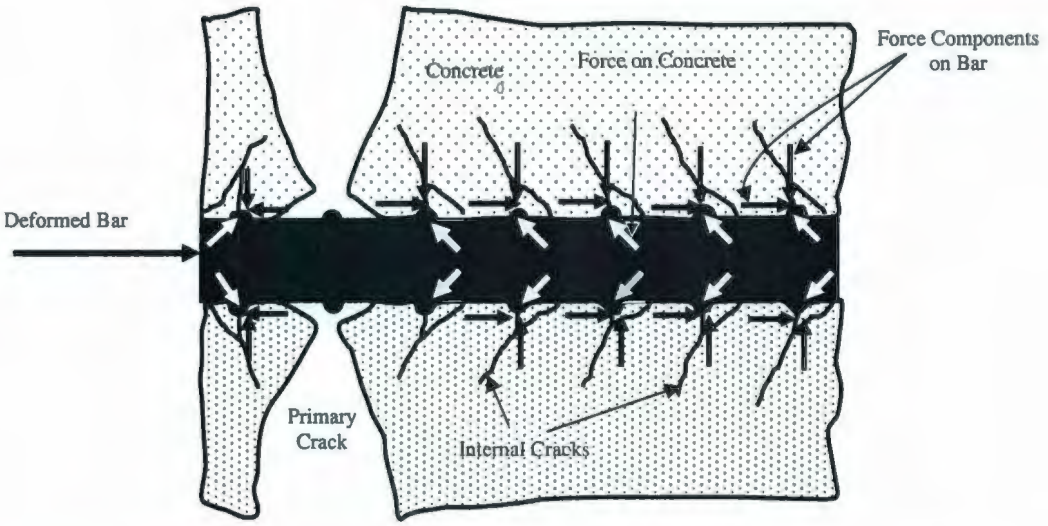

Fig. 2.9 Formation of Internal Cracks, Adapted from Goto (1971) [34]

Different variables, such as the percentage and distribution of reinforcing steel, bar size, bond properties, and shrinkage of concrete, are reported to have had an effect on tension stiffening (Clacrk and Cranston, 1979 [35]; Marzouk and Chen, 1993 [36]; Abrishami and Mitchell, 1996 [37]).

Fig. 2.10 shows a typical load-deformation response for a symmetrically reinforced axial member loaded in tension, where tension stiffening represents the difference between the member response and the bare steel bar response. The composite member response is initially linear elastic with uniform stresses in the concrete and steel along the length of the member, until the tensile strength of the concrete $f_t^{'}$ is reached and the member cracks at a load N_r. Once cracked, the concrete is not assumed to carry any tension at the cracks but it is still able to develop tensile stresses away from the crack as load is transferred from the reinforcing steel back into the surrounding concrete. Hence, stresses in the concrete vary between cracks along the length of the member, and this reduces the

average tensile stress in the concrete as indicated in Fig. 2.10 (Stevens et al., 1991[38]; Bischoff 1995; 2001 [39, 40]).

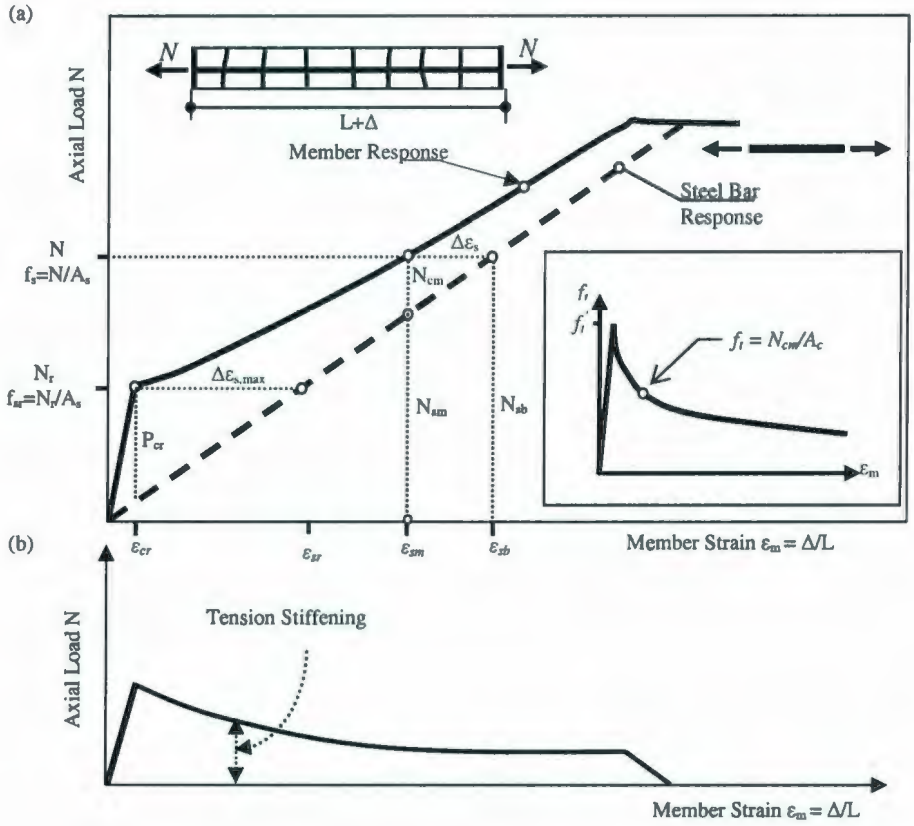

Fig. 2.10 Axial Load-Deformation Response and Tension Stiffening Effect
(a) Reinforced Concrete Member, (b) Concrete Contribution

The average tensile capacity of the concrete continues to decrease with increasing strain, as more cracks develop, and this is reflected by a reduction in tension stiffening with increasing load *N*. Once cracking has stabilized and no more transverse cracks develop, the observed decrease in the average concrete stress (and tension stiffening) continues but at a slower rate, mainly through loss of bond from internal cracking. N_r is the first cracking load, ε_{sr} is bare bar strain under axial load N_r, ε_s is the bare steel bar strain under a given

axial load N, ε_{sm} is the average strain in the reinforced concrete member, $\Delta\varepsilon_{s,max}$ is the jump in the steel strain at first cracking load, and ε_m average strain of the cracked member.

The first approach mentioned uses the concept of a tension stiffening strain $\Delta\varepsilon_s$, to stiffen the bare steel bar response ε_s in a fully cracked section with the concrete in tension ignored, see Fig. 2.10. For a given axial load N, the average strain in the steel reinforcement ε_{sm}, can be expressed *as* given by the following expression:

$$\varepsilon_{sm} = \varepsilon_s - \Delta\varepsilon_s = \beta\Delta\varepsilon_{s,\max} \tag{2.4}$$

The jump in steel strain at first cracking $\Delta\varepsilon_{s,max} = \varepsilon_{sr} - \varepsilon_{cr} = f_t'/\rho E_s$, while β is a factor that varies between one (just before first cracking) and zero (for no bond) that accounts for the variation of steel strains along the member length. ε_{cr} is the elastic strain in concrete at cracking and ε_{sr} is the bare steel strain at first cracking. E_S is the elastic modulus of the steel and ρ equals the reinforcing steel ratio A_S/A_c. A_c represents the area of concrete in tension affected by the transfer of bond forces, and A_S is the area of tension reinforcement. This approach was first introduced by Johnson, 1951 [41] in the form of:

$$\varepsilon_{sm} = \frac{1}{E_s}\left(f_s - \beta\frac{f_t'}{\rho}\right) \tag{2.5}$$

A number of different proposals have been made for the tension-stiffening factor β. Rostasy et al., 1996 [42] proposed using a value of $\beta = f_{sr}/f_s$ that varies inversely with the stress in the reinforcement and is also implicitly dependent on the reinforcing ratio.

$$\varepsilon_{sm} = \varepsilon_s\left(1 - \frac{1}{1+n\rho}\frac{f_{sr}^2}{f_s^2}\right) = \varepsilon_s\left(1 - \frac{f_{sr}^2}{f_s^2}\right) + \frac{f_{sr}}{f_s}\varepsilon_{cr} \tag{2.6}$$

This forms the basis of the method used to account for tension stiffening in the CEB-FIP Model Code for concrete structures, 1978 [43], where the cracking strain of concrete ε_{cr}, is neglected to obtain a more simplified expression for the average steel strain $\varepsilon_{sm}=\varepsilon_s(1 - f_{sr}^2 /f_s^2)$. This approximate expression actually represents the average extension of the steel reinforcement relative to the concrete, and is used to calculate crack widths. The more recent version of the Eurocode CEB-FIP 1990 Model Code, however, adopts a constant value of $\beta=0.4$ in the stabilized cracking region, with a transition curve between the uncracked and fully cracked regions (CEB-FIP Model Code, 1990 (MC-90) [44]). The average concrete stress can then be normalized with the concrete cracking strength, giving a tension stiffening bond factor $\beta = f_t/f_t^{'}$ that accounts for the variation of tensile stresses in the concrete between cracks. Collins and Mitchell, 1991 [45] propose using $\beta=(1+\sqrt{500\varepsilon_m})^{-1}$, Belarbi and Hsu suggest a value of $\beta=(\varepsilon_{cr}/\varepsilon_m)^{0.4}$ [46]; Fields and Bischoff, 2004 $\beta=e^{-0.8(\varepsilon_{cj}-\varepsilon_{cr})\times 10^3}$ [47]; Hwang and Rizkalla (1983) proposed an effective concrete tensile stress after cracking of $\beta=e^{-1000(\varepsilon_{cm}-\varepsilon_{cr})}$ [48]. Marzouk and Chen, 1995 [5], developed a model to express the tensile behavior of high strength concrete after cracking as $f/f_t^{'}=(\varepsilon_t/\varepsilon_t^{'})/[(\alpha(\varepsilon_t/\varepsilon_t^{'})-1)^{\beta}+(\varepsilon_t/\varepsilon_t^{'})]$, where α and β are tension stiffening constant and material dependent constant, respectively, see Fig. 2.11.

To account for the tension stiffening effect in simulating the cracking response of reinforced concrete structures, some investigators have artificially increased the stiffness of the reinforcing steel (Link et al., 1989 [49]; Massicotte et al., 1990 [50]; Lin and Scordelis, 1975 [51]; Gilbert and Warner, 1978 [52]; Cervenka et al., 1985; 1990 [53,

54]) by modifying its stress-strain diagram of reinforcing steel by considering the tension stiffening factor β.

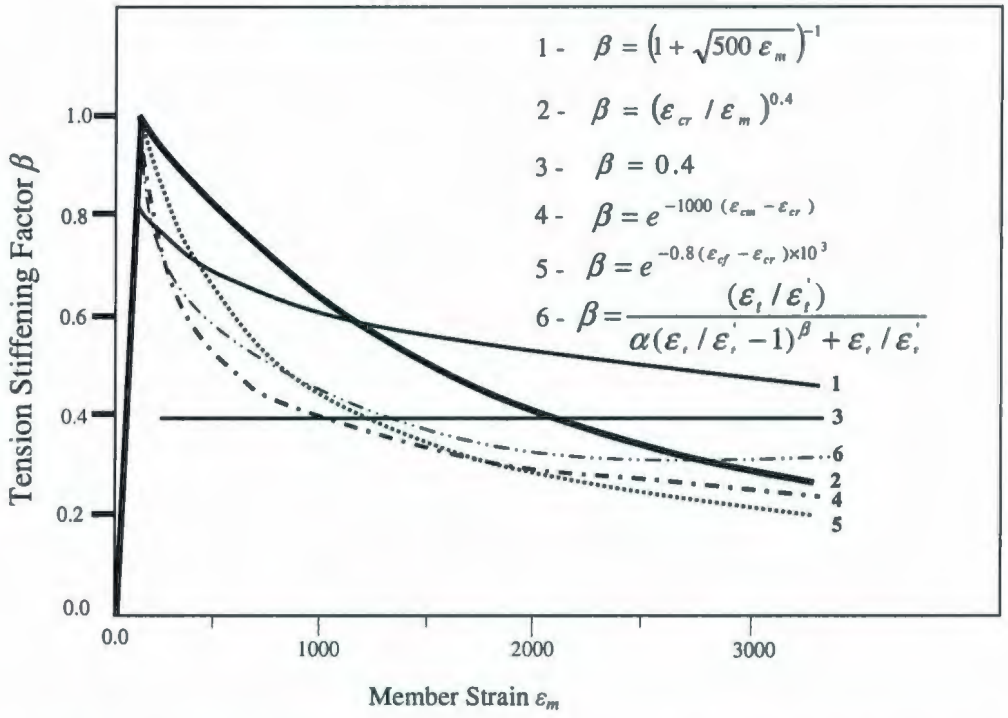

Fig.2.11 Range of Values Reported for Tension Stiffening Bond Factor β

An alternative approach to the modeling of the tension stiffening effect to include this phenomenon was that introduced by Scanlon, 1974 [55]. In this approach, the stress-strain curve of concrete in the tensile stress direction is modified by assigning a descending branch to account for the retained stiffness following cracking. By using this method different investigators have selected various shapes and strain levels, ε_{t0}, to determinate the artificially assigned softening branch, see Fig. 2.12. Many investigators have conducted research on the softening responses and reported the complete load-deformation diagrams of normal strength concrete under direct tension, see Fig. 2.12.

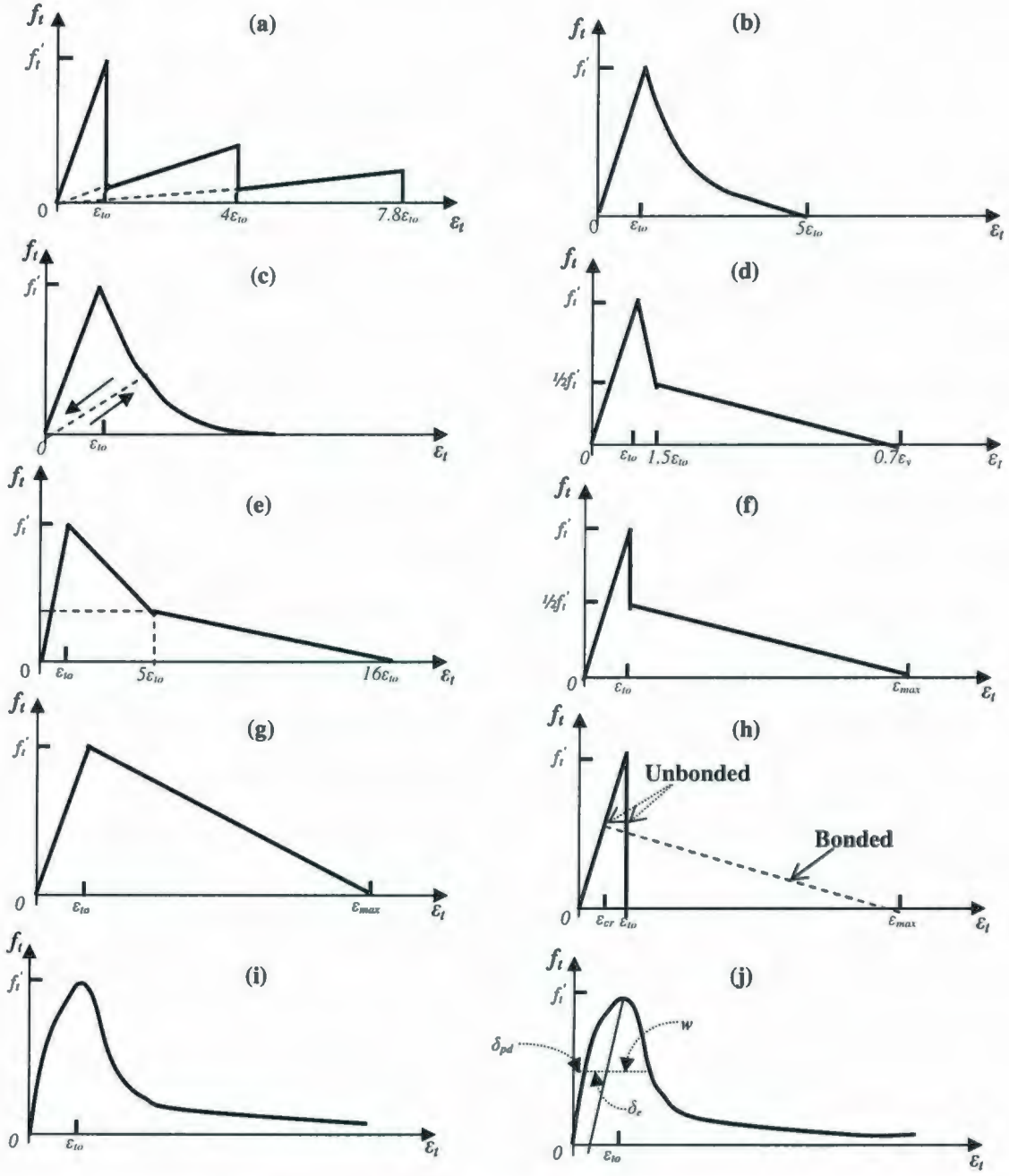

Fig. 2.12 Modeling of Concrete Tension Stiffening

(a) Steped unloading response (Scanlon, 1972); (b) Smooth unloading model (Lin and Scordelis, 1975); (c) Modified smooth unloading model (Mazars, 1981); (d) Bilinear unloading model (Cope et al., 1979); (e) Modified bilinear unloading model (Massicotte et al. , 1990); (f) Discontinuous unloading model (Damjanic and Owen, 1984); (g) Simple unloading model (Bazant and Oh, 1984); (h) Modified linear unloading model (Bergan and Holand, 1979); (i) Continuous Stress-deformation model (Guo and Zhang, 1987); (j) Continuous stress-crack width model (Gopalaratnam and Shah, 1985)

2.5 Control of Cracking in Reinforced Concrete Members

2.5.1 General Remarks

The Concept of random formation of cracks in reinforced concrete members had been discussed by Base et al., 1966 [56]; Broms and Lutz, 1965 [57], Beeby, 1979 [58]; and Hognestad, 1962 [59], who all have indicated that the final crack pattern in crack spacing can be expected to vary from a minimum crack spacing to maximum crack spacing that can be up to twice the minimum crack spacing.

The control of cracking can be as important as the control of deflection in flexural members. Crack control is also important to aesthetics of exposed concrete surfaces. Leonhardt, 1988 [60] conducted an extensive review of cracking in reinforced- and prestressed-concrete structures. Two extensive and independent testing programs were conducted by Rizkalla et al., 1983 [61, 62] to study the cracking behavior of reinforced concrete members subjected to pure uniaxial tension in the presence of transverse reinforcement. Panels of normal strength concrete (NSC) 34.5 MPa with thicknesses of 27, 178, and 254 mm, and subjected to uniaxial tension, were investigated. Williams, 1986 [63] prepared a technical report for the cracking behavior of NSC panels. The main objective of the report was to compare the results obtained from the experimental program performed on reinforced concrete panels with an average strength of 34.2 MPa and thickness of 250 mm with the existing design code and other formulae for the cracking response of reinforced concrete. Twelve prestressed concrete wall segments simulating portions of walls of secondary containment vessels were loaded by uniaxial or biaxial tensile loads to obtain load-deformation and cracking behavior (Simmonds et al.,

1979; 1980) [64, 65]. A typical specimen was 800 mm square by 260 mm thick, with concrete nominal compressive strength 31.7 MPa, reinforced in two directions and prestressed in one or two directions to provide data for use in calibrating the existing theoretical formulas for the crack width. Experimental program to investigate shear transfer in cracked containment vessel (Oesterle and Russell, 1980) [66] on large scale specimens subjected to biaxial tension and shear, the specimens were intended to simulate shear transfer with dimensions (1524 × 1524 × 610) mm with normal-strength concrete of 21.2 MPa.

Several of the most important crack-prediction equations are reviewed in this chapter. The control of cracking in a reinforced or prestressed concrete structure is usually achieved by limiting the stress increment in the bonded reinforcement to some appropriately low value and ensuring that the bonded reinforcement is suitably distributed. Many codes of practice specify maximum steel stress increments after cracking and maximum spacing requirements for the bonded reinforcement. Some codes include procedures for calculating design crack widths.

Permissible crack width varies with design codes. Acceptable values can vary between 0.1 mm and 0.4 mm. The smaller value may be suitable for water retaining and offshore structures and the larger value for structures in dry air or with protective membrane. The width of crack depends mainly on stress in steel after cracking. Other factors affecting crack width are thickness of concrete cover to reinforcement, bar diameter, bar spacing and the way they are arranged in the cross-section, bond properties of the bars, concrete strength and the shape of strain distribution.

2.5.2 Different Approaches for Estimating the Crack Spacing

Extensive previous investigations have been carried out with respect to crack spacing in reinforced concrete members. Leonhardt, 1977 [67] assumed a possible value for the crack spacing at the final crack stage S_L:

$$S_L = \frac{1}{2} L_0 + L_t \tag{2.7}$$

where, L_t is the transfer length that represents the length of active bond stress, and L_0 is the length of no bond stresses, and Leonhardt proposed a value for L_0 based on the experimental results as follows:

$$L_0 = \frac{f_{s2,cr}}{45} d \ (f_{s2,cr} \text{ in N/mm}^2) \tag{2.8}$$

where d is the diameter of the main reinforcement, and $f_{s2,cr}$ is the stress in the steel at the cracking stage.

Beeby 1972 [68], proposed an approach for the value of the average crack spacing S_b as shown in the following equation:

$$S_b = 1.33C + 0.08 d / \rho \tag{2.9}$$

where C is the concrete cover, d is the diameter of the main reinforcement, and ρ is the effective reinforcement ratio.

An attempt was made by Rizkalla et al., 1984 [61] to refine the crack spacing expression by using Beeby's expression where the value of the length L_0 is evaluated. Rizkalla recommended an expression based on the experimental results as follows:

$$S_m = 5(d - 7.2) + 1.33C + 0.08 d / \rho \tag{2.10}$$

where S_m is the average crack spacing mm; C is the concrete cover to the surface of the bar; ρ is the reinforcement ratio; and d is the diameter of the main reinforcement.

Based on the tension chord model, Marti et al., 1998 [69] developed the following model to estimate the crack spacing for fully developed crack pattern:

$$S_{rm} = \lambda S_{rm0} \tag{2.11}$$

where the value of S_{rm0} can be expressed as follows:

$$S_{rm0} = \frac{\phi f_t^{'} (1-\rho)}{2\tau_{b0}\rho} \tag{2.12}$$

where Φ is the bar diameter, $f_t^{'}$ is the tensile strength of concrete, ρ is the reinforcement ratio, τ_{b0} is the bond stress between the steel and the surrounding tensile concrete. Gilbert 2006; 2008 [70, 71] expressed the value of the maximum crack spacing as follows:

$$S_{\max} = \frac{\phi f_t^{'}}{2\tau_{b0}\rho} \tag{2.13}$$

The actual crack spacing at the stabilized cracking stage may be expressed as [52]:

$S = \lambda S_{max}$ where $0.5 \leq \lambda \leq 1.0$

2.5.3 Allowable Crack Width in Reinforced Concrete

The maximum crack width that may be considered not to impair the appearance of a structure depends on various factors including the position, length, and surface texture of the crack as well as the illumination in the surrounding area. According to Park and Paulay, 1975 [72], crack widths in the range 0.25 mm to 0.38 mm may be acceptable for aesthetic reasons. Crack width that will not endanger the corrosion of steel

reinforcement depends on the environment surrounding the structure. Table 2.1 shows the maximum allowable crack widths recommended by ACI Committee 224-2001 [73] for the protection of reinforcement against corrosion.

Table 2.1 Guide to reasonable crack widths, reinforced concrete under service load

Exposure condition	Crack Width	
	in	mm
Dry air or protective membrane	0.016	0.41
Humidity, moist air, or soil	0.012	0.30
Deicing chemicals	0.007	0.18
Seawater and seawater spray; wetting and drying	0.0006	0.15
Water retaining structures	0.004	0.10

For concrete structures of permanent character, dependent on the environmental conditions to which the structure is exposed, a material composition shall be selected and the nominal crack widths shall be limited as given in Table 2.2 in accordance with NS 3473-92[74]:

Table 2.2 Limiting values of nominal characteristic crack width w_k (NS 3473-92)

Environmental class	Reinforcement sensitive to corrosion, w_k	Reinforcement Slightly Sensitive to corrosion, w_k
SA	Special Consideration	Special Consideration
MA	0.10 mm	0.20 mm
NA	0.20 mm	0.40 mm
LA	0.40 mm	-

SA: Especially aggressive environment, MA: Severely aggressive environment, A: Moderately aggressive environment, LA: Mildly aggressive environment.

2.6 Crack Spacing and Width Approaches in the Different Structures Codes

2.6.1 CSA S474-2004; and NS 3473 E-1992

Both the Canadian offshore code CSA-04 [74], and Norwegian code NS-92 [75] provide similar approaches for calculating the value of crack spacing. According to CSA-S474-04, the average crack spacing of cracks normal to the reinforcement, S_m, may be calculated using the following equation:

$$S_m = 2.0(C + 0.1S) + k_1 k_2 d_{be}' h_{ef} b / A_s \quad (2.14)$$

where C = concrete cover, mm (not greater than 55 mm); S = bar spacing of the outer layer of the bars, mm; k_1 = coefficient that characterizes bond properties of bars (= 0.4 for deformed bars, and = 0.8 for plain bars); k_2 = coefficient to account for strain gradient = 0.25 $(\varepsilon_1+\varepsilon_2)/2\varepsilon_1$, ε_1 and ε_2 are the largest; and smallest tensile strains in the effective embedment zone; d_{be}' = equivalent bar diameter of the outer layer of the bars, mm; h_{eff} = effective embedment thickness, mm, taken as the greater of $(a_1+7.5d_{be})$ and $(a_2+7.5d_{be})$, but not greater than the tension zone or half the shell thickness (see Fig. 2.13); b = width of the section, mm; A_s = area of reinforcement within the effective embedment thickness, mm^2.

The crack spacing presented in the above equation includes two terms. The first term [2.0 (C + 0.1 S)] is expressed in terms of the concrete cover and bar spacing, and the second term $(k_1k_2d_{be}'h_{ef}b/A_s)$ is composed of the type of bar, diameter, effect of bond stress, and effect of strain gradient.

The Norwegain Code NS-S474E provides the following equation for the calculation of the average crack spacing:

$$S_m = 2(C + 0.1S) + k_1 k_2 \phi / \rho_t \qquad (2.15)$$

where C = concrete cover, mm; S = bar spacing of the outer layer of the bars, mm; k_1 = factor reflects the effect of the environment class on the reinforcement corrosion (0.4 for ribbed bar); k_2 = coefficient that takes account of the strain distribution over the cross section = 0.25 $(\varepsilon_1+\varepsilon_2)/2\varepsilon_1$, ε_1 and ε_2 are the largest; and smallest tensile strains in the effective embedment zone; ρ_t = the effective reinforcement ratio = A_s/A_c, A_c = the effective concrete area in accordance with Fig. 2.14, the part of the tensile zone that is assumed to contribute effectively to resist tensile forces transferred from the reinforcement to the concrete by bond, and A_s = the area of reinforcement of the tensile reinforcement.

It is obvious that both the CSA and NS codes present a similar equation for calculating the crack spacing, with a small difference attributed to the difference in the strain gradient and calculation of the effective reinforcement ratio.

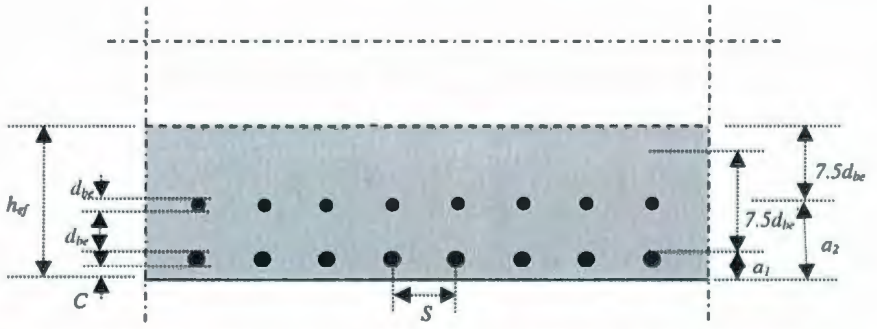

Fig. 2.13 Effective Embedment Thicknesses (CSA S474 2004 Code) [74]

The NS–92 code provides the following expressions for calculating crack width. Factor r is defined to account for the tension stiffening effect as follows:

$$w_k = 1.7\, w_m, \qquad w_m = r\, \varepsilon_1\, S_m \qquad (2.16)$$

$$r=1-\frac{\beta}{2.5k_1}(\frac{\sigma_{sr}}{\sigma_s})^2 \geq 0.4$$

ε_1 is the principal tensile strain at the level of the tensile reinforcement. In an uniaxial stress condition with the principal tension directed parallel to the reinforcement $\varepsilon_1=\varepsilon_s=\sigma_s/E_{sk}$; S_m is mean crack spacing; β is a coefficient that takes account of the type of action; k_1 is 0.4 for ribbed bar; σ_s is stress in the reinforcement in the crack; σ_{sr} is stress in the reinforcement at calculated crack load.

The CSA-S474-04 code recommends that the average crack width may be calculated as the product of the average crack spacing times the average tensile strain of concrete after considering the contribution of tension stiffening. The tension stiffening effect calculated according to the following Eq. 2.17 is going to reduce the crack width.

$$f_t=f_t^{'}/(1+\sqrt{500\varepsilon_1}),\ f_t^{'}=0.33\lambda\sqrt{f_c^{'}} \qquad (2.17)$$

where f_t is the average tensile stress (MPa); $f_t^{'}$ is the cracking strength of concrete (MPa); ε_1 is the principal concrete strain;

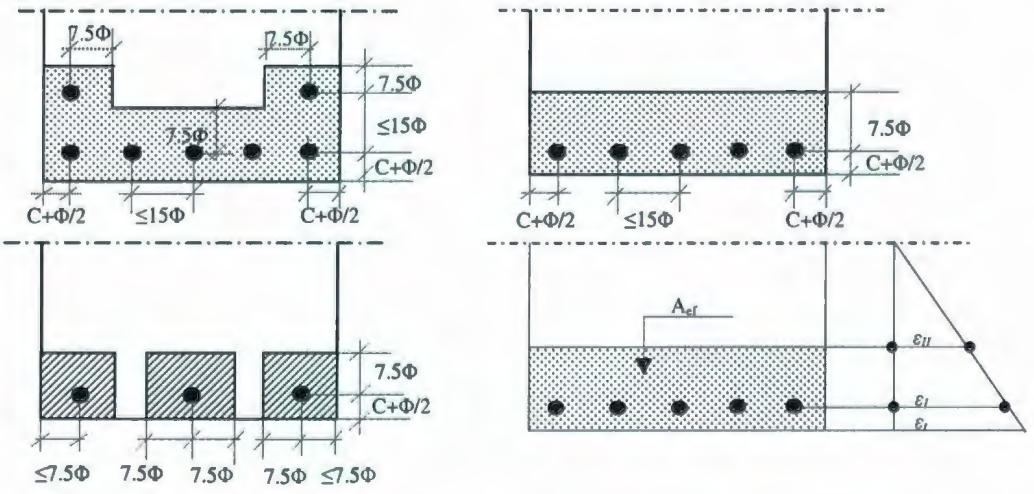

Fig. 2.14 Guidelines for Determination of Effective Concrete Area for Calculation of Crack Spacing (Shaded) [NS 3473 E 1992Code] [75]

2.6.2 Eurocode EC2 Provisions

In the Eurocode EC2 (2004) [76], the average crack spacing formula includes the concrete cover as a parameter in the first term of the formula. The average stabilized mean crack spacing S_m is evaluated from the following expression:

$$S_m = 2C + k_1 k_2 \frac{d_b A_{ceff}}{4 A_s} \tag{2.18}$$

where C = concrete cover; d_b = bar diameter; A_s/A_{ceff} = effective reinforcement ratio, see Fig. 2.15; k_1 = 0.8 for deformed bars and 1.6 for plain bars; and k_2 = 0.5 for bending and 1.0 for pure tension. In this approach, the EC2 code takes only the effect of the concrete cover and ignores the influence of the bar spacing of the outer layer of the reinforcing bars.

The characteristic crack width w_k is estimated by the next expression as:

$$w_k = \beta w_m, \qquad w_m = S_m \zeta \varepsilon_{s2} \tag{2.19}$$

w_k = Design crack width, S_m = Average stabilized crack spacing, ζ = A dimensionless coefficient between 0 and 1, representing the effect of the participation of concrete in the tension zone to stiffness of the member, ε_{s2} = Mean strain under relevant combination of loads and allowing for effects, such as tension stiffening or shrinkage, β = Coefficient relating the average crack width to the design value1.7 and 1.3, respectively, for a section where the minimum dimensions exceed 800 mm.

2.6.3 CEB-FIP 1990 Provisions

The crack spacing in CEB-FIP [44] code is presented in different expressions from previous codes (CSA, NS, and EC2). In this code, the value of the crack spacing is stated by the following expression:

$$S_m = \frac{2}{3} l_{s,\max} \tag{2.20}$$

$$l_{s,\max} = \frac{\phi_s}{3.6\,\rho_{s,ef}} \text{ , for stabilized cracking,} \tag{2.21}$$

$$l_{s,\max} = \frac{\sigma_{s2}}{2\tau_{bk}}\,\phi_s\,\frac{1}{1+\alpha_e\,\rho_{s,ef}} \text{ , for single crack formation} \tag{2.22}$$

where $l_{s,max}$ is the length over which slip occurs between the steel reinforcement and concrete; σ_{s2} = reinforcement stress at the crack location, N/mm^2; τ_{bk} = the value of the average bond stress, N/mm^2 = $1.8\,f_{ctm(t)}$; and $f_{ctm(t)}$ = the mean value of the concrete tensile strength at the time that the crack forms; α_e is the ratio of E_s/E_c. $\rho_{s,ef}$ = effective reinforcement ratio, $A_s/A_{c,ef}$; A_s = area of tension reinforcement, mm^2; and $A_{c,ef}$ = effective concrete area in tension, mm^2, see Fig.2.15; and for the sake of simplicity, $(1 + \alpha_e \rho_{s,eff})$ can be set equal to 1.

The CEB-FIP (CEB-90) code gives the following equation for calculation of the characteristic crack width:

$$w_k = l_{s\max}\,(\varepsilon_{s2} - \beta\varepsilon_{sr2} - \varepsilon_{cs}) \tag{2.23}$$

where ε_{cs} is the free shrinkage of concrete, generally a negative value, ε_{sr2} is the steel strain at the crack, under a force causing stress equal to f_{ctm} within A_{cef} [$\varepsilon_{sr2} = f_{ctm}/A_{cef}$

$(1+\alpha\rho_r)]$, ε_{s2} is the steel strain of transformed section in which the concrete in tension is ignored.

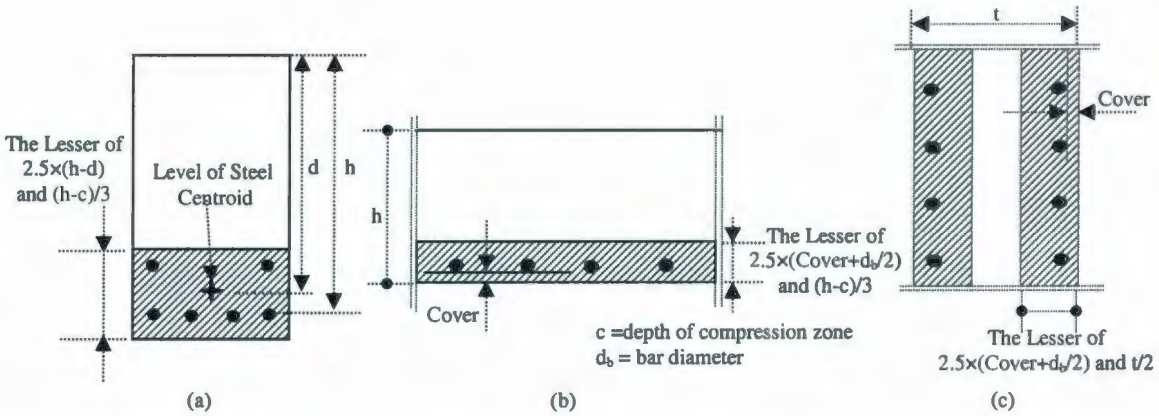

Fig. 2.15 Effective Area, A_{ceff} (a) Beam; (b) Slab; (c) Member in Tension (MC-90 or EC2)

2.6.4 ACI Approach through ACI 224R-01

ACI approach through ACI 318-01 [73] requirements for flexural crack control in beams and thick one-way slabs are based on the statistical analysis (Gergely and Lutz, 1968) [77] of maximum crack-width data from a number of sources. Based on the statistical analysis, the equations that were considered to best predict the probable maximum bottom and side crack widths are:

$$w = 0.076\beta f_s \sqrt[3]{d_c A}\times 10^{-3} \tag{2.24}$$

w = most probable maximum crack width, in.; f_s = reinforcing steel stress, ksi; d_c = thickness of cover from the extreme tension fiber to the closest bar, in.; A = area of concrete symmetric with reinforcing steel divided by number of bars, in.^{2}, as shown in Fig. 2.16; and β = ratio of distance between neutral axis and tension face to distance between neutral axis and reinforcing steel about 1.20 in beams.

The American Concrete Institute, Building code Requirements for reinforced concrete, ACI 318-2008 [78] controls flexural cracking by limiting the stress in the steel f_s at a cracked section to service load to ⅔ of the specified yield strength ($⅔f_y$). The spacing of reinforcement closest to the tension face, S, shall not exceed that given by:

$$S\ (in) = 15\left(\frac{40{,}000}{f_s}\right) - 2.5C_c \tag{2.25}$$

but not greater than $12(40{,}000/f_s)$, where C_c is the least distance from surface or reinforcement or prestressing steel to the tension face.

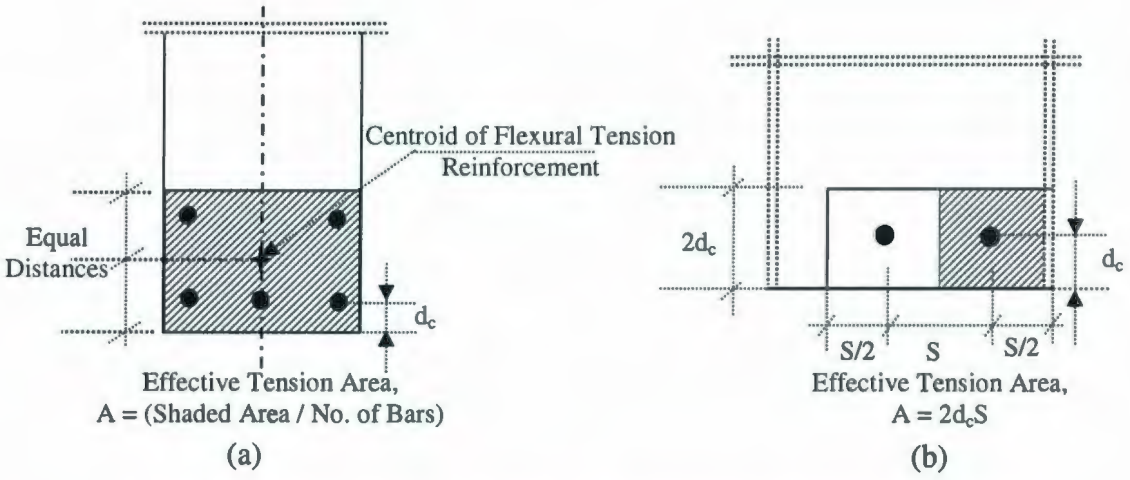

Fig. 2.16 Definitions of A, dc and S for the equations of Crack Width:
(a) Beam for 5 Bars; (b) Slab (ACI 224-01) [73]

2.7 Summary

The first part of this chapter presents a brief description for the nonlinear mechanical properties of the concrete in uniaxial and biaxial loading. Steel to concrete bond phenomenon, which allows longitudinal forces to be transferred from the reinforcement

to the surrounding concrete in a reinforced concrete specimen, is detailed in the second part of this chapter. The bond stress transfer mechanism of deformed bar is inherently three-dimensional, resulting from bearing stress that arises when the lugs of deformed bars push against the surrounding concrete.

Tension stiffening phenomenon can be defined as the increase in stiffness in a reinforced concrete member due to the interaction between concrete and reinforcement. As a member cracks, concrete between cracks rebound to its original state but is restrained by the reinforcement. The concrete between cracks is still able to develop tensile stresses away from the crack as load is transferred from the reinforcing steel back into the surrounding concrete, resulting in some tensile stresses in the concrete. Various methods and models of incorporating the tension stiffening effect in the cracking response of reinforced concrete members are discussed in the second part of this chapter.

The available codes approaches for the cracking behavior such as the Canadian Standards Association offshore code CSA-S474-04 (CSA 2004), Norwegain Council for Building Standardization code 3473E (NS 1992), the European Committee for Standardization Eurocode 2 (EC2-2004), the Comité Euro-Internationale du Béton et Fédération Internationale de la Précontrainte model code MC 90 (CEB-FIP 1990), and ACI Approach through ACI 224R-01, are presented in the last part of this chapter.

Chapter 3

Experimental Program

The primary objective of the experimental program is to study the cracking behavior of reinforced concrete panels with different concrete strengths subjected to pure tension (uniaxial or biaxial) in terms of tension stiffening behavior, cracking load, crack pattern, crack spacing, and crack width of these panels. Normal- and high-strength concrete were used. This chapter contains the details of the experimental program, test setup, description of the experimental equipments, methods used throughout the testing program, and specimen preparation.

3.1 Test Specimens

Nineteen specimens were tested as a part of this research program. The test panels represent thick normal and high strength reinforced concrete plates subjected to uniaxial or biaxial loading, which are used in offshore concrete structures and nuclear power plant construction.

The selected sizes of the tested panels are detailed in Table 1. Also, Table 1 shows the specimen's design configuration in detail presenting the plates' dimensions, concrete compressive strength $f_c^{'}$, reinforcement ratio (ρ), and ratio of concrete cover to the bar diameter (C_c/d_b), see Fig. 3.1.

Table 3.1–Reinforced concrete panel segments of the experimental program

Specimens Symbol	Specimen Dimensions (mm)	Concrete Strength f_c', (MPa)	Bar Diameter (mm)	Bar Spacing (mm)	Rft. Ratio %	C_c/d_b	Loading Ratio
NS-U-15-2.5-6	600×600×190	40	15	150	1.2	2.5	1:0
HS-U-15-2.5-6		90	15	150	1.2	2.5	1:0
NS-B1-15-2.5-6		35	15	150	1.2	2.5	1:1
HS-B1-15-2.5-6		75	15	150	1.2	2.5	1:1
HS-U-20-2.5-6		75	20	150	2.0	2.5	1:0
HS-B1-20-2.5-6		75	20	150	2.0	2.5	1:1
HS-U-20-2.5-4	900×900×260	80	20	300	1.2	2.5	1:0
HS-B1-20-2.5-4		75	20	300	1.2	2.5	1:1
HS-U-25-2.5-6		75	25	300	1.2	2.5	1:0
HS-U*-25-2.5-6		70	25	300	1.2	2.5	1:0
HS-B1-25-2.5-6		65	25	300	1.2	2.5	1:1
HS-U-25-1.5-6		75	25	300	1.2	1.5	1:0
HS-B1-25-1.5-6		70	25	300	1.2	1.5	1:1
HS-B2-25-2.5-6		60	25	300	1.2	2.5	2:1
HS-B3-25-2.5-6		65	25	300	1.2	2.5	3:1
HS-B4-25-2.5-6		65	25	300	1.2	2.5	4:1
HS-U-30-2.5-6	900×900×380	65	30	300	1.2	2.5	1:0
HS-B1-30-2.5-6		65	30	300	1.2	2.5	1:1
HS-U-30-1.5-6		65	30	300	1.2	2.5	1:0

The experimental program was undertaken to investigate the cracking response of thick concrete plates subjected to uniaxial and biaxial loading. Two types of concrete were tested:

a) A normal strength concrete (NSC) with a target strength of 35 MPa

b) A high strength concrete (HSC) with a target strength of 75 MPa.

In addition, three control cylinders having a nominal diameter of 100 mm and height of 200 mm were cast at the same time as the specimens for each concrete batch, and tested under uniaxial compression to relate specimen strength to standard material test results.

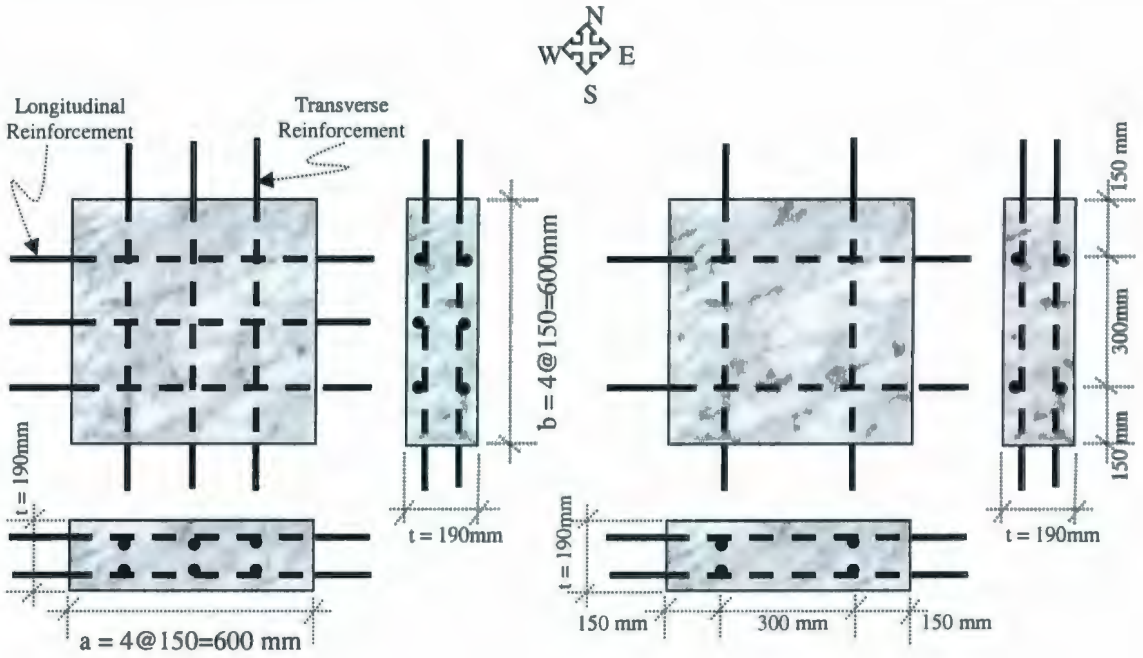
N
W
E
S
Longitudinal Reinforcement
Transverse Reinforcement
b = 4@150=600mm
t = 190mm
t = 190mm
a = 4@150=600 mm
150 mm
300mm
150 mm
t = 190mm
t = 190mm
150 mm
300 mm
150 mm

(a)

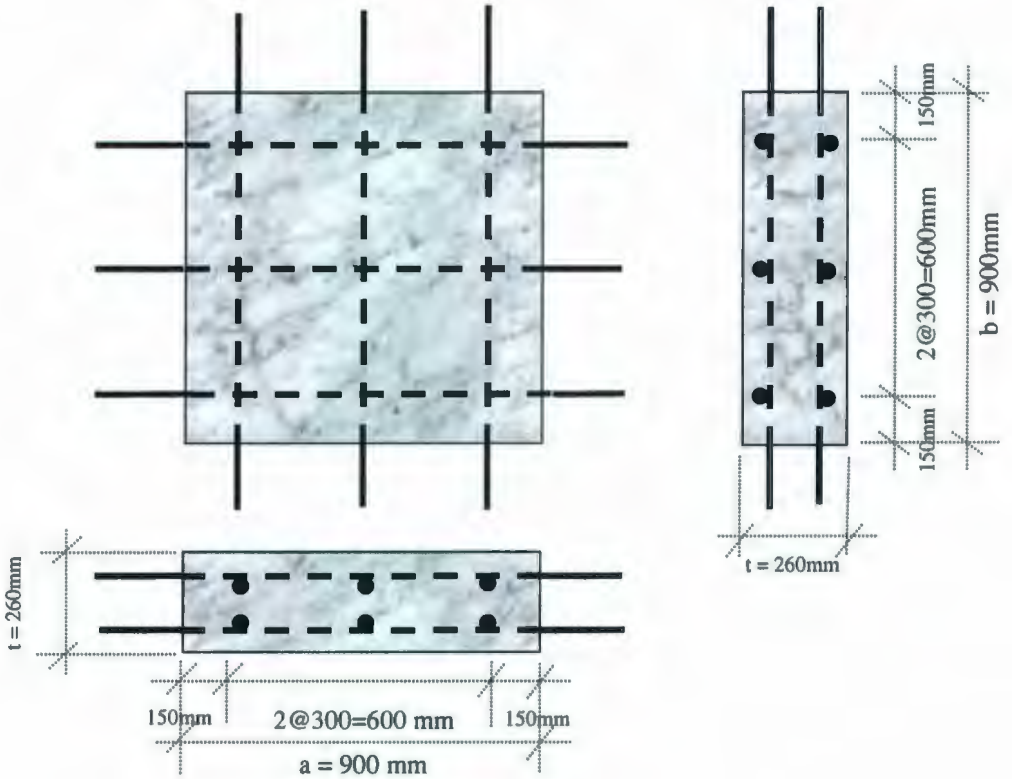
150mm
2@300=600mm
b = 900mm
150mm
t = 260mm
t = 260mm
150mm
2@300=600 mm
150mm
a = 900 mm

(b)

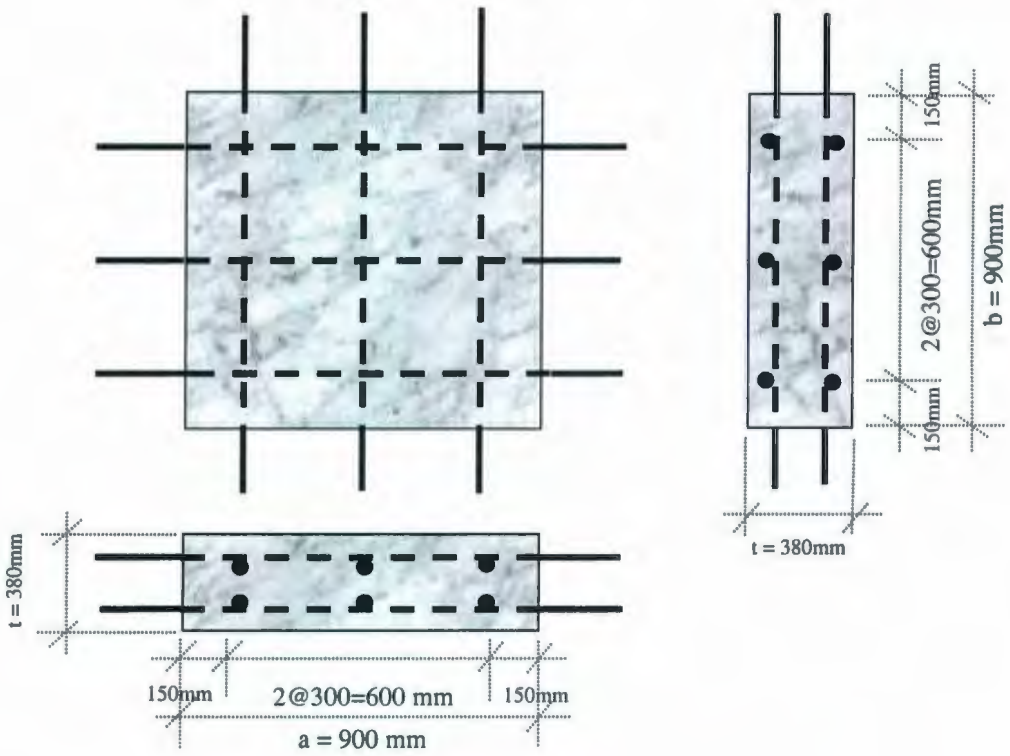

(c)

Fig. 3.1 Specimen Configurations and Dimensions

3.2 Specimen Variables

Several variables are considered in the present experimental investigation. These included the influence of concrete strength, reinforcement ratio, arrangement of reinforcement in the concrete section, concrete cover to the bar diameter proportion C_c/d_b, and applying the load into uniaxial and biaxial directions. Details of the individual specimens and the variables studied in each specimen are presented in Table 3.1.

Figure 3.2 illustrates the panels' name, where the first index indicates the type of the concrete, and the next indexes are the loading type, bar diameter, concrete cover to bar diameter ratio, and the number of the longitudinal reinforcing bars in the concrete section.

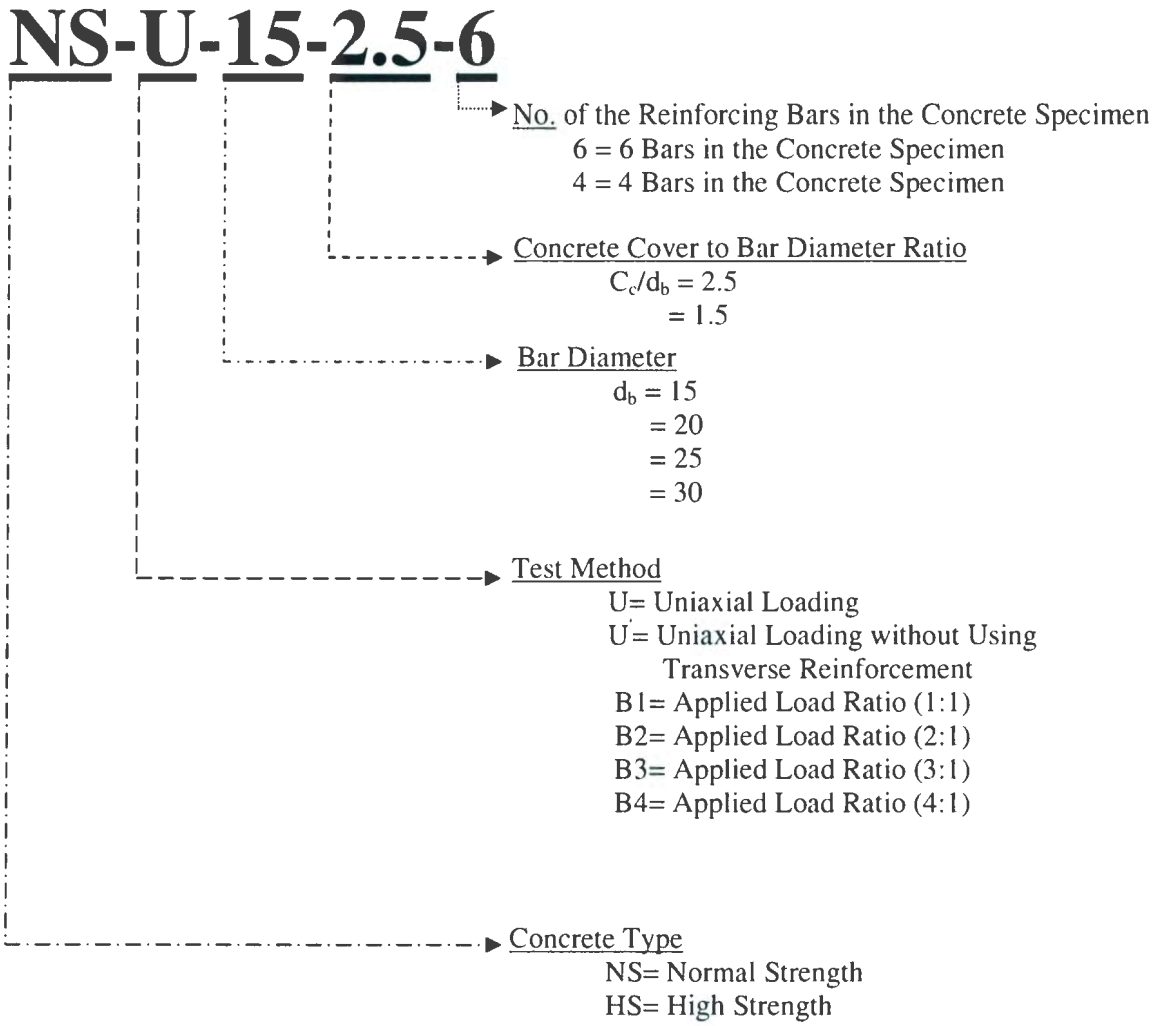

Fig. 3.2 Panel Identification Scheme

As shown in Fig. 3.2, this study considered two types of concrete, normal strength concrete (NSC), and high strength concrete (HSC). The load was applied using five different methods, uniaxial loading condition (1:0), biaxial loading condition with loading ratio 1:1, biaxial loading condition with loading ratio 2:1, biaxial loading condition with loading ratio 3:1, and biaxial loading condition with loading ratio 4:1. The effect of the bar diameter was investigated using four different bar diameters, 15, 20, 25,

and 30 mm. two different ratios for the concrete cover thickness to the bar diameters were used (C_c/d_b = 2.5, 1.5). Two reinforcement ratios (1.2 %, 2.0%) were used for reinforcing the concrete panels.

3.3 Test Setup and Instrumentation

3.3.1 Axial Testing Apparatus

Testing reinforced concrete panels under direct tension, either uniaxial or biaxial loading needs a special test setup. In the literature, many researchers fabricated test setups for the purpose of testing concrete panels to different kinds of loading in the axial directions (MacGregor et al., 1980 [79], Williams, 1986 [63], Hsu et al., 1995 [80], Cho et al., 2004 [81]). Each setup was manufactured according to the objectives of the research. Most of these test setups were built of steel that show deformations during the application of load, and consequently, may affect the experimental results to some extent.

A rigid and heavily reinforced concrete frame test setup was designed and fabricated at the structural laboratory of MUN [82]. The main function of this setup is to apply direct axial tension loads in one and/or two-dimensional directions; to simulate plane uniaxial and biaxial stress states. Details of this test setup are shown in Fig. 3.3. The test setup consists of three main parts, namely, fixed reaction frame, four moving parts, and in between 8 hydraulic jacks fixed to apply forces on the moving parts. Detailed explanation for each part will be presented in the rest of this section [82].

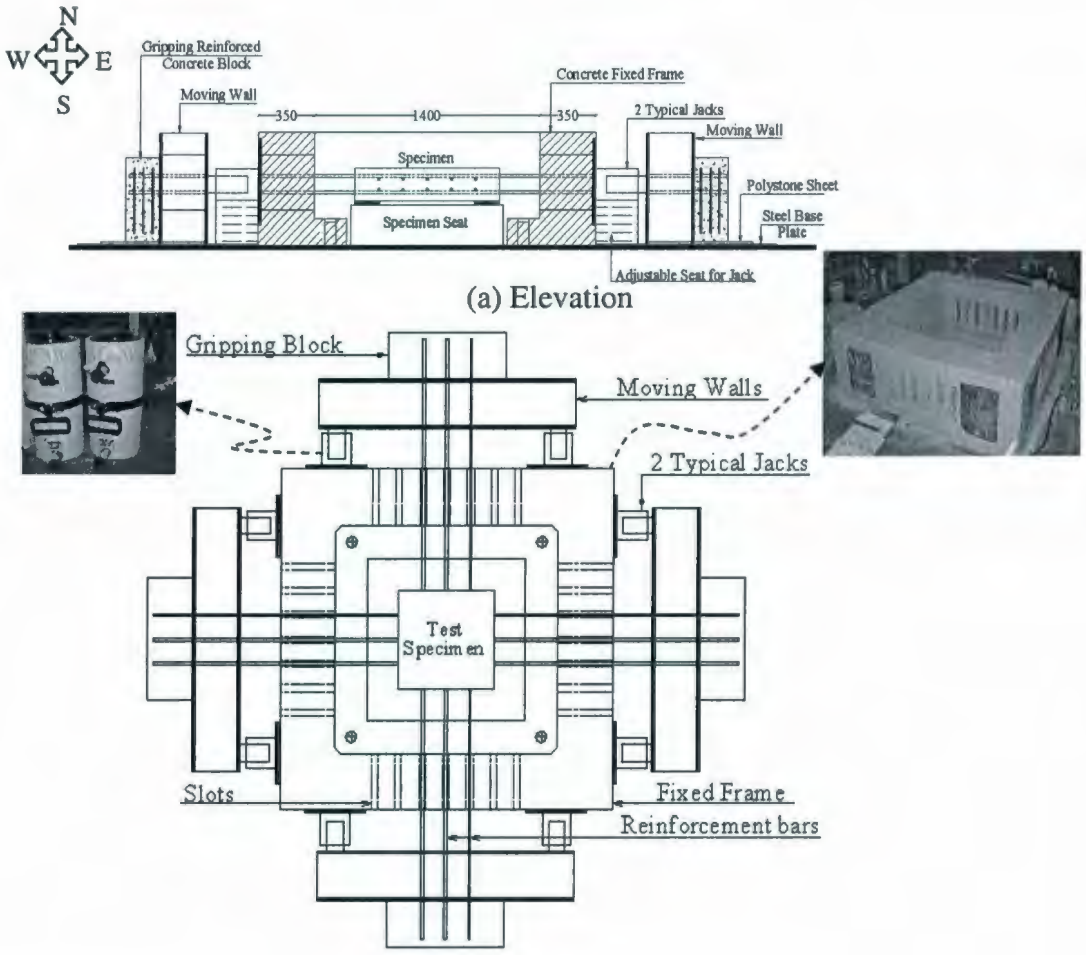

(a) Elevation

(b) Plan

Fig. 3.3- Test Setup

3.3.1.1 Fixed Reaction Frame

A fixed reinforced concrete frame was designed to take the reaction of the hydraulic jacks pushing against the moving parts. The concrete panel was cast and placed inside the free space area of fixed reaction frame. The frame is provided with twenty-eight slots, seven at each side. Through the slots, the reinforcement bars of the specimen were inserted inside the reaction frame. The slots are spaced at fixed distances equal 150 mm, see Fig. 3.3.

The frame is square in plan and with total height about 660 mm. The walls of the frame are 350 mm thickness. The frame has a concrete base casted at the same time with walls. The frame walls and the base were fixed to the laboratory structural concrete floor (thickness 1.0 m) through 8 threaded anchor bolts. Each anchor bolt is about 60 mm in diameter passing through the laboratory floor. The bolts were located in a grid form that has 600 mm spacing in the two-plane direction. The concrete used in casting the frame has target compressive strength equal to 40 MPa. The frame was reinforced with deformed steel rebars with a yield stress and ultimate tensile strength of 410 MPa and 650 MPa, respectively.

3.3.1.2 Four Moving Walls

The main objective of these parts is to apply tension loads for the steel bars in the two directions, and at the same time provide adequate anchorage length for gripping of the steel rebars. Therefore, four moving parts were placed at the four sides of the fixed frame, at a suitable distance for placing the jacks between the fixed frame and the moving walls. These parts are composite sections of concrete and steel; they were built using two steel plates at the front and back, welded in between with steel boxes around the bar slots. Then, reinforced concrete was cast between these plates to form the total section. The total thickness of the wall is 300 mm with about 660-mm height. The moving mechanism of the walls is facilitated through a sliding Teflon layer fixed on the bottom of the wall.

The moving walls were provided with slots for passing the steel bars through, and on the other sides of the moving walls, the steel bars protrude outside the moving walls, and are

embeded inside the concrete gripping blocks with equal and sufficient lengths to adjust the transferred loads to each reinforcing bar to provide uniformly distributed forces on the concrete panel, as illustrated in Fig. 3.4. The criterion of these gripping blocks is to transfer the tension load by bearing through a bearing base plate fixed on the moving wall for each bar.

3.3.1.3 Hydraulic Jacking System

Eight jacks were used to apply loads in the four directions of the frame walls, two jacks were fixed on each side of the setup. Each jack had 1000 kN capacity, and a maximum stroke of 635 mm (25 inch). To minimize local stresses in frame concrete under the jacking areas, different bearing steel plates were fixed on the jacks' locations. The jacks were connected through pipes, to apply load through hydraulic pumps. The jacking forces were distributed to apply load in the two directions with different ratios.

This setup can accommodate different testing conditions. It can test specimen size up to 1350 mm square, and the specimens can be with different thickness. The reinforcing bars can be placed in the specimens at different levels, using one or two layers of reinforcements within the specimen. The setup parts, fixed frame and the four moving walls, were provided with seven slots in each direction at 150 mm spacing. Thus, different bar spacing can be considered in the experimental investigation (150 mm, 300 mm, and 450 mm). The gripping system provided had the ability to pull out different bar diameters up to 30 mm without any slippage for the reinforcing bars.

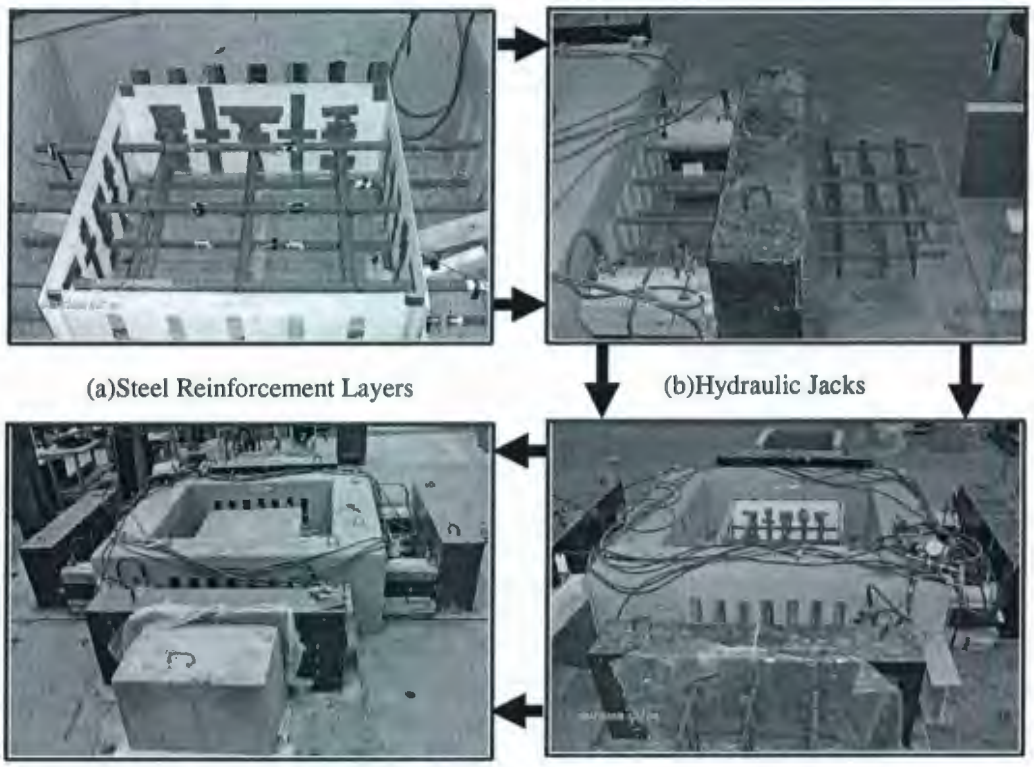

(a)Steel Reinforcement Layers (b)Hydraulic Jacks

(d)Specimen after Casting (c)Setup before Casting the Specimen

Fig. 3.4 Specimen Preparation Procedures

3.3.2 Measurement Devices

The load was measured using a hydraulic pressure transducer attached to the hydraulic jacks. The load was connected via the controller's valve to adjust the rate of the load application. The output voltage (10 V) from the controller was fed into the input channel of the data acquisition system.

The deformations were measured using number of linear potential differential transducers (LPDTs) that are attached to the top of concrete surface for measuring the deformations and cracking properties. The gauge length of these LPDTs is 50 mm, and mainly works on the basis of linear relationship between the resistance and displacement due to the

deformations occurrence, as shown in Fig. 3.5. Digital crack gauges with an accuracy of 0.001 mm were used to measure the crack width at regular interval of loading. Once the cracking occurs, the crack width readings are recorded using the crack gauges with a gauge length of 4.0 mm.

The LPDTs and the crack gauges were glued to the panel surface at different locations by epoxy, as illustrated in Fig. 3.5. These LPDTs and crack gauges were hooked up using separate channels of 10 V connected to the data acquisition system used in the present experimental investigation.

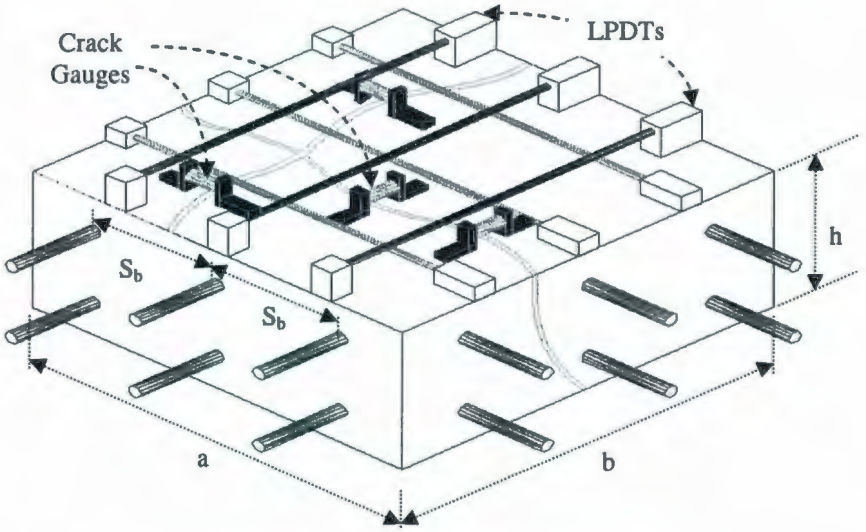

Fig. 3.5 Location of LPDTs and Crack Gauges

In addition, the strains were measured using electrical strain gauges. The strain gauges were 10 mm long, with a resistance of 120 Ω and a gauge factor of 2.07±0.5%. The strain gauges were affixed at different locations on the reinforcing bars of the top and the bottom layers in both north-south and east-west directions. The locations of the strain gauges were selected to provide sufficient information about deformation of the

reinforcing bars response at different location in the concrete panel. Fig. 3.6 shows a typical location of the concrete strain gauges on both top and bottom layers of the reinforcement. At each strain gauge location, the surface indentations of the reinforcement were ground smooth. In an effort to minimize the impact of the strain gauges on the bond characteristics of the steel, grinding was restricted to the smallest area that would permit placement of the strain gauges, and strain gauges were distributed in such a way that not more than two gauges were glued to each reinforcing bar, see Fig. 3.6.

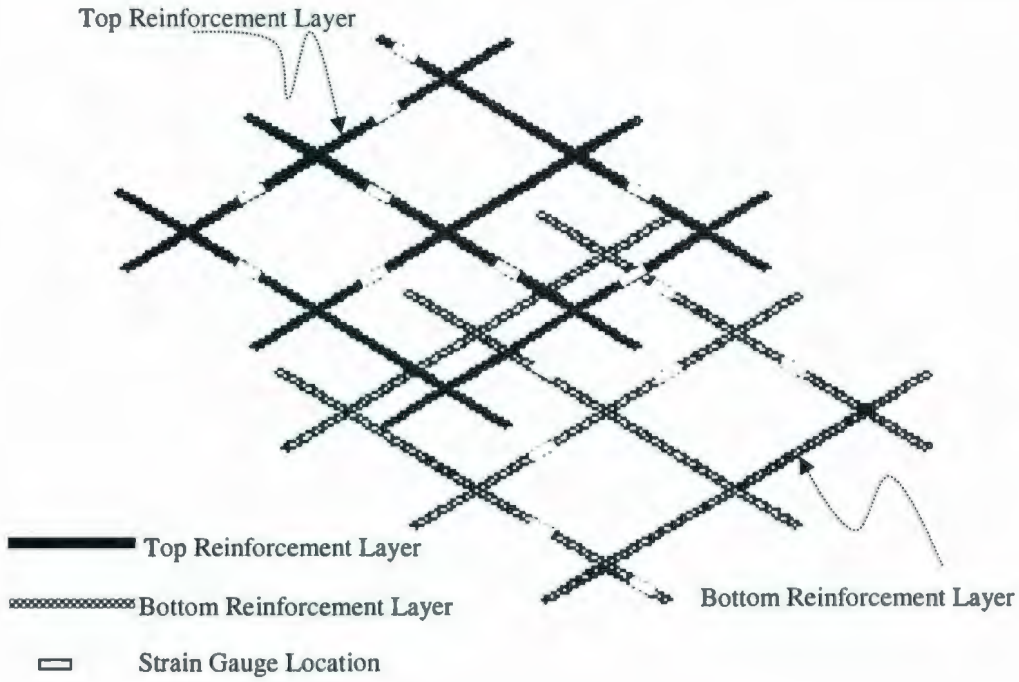

Fig. 3.6 Typical Location of Strain Gages

Gauges were attached to the reinforcing bars using an epoxy adhesive. After lead wires were attached, all gauges were covered with a layer of flow silicon to provide electrical

insulation. The outputs of the strain gauges were automatically logged into a 20 channel high speed data acquisition system connected to a computer.

3.4 Mix Design

Two levels of concrete strength, namely, normal-strength and high-strength concrete were used in the present experimental investigation. The mix proportions of normal- and high-strength concrete are shown in Table 3.2.

The normal-strength concrete test specimens were made of ordinary Portland cement (Type 10) CSA3-AS5 with a modified C_3A content of about 6%, and The high-strength concrete test specimens were made of CSA Cement type 10 E-SF cement blended with silica fume, as produced in Newfoundland. The coarse aggregate was crushed granite with a maximum nominal size of 19 mm. The fine aggregate had a composition identical to the coarse aggregate, with a fineness modulus (FM) of 3.02. Both types of aggregates were locally available. Due to the low water-cement ratios of the concrete mixtures, a superplasticizer of sulfonated naphthalene formaldehyde base, conforming to ASTM C 494 Type F, was employed. In addition, a nonchloride water-reducing agent of poly-hydroxy-carboxylic base, conforming to ASTM C 494 Type B and D, was used. The retarder was also useful in delaying the setting time so that the same consistency was achieved for all specimens prepared from each batch. The mixture proportions for the two batches are listed in Table 3.2.

The mixes design shown in Table 3.2 was used for all specimens constructed with normal- and high- strength concrete in this experimental program. The water to cement ratio = [w/(C+S.F.)] are 0.40, 0.29 for normal- and high-strength concrete.

Table 3.2: Mix Proportions for One Cubic Metre of the Two Types of Concrete Used

Normal Strength Concrete Mix (Target Compressive Strength = 35 MPa)							
Cement	Silica Fume	Fine Aggregate	Coarse Aggregate	Water Reducer	Superplastizer	Retarder	Water
400 kg	-	830 kg	1245 kg	-	-	-	160 ml
High Strength Concrete Mix (Target Compressive Strength = 70 MPa)							
Cement	Silica Fume	Fine Aggregate	Coarse Aggregate	Water Reducer	Superplastizer	Retarder	Water
400 kg	50 kg	713 kg	1070 kg	2.25 l ml	12.0 l ml	0.50 l ml	13 l ml

Three 100 mm diameter and height of 200 mm cylinders were cast from each batch. The cylinders were cabed with high-strength sulfur of 150 MPa at both ends and loaded about 8 MPa per minute in compression to failure.

3.5 Reinforcement Properties and Arrangements

Grade 400 reinforcing Canadian steel bars conforming CAN/CSA-G40.20-M92, were used. The reinforcement consisted of deformed bars 15 mm, 20 mm, 25 mm, and 30 mm in diameter; with average yield stress and ultimate tensile strength of 410 MPa and 650 MPa, respectively. The steel bars had a modulus of elasticity of 200 GPa. Two steel reinforcement ratios of 1.2% and 2% were used for the experimental program, as these ratios are commonly used in designing of offshore reinforced concrete panels. These

panels were equally reinforced in both directions. Fig. 3.7 shows the stress-strain relationship for the reinforcement for the various bar diameters used in the present study. The reinforcement was placed into two layers and the tension reinforcing bars were spaced according to details shown in Fig. 3.1, and as presented in Table 3.1. Both longitudinal and transverse reinforcing bars were passed through the slots in both reaction fixed frame and the four moving walls, as shown in Fig. 3.3.

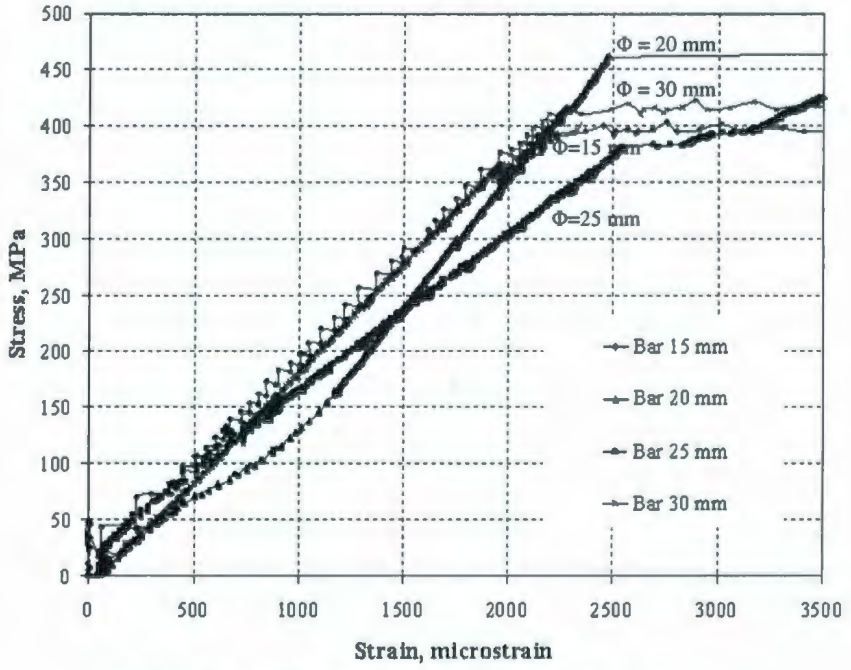

Fig. 3.7 Stress-Strain Curve of Steel Reinforcement

3.6 Mix Procedure

The following mixing procedure was developed for the production of a workable high-strength concrete mix:

1) Charge 100% of the coarse aggregate.
2) Batch 100% of cement.
3) Batch 100% of sand

4) Mix for 3-5 minutes after adding 70% of estimated water with superplasticizier.

5) Add 30% of mix water together with retarder and water reducer admixture.

3.7 Specimen Fabrication

3.7.1 Formwork

Special Plexiglass moulds were manufactured for casting the uniaxial and biaxial reinforced concrete panels, as shown in Fig. 3.8. The mould consisted of a base, and four walls. The base of the mould was secured in the base of test setup by screws spaced at 150 mm. Also, the vertical walls were stiffened with a wooden tie at the mid-height of the mould, to ensure that no distortion in the specimens occurred during casting.

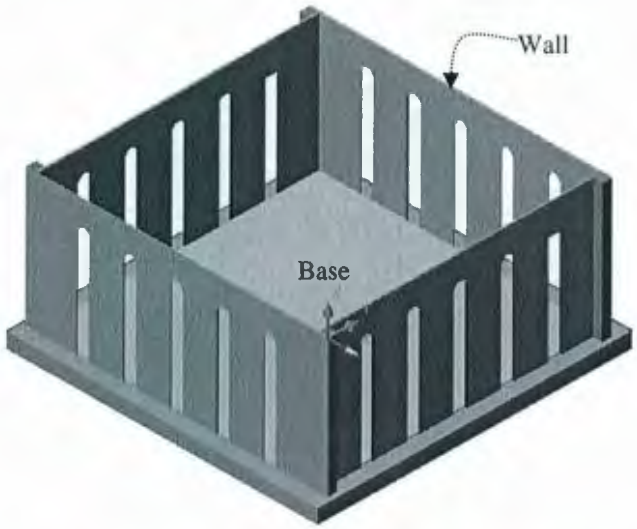

Fig. 3.8 Details of the Casting Formwork

3.7.2 Placing Reinforcement

The steel reinforcing bars were assembled in two stages. The first stage was performed by placing the lower layer of the reinforcement (longitudinal and transverse) in the

specimen. These reinforcing bars were passing through the slots in the frame and formwork in both north-south and east-west directions. The second stage of assembling the reinforcement was done by using wooden spacers on top of the lower layer of the steel reinforcement to support the top layer of reinforcement. Reinforcing bars for the top layer were inserted in their places in the panels following the same procedure used in assembling the bottom layer. The longitudinal and transverse reinforcement were tied together using steel wires for the top and bottom layers, see Fig. 3.4.

For uniaxial loading condition, all of the longitudinal reinforcing bars protruded outside the concrete panel, and were embedded inside the concrete gripping blocks (in east-west direction) with equal and sufficient lengths to adjust the transferred loads to each reinforcing bar to provide uniformly distributed forces on the concrete specimen. However, for biaxial loading condition, both the longitudinal and transverse reinforcement extended outside the concrete panel and embedded inside the concrete gripping blocks (in both east-west and north-south directions), as shown in Fig. 3.4.

3.7.3 Casting Concrete

Before placing the concrete, the formwork was thoroughly cleaned and the base and walls of formwork were slightly oiled. Concrete is poured in three layers and the compaction was achieved using a vibrator to consolidate the concrete. The top surface of the panel was finished, and a plastic cover was used to cover the mould to avoid drying out.

3.7.4 Curing

Two days after casting, the panel was de-moulded and fresh water was used for curing. This curing process was continued for three weeks to avoid shrinkage cracks, and then the panel was prepared for testing.

3.8 Test Procedure

The load was applied by using 1000 kN capacity hydraulic jacks. Load was transmitted from the loading jacks to the specimen by using a specially designed test setup and end gripping blocks, as shown in Fig. 3.4. All of the longitudinal reinforcing bars protruded outside the concrete panel, and embedded inside the concrete gripping blocks with equal and sufficient lengths to adjust the transferred loads to each reinforcing bar to provide uniformly distributed forces on the concrete specimen. Before applying the load to the specimen, initial measurements were recorded on the sensors, and the strain gauges. Load was applied in increments; a continuous record of the deformations was made using LPDTs. The readings of the strain gauges were also recorded for every incremental loading stage. In addition, the crack opening was measured at regular intervals using digital crack gauges with an accuracy of 0.001 mm. Once the cracking occurred, the crack width readings were recorded using the crack gauges. Fig. 3.9 presents a typical specimen during the test proceeding. After the start of loading, the load was never intentionally decreased until the test was completed. Since a large amount of strain energy was induced in the loading system, it was decided that testing be curtailed before complete failure of the reinforcing bar could occur. The tests were discontinued when one

of the following conditions were achieved: crack widths were judged to be extremely large; the steel had appreciably yielded; or the maximum capacity of the hydraulic jacks was reached.

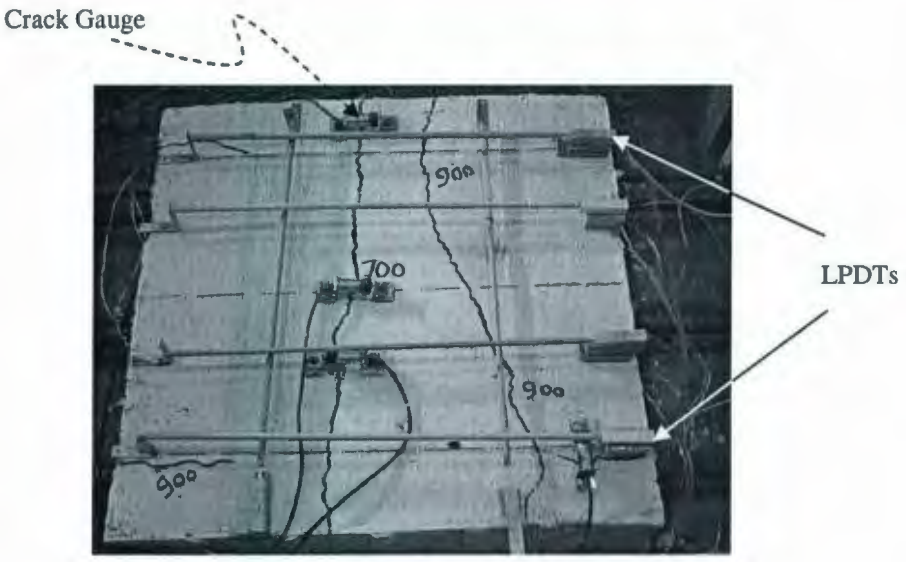

Fig.3.9 Typical Panel during Test

3.9 Summary of Experiments

An extensive experimental program was carried out to study the cracking behavior of reinforced concrete panels subjected to uniaxial and biaxial tension. In this experimental investigation, a total of nineteen reinforced concrete panels were fabricated and the effects of the concrete compressive strength, reinforcement ratio, and applying the load in the uniaxial or biaxial direction, were investigated. A special test setup was manufactured to conduct the present experimental investigation. The main purpose of this test setup was to apply the axial load in uniaxial and/or biaxial directions.

The strains of the steel bars were measured by strain gauges affixed to the bars. Also, LPDTs were attached to the top of concrete surface for measuring the deformations and cracking properties. In addition, digital crack gauges were used to measure the crack opening at regular intervals. The experimental data was continuously recorded from the load cells, LPDTs, and the strain gauges. Afterwards, the data was collected and processed automatically using a data acquisition system.

Chapter 4

Test Results and Discussion

In this chapter, the experimental results and observations obtained from the uniaxial and biaxial testing program are reported and analyzed. Firstly, cracking loads and cracking strength of concrete panels under axial loading for the different types of concrete are presented. Secondly, cracking properties including the crack width and spacing obtained from various measuring systems are detailed. The influence of various parameters that have profound effect on the tension stiffening response of thick HSC plates used for offshore concrete structure applications and nuclear containment structures, are discussed in details in the subsequent section. Finally, the effect of different factors on the cracking response (crack width and spacing) such as the reinforcement distribution in the concrete section, thickness of the concrete cover and applying the load into uniaxial and biaxial loading are examined.

4.1 Cracking Loads and Concrete Cracking Stresses

A reinforced concrete structure can easily crack due to its low tensile strength. Cracking loads can be captured at the point that shows the first change in the slope of the stress-strain curve, at which the first crack appears. Panels NS-U-15-2.5-6 and NS-B1-15-2.5-6 were cast with NSC, and subjected to uniaxial and biaxial tension loads (1:1), respectively. Panel NS-U-15-2.5-6 cracked approximately at a load of 240 kN, with an average tensile stress of 2.1 MPa that was sustained by the concrete, equivalent to 6% of

f_c', where f_c' is the compressive strength of the concrete resulting from cylinder tests. However, panel NS-B1-15-2.5-6 cracked when the tension force reached approximately 220 kN, and the average tensile stress of concrete was 1.92 MPa, which represents 5.5 % of f_c'.

Meanwhile, panels HS-U-15-2.5-6 and HS-B1-15-2.5-6 were cast with HSC, and tested under uniaxial and biaxial tension loads (1:1), respectively. At a tensile force of 400 kN, panel HS-U-15-2.5-6 started cracking, and with an average concrete tensile stress of 3.2 MPa, this is equivalent to 3.47% of f_c'. Panel HS-B1-15-2.5-6 cracked when the tension force reached approximately 310 kN, and the average tensile stress of 2.72 MPa was sustained by the concrete. This is equivalent to 3.6 % f_c'.

For thick HSC plates, the cracking response of panels HS-U-25-2.5-6 and HS-B1-25-2.5-6 is discussed. Panels HS-U-25-2.5-6 and HS-B1-25-2.5-6 were placed with HSC, and tested under uniaxial and biaxial tension loads (1:1), respectively. Panel HS-U-25-2.5-6 cracked approximately at a load of 650 kN, with an average tensile stress of 2.71 MPa that was carried by the concrete, equivalent to 3.6% of f_c'. However, panel HS-B1-25-2.5-6 cracked when the tension force attained approximately 595 kN, and the average tensile stress of concrete was 2.36 MPa, which represents 3.6 % of f_c'.

Test results revealed that use of HSC has a significant effect on the cracking behavior of axially loaded panels. Once the concrete strength was increased (125%) from 40 to 90 MPa, concrete tensile stress at the first cracking load increased by 52% for panels subjected to uniaxial loading. Also, for panels tested under biaxial loading, as the concrete strength was increased (115 %) from 35 to 75 MPa, the concrete stress at the

first cracking load increased by 42%, as shown in Table 4.1. Moreover, the experimental results show that applying the biaxial loading has some influence on the cracking behavior of the reinforced concrete panels. In comparison with panels tested under uniaxial loading conditions, applying the biaxial loading caused the tensile concrete strength to decrease by 8%, and 15% for NSC and HSC panels, respectively.

4.2 Cracking Properties (Crack Width and Spacing)

The cracking behavior of reinforced concrete panels subjected to uniaxial loading conditions can be discussed using an analysis of the cracking response of panels NS-U-15-2.5-6 and HS-U-15-2.5-6. Panel NS-U-15-2.5-6 was made with NSC and subjected to uniaxial loading in the east-west direction. As the tension force was applied, the average strain in the longitudinal upper and lower reinforcement bars increased gradually. When the tension force reached approximately 240 kN, the first crack appeared on the surface along the transverse reinforcement bar placed along the center line of the specimen in the north-south direction, as indicated in Fig. 4.1(a), at which an average tensile stress of 200 MPa was induced by the steel reinforcement bars in the east–west direction. The measured initial crack width was found to be equal to 0.122 mm. Another crack occurred at load 510 kN, on the surface along the first transverse reinforcement bar placed nearest to the east edge of the specimen and extended to approximately half width of the concrete panel, as shown in Fig. 4.1(a). At a steel stress of 270 MPa, which represents ⅔ of the yield stress of the reinforcement (f_y) (steel stress at the service load) [78], the measured crack width increased to 0.212 mm.

However, panel HS-U-15-2.5-6 was cast using HSC, and subjected to uniaxial loading in the east-west direction. When the tension force reached approximately 400 kN, two cracks occurred on the surface one along the first transverse reinforcement bar placed nearest to the west edge of the specimen and the other along the middle transverse bar; and the measured average tensile steel stress was 333 MPa. The measured initial crack opening was 0.21 mm. As the test progressed, another crack appeared at the first transverse reinforcement bar placed nearest to the east edge of the specimen, crossing the full width and thickness of the specimen at a load of 450 kN, and the measured average crack width was approximately 0.32 mm. Some cracks also occurred in the east-west direction at the end of the specimen. This phenomenon appears to be due to the bond failure between the reinforcement and concrete, as the reinforcing bars exceed the yielding stress, as shown in Fig. 4.1(b).

Meanwhile, as a result of applying the axial load in a biaxial direction, the cracking behavior can be investigated by analyzing the response of panels NS-B1-15-2.5-6, and HS-B1-15-2.5-6. Panel NS-B1-15-2.5-6 was cast with NSC and subjected to biaxial loading in the north-south and east-west directions with a loading ratio of 1:1. The average tensile strain in the longitudinal upper and lower reinforcement bars increased gradually in both directions. When the tension force reached approximately 220 kN, the first crack appeared along the surface perpendicular to the east-west direction right above the first transverse reinforcement bar near the west edge of the panel. The average tensile steel stress was 166 MPa. The measured initial crack width was found to be equal to 0.095 mm. At a tension force of 280 kN, the second crack occurred at 150 mm away from

the first crack in the north-south direction along the line at which the reinforcement was placed and eventually propagated to cross through the full width of the specimen. The measured average crack width was 0.14 mm. At the same time, two cracks occurred in the east-west direction along the surface right above the longitudinal reinforcement bars in the east-west direction, as shown in Fig. 4.1(c). At the serviceability limit and steel stress of 270 MPa, the measured crack width increased to 0.179 mm.

Identical to specimen NS-B1-15-2.5-6 in configuration and loading method, panel HS-B1-15-2.5-6 was made using HSC. While applying tensile load in the east-west direction, equal tensile load was simultaneously applied in the north-south direction. When the tension force reached approximately 310 kN, the first crack occurred along the surface perpendicular to the east-west direction right above the middle transverse reinforcement bar in the north-south direction, with an average tensile steel stress of 260 MPa. The measured initial crack width was found to be equal to 0.13 mm. As the test progressed, the second crack occurred approximately 150 mm away from the first crack in the north-south direction at a tension force of 330 kN along the line at which the steel bar was placed, and the measured average crack width was 0.19 mm. At the same time, two cracks occur in the east-west direction along the surface right above longitudinal reinforcement bars in the east-west direction, as indicated in Fig. 4.1(d).

The cracking behavior of thick HSC plates HS-U-25-2.5-6 and HS-B1-25-2.5-6 is detailed. Panel HS-U-25-2.5-6 was made with HSC and subjected to uniaxial loading in the east-west direction. When the tension force reached approximately 650 kN, the first crack appeared on the surface along the transverse reinforcement bar placed nearest to the

east edge of the panel, as illustrated in Fig. 4.1(i), at which an average tensile stress of 218 MPa was induced by the reinforcement bars in the east–west direction. The measured initial crack width was found to be equal to 0.102 mm. Another crack occurred at load 700 kN, on the surface along the first transverse reinforcement bar placed nearest to the west edge of the specimen and extended to approximately full width of the concrete panel, as shown in Fig. 4.1(i). At a steel stress of 270 MPa, which represents $\frac{2}{3} f_y$, the measured crack width increased to 0.282 mm.

HS-B1-25-2.5-6 was identical to panel HS-U-25-2.5-6 in configuration, but it was subjected to biaxial loading (1:1). When the tension force reached approximately 595 kN, the first crack occurred along the surface perpendicular to the north-south direction right above the middle transverse reinforcement bar in the east-west direction, with an average tensile steel stress of 200 MPa. The measured initial crack width was found to be equal to 0.095 mm. As the test progressed, the second crack occurred perpendicular to the first crack right above the first transverse reinforcement bar placed nearest to the east edge of the specimen at a tension force of 750 kN, as shown in Fig. 4.1(j).

Also, panel HS-B2-25-2.5-6 is identical to panel HS-U-25-2.5-6 in configuration, but it was subjected to biaxial loading (2:1). While applying tensile load in the north-south direction, double tensile load was simultaneously applied in the east-west direction. When the tension force reached approximately 610 kN, the first crack occurred along the surface perpendicular to the east-west direction right above the middle transverse reinforcement bar in the north-south direction, with an average tensile steel stress of 205 MPa. The measured initial crack width was found to be equal to 0.12 mm. As the test

progressed, the second crack occurred approximately 300 mm away from the first crack in the north-south direction at a tension force of 725 kN along the line at which the steel bar was placed near to east edge. As the load was increased, a crack occurred in the north-south direction along the surface right above reinforcement bars in the north-south direction near to west edge of the panel at load approximately of 1000 kN, as indicated in Fig. 4.1(p). At a steel stress of 270 MPa, which represents $\frac{2}{3} f_y$ the measured crack width increased to 0.354 mm.

HSC panel HS-U*-25-2.5-6 (without transverse reinforcement) is identical to panel HS-U-25-2.5-6. When the tension force reached approximately 700 kN, the first crack occurred along the surface perpendicular to the east-west direction at a distance of approximately 525 mm from the east edge, with an average tensile steel stress of 233 MPa. As the load was increased, a crack occurred in the north-south direction at load approximately of 900 kN, as indicated in Fig. 4.1(s). At a steel stress of 270 MPa, which represents $\frac{2}{3} f_y$ the measured crack width increased to 0.321 mm. In this panel without transverse reinforcement, most of the primary cracks developed randomly with increasing the applied load.

Cracks in the panels tested under biaxial loading propagated in both directions perpendicular to the load application, as the principal stresses take the same direction as the loading in the two orthogonal directions. The final crack patterns for all of the tested panels at the stabilized crack stage were marked manually at each stage of loading throughout the experiment, as shown in Fig. 4.1. Also, Fig. 4.2 shows the procedures for mapping of the cracks for various loading stages.

Table 4.1 Results from Reinforced Concrete Panel Tests

Specimens Symbol	f_c' (MPa)	f_t' (MPa)	$\varepsilon_{t(ex)}'$	Cracking Stage			Steel Stress		E_c MPa
				$P_{cr(ex)}$ (kN)	P_c (kN) Eq.4.3a	P_s (kN) Eq.4.3b	$f_{scr(ex)}$ (MPa)	f_{scr} (MPa) Eq.(4.6)	
NS-U-15-2.5-6	40	2.1	89.4	240	214	26	200	195	19740
NS-B1-15-2.5-6	35	1.92	91	220	194	26	166	175	19080
HS-U-15-2.5-6	90	3.2	133.1	400	354	46	333	295	29154
HS-B1-15-2.5-6	75	2.72	96.5	310	277	33	260	251	27900
HS-U-20-2.5-6	75	3.1	113	360	300	60	200	185	26283
HS-B1-20-2.5-6	75	2.96	97.6	335	280	55	186	175	29750
HS-U-20-2.5-4	80	3.0	115.5	330	295	35	270	277	26250
HS-B1-20-2.5-4	75	2.7	85.4	315	280	35	260	250	28270
HS-U-25-2.5-6	75	2.71	97.8	650	578	72	218	249	27950
HS-B1-25-2.5-6	65	2.36	96	595	531	64	200	231	26150
HS-U-25-1.5-6	75	2.7	105	490	436	54	165	250	26050
HS-B1-25-1.5-6	70	2.46	95	450	400	50	150	227	26150
HS-B2-25-2.5-6	65	2.42	105	610	544	66	205	222	22850
HS-B3-25-2.5-6	65	2.55	109	640	571	69	215	207	23300
HS-B4-25-2.5-6	65	2.61	113	655	585	70	220	190	23100
HS-U*-25-2.5-6	70	2.82	94.3	700	620	80	235	260	27600
HS-U-30-2.5-6	65	2.45	97	750	667	83	180	226	25350
HS-B1-30-2.5-6	65	2.1	90	700	615	85	182	193	24790
HS-U-30-1.5-6	65	2.32	96	580	516	64	140	213	24210

- *Panel without transverse reinforcement

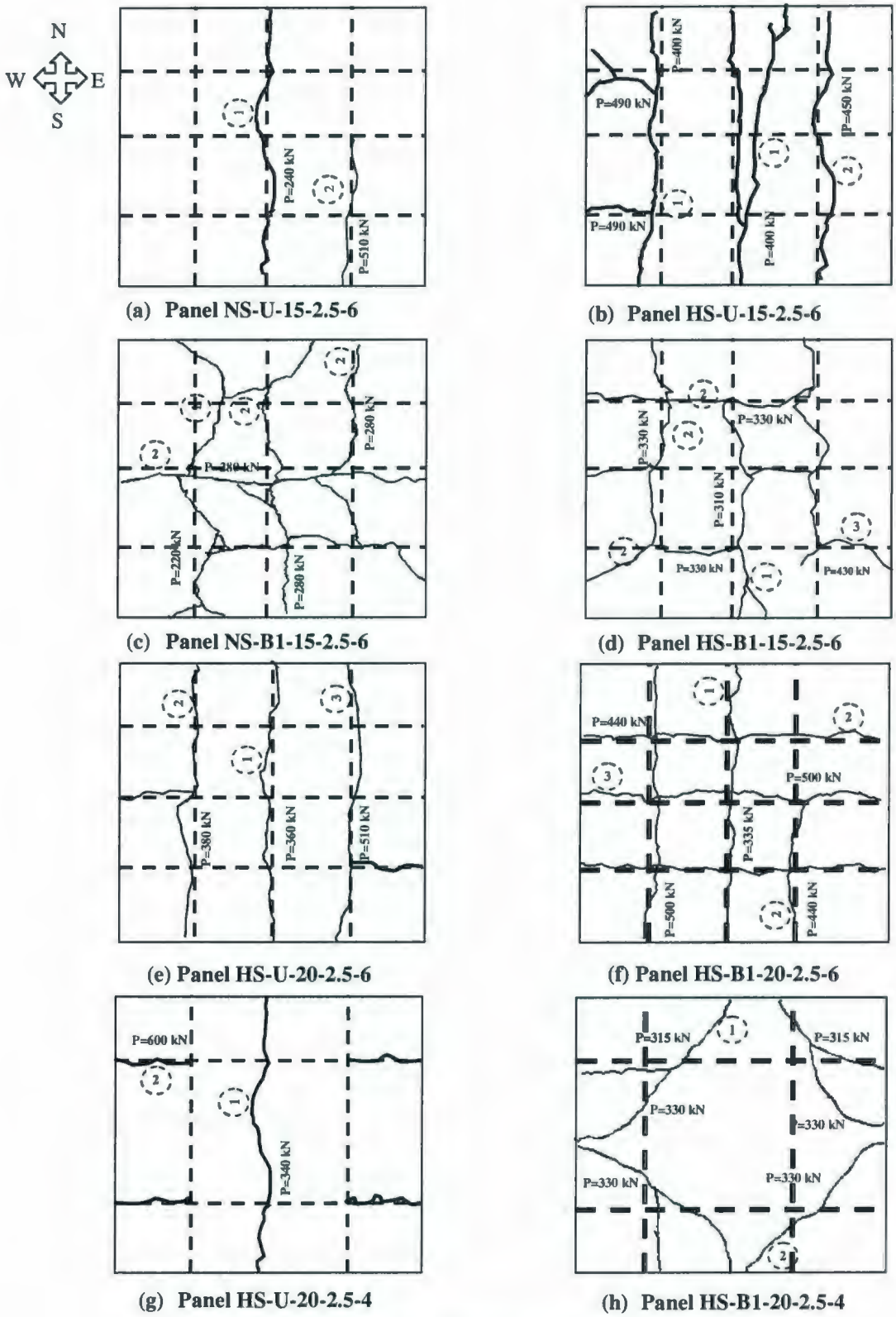

(a) Panel NS-U-15-2.5-6

(b) Panel HS-U-15-2.5-6

(c) Panel NS-B1-15-2.5-6

(d) Panel HS-B1-15-2.5-6

(e) Panel HS-U-20-2.5-6

(f) Panel HS-B1-20-2.5-6

(g) Panel HS-U-20-2.5-4

(h) Panel HS-B1-20-2.5-4

Fig. 4.1 Final Crack Patterns for the Tested Panels

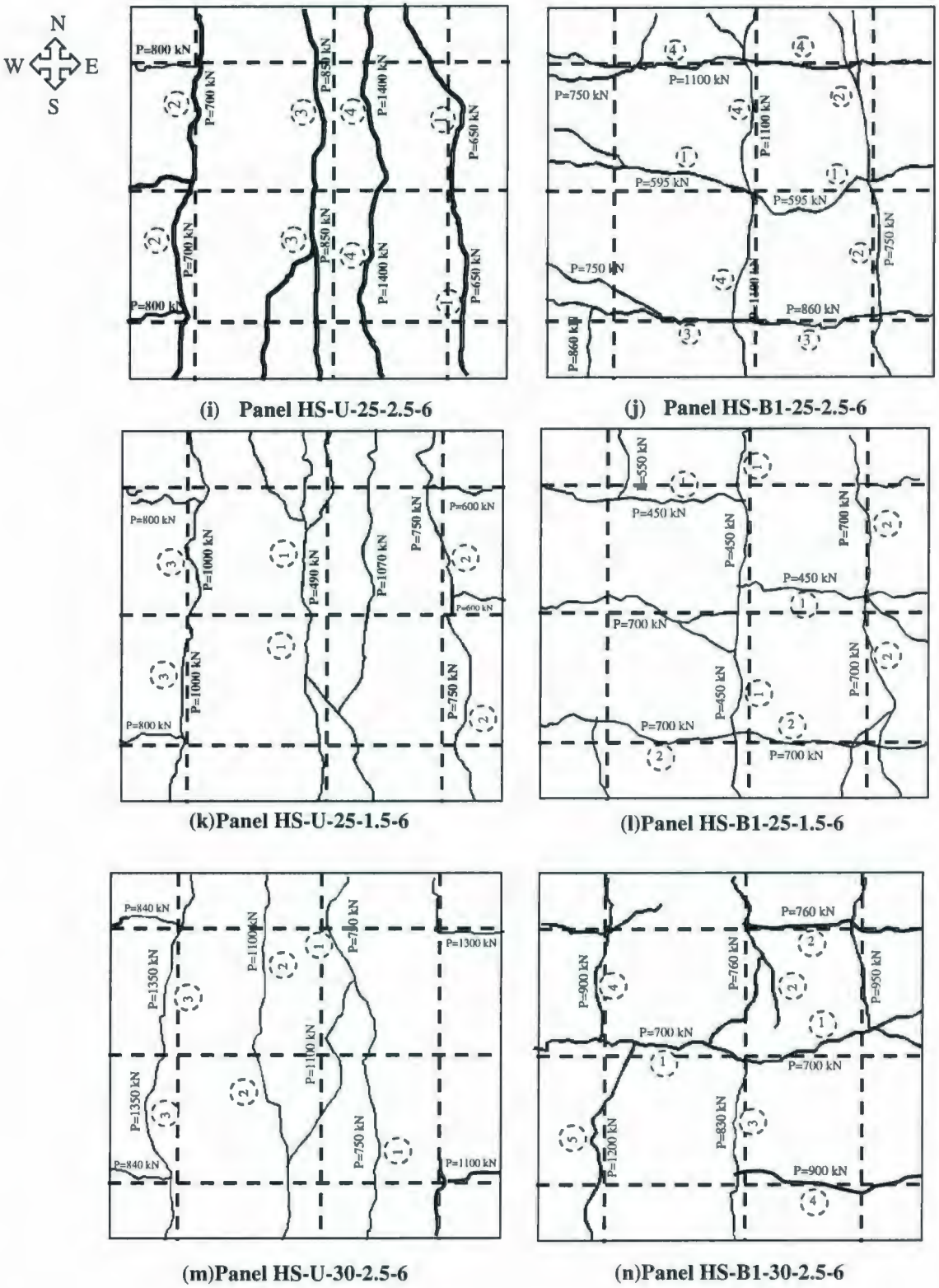

Fig. 4.1 Final Crack Patterns for the Tested Panels (Continued)

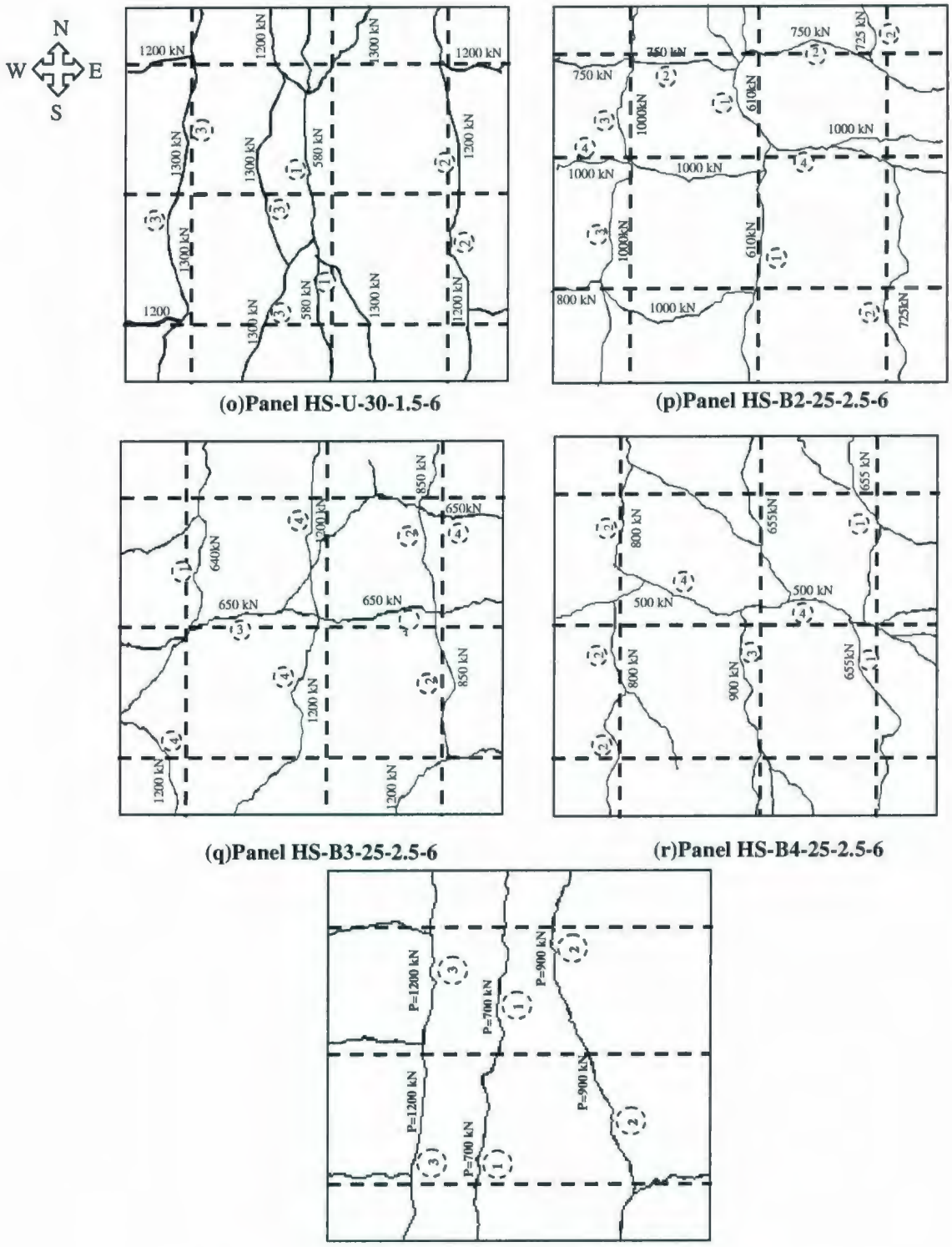

Fig. 4.1 Final Crack Patterns for the Tested Panels (Continued)

Fig. 4.2 Typical Crack Detection for Different loading Stages

4.3 Cracking of Concrete Panels under Axial Loading

4.3.1 Behavior before Cracking

The concrete strain was taken to be zero when the concrete was cast. Thus, the length of the concrete member at the time of casting is defined as the undeformed length of the member, L. The axial deformation measured from this undeformed condition was called Δ. The concrete strain, which is assumed to be uniform both over the cross section and along the length of the member, is given by $\varepsilon_t = \Delta/L$, assuming that the concrete and reinforcement bars are all rigidly anchored together. Hence, any change in length of the concrete must be accompanied by an identical change in the length of the reinforcement ($\varepsilon_t = \varepsilon_s$). For the equilibrium requirement, the internal stresses balance the applied load. Prior to cracking, the steel reinforcement and concrete behave elastically and tensile force

P in a panel is resisted partly by concrete and partly by the main longitudinal reinforcement in accordance to the stiffness of the concrete and steel bar sections [83, 46].

$$P = P_c + P_s = (E_c A_c + nE_c A_s)\varepsilon_t \tag{4.1}$$

And the tensile stress of the concrete can be expressed as following,

$$f_t = \frac{P}{A_c} - \rho E_s \varepsilon_t \tag{4.2}$$

in which E_c is the modulus of elasticity of concrete; A_c is the cross-section area of concrete; A_s is the area of the reinforcement; A_g is the gross-sectional area of the reinforced concrete panel (A_c+A_s); $(EA)_{uc}$ is the stiffness of the uncracked cross section; and ε_t is the tensile strain of concrete. Hence, each load transferred into concrete and reinforcement can be expressed as follows [83]:

$$P_c = (\frac{1}{1+n\rho})P \tag{4.3a}$$

$$P_s = (\frac{n\rho}{1+n\rho})P \tag{4.3b}$$

where P_c and P_s are the loads sustained by concrete and reinforcement, respectively; n is the modular ratio of concrete and reinforcement. At the time when the first crack occurs, $P = P_{cr}$, $\varepsilon_t = \varepsilon_t'$, and $E_c \varepsilon_t' = f_t'$. This can be written as follows:

$$P_{cr} = (E_c A_c + nE_c A_s)\varepsilon_t' \tag{4.4}$$

$$f_t' = \frac{P_{cr}}{A_c} - \rho E_s \varepsilon_t' \tag{4.5}$$

and the steel stress at cracking load can be calculated as follows [83]:

$$f_{scr} = \frac{P_{cr}}{A_s} = f_t' \left(\frac{1}{\rho} - 1 + n\right) \tag{4.6}$$

Table 4.1 summarizes the loads and the measured concrete strains at the cracking stage for different concrete specimens, obtained from the experiments. Tensile strength f_t' for different concrete specimens, obtained from the experiments conducted on the concrete plates, is also presented in Table 4.1.

The cracking load was selected at the point where the slope of the stress-strain curve abruptly changes, and where this change can be observed in every specimen. In the mean time, Table 4.1 shows a comparison between the steel stress at the cracking stage observed experimentally and the calculated steel stress from Eq. (4.6).

Prior to the cracking of the concrete member, steel reinforcement and concrete behave elastically and there is a compatibility condition between the concrete and reinforcing steel bars (Belarbi and Hsu, 1994 [46]; and Cho et al., 2004 [82]). The concrete and steel bars share the applied load in accordance to the stiffness of each material without any slippage between them. These stresses and strains can be approximately related by a straight line expressed as:

$$f_t = E_c \varepsilon_t \tag{4.7}$$

The normalized concrete stresses f_t/f_t' obtained from Eq. (4.2), and their corresponding measured strains ε_t are plotted in Fig. 4.3. These stresses and strains can be expressed by straight line as shown in the following equation:

$$\frac{f_t}{f_t'} = \frac{\varepsilon_t}{102 \times 10^{-6}} \tag{4.8}$$

The average value for all the measured cracking strains for each panel tested in the experimental program conducted in the present study is found to be about 102 microstrains.

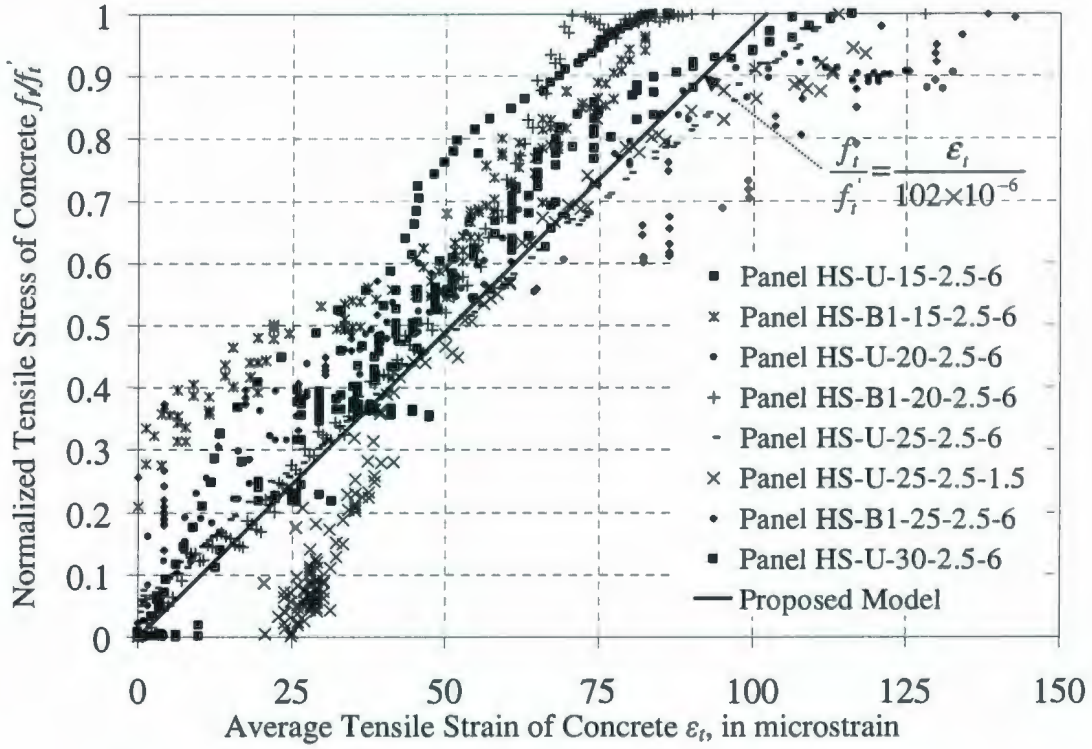

Fig.4.3-Ascending Branch of Tensile Stress-Strain Curves of Concrete

Cracking stress was found to be related to the square root of the cylinder compression strength for the normal strength concrete specimens as:

$$f_t' = 0.34\sqrt{f_c'} \quad \text{(MPa)} \tag{4.9}$$

The modulus of elasticity of the normal strength concrete can be obtained by substituting Eqs. (4.7) and (4.9) into Eq. (4.8):

$$E_c = 3330\sqrt{f_c'} \quad \text{(MPa)} \tag{4.10}$$

This developed equation for the modulus of elasticity of NSC shows a good agreement with the prvious proposed values for the modulus of elasticity of NSC [46, 81].

For high strength concrete the cubic root of the compressive stress ($f_c^{1/3}$) provides a good representation of the tensile strength for the high strength concrete (Marzouk, and Chen, 1995 [5]), as presented in the following equation:

$$f_t' = \beta \sqrt[3]{f_c'} \quad \text{(MPa)} \tag{4.11}$$

where β is a coefficient ranging from 0.6 - 0.7.

Also, the average value of the modulus of elasticity of the high strength concrete can be attained by substituting Eqs. (4.7) and (4.11) into Eq. (4.8):

$$E_c = 6400 \sqrt[3]{f_c'} \quad \text{(MPa)} \tag{4.12}$$

4.3.2 Behavior after Cracking

Based on the experimental results, constitutive relationships were developed to relate the average stress to average strain for orthogonally reinforced concrete plate segments. Fig. 4.3 shows the best mathematical form to fit the descending branches after cracking of the experimental stress-strain curve of HSC concrete plates subjected to axial loading conditions. After cracking occurrence, the steel carries all the tensile force at the crack locations. The following model can represent the best fit of descending branch for the HSC plates after cracking, taking into consideration the influence of transverse bars:

$$\frac{f_t}{f_t'} = e^{\frac{-0.0008}{\alpha_{trans}}(\varepsilon_t - \varepsilon_0)} \tag{4.13}$$

The influence of the transverse bar on the stress distribution of the panels tested under uniaxial and biaxial loading conditions can be considered by a factor α_{trans}, where the value of α_{trans} is found to be equal to approximately between 0.92 – 0.95.

Fig. 4.4 shows a comparison of the previously proposed models (Hawng and Rizkalla, 1983 [48]; Shima et al., 1987 [84]; Marzouk and Chen, 1995; 1993 [5, 36]; Fields and Bischoff, 2004 [47]), inclusive of the proposed model in Eq. (4.13) the descending portion in this study. All of these models were obtained from the experimental study for the behavior reinforced concrete members under axial loading. The proposed model represents an average value between the previously proposed models for tensile stress-strain response of reinforced concrete, as shown in Fig. 4.5.

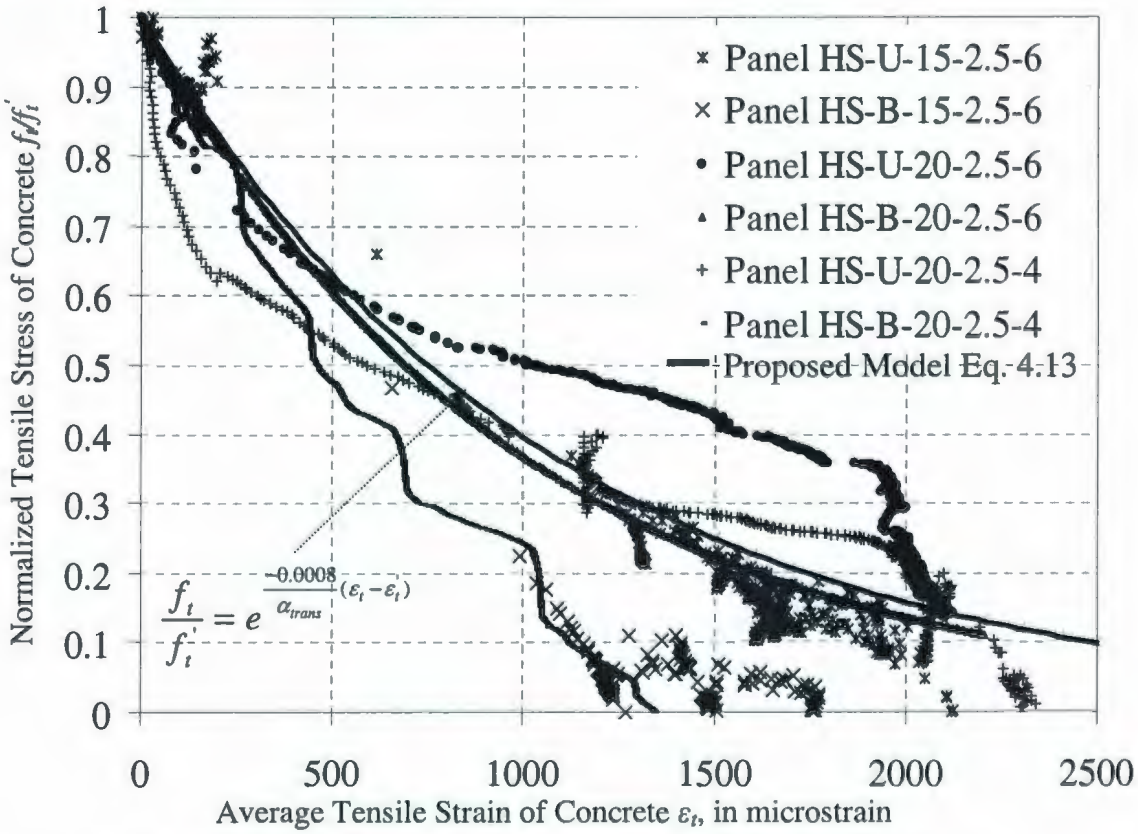

Fig. 4.4 -Descending Branch of Tensile Stress-Strain Curves of Concrete

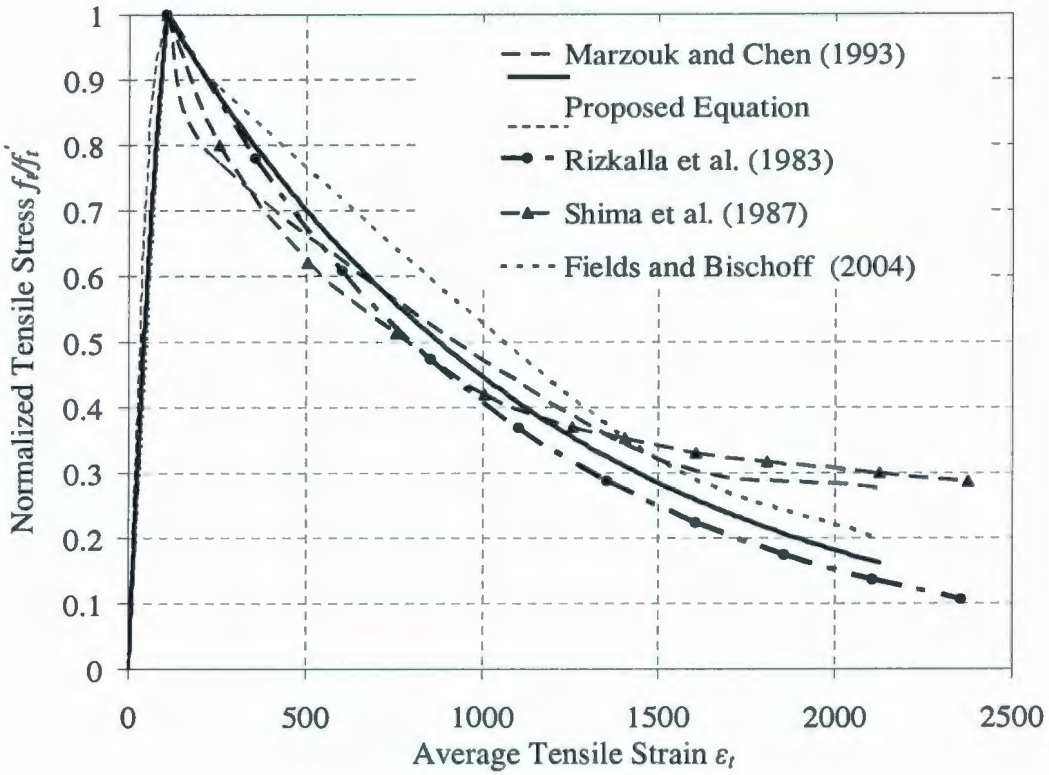

Fig. 4.5-Average Stress Strain of Concrete

4.4 Factors Affecting the Tension Stiffening Response of Axial Tension HSC Thick Plates

A comprehensive experimental investigation was conducted to study the tension stiffening response of reinforced concrete panels with different concrete strength under axial tension (uniaxial or biaxial). This section is investigating the influence of various parameters such as concrete strength, reinforcing bar distribution, concrete cover thickness, and applying the axial load into biaxial direction on the response of thick HSC plates used for offshore concrete structure applications and nuclear containment structures.

4.4.1 Effect of Higher Compressive Strength on the Tension Stiffening

The experimental results showed that, changing the compressive strength of concrete led to significant changes in the tension stiffening and cracking behavior of the reinforced concrete panels. Figs. 4.6 and 4.7 illustrate the influence of using HSC on the tension stiffening behavior of reinforced concrete panels under uniaxial and biaxial loading, respectively. The changes can be summarized in the following observations: a rise of the cracking load due to a higher tensile strength of HSC; an increase of the cracking strain was observed in the case of the HSC panel due to higher cracking load; and lower strains and greater tension stiffening effects at a given load level due to improvement of the bond of the reinforcing steel bars to the high strength concrete matrix.

Generally, four distinct regions characterized the typical tension stiffening behavior of the panels tested under axial loading, including: the uncracked phase where the concrete composite showed a linear and elastic behavior; crack formation phase in which the axial stiffness of the concrete panel gradually decreased due to cracks occurrence; stabilized cracking phase where the concrete panels and the bare reinforcing bars showed almost an identical slope for the stress-strain response; and failure phase that accompanied the yielding of the reinforcement, as illustrated in Fig. 4.6.

HSC sustained tension forces well up to the point of the first crack occurrence, corresponding to higher steel stress levels compared to NSC panels, as implied in Figs 4.6 and 4.7. The panels placed with HSC showed a larger discrepancy in the members' strain at the cracking load due to its brittle nature, where it led to a tension stiffening response that can be quite different from that of NSC. On the other hand, after the first crack

appearance, the slope of the stress-strain curve for the HSC panels radically decreased up to the yield point of the reinforcement with continuous variation of the slope through several steps. This indicated an additional cracks occurrence in the panel.

Experimental results showed that using high strength concrete (HSC) led to an obvious improvement for the tension stiffening contribution ($\Delta\varepsilon_s = \varepsilon_{s2} - \varepsilon_{sm}$), compared to normal strength concrete (NSC). Fig. 4.6 illustrates the relative improvement of tension stiffening effect $[(\Delta\varepsilon_{s,HSC} - \Delta\varepsilon_{s,NSC})/\Delta\varepsilon_{s,NSC}]$ for different levels of the steel stress, when changing concrete compressive strength from NSC ($f_c^{'}$ = 40 MPa) of panel NS-U-15-2.5-6 to HSC ($f_c^{'}$ = 90 MPa) of panel HS-U-15-2.5-6. A continuous increase was noted for tension stiffening response of the HSC panels compared with the NSC panels, till the concrete reached the cracking stage of the HSC, which was corresponding to high level of steel stress ($f_s \approx 333$ MPa), as illustrated in Fig. 4.6. The improvement of the tension stiffening $[(\Delta\varepsilon_{s,HSC} - \Delta\varepsilon_{s,NSC})/\Delta\varepsilon_{s,NSC}]$ increased gradually up to approximately 300% at the crack formation of the HSC panel. The tension stiffening response of the HSC panel dropped suddenly after cracking formation stage where the relative tension stiffening $[(\Delta\varepsilon_{s,HSC} - \Delta\varepsilon_{s,NSC})/\Delta\varepsilon_{s,NSC}]$ decreased to 40%, as shown in Fig. 4.6. This abrupt decrease in the tension stiffening of the HSC panels after crack formation reflected the brittle nature of the HSC.

Comparisons for the average tensile stress-strain relationship between NSC and HSC panels tested under uniaxial and biaxial loading conditions are presented in Figs. 4.8 and 4.9, respectively. The tensile strains of concrete were obtained and averaged from four LPDTs that were installed at several locations to the surface of the specimens, as the

average strain from the LPDTs reflected the global behavior of the cracked reinforced concrete panels under the applied tensile load. Thus, the average strain ε_t can be determined as:

$$\varepsilon_t = \frac{\frac{1}{n}\sum_{i=1}^{n}\Delta_i}{l_g} \tag{4.14}$$

where Δ_i is the individual reading from LPDTs; n is the number of the LPDTs attached to the concrete surface to measure the deformation; and l_g is the gauge length of the LPDTs. The tensile strength of the concrete increased as compressive strength was increased. However, the tensile strength increased slightly at a much lower rate compared to the compressive strength. Also, it can be seen that the initial axial stiffness of HSC panels appeared to be higher than that of NSC panels, reflecting the stiffer nature of HSC. However, the stress-strain curve of HSC panels descended more sharply after the peak stress in comparison to NSC panels that showed a gradual decrease, confirming the higher brittle nature of HSC. The maximum observed ultimate strain value ε_{max} measured from the experimental tests, was approximately equal to 16-20 times the value of strain at cracking ε_t'.

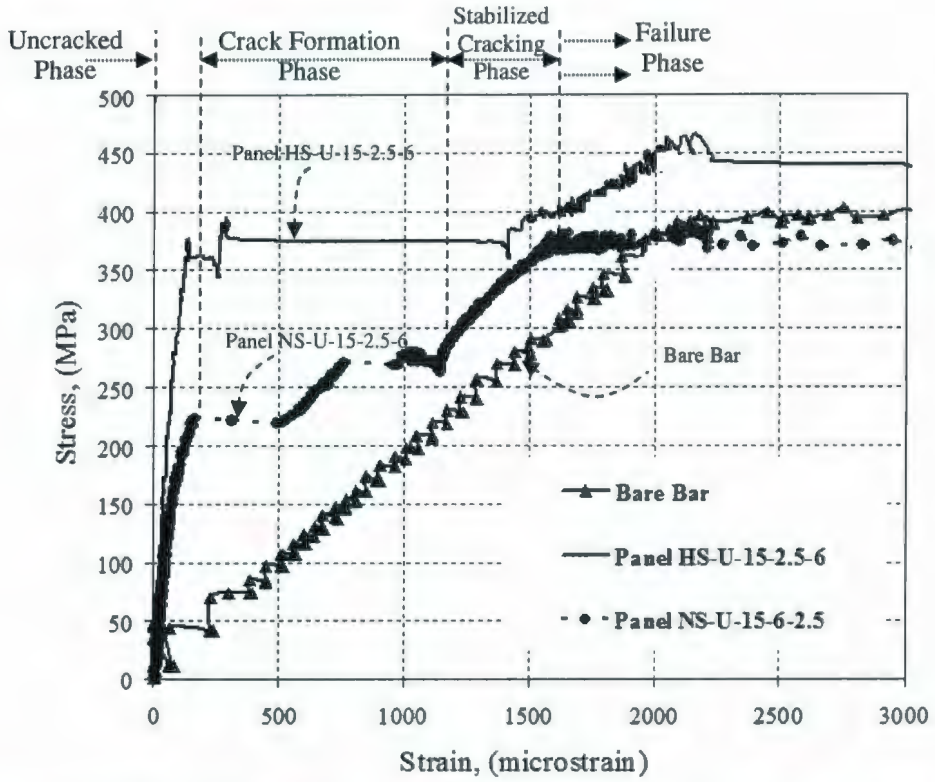

Fig. 4.6- Average Stress-Strain Curves for Plates NS-U-15-2.5-6 and HS-U-15-2.5-6

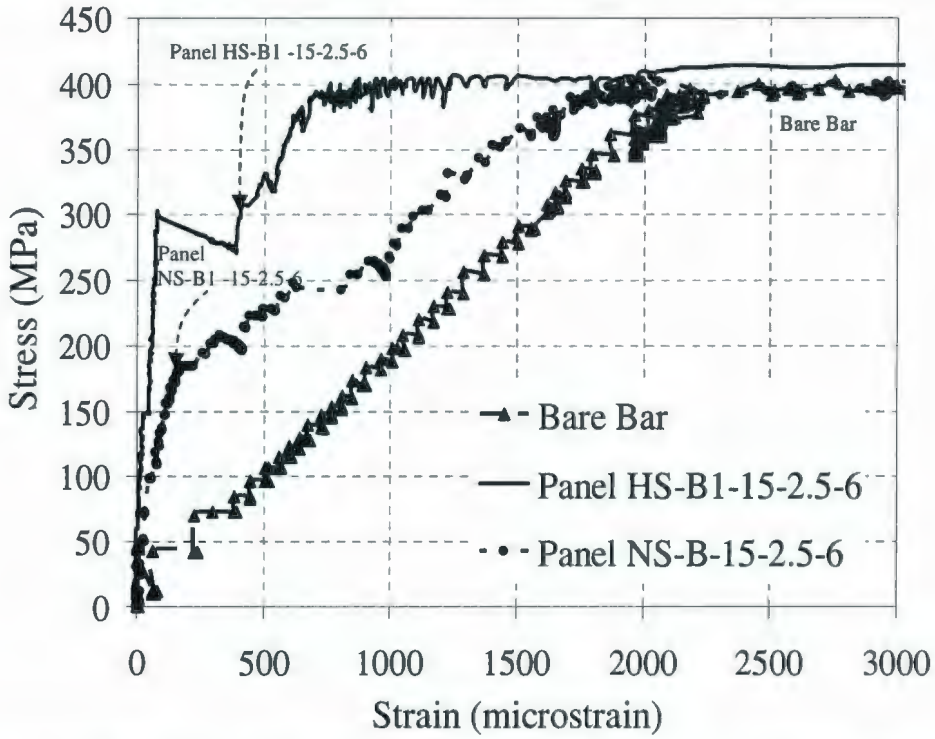

Fig.4.7- Average Stress-Strain Curves for Plates NS-B1-15-2.5-6 and HS-B1-15-2.5-6

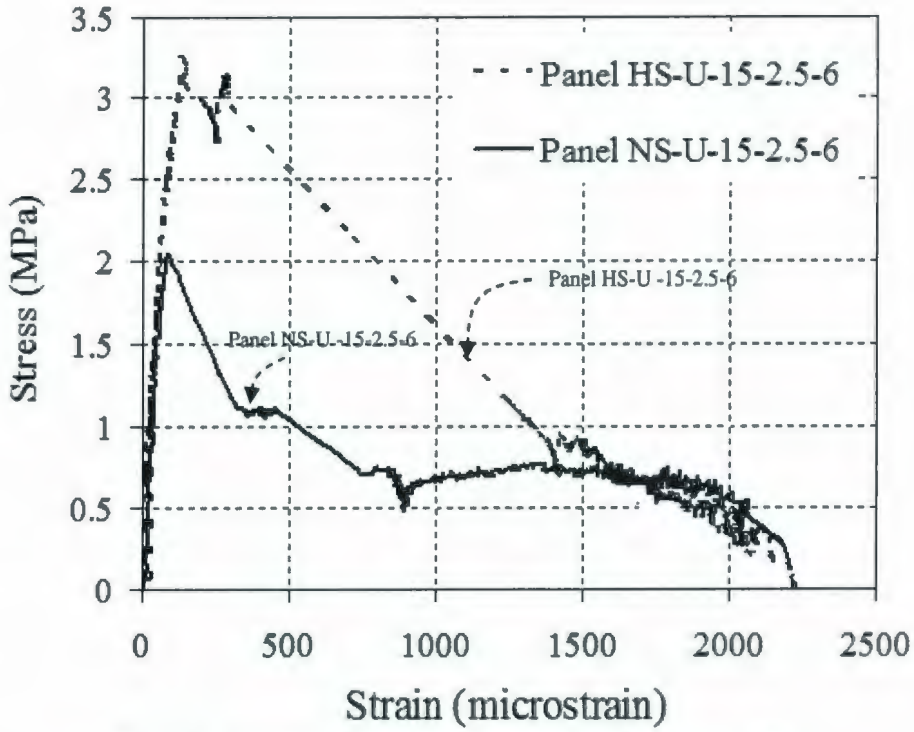

Fig.4.8- Average Stress-Strain curves of Concrete for Plates NS-U-15-1.5-6 and HS-U-15-1.5-6

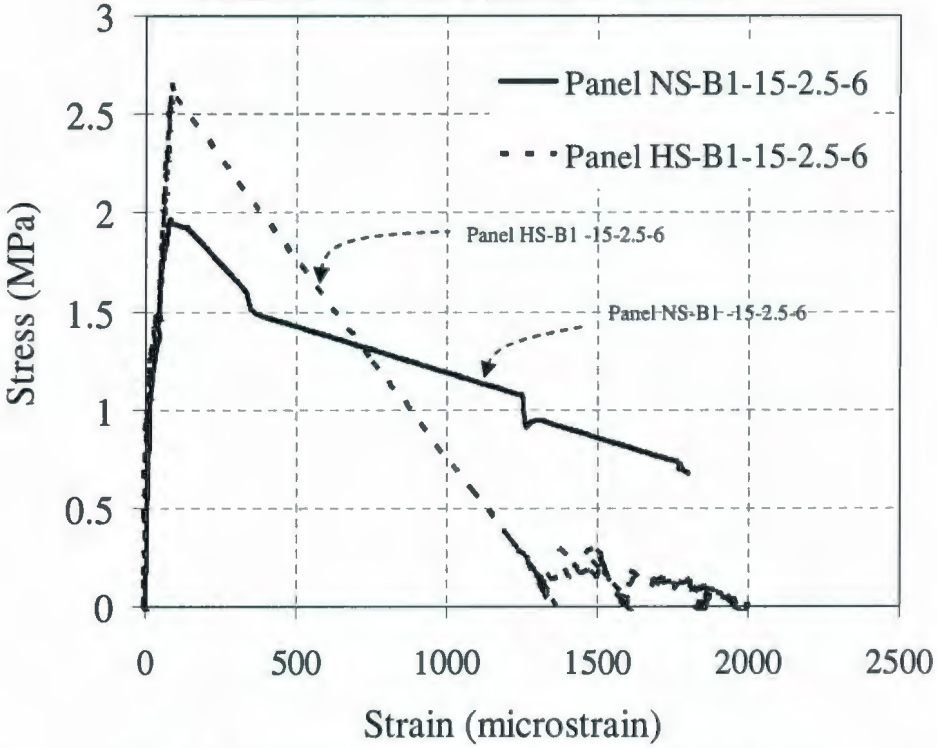

Fig. 4.9- Average Stress-Strain Curves of Concrete for Plates NS-B-15-2.5-6 and HS-B-15-2.5-6

4.4.2 Effect of Reinforcement Ratio

The influence of changing the reinforcement ratio on the tension stiffening and cracking response can be examined by comparing the experimental results of specimens HS-U-15-2.5-6 (ρ = 1.2%) and HS-U-20-2.5-6 (ρ = 2%). In this series of tests, the layout of the bars was identical, but the diameter varied from 15 mm to 20 mm, where a constant reinforcing bar spacing of 150 mm was chosen, as shown in Table 3.1. There is a trend whereby the concrete surrounding the smaller bar diameter carried a higher stress at the same steel stress level than that surrounding the larger bar diameter for the same bar spacing, especially during the crack formation stage, as shown in Fig. 4.10. Thus, the tension stiffening contribution decreased for the panels with higher reinforcing bar diameters. Also, increasing the reinforcement ratio by increasing the bar diameter had an insignificant influence on the cracking strength of concrete, where changing the reinforcement ratio from 1.2% to 2% caused the tensile strength to drop by 3%, see Table 4.1.

Meanwhile, the effect of the reinforcement ratio on the tension stiffening behavior can be investigated by changing the bar spacing and using the same bar diameter. Figs. 4 (e) and (g) represent the crack patterns for the specimens HS-U-20-2.5-6 (ρ = 2%) and HS-U-20-2.5-4 (ρ = 1.2%), respectively. The analysis of the failure mechanism and the final crack pattern recorded for panel HS-U-20-2.5-4 showed that the cracks locations were not significantly affected by the location of the transverse bars as the spacing between these bars exceed the required length to develop the tensile strength of concrete compared with the other specimen (HS-U-20-2.5-6) with closer transverse bar spacing.

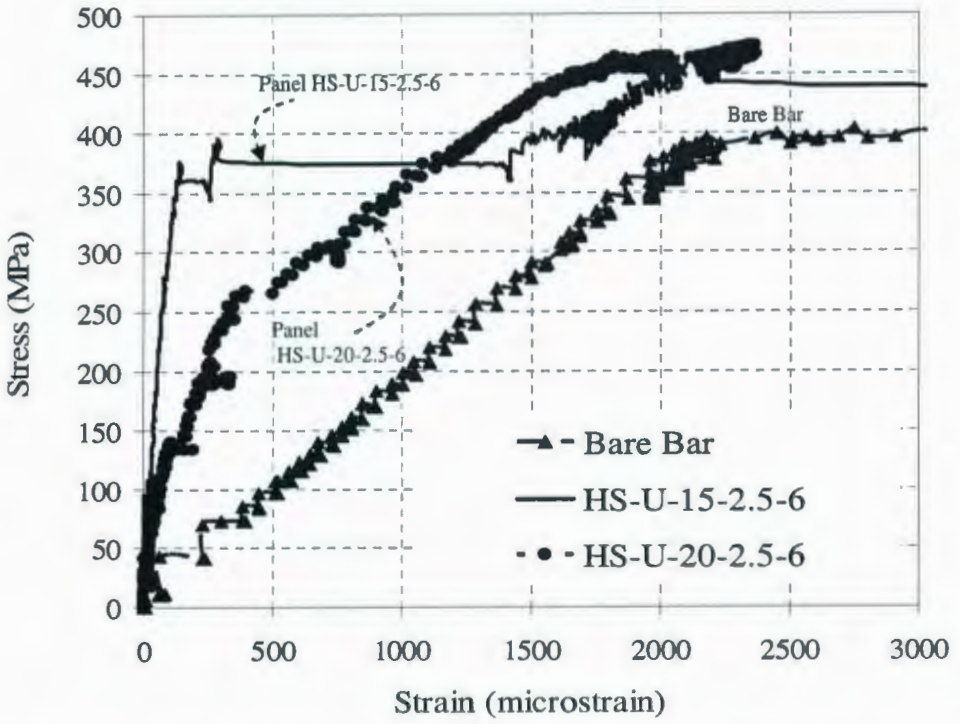

Fig. 4.10- Average Stress-Strain Curves for HS-U-15-2.5-6 and HS-U-20-2.5-6

The influence of changing the bar spacing between the longitudinal reinforcement on the tension stiffening behavior ($\Delta\varepsilon_s = \varepsilon_{s2} - \varepsilon_{sm}$) can be investigated by comparing the response of panels HS-U-20-2.5-6 (ρ = 2%, S_b = 150 mm) and HS-U-20-2.5-4 (ρ = 1.2%, S_b = 300 mm). In this series of test, the reinforcing bar diameter was identical, but longitudinal bar spacing was changed from 150 mm to 300 mm, as shown in Table 3.1. These two panels were tested under uniaxial loading.

Fig. 4.11 illustrates that, concrete tension stiffening contribution decays with strain at a rate that increases with bar spacing. Before the cracking stage, both panels HS-U-20-2.5-6, HS-U-20-2.5-4 showed almost the same tension stiffening contribution for the concrete, as the relative variation of the tension stiffening did not exceed (10%). The improvement of the tension stiffening for panel HS-U-20-2.5-6 increased gradually up to

70% through the crack formation phase, compared with panel HS-U-20-2.5-4. However, this improvement diminished gradually to 20% at the stabilized cracking phase, as shown in Fig. 4.11.

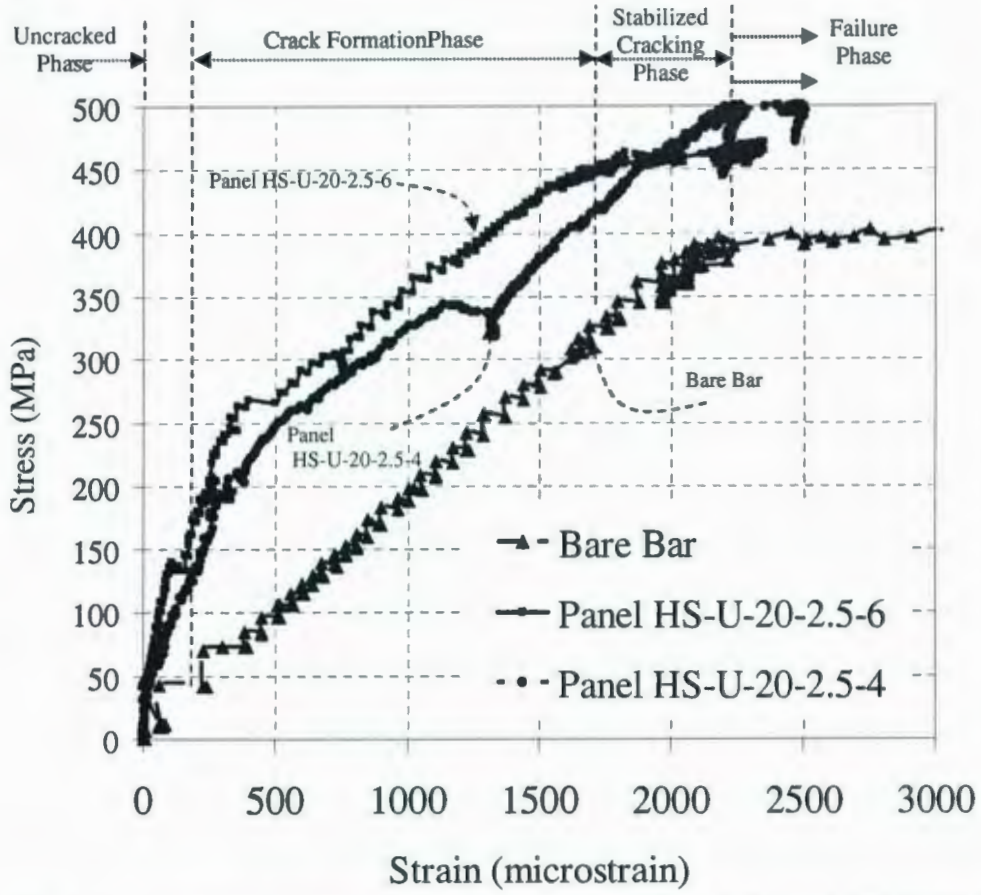

Fig.4.11- Average stress-strain curves plates HS-U-20-2.5-6 and HS-U-20-2.5-4

The influence of the distribution of the reinforcement on the tension stiffening response was more significant in case of applying the load in biaxial direction. This effect can be studied by considering the tensile stress-strain response for panels HS-B1-20-2.5-6 (S=150 mm) and HS-B1-20-2.5-4 (S=300 mm). Fig. 4.12 shows that, after cracking stage the tension stiffening increased gradually through the crack formation and stabilized cracking phases, the improvement of the tension stiffening increased gradually up to

approximately 100% through the crack formation phase. At high steel stress level (350 MPa), the tension stiffening contribution for the panel with high bar spacing (S_b = 300 mm) diminished to zero, however the other panel with lower bar spacing (S_b = 150 mm) showed some tension stiffening contribution for the concrete between cracks, as shown in Fig. 4.12. As a conclusion, the concrete tension stiffening contribution between cracks decays with strain at a rate that increases with the bar spacing for panels subjected to uniaxial and biaxial loading.

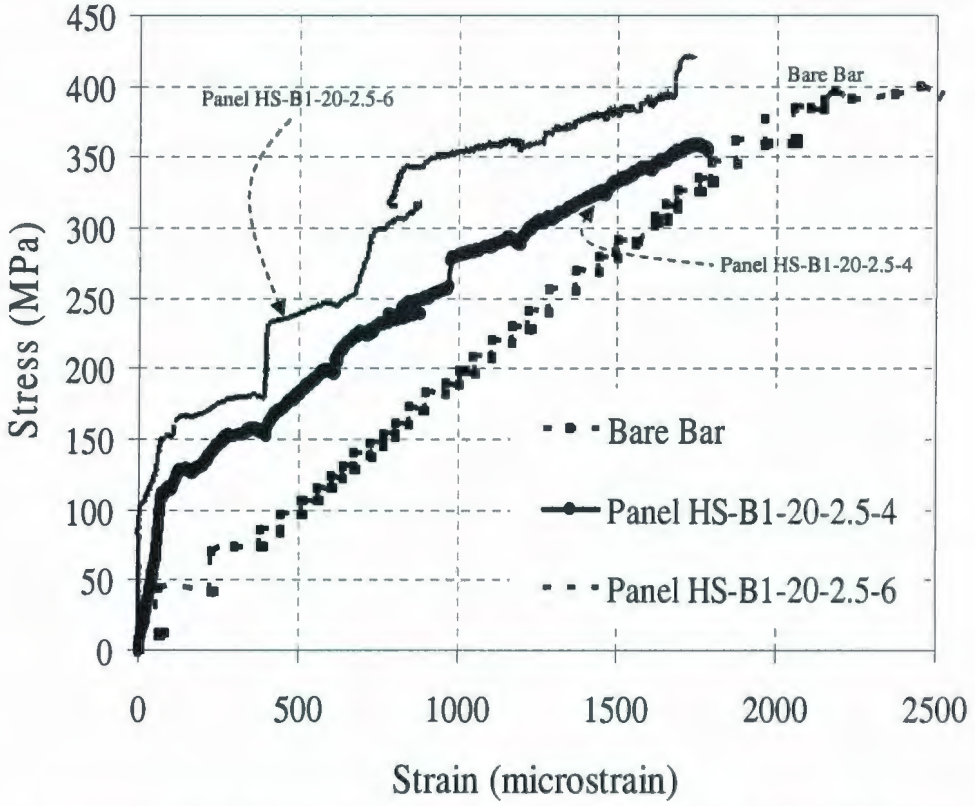

Fig.4.12- Average Stress-Strain Curves for plates HS-B1-20-2.5-6 and HS-B1-20-2.5-4

4.4.3 Effect of Concrete Cover on Tension Stiffening Response

Practical solution to protect the steel against the corrosion in harsh environmental conditions is by increasing the concrete cover, where using the reinforced concrete

sections with thick concrete cover is common in offshore and containment structures. Thus, one of the major objective of this study is to summarize and assess the effect of increasing the concrete cover on the tension stiffening behavior of HSC panels subjected to in-plane axial stress condition (uniaxial and biaxial) that is the case in some of the offshore and containment structures for nuclear power plants.

The effect of increasing the thickness of the concrete cover on the tension stiffening phenomena can be investigated by analyzing the experimental results of panels HS-U-25-1.5-6 (C_c/d_b = 1.5) and HS-U-25-2.5-6 (C_c/d_b = 2.5). In this series of test, the layout of the reinforcement was identical, where a constant reinforcing bar spacing of 300 mm and the reinforcement ratio of 1.2%, were chosen, but the concrete cover increases from 37.5 mm to 62.5 mm. These panels were tested under uniaxial loading condition. Fig. 4.13 shows that, there is a trend whereby the concrete surrounding reinforcing bars in both panels HS-U-25-1.5-6 and HS-U-25-2.5-6 provided almost the same tension stiffening contribution before the cracking occurrence. However, immediately after the cracking load, the concrete tension stiffening contribution was higher in HSC panels with thicker concrete cover for various steel stress level, as shown in Fig. 4.13.

The results for the average stress-strain relationship of concrete for panels HS-U-25-2.5-6 and HS-U-25-1.5-6 with the same bar diameter and spacing but varying concrete cover thickness are shown in Fig. 4.14. Panel HS-U-25-1.5-6 with the smaller concrete cover showed a faster decrease in the stress carried by the concrete between cracks with increasing the average concrete strain, compared with panel HS-U-25-2.5-6 with thicker concrete cover.

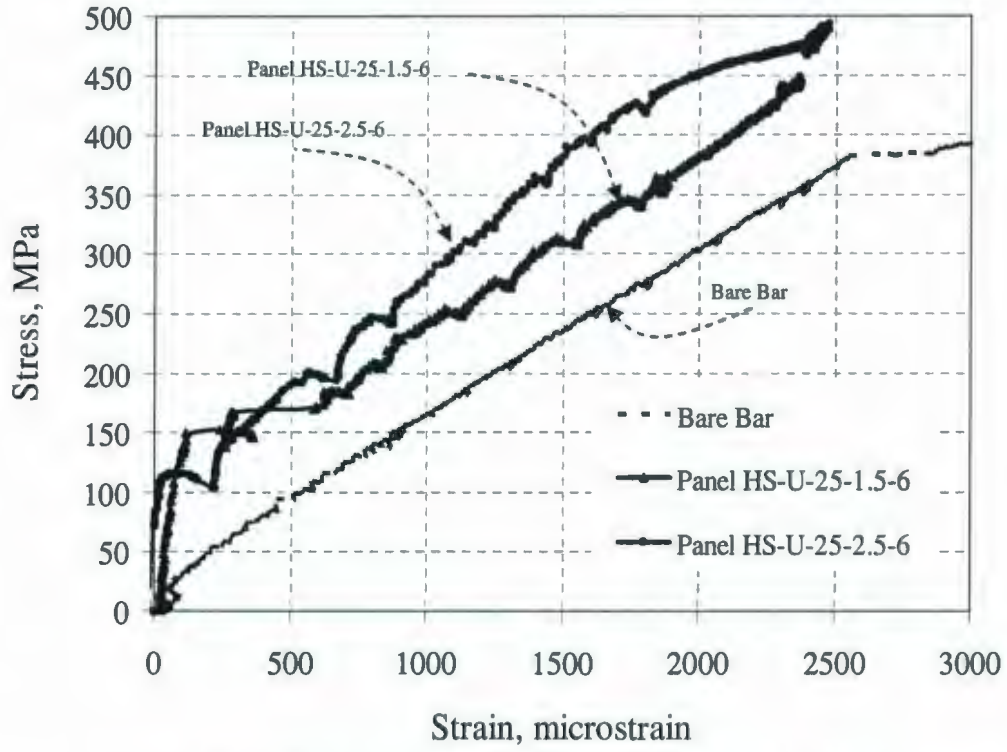

Fig.4.13- Average stress-strain curves for plates HS-U-25-2.5-6 and HS-U-25-1.5-6

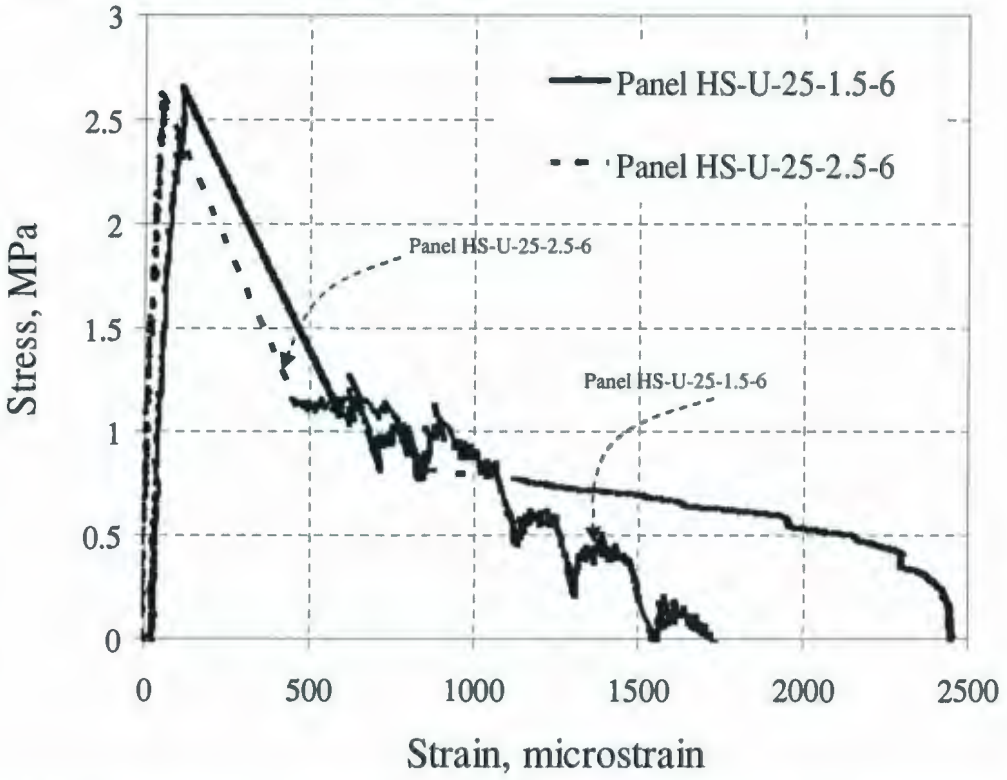

Fig.4.14 Stress-Strain Curves of Concrete for Plates HS-U-25-2.5-6 and HS-U-25-1.5-6

4.4.4 Effect of d_b/ρ_{eff} Ratio on the Tension Stiffening of Thick HSC Panel

The bar diameter-steel percentage proportion (d_b/ρ_{eff}) is proved to be one of the influential parameter on the tension stiffening and cracking behavior of the thick high strength reinforced concrete panel.

Based on the experimental program results, for specimens with d_b/ρ_{eff} ratio that was approximately 150 cm and above, consistent stress-strain response that exhibited similar characteristic features were obtained. Fig. 4.15 plots the stress-strain relationship for panels the HS-U-20-2.5-4 (d_b/ρ_{eff} = 166 cm), HS-U-25-2.5-6 (d_b/ρ_{eff} = 208 cm), and HS-U-30-2.5-6 (d_b/ρ_{eff} = 250 cm), tested under uniaxial loading. Before the cracking stage, stresses and strains increased linearly. The initial crack caused notable increase in the member strain that influence the average stress-strain curves significantly. The axial stiffness of the composites decreased gradually with each additional crack until a stabilized crack pattern was developed. When the panels reached the stabilized cracking phase, the average stress-strain curve of the reinforced panels and that of a bare reinforcing bar had almost identical slopes, as shown in Fig. 4.15.

However, different response was obtained for HSC panels with d_b/ρ_{eff} ratio that was less than 150 cm, as shown in Fig. 4.15. For panel HS-U-15-2.5-6 with (d_b/ρ_{eff} = 125 cm), after the first crack corresponding to high steel stress level ($f_s \approx$ 333 MPa), all subsequent cracks developed without a significant further increase in total load. This was due to yielding of the steel reinforcement at this loading level, immediately after the formation of the first cracking. Thus, the reinforcing bars reached yielding stress stage before

occurance of stabilized crack pattern. Fig. 4.15 displays that the lower the value of d_b/ρ_{eff} proportion, the higher the concrete tension stiffening response was obtained.

Fig. 4.16 shows the results for the average stress-strain relationship of HSC panels with different ratios of the bar diameter to reinforcement ratio (d_b/ρ_{eff}). The experimental results indicated that, after the peak concrete stress, the stress-strain curve of HSC panel HS-U-15-2.5-6 with d_b/ρ_{eff} = 125cm showed higher tension stiffening contribution for the concrete between cracks in comparison with the other panels with higher values for (d_b/ρ_{eff}) for various levels of concrete strains.

Fig. 4.17 shows the stress level in the reinforcement at the time when the first crack formed (f_{scr}) for different values of d_b/ρ_{eff} for both panels subjected to uniaxial and biaxial loading. It is obvious that the steel stress at cracking stage was sensitive to the value of d_b/ρ_{eff}, where the lower the value of d_b/ρ_{eff}, the higher the measured value of the steel stress at cracking for panels subjected to unaxial and biaxial loading conditions. This interesting result makes it possible to prevent crack formation under service load by using HSC panels with d_b/ρ_{eff} ratio that is less than 150 cm, which implies utilizing well distributed reinforcing bars in the concrete section, for the crack control and durability concerns.

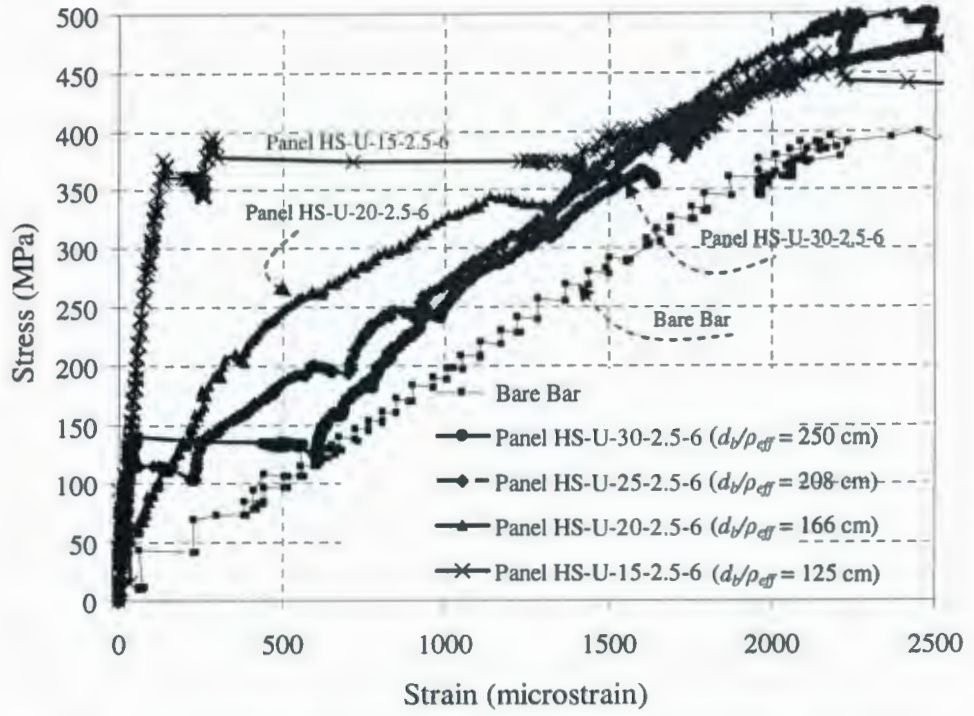

Fig. 4.15 Average Stress-Strain Curves of Reinforcement for Panels under Axial Loading for Different Values for d_b/ρ_{eff}

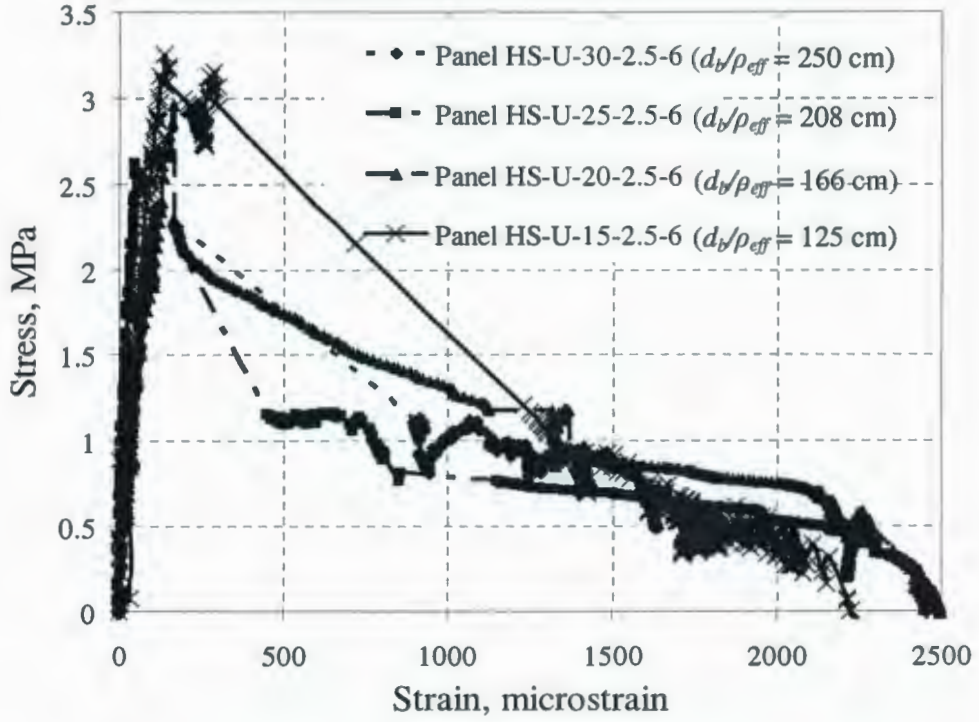

Fig. 4.16 Average Stress-Strain Curves of Concrete for Panels under Axial Loading for Different Values for d_b/ρ_{eff}

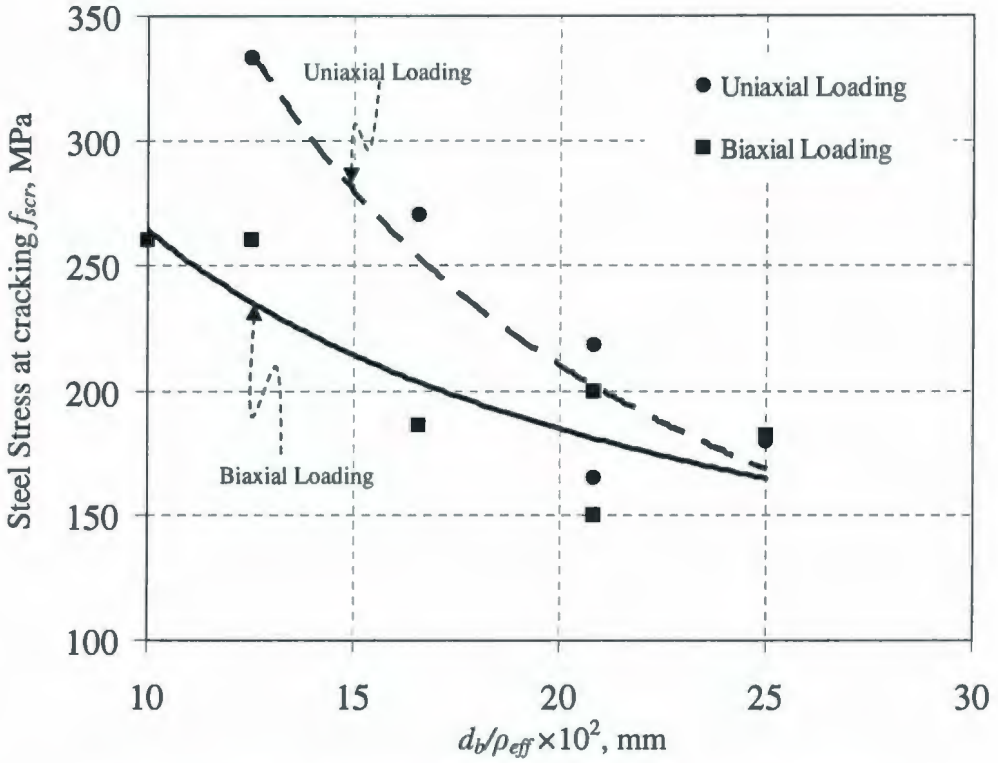

Fig. 4.17 Stress in Reinforcement at the Onset of Cracking Stage

4.4.5 Effect of Applying the Load into Biaxial Direction

The experimental test results presented in this study can be used to provide a clear understanding for the influence of applying the axial load into biaxial direction compared with the panels tested under uniaxial loading.

A comparison for the stress-strain response of reinforced HSC panels HS-U-20-2.5-4 and HS-B1-20-2.5-4 tested under uniaxial and biaxial loading (1:1), respectively, is presented in Fig. 4.18. Prior to cracking stage, a slight difference for the tensile stress-strain response was observed, where both panels have almost the same axial stiffness before the cracks occurence. However, after cracking stage the effect of applying the load into biaxial direction became more obvious. HSC concrete panels subjected to biaxial loading

showed lower tension stiffening contribution of concrete for different steel stress levels in comparison with the identical panels tested under uniaxial loading. This reduction in the tension stiffening was more obvious during the crack formation and the stabilized crack phases, as illustrated in Fig. 4.18. The main reason for this reduction in the tension stiffening was the gradual degradation of the axial stiffness of the reinforced concrete panel due to the additional cracks in the transverse direction.

The reduction of the tension stiffening contribution of concrete between cracks due to applying the axial into biaxial direction became more obvious as the reinforcing bar diameter was increased, as shown in Fig. 4.19. After cracking stage, panel HS-B1-30-2.5-6 tested under biaxial loading showed almost the same response as the bare bar, with sligh contribution for the concrete between cracks, in comparison with panel HS-U-30-2.5-6 that showed some tension stiffening contribution for the concrete after cracking occurrence.

Also, applying the axial load into biaxial direction reduced the tensile strength capacity of the concrete section. This reduction ranges between 5%-15%, as presented in Table 4.1. Generally, the concrete stresses resulting from the biaxial tension tests were lower than those from the uniaxial tension tests, and the average contribution of the concrete after cracking decreased at a higher rate with increasing the strains as the load was applied in biaxial direction, as shown in Fig. 4.20. The main reson for this effect is the higher axial degradation in the axial stiffness due to the development of the cracks in both directions as the load was applied in biaxial.

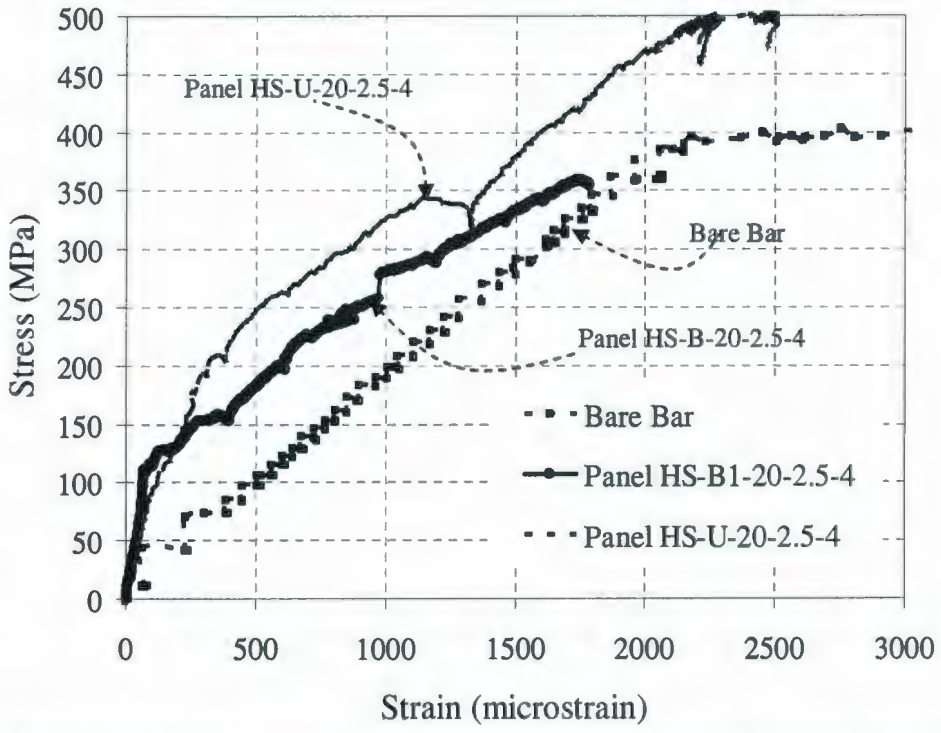

Fig. 4.18 Average Stress-Strain Curves for Plates HS-U-20-2.5-4 and HS-B1-20-2.5-4

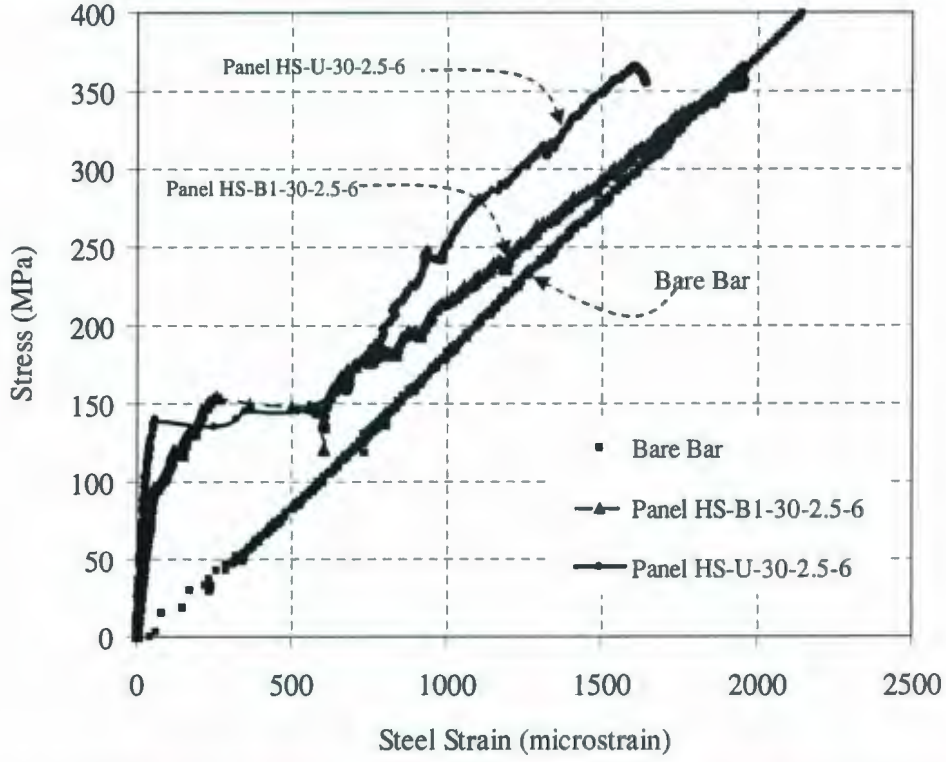

Fig. 4.19 Average Stress-Strain Curves for Plates HS-U-30-2.5-6 and HS-B1-30-2.5-6

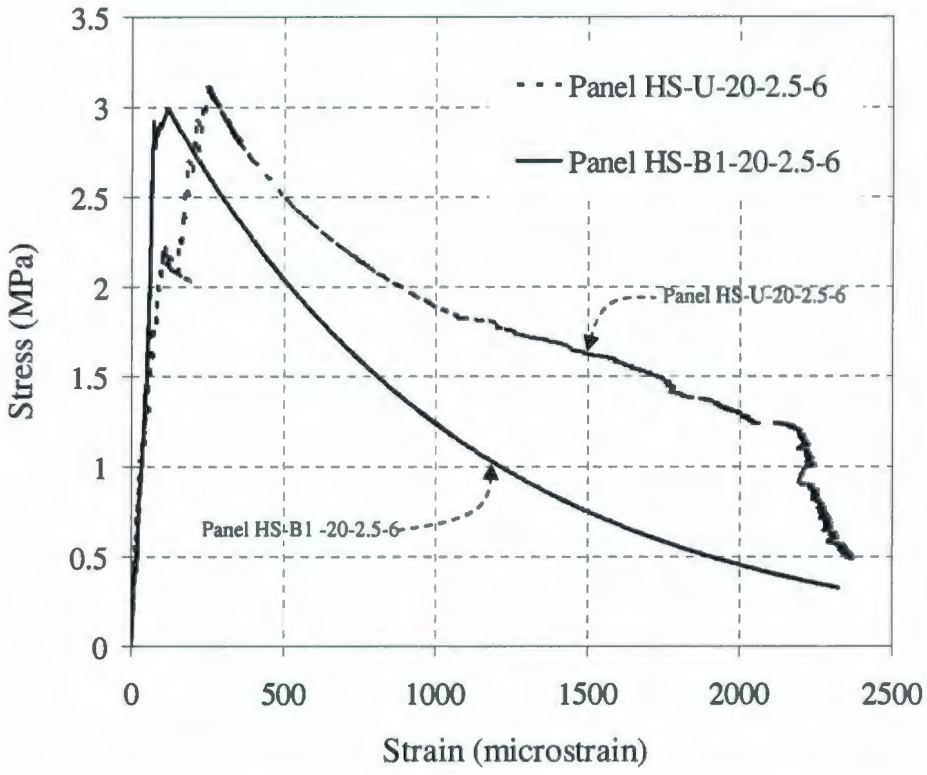

Fig.4.20 Average Stress-Strain Curves of Concrete for Plates HS-U-20-2.5-6 and HS-B1-20-2.5-6

4.4.6 Effect Biaxial Loading Ratio (P_1/P_2)

As detailed in chapter 3 (Fig. 3.2), this study considered five types of tension loads, 1:0, 1:1, 1:2, 1:3, and 1:4, as shown in Fig. 4.21. These ratios are corresponding to 90, 45, 26.5, 18.5 and 14 degrees expressed by an angle in the first quadrant of the tension-tension region, respectively.

Table 4.1 shows that tensile strength of the concrete panels decreased as the loading ratio was changed from 1:4 to 1:1. The tensile strength of the concrete was found to be 2.71, 2.36, 2.42, 2.55, and 2.61 for panels HS-U-25-2.5-6 (1:0), HS-B1-25-2.5-6 (1:1), HS-B2-25-2.5-6 (1:2), HS-B3-25-2.5-6 (1:3), HS-B4-25-2.5-6 (1:4); respectively.

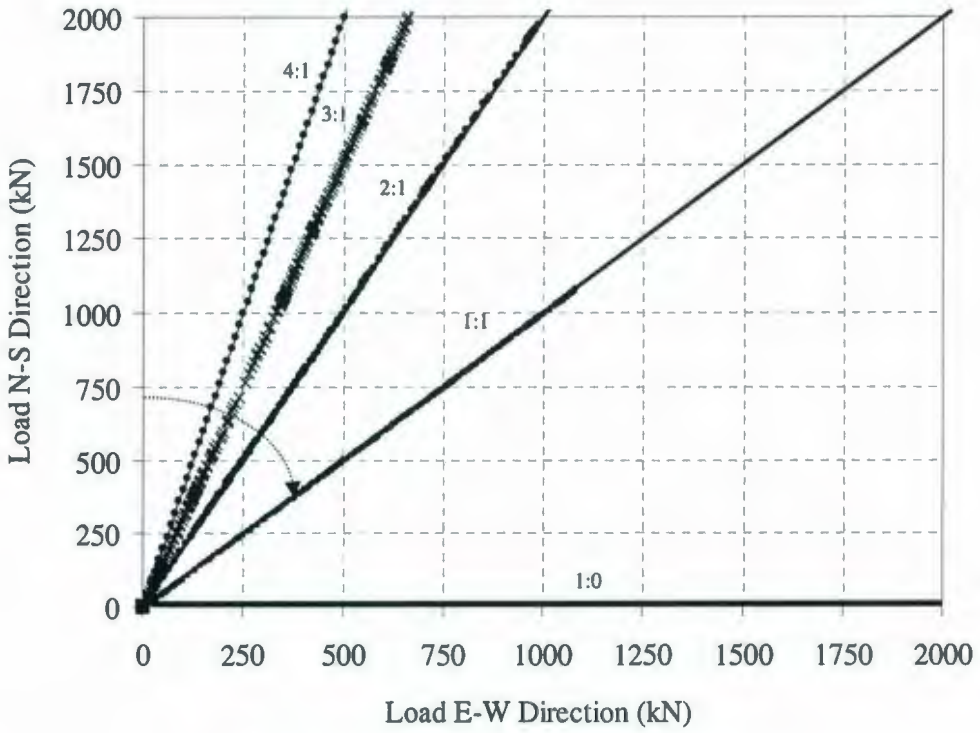

Fig. 4.21 Applied loads in two directions

Furthermore, the tension stiffening contribution for the concrete between cracks was decreased as the loading ratio (P_1/P_2) is changed from 1:4 to 1:1. Fig. 4.22 shows a comparison of the tension stiffening response of the thick concrete panels between panels HS-B1-25-2.5-6, HS-B2-25-2.5-6, HS-B3-25-2.5-6, and HS-B4-25-2.5-6. At steel stress level of approximately 300 MPa, the tension stiffening of the concrete between cracks for panels HS-B1-25-2.5-6 (1:1) and HS-B2-25-2.5-6 (1:2) diminished and these panels show a response similar to the bare bar. However, at the same steel stress level, panels HS-B3-25-2.5-6 (1:3) and HS-B4-25-2.5-6 (1:4) showed some tension stiffening response for the concrete between cracks, as shown in Fig. 4.22.

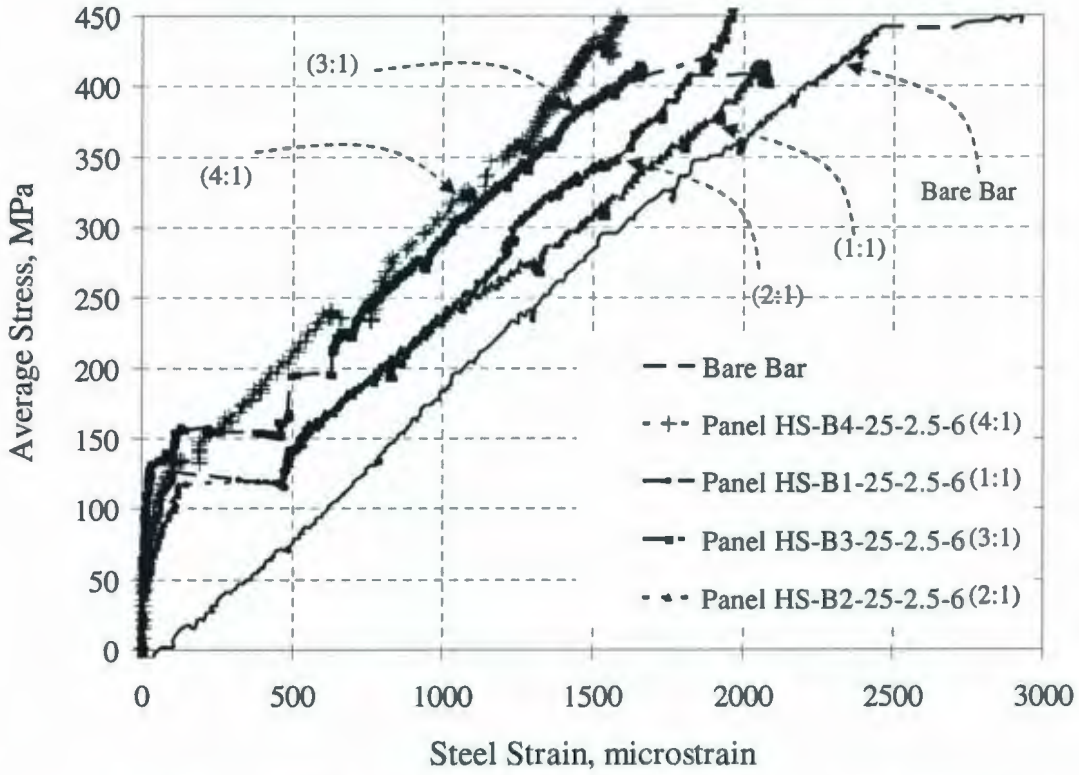

Fig. 4.22- Average Stress-Strain Curves for Panels subjected to Different Loading Ratio in the Orthogonal Direction

4.4.7 Effect of Transverse Reinforcement Presence

The presence of the transverse reinforcement in the concrete appears to cause a reduction in the tension stiffening effect of thick HSC panels. A comparison for the stress-strain response of reinforced HSC panels reinforced with transverse reinforcement (panel HS-U-25-2.5-6) and without transverse reinforcement (panel HS-U*-25-2.5-6), is presented in Fig. 4.23. Also, Fig. 4.24 presents a comparison of the average stress-strain curves of concrete between panels HS-U-25-2.5-6, and HS-U*-25-2.5-6. It is evident that prior to cracking stage, a slight difference in behavior of the tensile stress-strain response was observed. However, after cracking stage the effect of the presence of transverse reinforcement became more obvious.

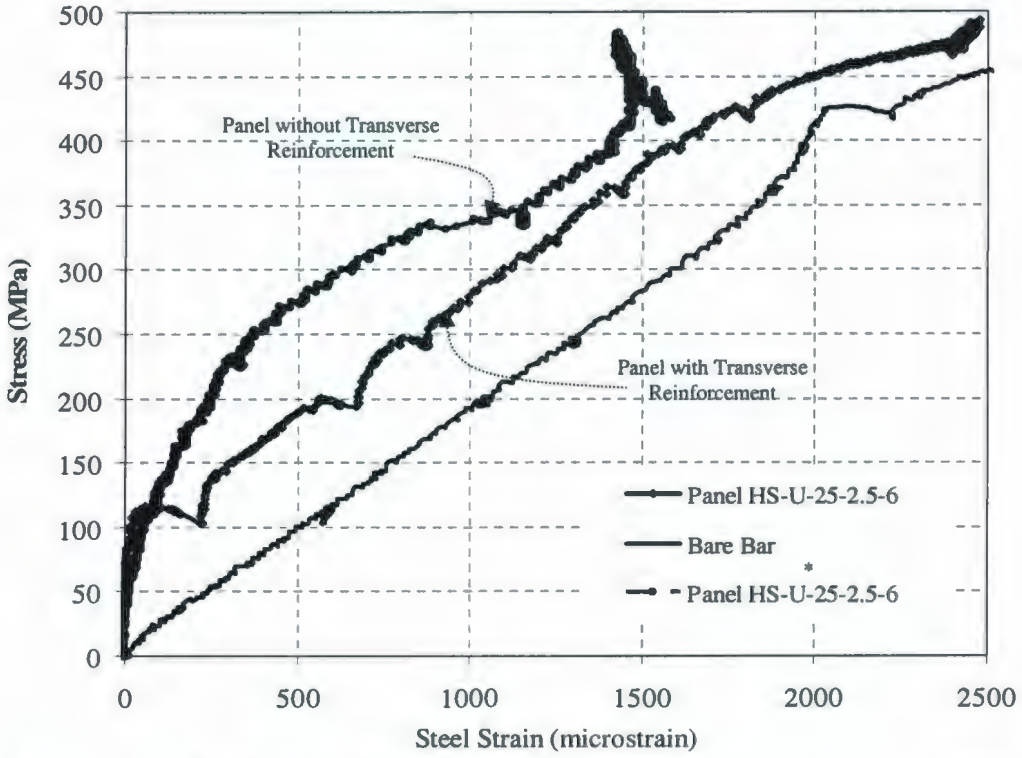

Fig.4.23 Effect of Transverse Reinforcement on the Tension Stiffening Response

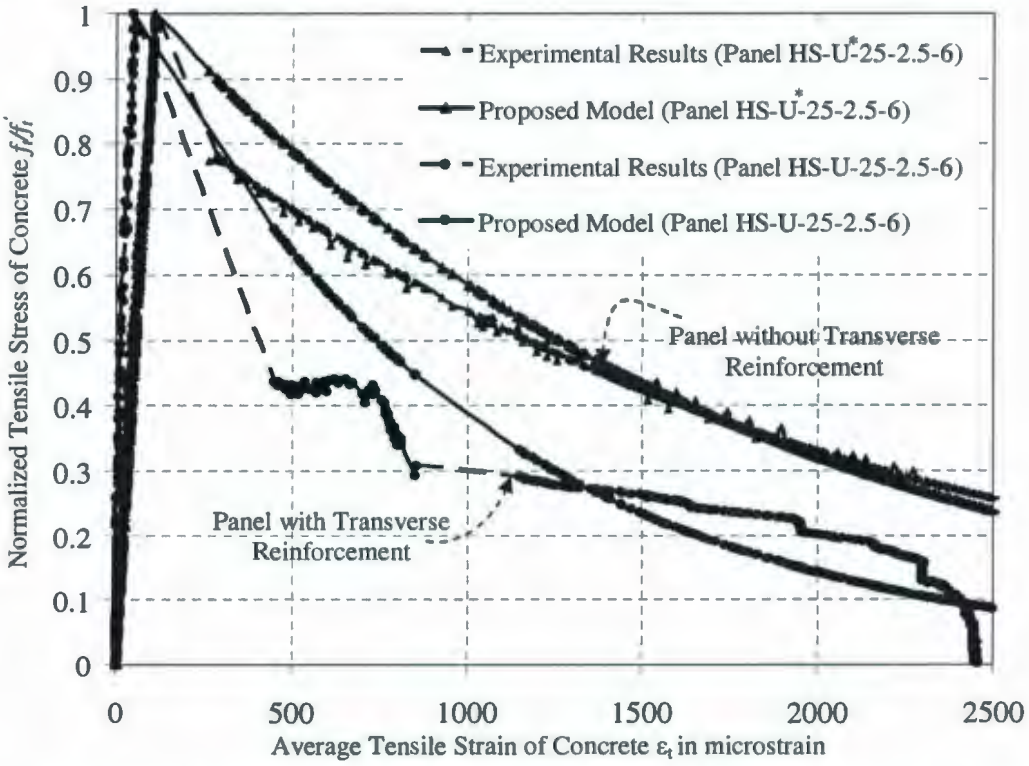

Fig. 4.24 Effect of transverse reinforcement on average stress-strain curves of concrete

Generally, the panel with the transverse reinforcement showed lower tension stiffening contribution of concrete for different steel stress levels in comparison to the identical panel without transverse reinforcement.

4.5 Factors Affecting the Crack Width and Spacing of Axial Tension HSC Thick Plates

The above experimental investigation revealed that the spacing and width of the cracks developed in thick reinforced concrete panels tested under axial loading application at a given steel stress level, are governed by some variables such as, the concrete strength, thickness of the concrete cover, reinforcement ratio, applying the load into uniaxial or biaxial directions.

To enable an accurate crack spacing measurements to be obtained, the tested panels were carefully inspected at each load step. The cracks were marked manually on all specimens at each load increment. Crack mapping of the specimen was depicted by means of photographs at each stage of loading throughout the experiment. These photographs were imported into a computer-aided AutoCAD, tools and the spacing was measured and averaged using the software.

This section discusses and summarizes the main test results of the tensile cracking response of some of the tested panels, showing the relative significance of the effects of individual variable on the measured crack spacing and width observed in the present experimental study.

4.5.1 The Effect of the Concrete Strength, f_c'

Table 4.2 shows the measured results for the average crack spacing of the different panels in the experimental investigation conducted in the present study. The influence of concrete strength can be typically explained by comparing the cracking behavior of NSC panel NS-U-15-2.5-6 with HSC panel HS-U-15-2.5-6 as these panels were tested under uniaxial loading condition; and panels NS-B1-15-2.5-6 and HS-B1-15-2.5-6 as tested under biaxial loading condition. The experimental results presented in Table 4.2 indicate that, changing the compressive strength of concrete has insignificant effect on the measured value of the crack spacing, where other variables are kept constant.

Comparison for the average crack width measured at different levels of steel stress between normal and high strength reinforced concrete panels tested under biaxial loading condition is presented in Fig. 4.25. The influence of using HSC on the average crack width can be summarized in the following observation: At the same steel stress level, the higher the compressive strength of the concrete, the lower the value of the average crack width. Also, using the high strength concrete causes the concrete to crack at a higher steel stress level compared with panel casted with NSC, as shown in Fig. 4.25.

The value of the average crack width for panels NS-B1-15-6-2.5, and HS-B1-15-2.5-6 reached approximately 0.179 mm, 0.145 mm, respectively, at the stress in reinforcement equal to service load ($\frac{2}{3} f_y$ = 270 MPa) [78]. Thus, the test results showed that as the concrete strength was increased by 115% the average crack width decreased by 20%, at the serviceability limit.

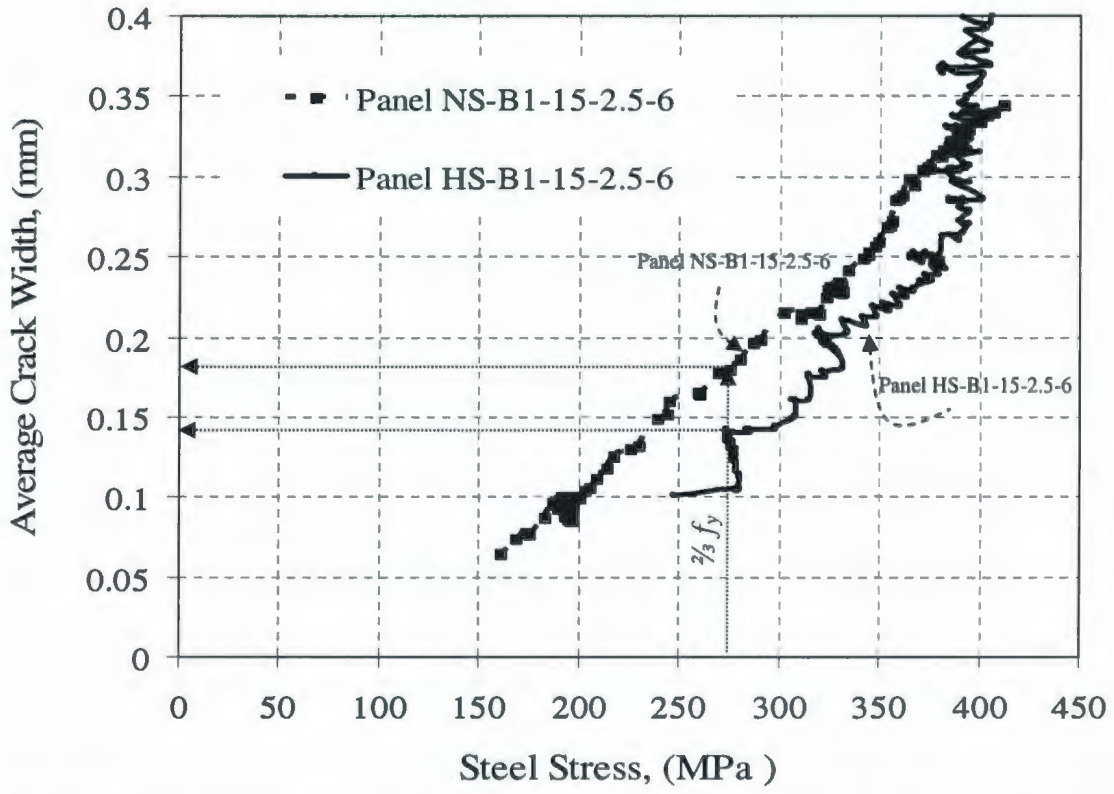

Fig. 4.25 Crack Width versus Steel Stress for Panels NS-B1-15-2.5-6, and HS-B1-15-2.5-6

4.5.2 Effect of the Reinforcement Ratio

The influence of changing the reinforcement ratio on the cracking response can be examined by comparing the experimental results of specimens HS-B1-15-2.5-6 (ρ=1.2%) and HS-B1-20-2.5-6 (ρ = 2%). In this series of tests, the layout of the bars was identical, but the diameter varied from 15 mm to 20 mm, where a constant reinforcing bar spacing of 150 mm was chosen, as shown in Table 3.1. It may be seen from Table 4.2 that there was no significant change in the measured value of the average crack spacing, due to the variation of the reinforcement ratio as the bar diameter was changed. Also, increasing the

reinforcement ratio by increasing the bar diameter has an insignificant influence on the average crack width of concrete, as shown in Fig. 4.26.

Meanwhile, the effect of the reinforcement ratio on the cracking response can be investigated by changing the bar spacing and using the same bar diameter. Table 4.2 presents the crack spacing for the specimens HS-U-20-2.5-6 (ρ = 2%) and HS-U-20-2.5-4 (ρ = 1.2%). In this series of test, the bar diameter of the reinforcement, and geometrical properties of the cross section were identical, but the spacing between the reinforcement was changed from 150 mm to 300 mm, as shown in Table 3.1.

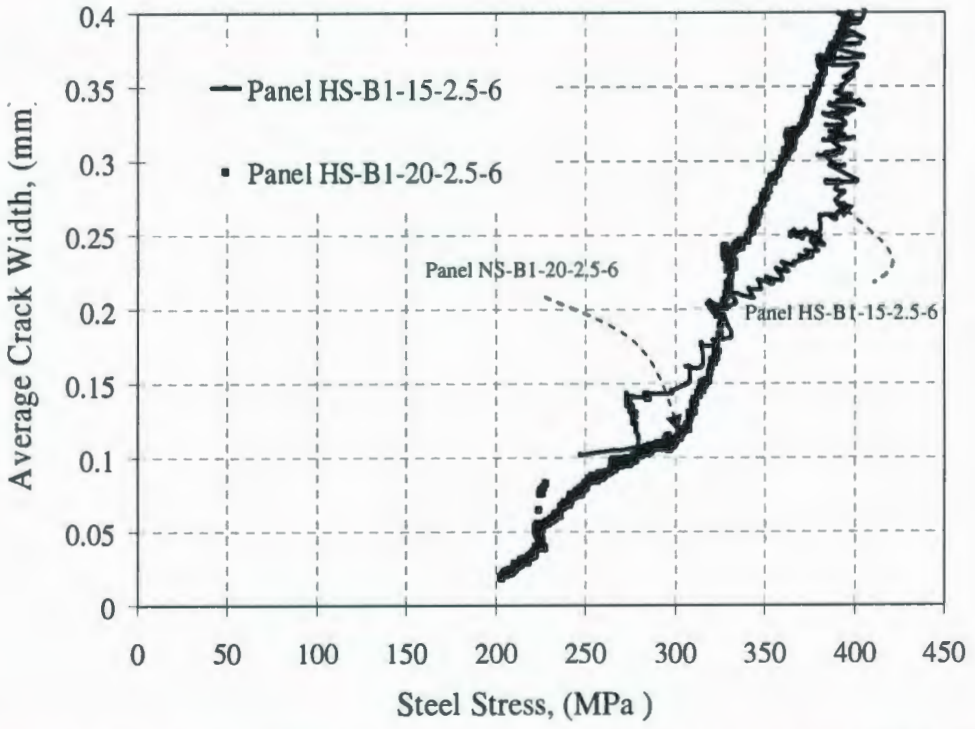

Fig. 4.26 Crack Width versus Steel Stress for Panels HS-B1-15-2.5-6, and HS-B1-20-2.5-6

The experimental data indicated that as the bar spacing increased by 50%, the crack spacing at the stabilized cracking stage also increased by 37% and 46% for the panels tested under uniaxial and biaxial loading, respectively, as shown in Fig. 4.27.

Table 4.2: Measured Average Crack Spacing and Crack Width at Service load

Specimen Serial	Specimen Number	C_c/d_b	Bar Spacing (mm)	d_t/ρ_{eff}, (cm)	Measured Average Crack spacing (mm)	Crack Width at service Load, $\frac{2}{3}f_y$, (mm)
1	NS-U-15-2.5-6	2.5	150	125	151	0.212
2	NS-B1-15-2.5-6	2.5	150	125	144	0.179
3	HS-U-15-2.5-6	2.5	150	125	152	-
4	HS-B1-15-2.5-6	2.5	150	125	151	0.145
5	HS-U-20-2.5-6	2.5	150	100	150	0.089
6	HS-B1-20-2.5-6	2.5	150	100	148	0.12
7	HS-U-20-2.5-4	2.5	300	166	240	0.17
8	HS-B1-20-2.5-4	2.5	300	166	275	0.215
9	HS-U-25-2.5-6	2.5	300	208	270	0.282
10	HS-B1-25-2.5-6	2.5	300	208	290	0.358
11	HS-U-25-1.5-6	1.5	300	208	240	0.233
12	HS-B1-25-1.5-6	1.5	300	208	285	0.306
13	HS-B2-25-2.5-6	2.5	300	208	290	0.354
14	HS-B3-25-2.5-6	2.5	300	208	295	0.317
15	HS-B4-25-2.5-6	2.5	300	208	300	0.308
16	HS-U*-25-2.5-6	2.5	300	208	295	0.321
17	HS-U-30-2.5-6	2.5	300	250	290	0.335
18	HS-B1-30-2.5-6	2.5	300	250	305	0.394
19	HS-U-30-1.5-6	1.5	300	250	230	0.26

Fig. 4.28 presents a comparison for the average crack width between panels HS-U-20-2.5-6, and HS-U-20-2.5-4. This figure illustrates the significant effect of the bar spacing on the values of the average crack width for the different level of steel stress, where the higher the bar spacing the higher the value of the average crack width.

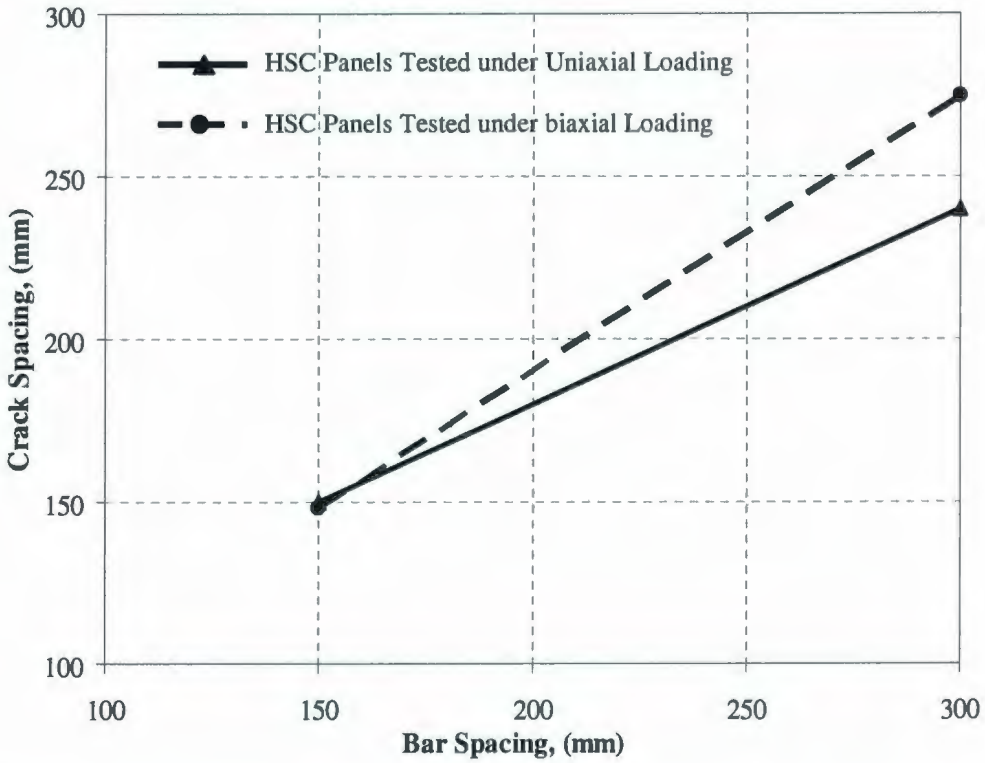

Fig. 4.27 Effect of the Bar spacing on the Average crack Spacing

Also, it confirms that the well distribution of reinforcement in the concrete section provides adequate control for primary crack width, considering the significant influence of the spacing between the reinforcement in the concrete section. At a steel stress equal to the stress in reinforcement at service load ($\frac{2}{3} f_y$) [78], the measured average crack width was found to be 0.17 mm, and 0.089 mm for panels HS-U-20-2.5-4 and HS-U-20-2.5-6, respectively. Increasing the bar spacing by 50%, the average crack width increased by 47% and 46% for the panels tested under uniaxial and biaxial loading, respectively, as presented in Table 4.2.

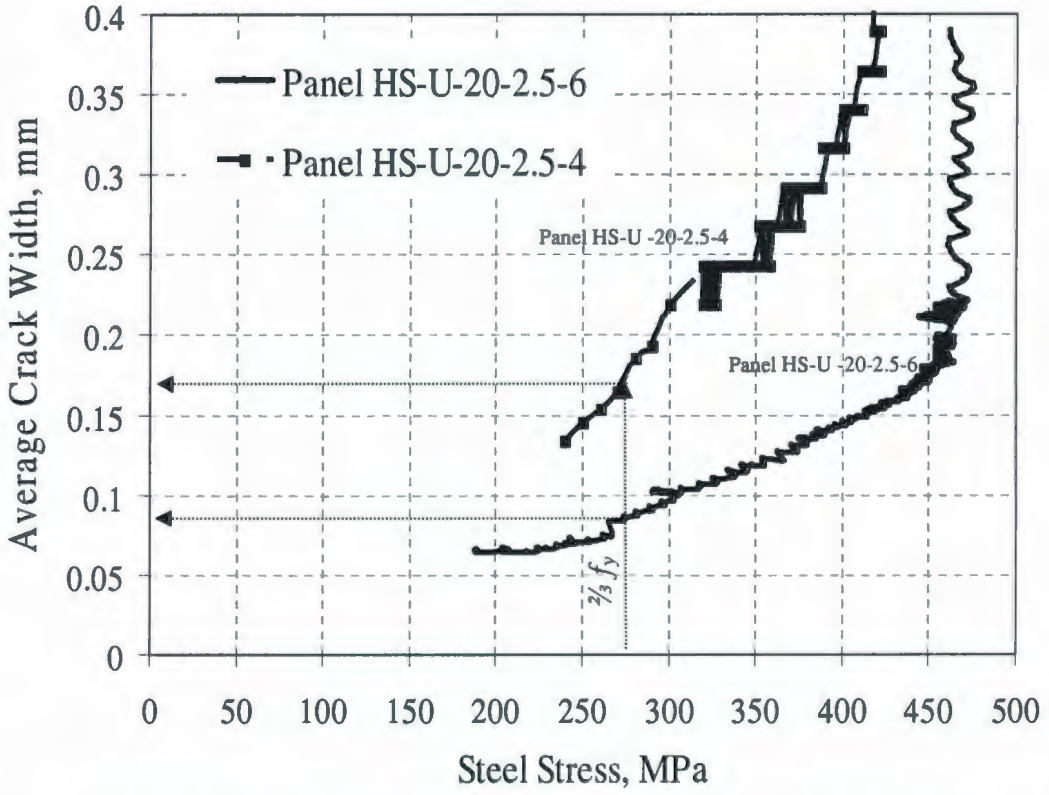

Fig. 4.28 Crack Width versus Steel Stress for Panels HS-U-20-2.5-6, and HS-U-20-2.5-4

4.5.3 Effect of the Concrete Cover Thickness

It has been realized that the most practical means of protecting the reinforcement of the offshore structures against corrosion, is by increasing the thickness of the concrete cover. Thus, one of the main goals of this experimental study is to investigate the effect of varying the concrete cover thickness on the cracking response of axially load HSC panels.

The test results for panels HS-U-25-1.5-6 (C_c/d_b= 1.5) and HS-U-25-2.5-6 (C_c/d_b=2.5) indicated that as the concrete cover thickness was increased from 37.5 mm to 62.5 mm, the crack spacing increased from 240 mm to 270 mm, respectively, where both panels

were tested under uniaxial loading. Also, for panels HS-B1-25-1.5-6 (C_c/d_b= 1.5) and HS-B1-25-2.5-6 (C_c/d_b=2.5) subjected to biaxial loading, the crack spacing increased from 285 mm to 290 mm, respectively. The experimental results showed that, the cracks occurrence was highly developed on the locations of the reinforcement in the perpendicular directions for panels subjected to biaxial loading compared with the panels tested under uniaxial loading state, see Fig. 4.29. This effect is mainly due to the effect of the splitting stresses in case of applying the load in biaxial directions.

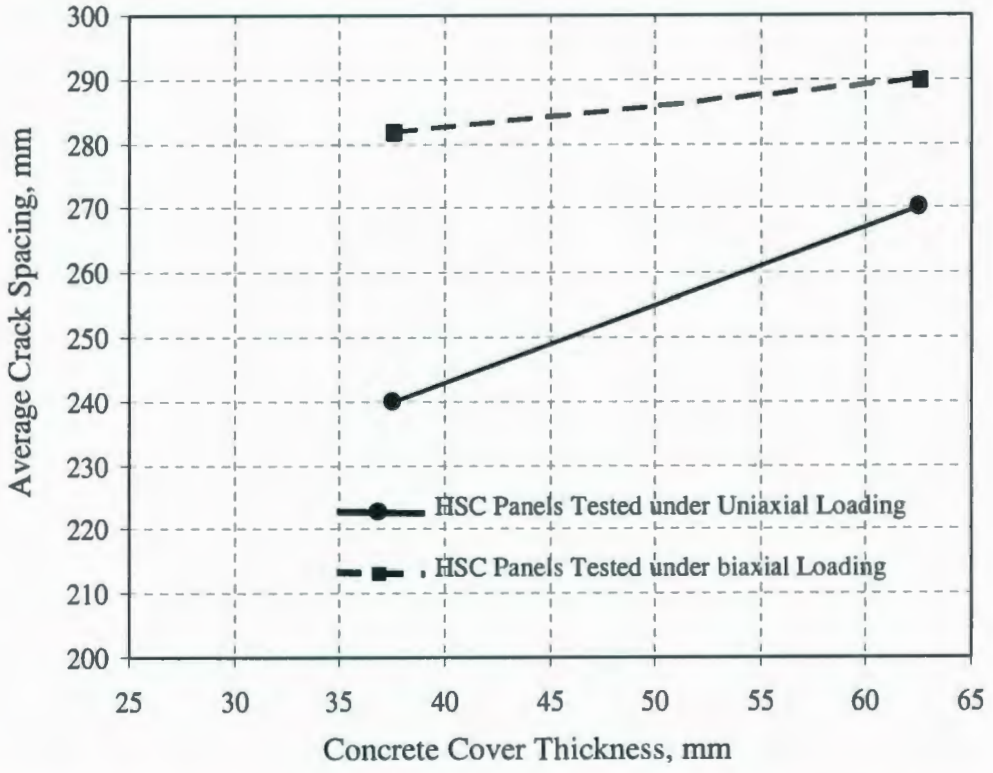

Fig. 4.29 Effect of the Concrete Cover Thickness on the Average crack Spacing

Fig. 4.30 plots the measured average crack width for various steel stress levels for panel (HS-U-25-2.5-6) with concrete cover equal to 62.5 mm, compared with panel (HS-U-25-1.5-6) with concrete cover equal to 37.5 mm. At service load ($\frac{2}{3} f_y$), the measured value

of the average crack width for panels HS-U-25-2.5-6 and HS-U-25-1.5-6 were 0.282 and 0.233 mm, respectively. Also, Fig. 4.31 represents the experimental results for the average crack width of panels HS-B1-25-2.5-6 (C_c = 62.5 mm), and HS-B1-25-1.5-6 (C_c = 37.5 mm), tested under biaxial loading. At service load ($\frac{2}{3} f_y$), the observed value of the average crack width for panels HS-B1-25-2.5-6 and HS-B1-25-1.5-6 were 0.358 and 0.306 mm, respectively. The test results indicated that as the concrete cover increased by 40%, the recorded value for the average crack width increases by 17% and 12% for panels subjected to uniaxial and biaxial loading, respectively.

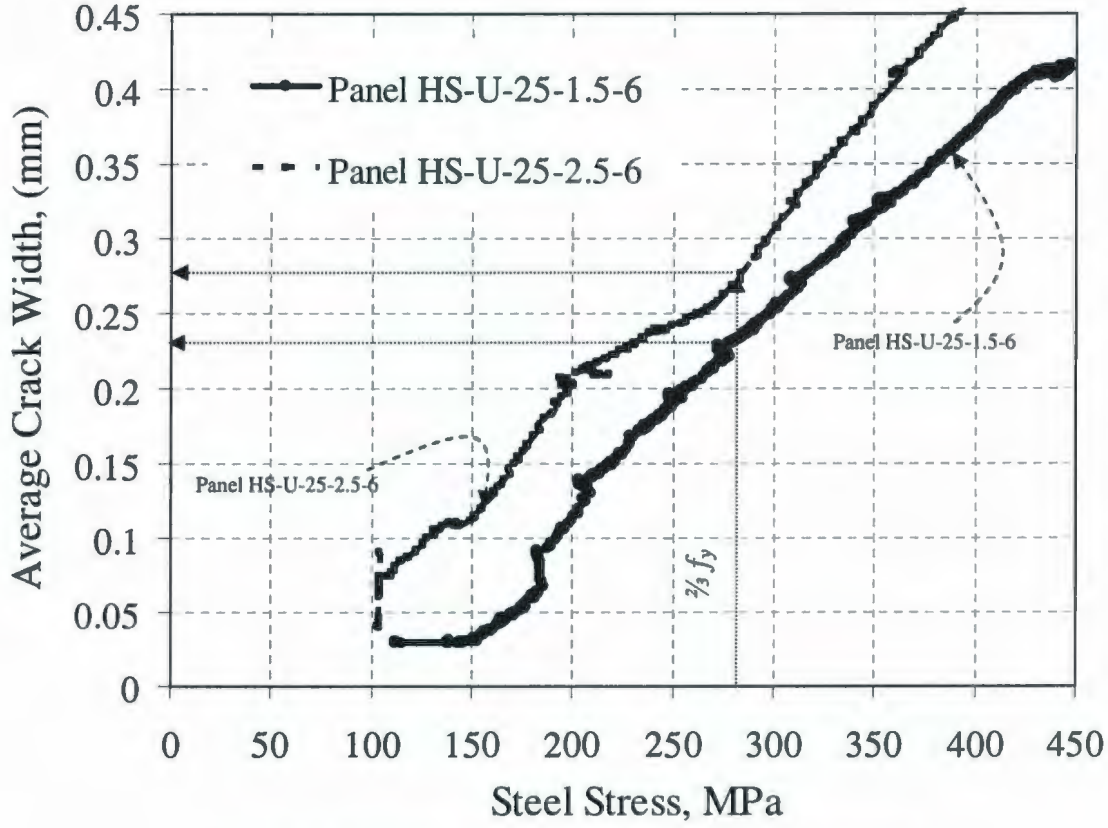

Fig. 4.30 Crack Width versus Steel Stress for Panels HS-U-25-2.5-6 and HS-U-25-1.5-6

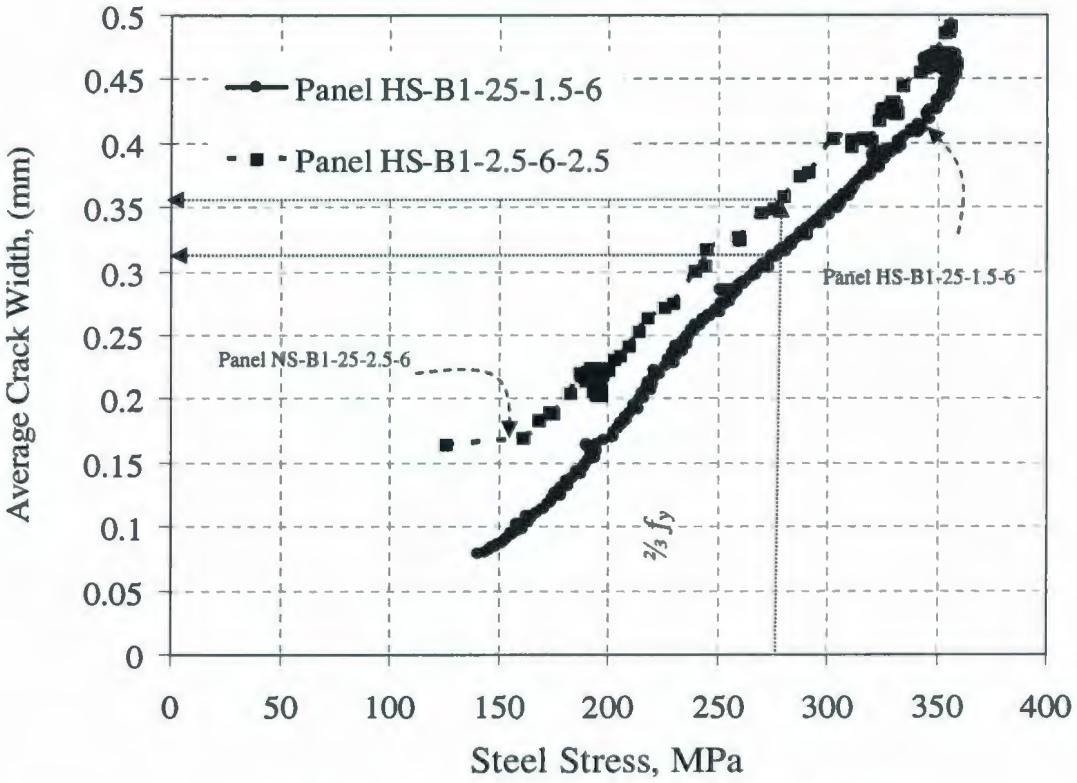

Fig. 4.31 Crack Width vs. Steel Stress for Panels HS-B1-25-2.5-6 and HS-B1-25-1.5-6

4.5.4 Effect of Biaxial Load Application

The experimental test results presented in this study can be used to provide a clear understanding for the cracking behavior of reinforced concrete structures subjected to biaxial tension.

Generally, panels subjected to biaxial tension loading showed higher values for the crack spacing compared with the corresponding panels tested under uniaxial tension load, as presented in Table 4.2. For panels tested under biaxial loading, most of the cracks propagated approximately along the location of the reinforcing bars in both directions. Thus, the measured values for the crack spacing were found to be very close to the spacing between the reinforcing bars in both directions. However, for the panels

subjected to uniaxial loading, the cracks propagated not only along the transverse bars location but also between these bars in case the spacing between the transverse bars was higher than the required distance to develop the tensile strength of the concrete, see Table 4.2.

The influence of applying the axial loading in biaxial direction on the crack width can be investigated by comparing the experimental results of panels HS-U-30-2.5-6 and HS-B1-30-2.5-6 tested under uniaxial and biaxial loading (1:1), respectively. There was a trend whereby the panel subjected to biaxial loading condition showed higher values for the average crack width for the different levels of the steel stress than that the panel tested under uniaxial loading, as shown in Fig. 4.32. This increase in the average value of the crack width thanks to the higher value of the measured average crack spacing for the panels tested under biaxial loading condition compared with the corresponding panels subjected to uniaxial loading condition. At service load ($\frac{2}{3} f_y$), the measured values of the average crack width for panels HS-U-30-2.5-6 and HS-B1-30-2.5-6 were 0.335 and 0.394 mm, respectively. Thus, the average crack width increased by 14 % due to applying the load into biaxial direction (1:1).

4.5.5 Effect Biaxial Loading Ratio (P_1/P_2) on the Cracking Response

The test results can be used to identify the cracking behavior of reinforced concrete structures subjected to biaxial tension, such as containment walls of nuclear power plants when subjected to monotonic biaxial tension. To simulate the actual behavior of the offshore and nuclear power structures, the biaxial load was applied using various ratios

such as 1:1, 1:2, 1:3, and 1:4 in the perpendicular directions, as this research ultimately aims to investigate the cracking behavior of concrete panels modeled on nuclear power plant containment walls when subjected to monotonic biaxial tension.

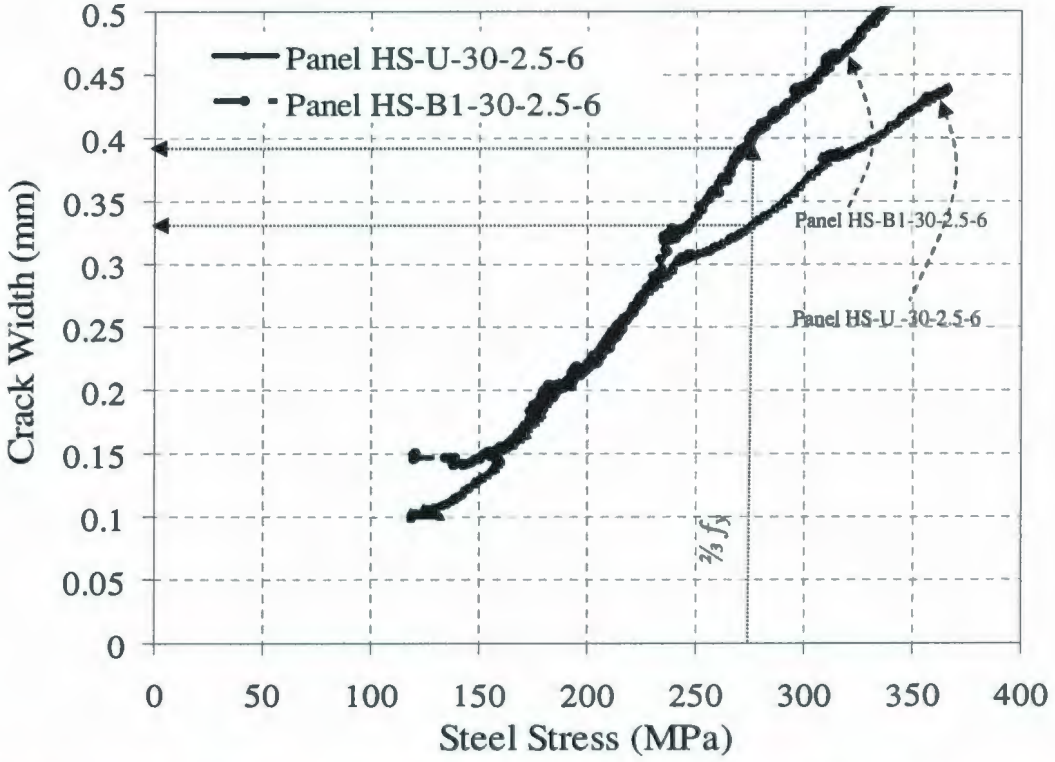

Fig. 4.32 Crack Width vs. Steel Stress for Panels HS-U-30-2.5-6, and HS-B1-30-2.5-6

These panels subjected to biaxial loading with different ratios showed approximately similar average crack spacing as the cracks extended over the locations of the reinforcing bars in the perpendicular direction.

Fig. 4.33 shows a comparison of the average crack width for panels HS-U-25-2.5-6, HS-B1-25-2.5-6, HS-B2-25-2.5-6, HS-B3-25-2.5-6, and HS-B4-25-2.5-6, at different levels of steel stress. There was a general tendency that measured average crack width increased as the loading ratio changed from 1:4 to 1:1. At the service load level (⅔ f_y), the

measured average crack width was found to be 0.282, 0.358, 0.354, 0.317, and 0.308 for panels HS-U-25-2.5-6, HS-B1-25-2.5-6, HS-B2-25-2.5-6, HS-B3-25-2.5-6, HS-B4-25-2.5-6, respectively, as shown in Fig. 4.33.

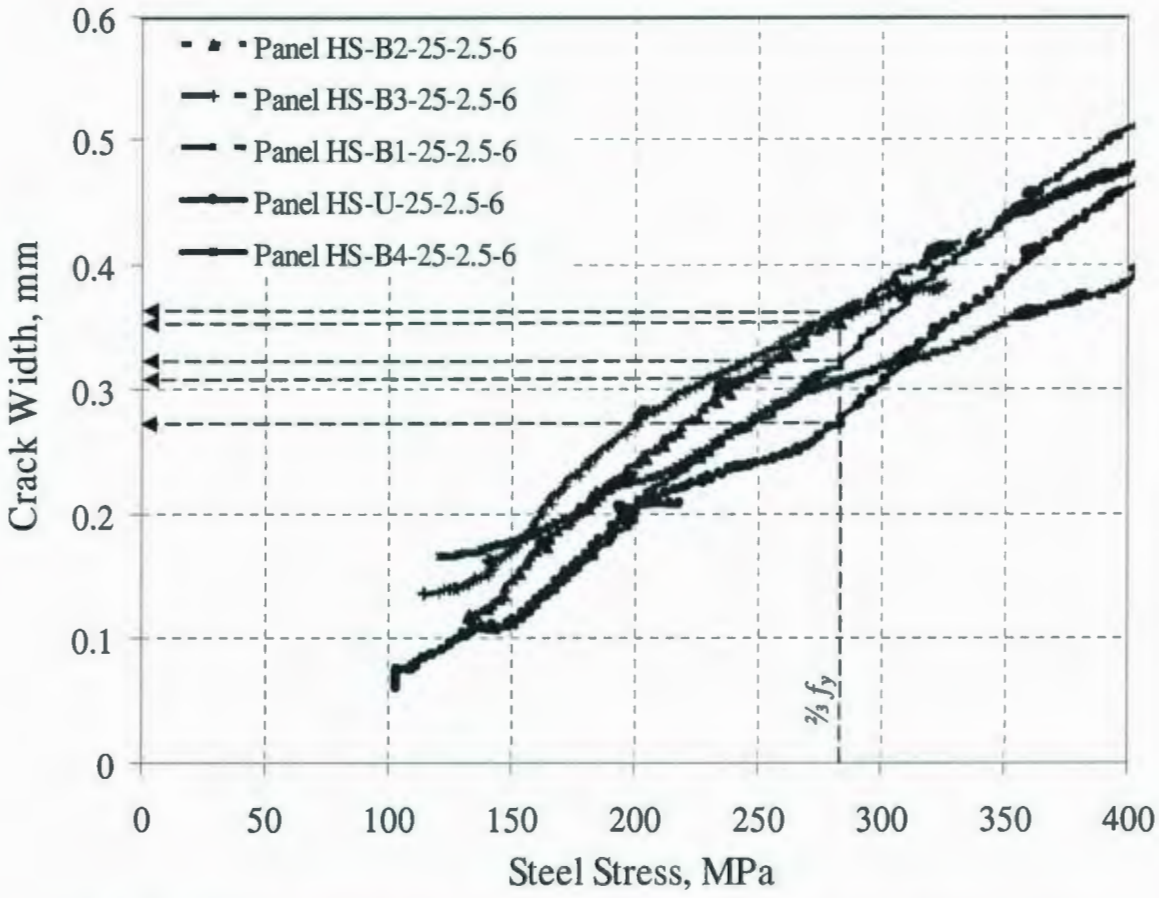

Fig. 4.33 Average Stress-Strain Curves for Panels Subjected to Different Loading Ratio in the Orthogonal Direction

4.6 Summary

An experimental investigation was carried out to study the cracking behavior of reinforced concrete panels with different concrete strengths subjected to pure tension (uniaxial or biaxial loading). The pre- and post-tensile behavior of the concrete panels is

discussed. The best fit to the test results is developed for pre- and post-cracking stress-strain behavior of HSC panels. Influences of the main parameters that affect cracking behavior and the tension stiffening response of the reinforced concrete panels are investigated, such as the compressive strength, reinforcement ratio, concrete cover thickness, and applying the load in biaxial directions.

Compared with NSC panels, HSC panels show lower strains and greater tension stiffening effects at a given load level thanks to the corresponding improvement of the bond between the reinforcing steel bars and the high strength concrete matrix. The concrete tension stiffening contribution between cracks decays at higher rate with increasing the bar spacing, for various loading stages. This effect is more obvious in case of applying the axial load into biaxial direction.

HSC concrete panels tested under biaxial loading show lower tension stiffening contribution of concrete for different steel stress levels in comparison to the identical panels subjected to axial loading. Applying the load in the biaxial direction reduces the tensile strength capacity of the concrete section. This reduction ranges between 5%-15%. The increase in concrete cover to the main reinforcement leads to higher tension stiffening response for different level of the steel stress, the main reason for the reduction in the tension stiffening repose in case of panels with smaller concrete cover is the development of the splitting cracks.

Chapter 5

Concrete and Steel Stresses and Bond Characteristics

5.1 Introduction

The transfer of forces across the interface between concrete and steel reinforcing bars is of fundamental importance to investigate the cracking behavior of reinforced concrete structures. Bond stress is the equivalent unit shear stress acting parallel to the reinforcing bars on the interface between the bars and concrete. Due to the transfer of forces through bond stress between the concrete and the reinforcing bars, the stress in the reinforcing bars changes along its length to satisfy the equilibrium between the reinforcing bars and the concrete.

In this chapter, an analytical model is developed for predicting the complete distribution of the slip, bond stress, and concrete and steel stresses at different loading stages. This analytical model is derived based on the relationship between the local bond stress and the second derivative of the slip between the steel bar and the concrete section. The boundary conditions controlling the cracking behavior of the reinforced concrete members are considered, to ensure an accurate prediction for the response of the member under the applied load. Moreover, the analytical derivation considers the influence of the main factors that affect the cracking behavior such as the tensile strength of concrete, bond characteristics, and reinforcement ratio.

To validate the proposed model, a series of verification tests is performed to measure the reliability of this model. The analytical predictions are compared to the results of various experimental investigations conducted on different reinforced concrete members.

5.2 Analytical Procedure

A reinforced concrete member is subjected to axial tension is shown in Fig. 5.1, the applied load P is carried partly by the concrete section P_{cx}, and partly by reinforcing steel P_{sx} at any section located at distance x from the crack face. Considering the equilibrium of the horizontal forces, the total load can be expressed as following:

$$P = P_{cx} + P_{sx} \tag{5.1}$$

Assuming that both concrete and steel behave elastically:

$$P = A_c E_c (\varepsilon_{cx} + n\rho \varepsilon_{sx}) \tag{5.2}$$

where A_c, E_c, *and* ε_{cx} are the concrete cross sectional area; concrete modulus of elasticity; and concrete strain, respectively; ε_{sx} is the steel strain; ρ is the reinforcement ratio A_s/A_c; and n is the modular ratio that represents the ratio of the modulus of elasticity of the steel reinforcement E_s to the modulus of elasticity of concrete E_c.

P_{cx} is zero at the cracked face and maximum at a distance of L_t that represents the transfer length. The transfer length is the embedded length required to satisfy the following condition, at $x = L_t$ the strains in steel and concrete are equal ($\varepsilon_{sx} = \varepsilon_{cx}$), as illustrated in Fig 5.1.

The local slip w_{sx} between the reinforcement and the concrete section is an accumulation of the strain differences between the reinforcement and the concrete within the transfer

length. Thus, the local slip can be defined as the total difference in elongations between the reinforcement and the concrete measured over the length x and the center of the segment [24],

$$w_{sx} = \int_{x}^{s_b/2} (\varepsilon_{sx} - \varepsilon_{cx}) dx \tag{5.3}$$

where, S_b is the segment length that represents the crack spacing between two consecutive cracks.

$$\frac{dw_{sx}}{dx} = -(\varepsilon_{sx} - \varepsilon_{cx}) \tag{5.4}$$

Eq. (5.2) can be retransformed as:

$$\varepsilon_{cx} = \frac{P}{A_c E_c} - n \varepsilon_{sx} \rho \tag{5.5}$$

Substituting the value of ε_{cx} in Eq. (5.5) into Eq. (5.4):

$$\frac{dw_{sx}}{dx} = -(\varepsilon_{sx} - \frac{P}{A_c E_c} + n \varepsilon_{sx} \rho) \tag{5.6}$$

$$\frac{dw_{sx}}{dx} = \frac{P}{A_c E_c} - \varepsilon_{sx} (1 + n\rho) \tag{5.7}$$

$$n\rho = \frac{E_s A_s}{E_c A_c}, E_c A_c = E_s A_s / n\rho \tag{5.8}$$

Substituting Eq. (5.8) into Eq. (5.7)

$$\frac{dw_{sx}}{dx} = \frac{n\rho \sigma_s}{E_s} - \varepsilon_{sx} (1 + n\rho) = n\rho \varepsilon_s - \varepsilon_{sx} (1 + n\rho) \tag{5.9}$$

where ε_s is the steel strain at crack location ($\varepsilon_s = P/A_s E_s$)

$$\frac{d^2 w_{sx}}{dx^2} = -(1+n\rho)\frac{d\varepsilon_{sx}}{dx} \tag{5.10}$$

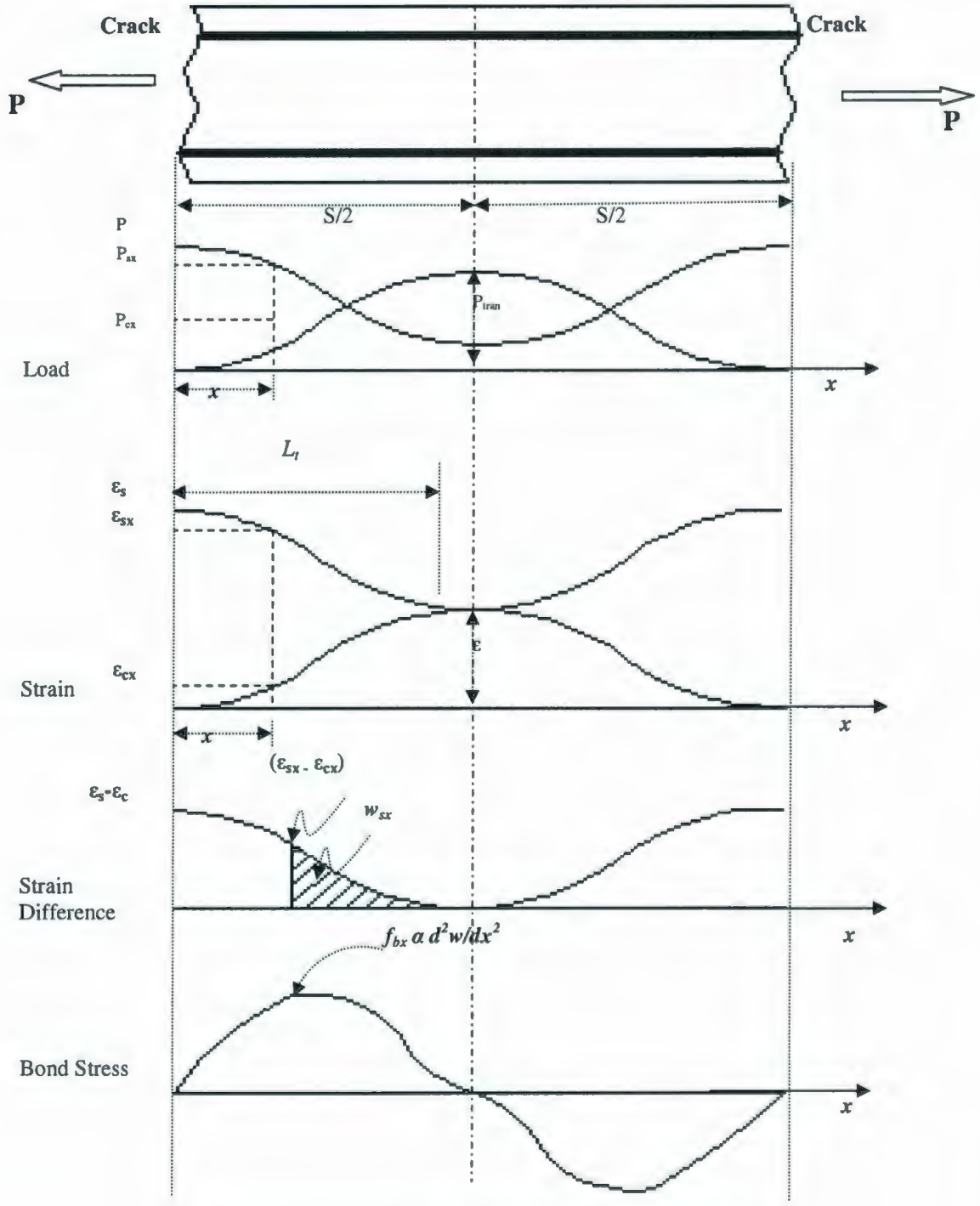

Fig. 2 Loads, Strain, Slip, and Bond Stress Distribution

The local bond stress f_{bx} can be defined by considering the equilibrium of the free body diagram in Fig. 5.2:

$$P_s + f_{bx}\,\Sigma o\,dx = P_s + dP_s,$$

$$f_{bx} = -\frac{dP_{sx}/dx}{\Sigma o} = -\frac{A_s E_s}{\Sigma o}\frac{d\varepsilon_{sx}}{dx} \tag{5.11}$$

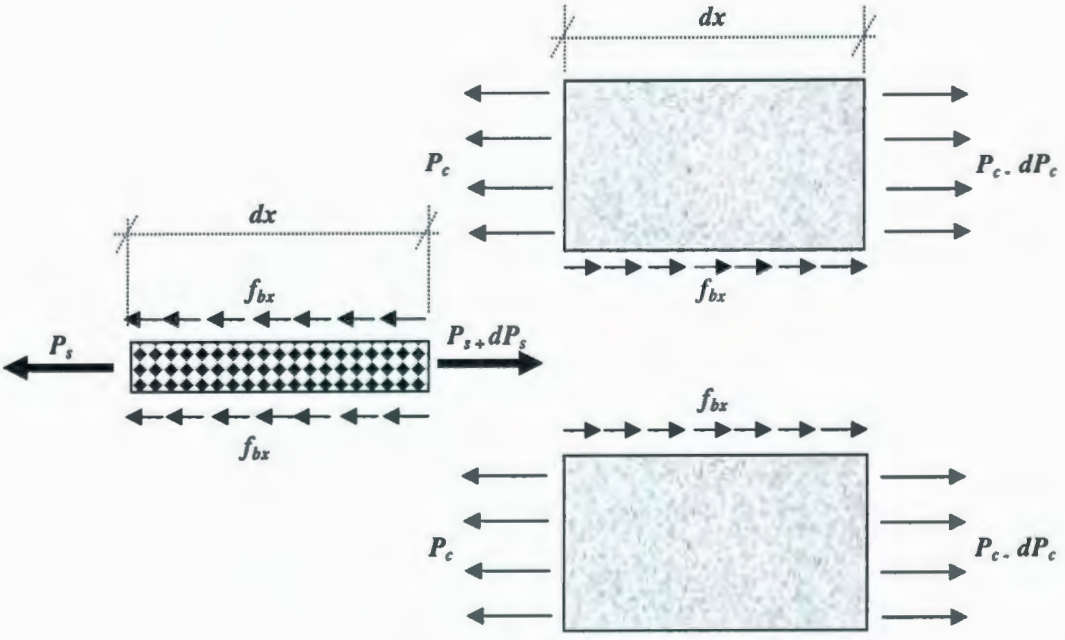

Fig. 5.2 Free body Diagram for the Load Transfer from Steel to Concrete

where Σo is the surface area per unit length of the reinforcement

$$\frac{d\varepsilon_{sx}}{dx} = \frac{f_{bx}\,\Sigma o}{A_s E_s} \tag{5.12}$$

Substituting Eq. (5.12) into Eq. (5.10),

$$\frac{d^2 w_{sx}}{dx^2} = -\,(1+n\rho)\frac{f_{bx}\,\Sigma o}{A_s E_s}$$

$$\frac{d^2 w_{sx}}{dx^2} - (1+n\rho)\frac{\Sigma o}{A_s E_s} f_{bx} = 0 \qquad (5.13)$$

This differential equation represents the basic relationship between the second derivative of the local slip w_{sx}, and the local bond stress f_{bx}, where this differential equation of basic importance for slips and bond between the concrete and the reinforcing bars. Bond behavior is a key aspect of the cracking behavior of reinforced concrete since it controls the ability of the reinforcement to transfer tensile stresses to concrete.

The proposed analytical model presented in this study based on the mathematical solution for the differential equation that relates the bond stress to the second derivative of the slip between the concrete and steel bars, presented in Eq. (5.13). This solution for the differential equation must satisfy the known values of the parameters at the cracked section and the center of the segment location. The second derivative of slip changes proportionally with the bond stress distribution along different sections from the crack face as proved in Eq. (5.13), and as shown in Fig. 5.1.

To solve the differential equation that expresses the relationship between the bond stress and the second derivate of the slip in Eq. (5.13), polynomial equation from the third degree, that reflects a precise distribution for the second derivative of the slip (bond stress distribution) between the successive cracks, is proposed in solving the differential equation. This solution considers the boundary conditions that control the cracking behavior, as well as the bond characteristics between the reinforcing bars and the concrete, as detailed in the following derivation:

$$\frac{d^2 w_s}{dx^2} = A_1 + A_2 X + A_3 X^2 + A_4 X^3 \qquad (5.14)$$

$$\frac{dw_s}{dx} = A_1 X + \frac{A_2}{2} X^2 + \frac{A_3}{3} X^3 + \frac{A_4}{4} X^4 + C_1 \tag{5.15}$$

$$w_x = \frac{A_1}{2} X^2 + \frac{A_2}{6} X^3 + \frac{A_3}{12} X^4 + \frac{A_4}{20} X^5 + C_1 X + C_2 \tag{5.16}$$

$$\frac{d^3 w_s}{dx^3} = A_2 + 2A_3 X + 3A_4 X^2 \tag{5.17}$$

In the proposed solution for the differential equation, there are six constants (A_1, A_2, A_3, A_4, C_1, and C_2) to be determined by considering the boundary conditions that satisfy the known values of the parameters at the cracked section and at the center of the segments. The boundary conditions are of fundamental importance in prediction of cracking behavior of reinforced concrete structures, as illustrated in Fig. 5.1, and are given as follows:

1- At $x = S/2$, the value of the slip $w_x = 0$. At the mid distance between two consecutive cracks, the slip should equal to zero because of the symmetry and the compatibility condition between the steel reinforcement and the concrete material ($\varepsilon_c = \varepsilon_s$). Thus, Eq. (5.16) can be retransformed as follows:

$$0 = \frac{A_1}{8} S^2 + \frac{A_2}{48} S^3 + \frac{A_3}{192} S^3 + \frac{A_4}{640} S^5 + C_1 S + C_2 \tag{5.18}$$

2- At $x = zero$ the value of $dw_x/dx = -\varepsilon_s$. At the crack location, the value of $\varepsilon_{cx} = 0$, and the first derivative for the slip is equal to the steel strain ($dw_x/dx = -\varepsilon_s$), see Eq. (5.4). Substituting this value for the first derivative of the slip into Eq. (5.15), leads to:

$$-\varepsilon_s = C_1 \tag{5.19}$$

3- At $x = L_t$, the value of $dw_x/dx = 0$, where the compatibility between steel and concrete is attained ($\varepsilon_{sx} = \varepsilon_{cx}$) at the transfer length L_t section. Thus, the first derivative for the local slip at that section will equal to zero, consequently, Eq. (5.15) can be expressed as:

$$0 = A_1 L_t + \frac{A_2}{2} L_t^2 + \frac{A_3}{3} L_t^3 + \frac{A_4}{4} L_t^4 + C_1 \tag{5.20}$$

4- At x = 0, the value of $d^2w_x/dx^2 = 0$, where the bond stress is zero at the crack face. Eq. (5.13) shows a proportional relationship between the bond stresses f_{bx} and the second derivative for the local slip between the steel reinforcement and concrete, see Fig. 5.1, substituting by the above relationship into Eq.(5.14):

$$0 = A_1 \tag{5.21}$$

5- At x = S/2, the value of $d^2w_x/dx^2 = 0$. Based on the experimental work results, it is observed that the bond stresses are zero at center of the segment. As a result, the second derivative of the local slip at this section is equal to zero, as it changes proportionally with the bond stress, and Eq. (5.14) can be rewritten as follows:

$$0 = A_1 + \frac{A_2}{2} S + \frac{A_3}{4} S^2 + \frac{A_4}{8} S^5 \tag{5.22}$$

Based on the experimental results, the peak bond stress occurs at a distance Z = (0.15-0.25)L_t from the crack face (Yang and Chen, 1988) [29], where the test results showed that the peak bond stress occurs at the section closer to the crack face than to the other end of the transfer length L_t.

6- At x = Z, the value of $d^3w_x/dx^3 = 0$. Substituting by the value of Z into Eq. (5.17) leads to:

$$0 = A_2 + 2A_3 Z + 3A_4 Z^2 \tag{5.23}$$

By solving Eqs. (5.18) through (5.23) simultaneously, the value of the six constants (A_1, A_2, A_3, A_4, C_1, and C_2) can be obtained based on the six boundary conditions mentioned earlier as follows:

$$\begin{bmatrix} \frac{S^2}{8} & \frac{S^3}{48} & \frac{S^4}{192} & \frac{S^5}{640} & \frac{S}{2} & 1 \\ 0 & 0 & 0 & 0 & 1 & 0 \\ L_t & \frac{L_t^2}{2} & \frac{L_t^3}{3} & \frac{L_t^4}{4} & 1 & 0 \\ 1 & 0 & 0 & 0 & 0 & 0 \\ 1 & \frac{S}{2} & \frac{S^2}{4} & \frac{S^3}{8} & 0 & 0 \\ 0 & 1 & 2Z & 3Z^2 & 0 & 0 \end{bmatrix} \begin{bmatrix} A_1 \\ A_2 \\ A_3 \\ A_4 \\ C_1 \\ C_2 \end{bmatrix} = \begin{bmatrix} 0 \\ -\varepsilon_s \\ 0 \\ 0 \\ 0 \\ 0 \end{bmatrix} \tag{5.24}$$

$$[C]_{6X6}\,[A]_{6X1} = [V]_{6X1}$$

$$[A]_{6X1} = [C]^{-1}_{6X6}\,[V]_{6X1} \tag{5.25}$$

where Z is the distance from crack at which the bond stress reaches the maximum value, S is the spacing between the sucssive cracks.

Solving the previous Eq. (5.25), the value of the constants can be evaluated as following:

$$A_1 = Zero \tag{5.26}$$

$$A_2 = -\varepsilon_s \frac{12(S-3Z)ZS}{L_t^2(-6S^2Z + 2L_tS^2 + 18Z^2S - 3SL_t^2 - 24Z^2L_t + 12ZL_t^2)} \tag{5.27}$$

$$A_3 = \varepsilon_s \frac{6(S^2-12Z^2)}{L_t^2(-6S^2Z + 2L_tS^2 + 18Z^2S - 3SL_t^2 - 24Z^2L_t + 12ZL_t^2)} \tag{5.28}$$

$$A_4 = -\varepsilon_s \frac{12(S-4Z)}{L_t^2(-6S^2Z + 2L_tS^2 + 18Z^2S - 3SL_t^2 - 24Z^2L_t + 12ZL_t^2)} \tag{5.29}$$

$$C_1 = -\varepsilon_s \tag{5.30}$$

$$C_2 = -\varepsilon_s \frac{S(S^5 - 14S^4Z + 30Z^2S^3 - 80L_t^3S^2 + 240S^2ZL_t^2 + 120L_t^4S - 720SZL_t^2 + 960Z^2L_t^3 - 480ZL_t^4)}{L_t^2(-6S^2Z + 2L_tS^2 + 18Z^2S - 3SL_t^2 - 24Z^2L_t + 12ZL_t^2)} \quad (5.31)$$

From the solution of the previous differential equation Eq. (5.13), the six constants (A_1, A_2, A_3, A_4, C_1, and C_2) depend on four parameters, which are the length of the segments (the crack spacing S), the transfer length L_t, the location of the peak bond stress from the crack face Z, and the steel strain at the crack location ε_s.

The above model was proposed by Somayaji and Shah, 1981 [24] to predict the cracking response of a reinforced concrete member. That model assumed that the peak bond stress moves to the center of the transfer length L_t, neglecting the actual distribution of bond stress, where, the test results proved that the local peak bond stress occurs at section closer to the crack face than the other end of the transfer length (ACI Committee 408) [85].

5.3 The Transfer Length (L_t)

Transfer length L_t is defined as the embedded bonded length required to develop the condition that the strain in steel equal to the concrete strain (at $x = L_t$, $\varepsilon_{cx} = \varepsilon_{sx}$). Accurate estimation for the transfer length is crucial to represent the cracking behavior of reinforced concrete. Cracks occur whenever the principal tensile stress due to the applied load exceeds the tensile strength of concrete. At the initial crack formation stage, a portion of the element between cracks exists over which steel and concrete strains are equal, and slips are not produced. The crack pattern is developed fully if all the crack spacing varies between L_t and $2L_t$ as shown in Fig. 5.3, this phase referred to as stabilized

crack formation. The steel stress reaches its minimum where the slip is zero and the bond stress changes its sign. This point is approximately half way between the cracks.

Based on CEB-FIP 1990 (MC-90) [44], this value for the transfer length L_t is given by the following equations:

$$L_t = \frac{d_b}{3.6\rho_r}, \text{ for stabilized cracking} \tag{5.32}$$

$$L_t = \frac{\sigma_{s2}\, d_b}{2\tau_{bk}\,(1+n\rho_r)}, \text{ for Single crack deformation} \tag{5.33}$$

where, d_b = bar diameter (mm), σ_{s2} = Steel stress at the crack, τ_{bk} = Bond stress, $n = E_s/Ec$, and ρ_r is the steel reinforcement ratio and it is defined as ($\rho_r = A_s/A_{cef}$) and A_{cef} is the effective tension area around the steel reinforcement as shown in the Fig. 5.4.

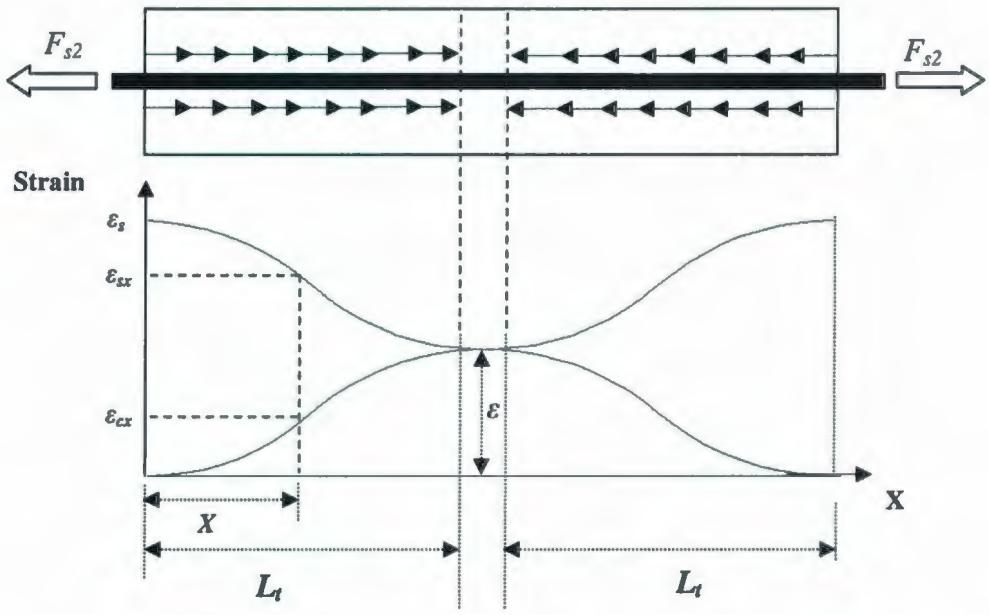

Fig. 5.3 Steel and Concrete Strain Distribution between the Consecutive Cracks

Obviously, the value of the transfer length is dependent on the geometrical conditions of the segments, such as the ratio of rigidity of the reinforcement to that of the concrete, the

reinforcement ratio, the average value of the bond stress, and the diameter of the reinforcement.

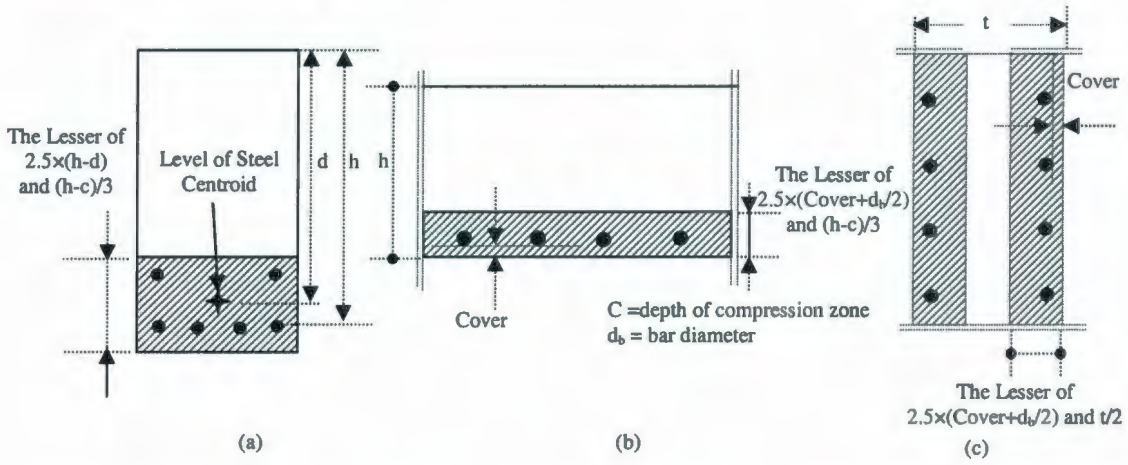

Fig. 5.4 Effective Area, A_{ceff} (a) Beam; (b) Slab; (c) Member in Tension (MC-90 and EC-91)

5.4 Comparison with Experimental Results

A series of verification tests, involving various types of structural elements and loading conditions, is conducted to measure the reliability of the model. The selection of the test series is based on that the test must allow the verification of the model in various loading conditions. Evaluating the constants (A_1, A_2, A_3, A_4, C_1, and C_2) using Eqs. (5.26) through (5.31), enables predicting the bond characteristics and cracking behavior of reinforced concrete member subjected to tension stresses at any loading stage using the above analytical model. The comparisons between the measured experimental data and the predicted analytical results are presented in terms of bond stress and slip distribution, steel and concrete stress distribution.

5.4.1 Bond and the Slip Distribution between the Consecutive Cracks

Tests on various tension members were conducted by Yang and Chen, 1988 [29], to determine the distributions of the slip between the reinforcing steel and the concrete. The distribution of the slip between the steel bars and concrete matrix at any section between the successive cracks can be evaluated using the proposed model in Eq. (5.16). Figs 5.5(a, b) show the predicted slip distribution along different sections of axially loaded member according to Eq. (5.16), compared with the experimental test results [29], as well as the results from previous analytical model proposed by Yang and Chen, 1988 [29]. The results of proposed analytical model shown in Figs. 5.5 (a, b) provide a satisfactory agreement between the predicted response as compared with the measured experimental results. Also, Figs. 5.5 (a, b) confirm that, the slip between the steel bar and the concrete matrix reaches its maximum value at the crack location.

Moreover, the test results conducted on specimens at the institute of metallurgy-Architecture of China [87] are used as further verification for the proposed model. Figs. 5.6 (a, b, c) show the calculated values of the local slip at different levels of steel stress based on the previous analytical models proposed by Somayaji and Shah, 1981 [24], and Yang and Chen, 1988 [29]. The value of local slip at the crack face can be estimated theoretically by substituting with $x = 0$ into the proposed Eq. (5.16).

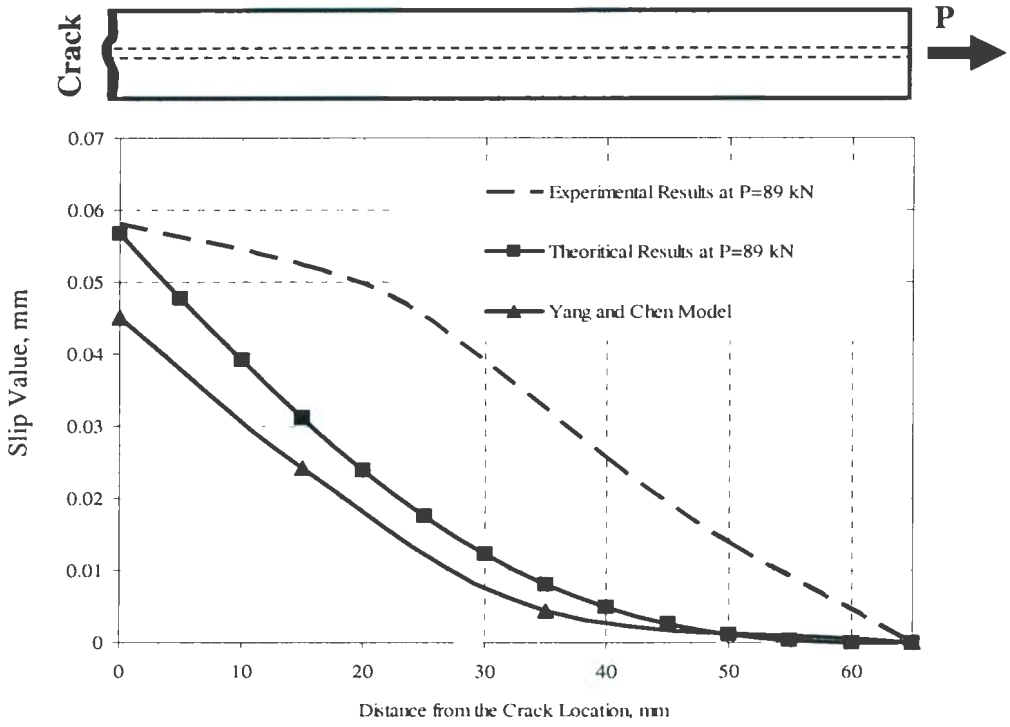

(a) Specimen A_3 [86]

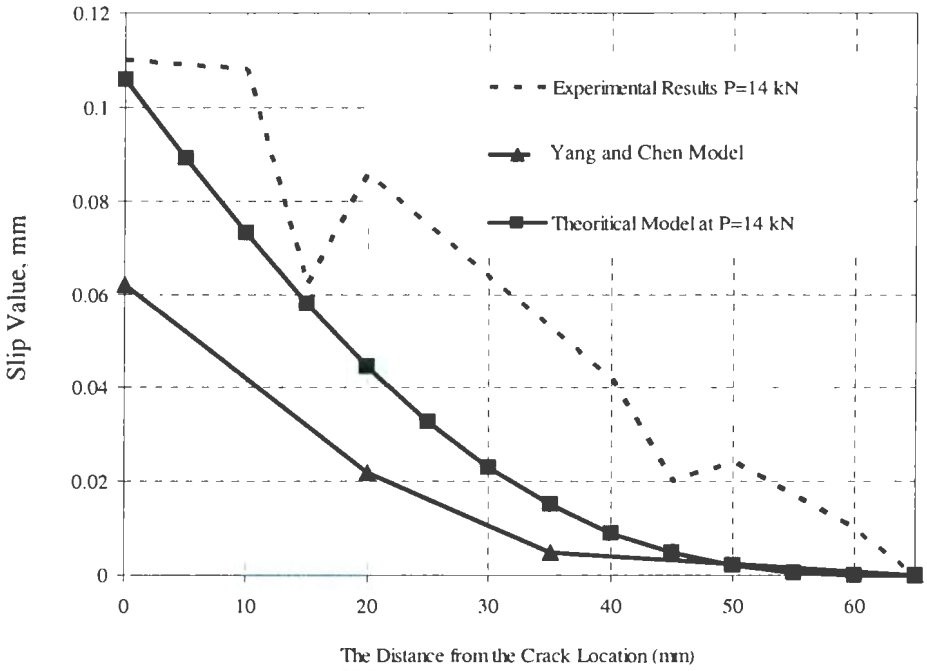

(b) Specimen A_4 [86]

Fig. 5.5 Comparison of Theoretical Model and Experimental Values of Slip [86]

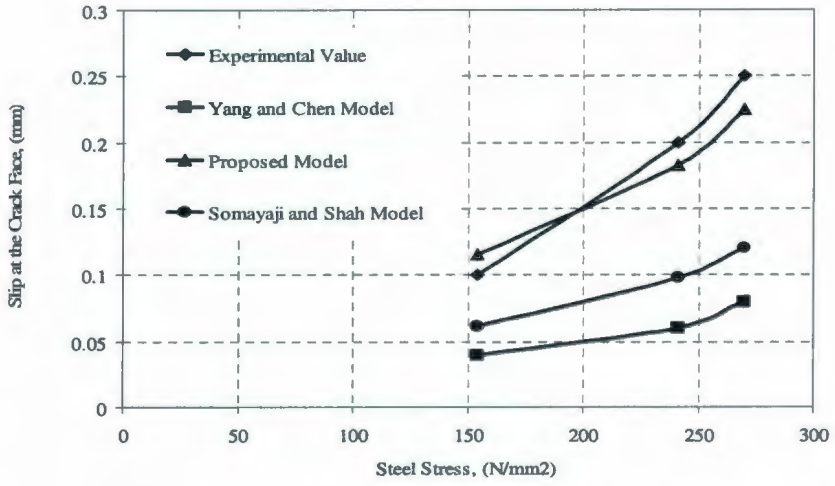

(a) Specimen No. 1 [87]

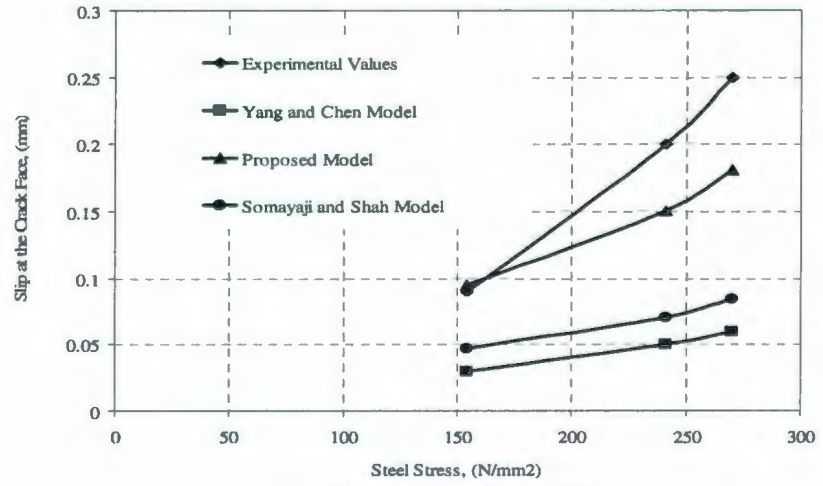

(b) Specimen No. 2 [87]

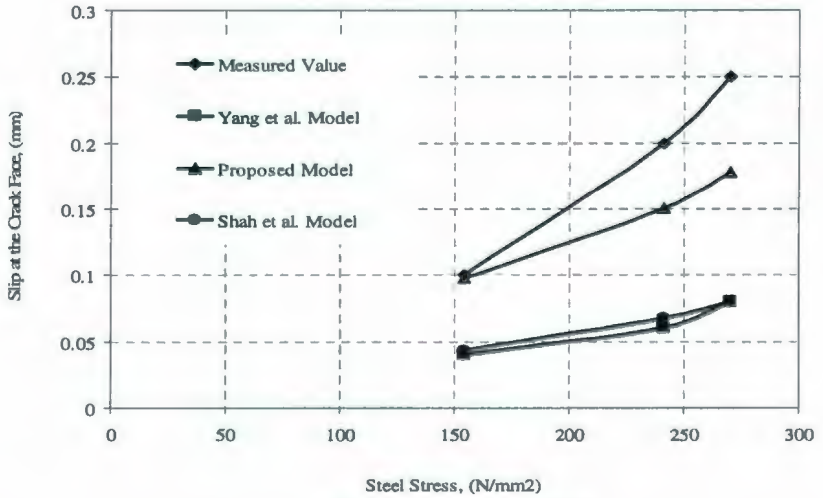

(c) Specimen No. 3 [87]

Fig. 5.6 Theoretical and Experimental Local Slip at the Crack Face [87]

The model can be utilized to predict the manner in which the bond stress is distributed along the length of the member. Eq. (5.13) shows a proportional relationship between the bond stress f_{bx}, and second derivative of the slip d^2w_x/dx^2. Thus, the relationship between the bond stress and the second derivative of the slip can be expressed as:

$$\frac{d^2 w_s}{dx^2} = (1+n\rho)\frac{\Sigma o}{A_s E_s} f_{bx} = \beta f_{bx} \tag{5.34}$$

where β is a constant coefficient depends on the material and geometrical properties of the steel bars ($\beta = [(1 + n\rho)\Sigma o/A_sE_s]$). Substituting by the equation of the second derivative of the slip Eq. (5.14) into Eq. (5.34), the local bond stress distribution at different sections along the members' length can be predicated as presented in the following equation:

$$f_{bx} = \frac{1}{\beta}\frac{d^2 w_s}{dx^2} = \frac{1}{\beta}(A_1 + A_2 X + A_3 X^2 + A_4 X^3) \tag{5.35}$$

Therefore, the bond stress distribution can be determined between the consecutive cracks using Eq. (5.35). Fig. 5.7 shows a comparison between the results of the local bond stress distribution based on the derived Eq. (5.35), and the experimental work results for specimen A_4 conducted by Jiang et al., 1984 [25] at two different loading stages. From the experimental results and the analytical model, it is observed that the local peak bond stress occurs at a section situated closer to the crack face than the other end of the transfer length L_t.

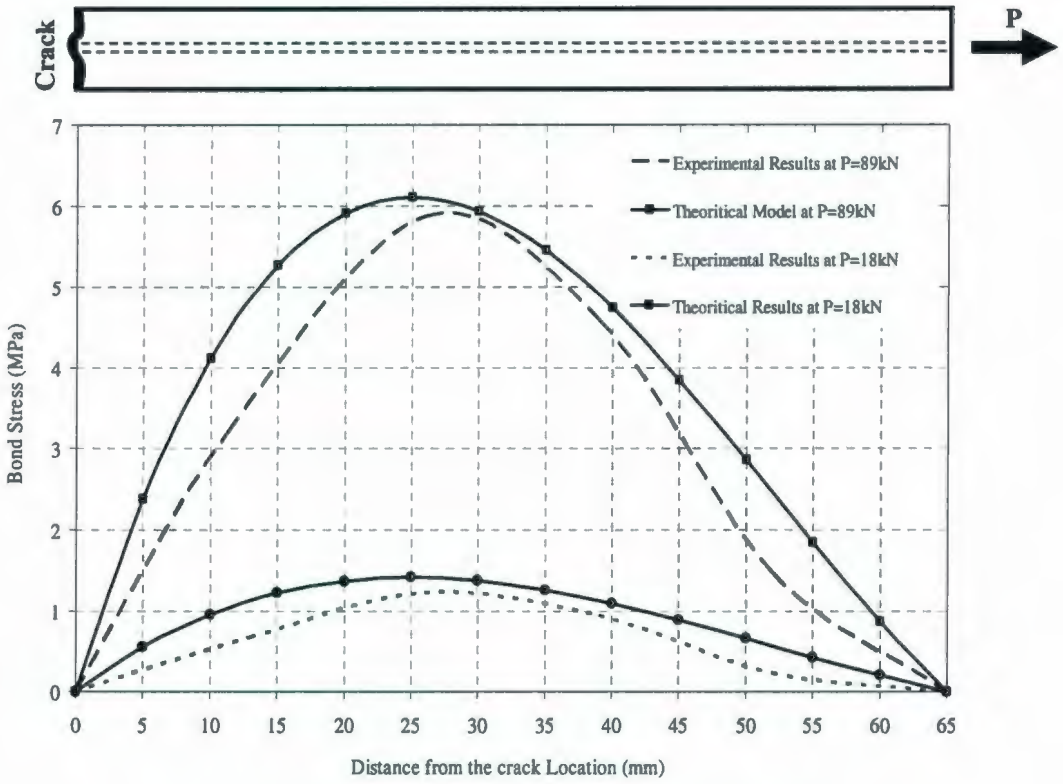

Fig. 5.7 Bond Stress Distribution for Specimen A_4 [25]

5.4.2 Steel and Concrete Stress Distribution

The manner in which the axial load is shared between the concrete and the reinforcement along the length of a member can be evaluated by considering the distribution and magnitude of the bond stress between cracks that is presented in Eq. (5.35). The load component resisted by concrete P_{cx} at any section between the successive cracks, is the accumulation of the transferred bond stress, thus, the value of P_{cx} carried by section at a distance x from the crack face can be expressed as:

$$P_{cx} = \int_0^x f_{bx}\, u\, dx \tag{5.36}$$

where f_{bx} is the local bond stress at a distance x from the crack face; u is perimeter of the reinforcement. Substituting the value of bond stress in Eq. (5.35) into Eq. (5.36):

$$P_{cx} = \int_0^x [\frac{u}{\beta}(A_1 + A_2 X + A_3 X^2 + A_4 X^3)]dx$$

$$P_{cx} = \frac{u}{\beta}(A_1 X + \frac{A_2}{2} X^2 + \frac{A_3}{3} X^3 + \frac{A_4}{4} X^4) \quad (5.37)$$

Eq. (5.37) represents the distribution of the load carried by the concrete section at various locations from the crack sections. The value of tensile stress of the concrete at any section from the crack face can be evaluated as follows:

$$f_t = \frac{P_{cx}}{A_c (1 + n\rho)} \quad (5.38)$$

Fig. 5.8 represents the distribution of the estimated values of concrete stress distribution at the cracking stage for different sections from the crack face, for specimen A_4 conducted by Jiang et al., 1984 [25] using the proposed Eq. (5.38). It is obvious that, the value of the concrete stress is equal to zero at the crack face, and reaches its maximum value at a distance equal to the transfer length L_t from the crack face.

The predicted value of the tensile strength of concrete f_t' is equal to 1.88 MPa, as presented in Fig. 5.8, showing a favorable congruent with the value of cracking strength of normal strength concrete according to CSA-S474-04 ($f_t' = 0.33\lambda\sqrt{f_c'}$ = 1.94 MPa). In the mean time, the value of concrete cracking strain is equal to 98 microstrains, which is very close to the proposed value of the concrete cracking strain recommended by Belarbi and Hsu, 1994 [46]; and Marzouk and Chen, 1995 [5].

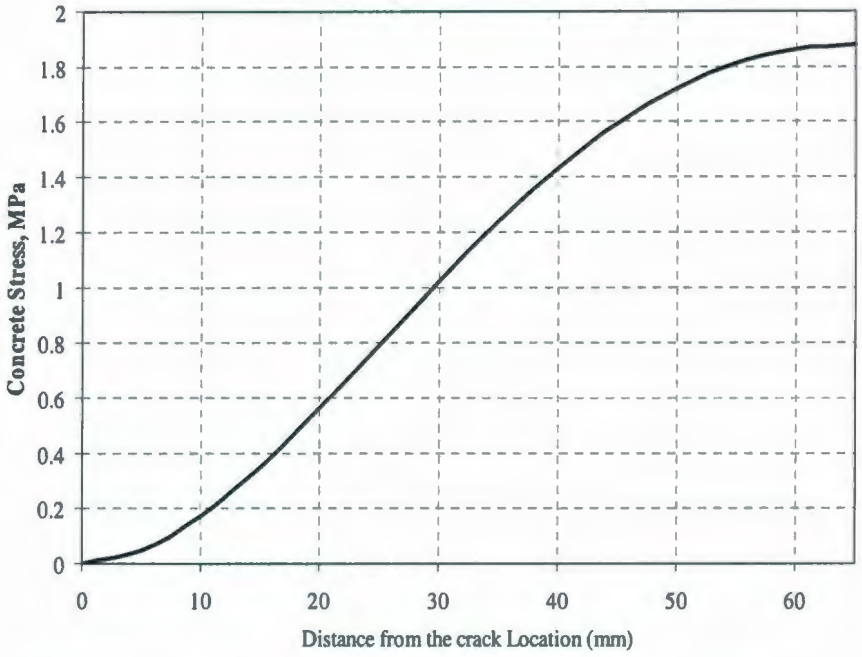

Fig.5.8 Distribution of the concrete stress for specimen A_4 [25]

Similarly, the distribution of load component carried by steel reinforcement P_{sx} can be determined ($P_{sx} = P_T - P_{cx}$). Consequently, steel stress distribution can be evaluated for various sections from the crack face. Fig. 5.9 shows a comparison between the results of the analytical model for calculating the steel stress distribution between the successive cracks and the experimental results for specimen A_4 tested by Jiang et al., 1984 [25] for two stages of loading, favorable agreement between the experimental and theoretical results is noted.

Figs 5.7 and 5.9 demonstrate that, the bond stress at any point is proportional to the rate of change of the steel stress in the reinforcement df_{sx}/dx at the same point, where bond stress must be present whenever the stress or force in a reinforcing bar changes from point to point along the length of the bar to keep the equilibrium.

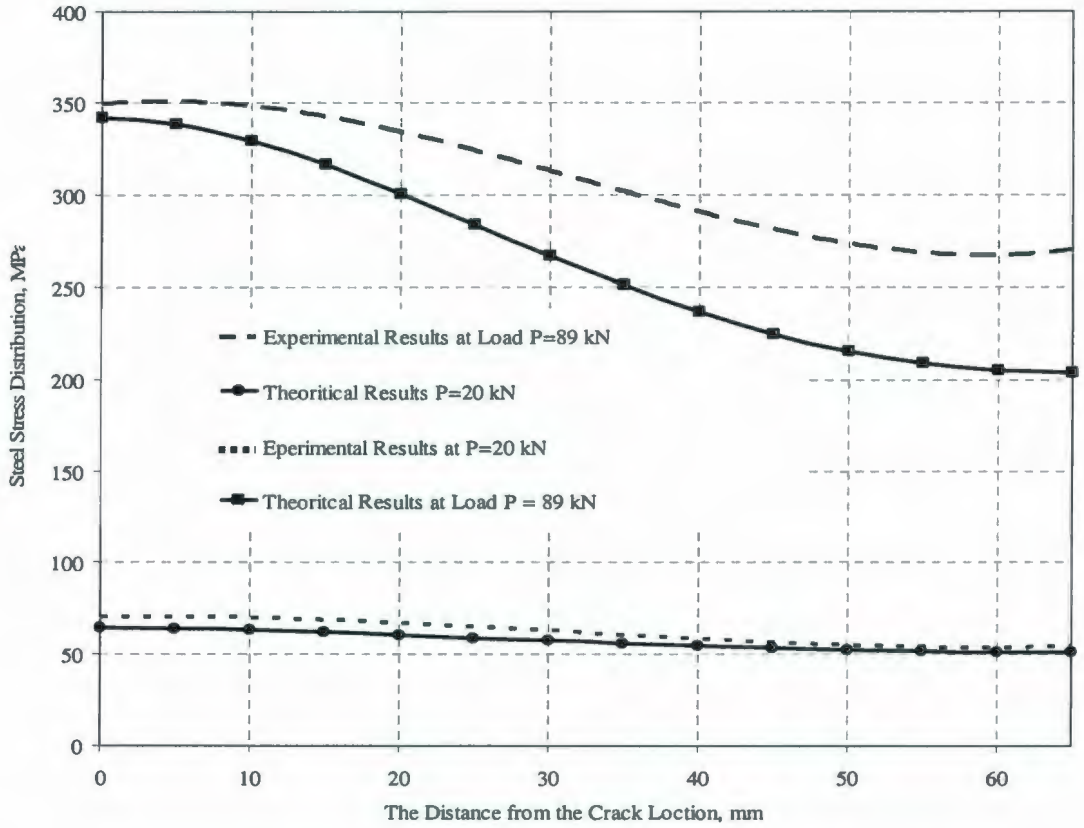

Fig. 5.9 Analytical and Experimental Steel Stress Distributions [25]

This observation can be explained by the free-body diagram in Fig. 5.10. If f_{s2} is greater than f_{s1}, the bond stress, f_{bx}, must act on the surface of the bar to maintain equilibrium. Summing forces parallel to the bar, one finds the equilibrium for the free body of differential steel of length dx is:

$$(f_{s2} - f_{s1})\frac{\pi d_b^2}{4} = f_{bx}(\pi d_b)dx$$

$$f_{bx} = \frac{(f_{s2} - f_{s1})d_b}{4dx} = \frac{d_b}{4}\frac{df_{sx}}{dx} \tag{5.39}$$

$$f_{bx} \propto \frac{df_{sx}}{dx} \tag{5.40}$$

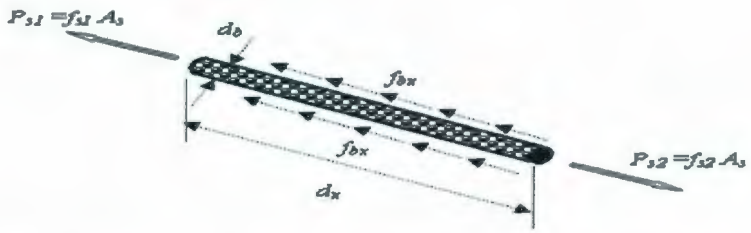

Fig. 5.10 Relationship between Change in Bar Stress and Bond Stress

To check the suitability of proposed analytical model for predicting the response of thick reinforced concrete specimens, which is the case for offshore structures, the results of the proposed model are compared with the experimental test results conducted in this study on thick reinforced normal and high strength concrete panels. Figs 5.11(a, b) show the concrete stress distribution at different sections between two consecutive cracks at the cracking stage for panels NS-U-15-2.5-6, and HS-U-15-2.5-6, respectively. Based on the proposed model, the value of the tensile strength for normal and high strength concrete is found to be 2.22 MPa and 3.26 MPa, respectively, see Fig. 5.11. The test results revealed that, the tensile strength of concrete for the normal and high strength concrete panel is 2.1 MPa, and 3.2 MPa, respectively. These results show a favorable agreement with the predicted value of tensile strength concrete.

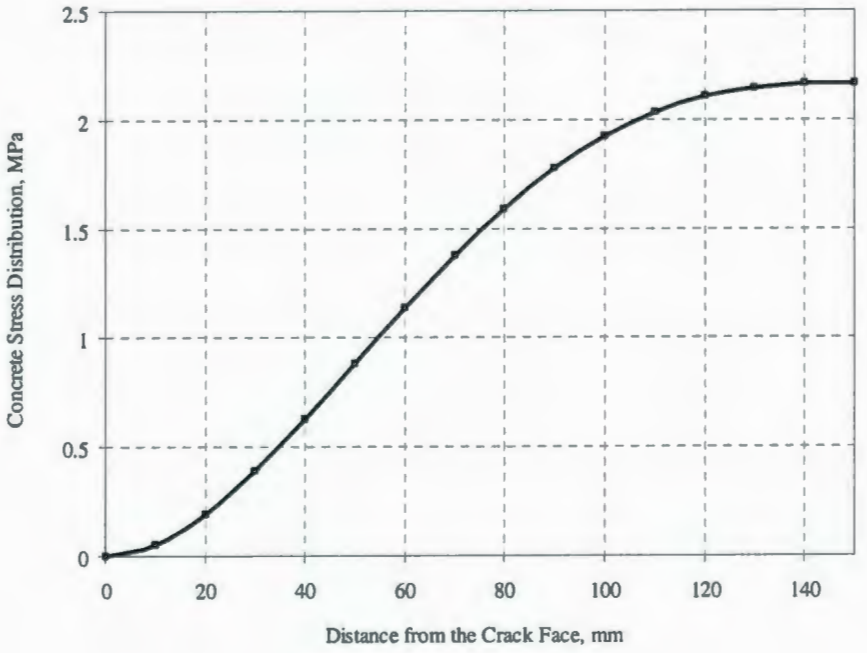

(a) Panel (NS-U-15-2.5-6)

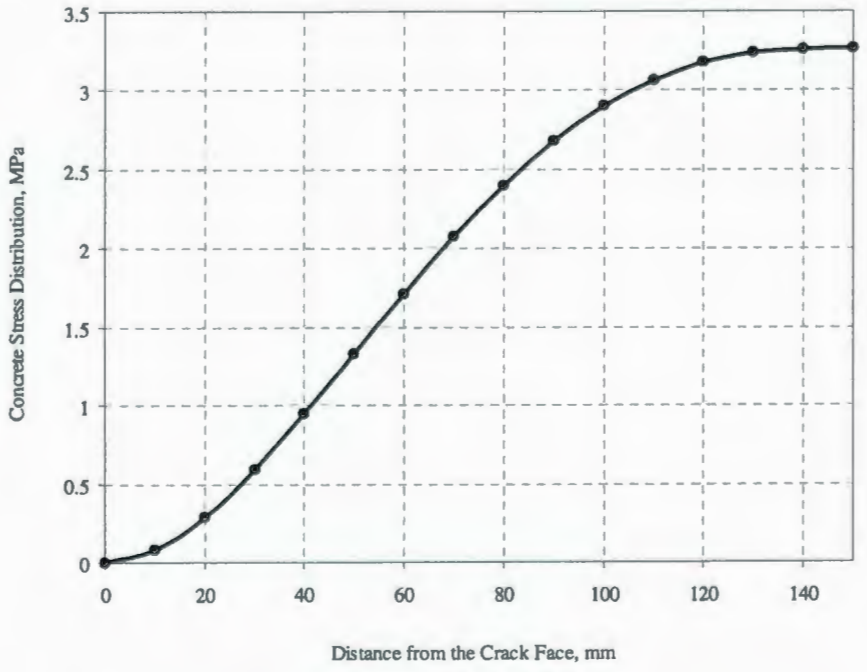

(b) Panel (HS-U-15-2.5-6)

Fig. 5.11 Concrete Stress Distribution at the Cracking Load

5.5 Summary

A rational model is developed for predicting the bond characteristics and the cracking behavior of reinforced concrete member under tension stresses. The derivation of the analytical model is based on the solution of the deferential equation, which relates the local bond stress to the second derivative of the slip between the steel bar and the concrete section. The model enables the determination of the complete distribution of the slip, bond stress, and concrete and steel stresses at different loading stages. The influence of the main factors that affect the cracking behavior, such as the tensile strength of concrete, and reinforcement ratio on the bond stress distribution, are taken into consideration. Moreover, this model considers all the boundary conditions that have profound effect on the cracking behavior at different sections between cracks, to provide an accurate prediction for the response of the member under the applied load.

The predicted values using the proposed analytical model are compared to results of various experimental investigations conducted on thick reinforced concrete panels loaded axially in tension conducted in the present study. The model preformed satisfactorily as compared with the experimental data for the different levels of the steel stress.

Chapter 6

Bond Effects on the Cracking Response

6.1 Introduction

The safety and proper design of the enormous yet indispensable structures such as offshore oil platforms and containment structures for nuclear power plants need a clear understanding of the cracking behavior and bond characteristics. The transfer of the forces across the interface between concrete and steel reinforcing bars is of fundamental importance in analyzing of reinforced concrete structures behavior. Forces are transferred from the reinforcing bars to the surrounding concrete primarily by inclined compressive forces radiating out from the bars (Abrams, 1913[88]; Losberg and Olsson, 1979[89]). As a result, the forces on the concrete have longitudinal and radial components. The radial component causes circumferential tensile stresses in the concrete around the bars (Goto, 1971) [23]. Eventually, the concrete splits parallel to the bars and the resulting cracks propagate out to the surface of the reinforced concrete panels. Once these cracks develop, the bond transfer drops rapidly unless transverse reinforcement is provided to restrain the opening of the splitting cracks.

Several research studies were conducted on the transfer of forces across the interface between concrete and steel reinforcing bars, and the splitting cracks influences on the cracking response of RC members. Abrishami and Mitchell, 1996 [37] investigated the influence of splitting cracks on tension stiffening of reinforced concrete tension members considering the effect of different sizes of reinforcing bars. The bond strength

characteristics of high strength concrete under monotonic and cyclic pull out loading were studied by Alavi-Fard and Marzouk, 2002; 2004 [27, 28], considering the load history, confining reinforcement, bar diameter, concrete strength, and the rate of pull out loading. Azizinamini et al., 1993; 1995 [90, 91] conducted a research study to evaluate the bond performance of reinforcing bars embedded in high-strength concrete. Maekawa et al., 2003 [92] studied the bond stress transfer mechanism of the deformed bar, the typical distribution of the local bond stress in concrete was defined, taking into account the average post cracking tensile behavior.

The current chapter analyzes the relationship between the bond and the splitting forces, resulting from the bearing of lugs of the reinforcing steel bars. Effects of the confinement provided by the tensile resistance of the concrete cover and transverse reinforcement on the splitting occurrence are investigated, as the transverse reinforcing bars provide additional tensile resistance to the bond failure across the splitting plane. Influence of the forces that tend to split the concrete cover around the bars, on the cracking behavior of orthogonally reinforced concrete panels subjected to in-plane axial stresses, is discussed. Furthermore, this study is extended to provide simple design equations for evaluating the tensile strength of normal and high strength reinforced concrete thick plates subjected to biaxial loading condition, considering the secondary effect of the splitting stress on the cracking behavior of these members. Results of the experimental program conducted in the present research, as well as the available experimental data of various experimental investigations, are utilized to validate the reliability of the proposed model. In all of the

studied cases, the model performed satisfactorily with respect to the measured responses from the experimental work.

6.2 Review of the Bond Mechanism

Bearing stress arises when the lugs of the deformed bars push against the surrounding concrete. Conical compression struts are developed as the reinforcing bars are stretched out, as shown in Fig. 6.1. These inclined forces are not perpendicular to the surface of the bar lugs due to the friction forces between the surface of the lugs and the surrounding concrete. The conical bond action between bar and concrete can be resolved into radial and tangential components. The splitting force is the radial component of the force applied on the concrete by the reinforcing bars (Canbay and Frosch, 2005 [93]). These radial forces are generated by the longitudinal bar forces that can be calculated according to the following Eq. (6.1):

$$F_l = \Sigma A_s f_s \tag{6.1}$$

where F_l is the forces carried by the longitudinal reinforcing bars, A_s is the area of the longitudinal steel reinforcement, f_s is the stress on the reinforcing bar. The radial force F_{sp} can be related to the longitudinal force F_l through the geometrical relationship shown in Fig. 6.1 and as provided by Eq. (6.2)

$$\tan\alpha = \frac{F_{sp}}{F_l} \tag{6.2}$$

where α is the angle of inclination of the forces radiating from the reinforcing bars.

The radial component F_{sp} of the inclined compressive force is balanced by circumferential tensile stresses in the concrete surrounding the bar (Tepfers, 1973 [94]; MacGregor and Bartlett, 2000 [95]). The mechanical locking of lugs with surrounding concrete is the major component transfers tensile stress from a deformed bar to concrete. The resultant force exerted by the lug on the concrete is inclined.

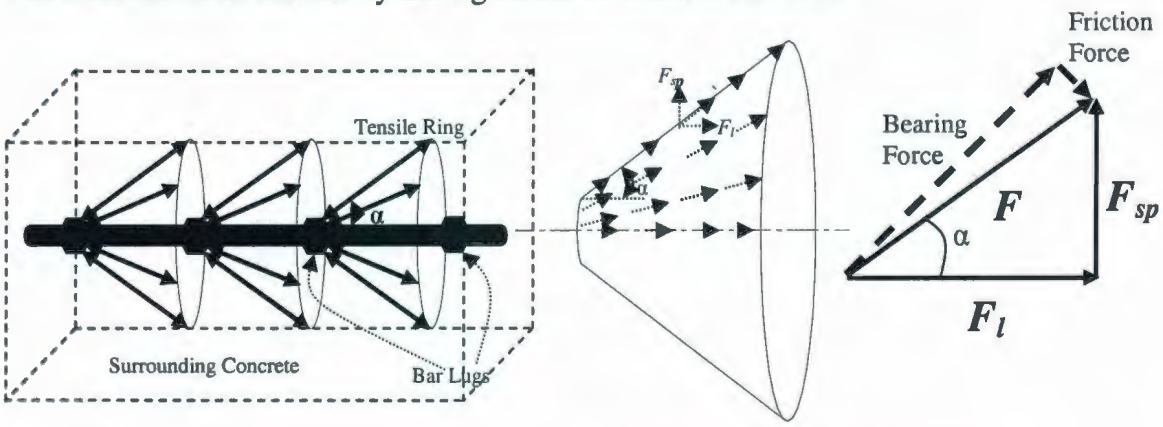

Fig. 6.1 Tensile stress Rings in Concrete Balance Radial Components of Inclined Compressive Stresses

The radial stress causes tensile ring stress and splitting cracks if the splitting stress exceeds the cracking strength of concrete. Also, the bond stress can lead to primary cracks if its summation over a certain length exceeds the concrete tensile strength. Two types of failure modes are distinguished: (a) pull-out failure if adequate confinement is provided by the concrete cover or by transverse reinforcement; and (b) splitting failure with drop of bond stress if concrete cover splits along the reinforcing bar, see Fig.6.2 (Harajli, 1994 [96]; CEB-FIP, 1990 [44]). In this figure, τ_s represents the peak local bond stress in the pull-out failure; and τ_{sp} is the splitting bond resistance due to the development of splitting cracks.

The ability of a deformed bar to transfer its load into the surrounding concrete is typically limited by failure of this ring of tension when the thinnest part of the ring splits (splitting failure), unless transverse reinforcement is provided to restrain the opening of the splitting crack.

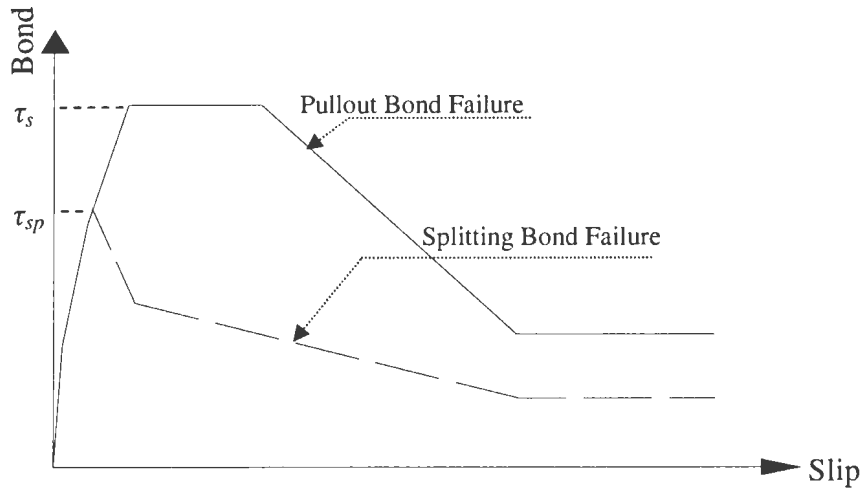

Fig. 6.2 Schematic Representation of Bond Stress vs. Slip Relationship

The damage proceeds outward from the reinforcing bar lug region toward the top surface that is through the cover, as well as downward into the interior of the specimen. Thus, the presence of the concrete cover of the specimens is important in providing confinement to absorb the fracture energy associated with the splitting cracking process.

Typical splitting crack surfaces (MacGregor, and Bartlett, 2000 [95]) are shown in Fig. 6.3; the splitting cracks tend to develop along the shortest distance between a bar and the surface or between two bars. Two different splitting failure planes can develop. Side splitting occurs when a horizontal split extends at the level of bars, and face splitting occurs when vertical split develops below the bars (Kemp, 1986 [97]; Canbay and Frosch, 2005 [93]), as shown in Fig. 6.3. The circles that touch the edges of the member,

where the distances are shortest, are considered the effective area that provided the splitting resistance. Thus, the load at which splitting failure develops is a function of the minimum distance from the bar to the surface of the concrete or to the next bar; the tensile strength of the concrete; and the average bond stress between the reinforcement and the concrete.

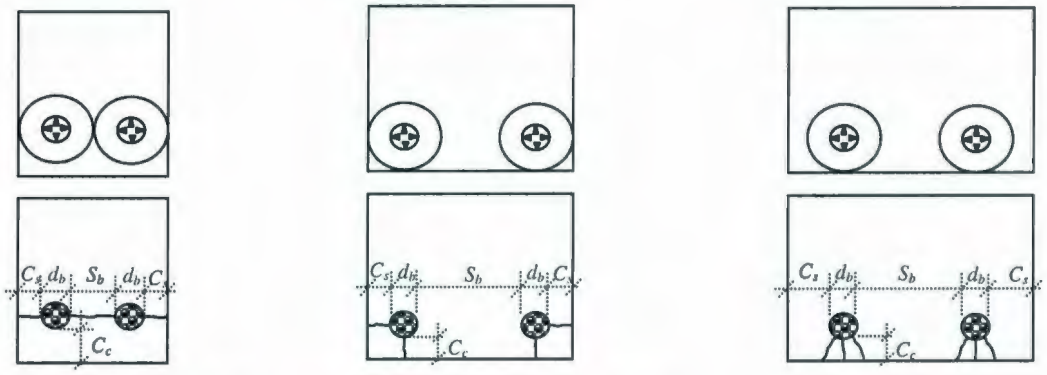

(a) Side Splitting, side cover and two thirds the bar spacing both less than bottom cover.

(b) Side splitting and face splitting, side cover = bottom cover, both less than two thirds the bar spacing.

(c) Face splitting, bottom cover less than side cover and two thirds the bar spacing.

Fig. 6.3 Typical Splitting Failure Surfaces

Based on the experimental results conducted in the present study, the splitting cracking occurrence is highly pronounced in case of using high bar diameter. However, if a bar with a relatively small diameter is embedded in large block of concrete, the bar might pull out of the concrete (pull out failure) or reach its yield stress, before splitting cracks occurrence.

6.3 Development of Side and Face Splitting Cracks

The three-dimensional bond action mechanism between the concrete section and the reinforcing bars generates a radial splitting force F_{sp} around the bar circumference. The

relationship between radial splitting forces F_{sp} and longitudinal force F_l can be expressed as presented in Eq. 6.3 and as shown in Fig.6.1.

$$F_{sp} = F_l \tan\alpha \tag{6.3}$$

Radial splitting force F_{sp} is developed around the reinforcing bar when the steel bar is in tension, and it causes the splitting of concrete based on the tensile strength of concrete and the clear cover thickness. The circle that can be drawn within the section of a panel around the reinforcing bar is considered the effective concrete restraining portion that provides the confinement for the splitting action of the reinforcing bar, as shown in Fig. 6.4. Internal pressure of f_{sp} is acting within a circular hole with diameter d_b that represents the bar diameter embedded in a concrete section. Considering a cylindrical prism of concrete of diameter 2C, containing a bar with a diameter of d_b. The radial component force on the concrete causes an internal splitting pressure f_{sp} on a portion of the cross section of the reinforced concrete panel, as shown in Fig. 6.4. This pressure is equilibrated by the tensile stress in concrete on either sides of the bar. The distribution of these stresses is arbitrarily assumed to be of a parabola, as illustrated in Fig. 6.4. Splitting is assumed to occur when the maximum tensile stress induced in the concrete rings reaches the tensile strength of the concrete f_t', to satisfy the equilibrium condition in a panel of length equal to l.

Thus, the main assumptions, which are made in this study are: the effective area that provides the confinement for the splitting cracks is simulated by the concrete section surrounded by the circle of radius of C, as shown in Fig. 6.4; the distribution of the tensile stresses in concrete around the reinforcing bars follows 2nd degree parabola; the

angle of inclination of the forces radiating from the reinforcing bars depends on the relationship in Eq. (6.2); and the replacement of the concentrated forces on the lugs of the reinforcement with a force that is uniformly distributed along the length of the bar.

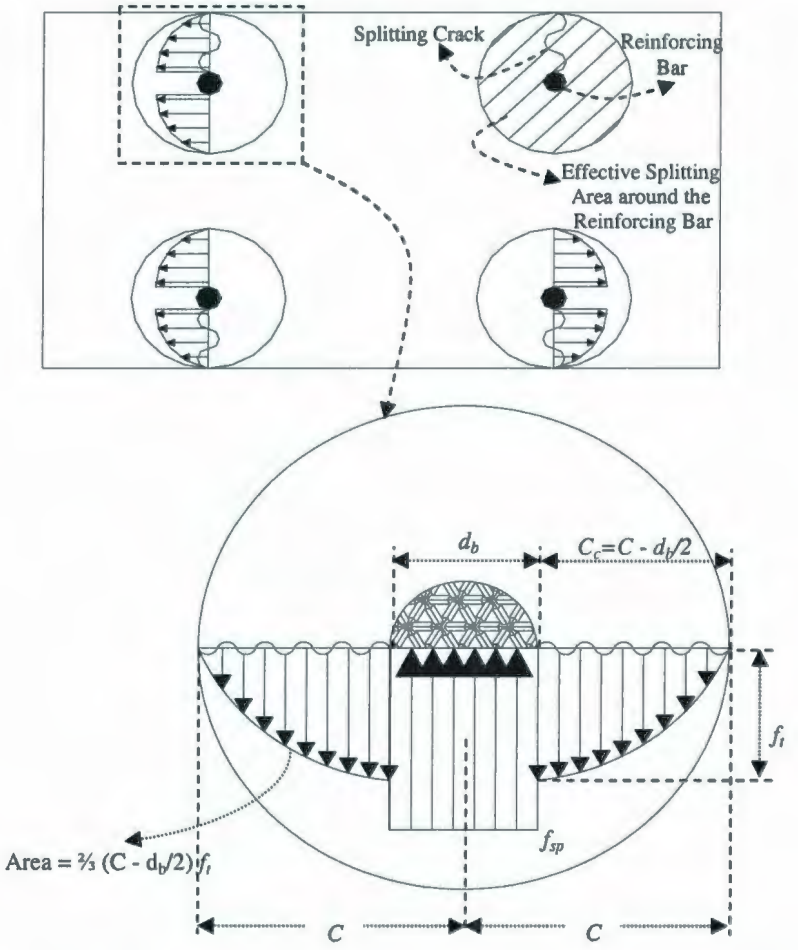

Fig. 6.4 Stresses Distribution in the Effective Circular Area of Concrete around the Reinforcing Bars

The splitting force generated by bond action may be obtained by integrating the splitting stresses around and along the length of the reinforcing bar as shown in Fig. 6.5. Thus, the total splitting force can be expressed as following:

$$F_{sp} = \int_0^l \int_{-\pi/2}^{\pi/2} f_{sp} \frac{d_b}{2} \cos\theta . d\theta . dl \tag{6.4}$$

where f_{sp} is the splitting stress, d_b is the longitudinal bar diameter, and l is the embedded length of the reinforcing bars. The splitting stresses are assumed to be uniform around the bar circumference and along the bond length, thus the integration may be evaluated to give:

$$F_{sp} = \int_0^l f_{sp}\, d_b\, dl = f_{sp}\, d_b\, l \tag{6.5}$$

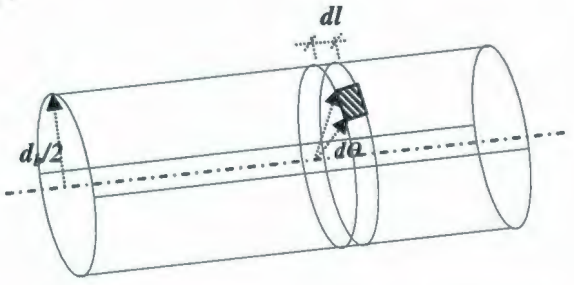

Fig. 6.5 Splitting Stress Distribution Due to Bearing of the Lugs of the

These internal splitting forces are equilibrated by the tensile stress of the concrete surrounding the reinforcing bars, as shown in Fig. 6.4. Considering the equilibrium in vertical direction, the splitting stress f_{sp} can be expresses as:

$$\frac{f_{sp}\, d_b\, l}{2} = \frac{2}{3}(C - \frac{d_b}{2})\, f_t\, l \tag{6.6}$$

$$f_{sp} = \frac{4}{3}(\frac{C}{d_b} - \frac{1}{2})\, f_t \tag{6.7}$$

At the time when the splitting crack occurs, the concrete stress f_t in Eq. (6.7) reaches the tensile strength of the concrete f_t'.

Therefore, the radial splitting pressure required to cause the splitting crack can be determined by:

$$f_{sp} = \frac{4}{3}\left(\frac{C}{d_b} - \frac{1}{2}\right) f_t' \tag{6.8}$$

Inserting the value of the splitting stress from Eq. (6.8) into Eq. (6.5), leads to the following expression for evaluating the force that causes the splitting crack:

$$F_{sp} = \frac{4}{3}\, l\left(C - \frac{d_b}{2}\right) f_t' \tag{6.9}$$

The value of $(C\text{-}d_b/2)$ represents the clear concrete cover C_c over the steel reinforcing bars, thus, the splitting force to cause cracking can be expressed as:

$$F_{sp} = \frac{4}{3}\, l\, C_c\, f_t' \tag{6.10}$$

Based on the derived Eq. (6.10), for the side-splitting failure case ($C_s < C_c$) shown in Fig. 6.3(a), the force F_{sp} that causes splitting cracking can be calculated using the following equation:

$$F_{sp} = l\left[\frac{8}{3} C_s + (n-1) S_b\right] f_t' \tag{6.11}$$

where, F_{sp} is the force that causes the splitting crack; f_t' is the concrete tensile strength; C_s is the side clear cover; n is the number of the reinforcing bars, and S_b is the spacing between the longitudinal reinforcing bars. In case of using equal side and face concrete cover in a reinforced concrete member ($C_s = C_c$), the possibility of side and face splitting cracks occurrence are equal, as shown in Fig. 6.3(b), and the force required to cause splitting F_{sp} can be expressed as the following equation:

$$F_{sp} = \frac{4}{3} C_s\, l\, f_t' = \frac{4}{3} C_c\, l\, f_t' \tag{6.12}$$

For the face-splitting cracking ($C_s > C_c$), as shown in Fig. 6.3(c), the total force required to cause splitting cracks F_{sp} can be calculated using the following equation:

$$F_{sp} = \frac{4}{3} C_c \, l \, f_t' \tag{6.13}$$

For a reinforced concrete member subjected to tensile stresses, the oblique angle α of the forces radiating from the reinforcing bars can be directly calculated using F_{sp} (Eqs.6.11 through 6.13) and F_l (Eq. 6.1). In this study, the experimental results conducted in the present experimental investigation parallel with the available experimental results in the literature (Chinn et al.,1955 [98]; Chamberlin, 1958 [99]; Ferguson and Breen, 1965 [100]; Goto, 1971 [23]; Abrishami and Mitchell, 1992, 1996 [26, 37]; Azizinamini et al., 1999 [91]), are utilized in an attempts to develop design criteria for the relationship between the radial splitting (F_{sp}) and the longitudinal (F_l) forces. Thus, the values of the oblique angle (α) are calculated based on Eq. 6.2 for different values of C_c/d_b. A good fit to the experimental test results is obtained using the following prediction equations for both normal and high strength concrete specimens, as presented in Figs. 6.6, 6.7:

$$\tan\alpha = 0.073 e^{1.81\sqrt{\frac{C_c}{d_b}}} \text{, for normal strength concrete} \tag{6.14}$$

$$\tan\alpha = 0.121 e^{1.53\sqrt{\frac{C_c}{d_b}}} \text{, for high strength concrete} \tag{6.15}$$

where α is the oblique angle of stress due to the bearing of the bar lugs against the surrounding concrete, and C_c/d_b represents the ratio between the clear concrete cover and the bar diameter. These design criteria are proposed based on a comprehensive experimental data obtained from the experimental program conducted in the present study, as well as the test data available in the literature.

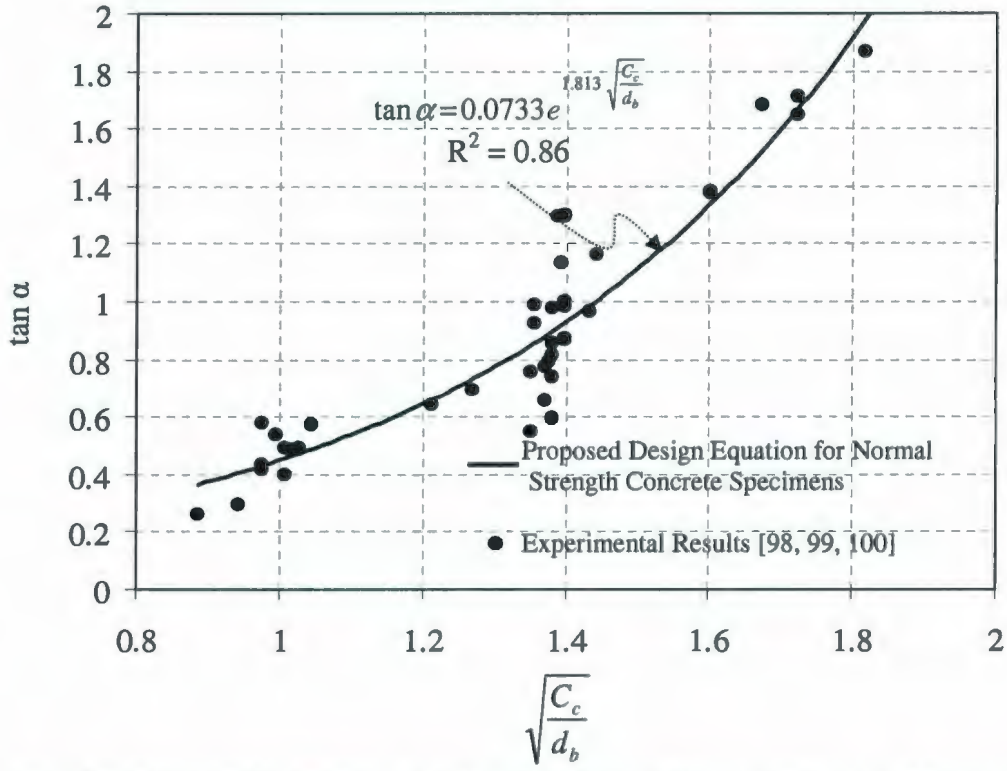

Fig. 6.6 Value of the Oblique Angle α for Normal Strength Concrete Members

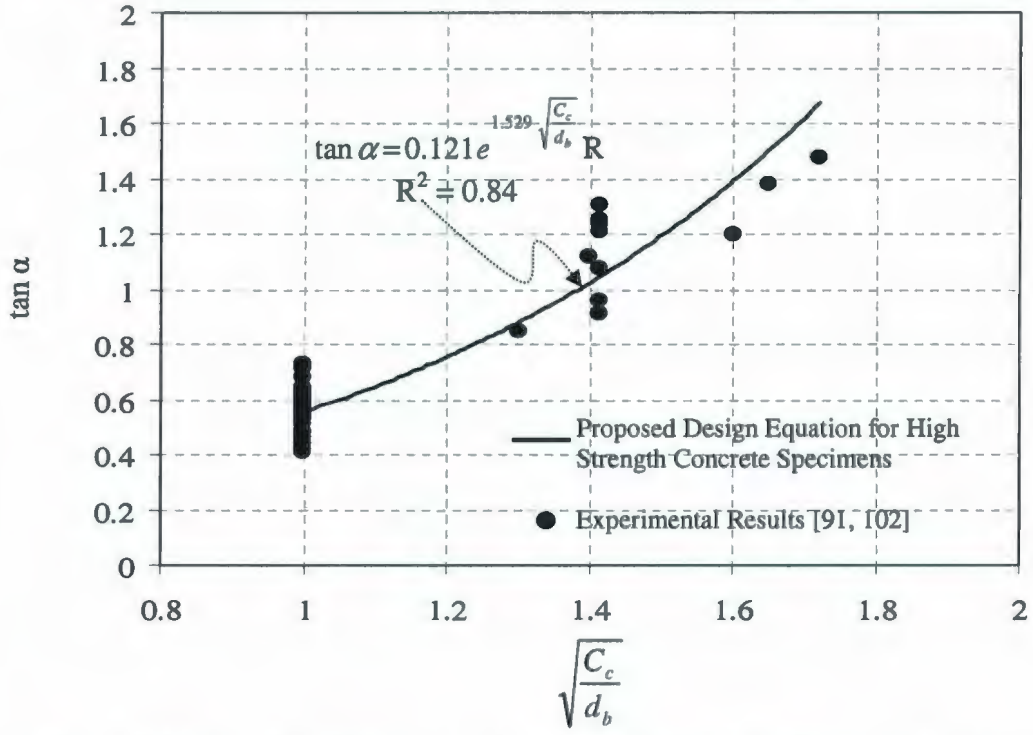

Fig. 6.7 Value of the Oblique Angle α for High Strength Concrete Members

The correlation coefficient, R^2, is a measure of the compatibility between the experimental data and the predicted values based on equations 6.14 and 6.15. For normal- and high-strength concrete specimens, the value of R^2 is found to be 0.86 and 0.84, respectively, see Fig. 6, and 7. Thus, for reinforced concrete with its usual wide scatter in data, on average base $R^2 = 0.85$ is generally accepted as a satisfactory indication of compatibility. Also, the results from the proposed equations for predicting the relationship between the radial splitting and the longitudinal bond stresses show a good agreement with the previous measurements of the angle α, at which the compressive struts radiate from the bar lugs, reported by (Goto, 1971 [23]; Tepfers, 1973 [94]; and Tepfers and Olsson, 1992 [101]; Esfahani and Regan, 1998 [102]).

6.4 Analytical Expression of Splitting and Bond Stresses Relationship

The equilibrium between the applied longitudinal force F_l carried by the reinforcing bars ($F_l = A_s f_s$) and the resisting bond force ($A_b \tau_{sp}$) can be expressed as follows [93, 102]:

$$A_s f_s = A_b \tau_{sp} \tag{6.16}$$

In the present study, the proposed model in equations (6.14) and (6.15) for predicting the relationship between the splitting and the longitudinal forces can be used to evaluate the value of the splitting bond strength τ_{sp} of the concrete surrounding the reinforcing bars. Substituting by the value of f_{sp} in Eq. (6.8) into Eq. (6.14), and Eq. (6.15), the equations to evaluate the splitting bond strength for normal and high strength concrete can be expressed as:

$$\tau_{sp} = 18.3 \frac{A_{sp}}{A_b}\left(\frac{C}{d_b} - \frac{1}{2}\right) f_t' \, e^{-1.81\sqrt{\frac{C_c}{d_b}}} \text{ , for the normal strength concrete} \quad (6.17)$$

$$\tau_{sp} = 11.1 \frac{A_{sp}}{A_b}\left(\frac{C}{d_b} - \frac{1}{2}\right) f_t' \, e^{-1.53\sqrt{\frac{C_c}{d_b}}} \text{ , for high strength concrete} \quad (6.18)$$

where τ_{sp} is the splitting bond stress, A_b is the bond surface area of the reinforcement($\pi d_b l$); A_{sp} is the area that provides confinement for the splitting stresses($C_c l$). These equations reflect the effect of the concrete tensile strength f_t', and C/d_b ratio on the bond characteristics of concrete.

Meanwhile, the average value of the steel stress at the splitting failure can be predicted based on the equilibrium between the applied bar forces ($A_s f_s$) and the resisting bond force ($A_b \tau_{sp}$), as given by Eq. (6.16). Thus, the average value of the steel stress at the splitting failure can be predicted.

$$f_s = \frac{A_b \tau_{sp}}{A_s} = \frac{4\tau_{sp} l}{d_b} \quad (6.19)$$

where, A_b is the surface area of the bar over the splice length ($\pi \, d_b \, l$); l is the embedded length; A_{sp} is the area that provides confinement for the splitting stresses ($C \, l$); A_s is the cross sectional area of the longitudinal reinforcing bars ($\pi \, d_b^2/4$).

A series of verification tests is conducted to measure the reliability of the model for predicting the value of the splitting bond strength. The selection of the test series was based so that the test must allow the verification of the model for normal and high strength concrete. The validity of the proposed expressions in equations 6.17 and 6.18 are based on the literature survey (Chinn et al., 1955 [98], Hamad and Itani, 1988 [102]).

Tables 6.1 and 6.2 present a comparative study between the measured value of splitting bond and steel stresses at the splitting failure and the corresponding predicted values, for normal and high-strength concrete specimens, respectively.

As a further verification, Table 6.3 presents the average μ, standard deviation σ^2, and the coefficient of variance (σ^2/μ) for the ratio of the experimental and theoretical results of the various experimental results available in the literature for both normal and high strength concrete specimens (Chamberlin, 1956 [99]; Azizinamini et al., 1999 [103]).

The statistical values presented in Tables 6.1 through 6.3 shows a favorable agreement between the measured experimental and the predicted results based on the proposed model.

Esfahani and Rangan, 1998 [104] conducted an experimental program to evaluate the influence of different parameters such as the C_d/d_b ratio, and f_t' on bond stress, using pull-out test on various normal and high strength concrete specimens.

The results of that experimental investigation [104] are used as a further confirmation of the accuracy of the analytical approach developed in this study (Equations 6.17, 6.18). Figs. 6.8 (a, b) present the results of the proposed model expressed in Eqs. (6.17) and (6.18), as well as, the modified Tepfers' model proposed by Esfahani and Rangan [104], and ACI 318R-08 approach [78], compared with the experimental results for normal and high strength concrete members. Fig. 6.8 shows the importance of concrete cover in increasing of the bond stress between the reinforcing bars and the surrounding concrete. The proposed design equations are able to adequately predict the bond behavior of reinforced concrete specimen with different concrete cover, as shown in Fig. 6.8.

Table 6.1- Comparison between the Experimental and predicted values of u_{sp}, and f_s (Noraml Strength Concrete Specimens)

Specimen No.	f_c', MPa	$\tau_{sp(exp)}$, MPa	$f_{s(exp)}$, MPa	$\tau_{sp(cal)}$, MPa	$f_{s(cal)}$, MPa	$\tau_{sp(exp)}/\tau_{sp(cal)}$	$f_{s(ex)}/f_{s(cal)}$
D1*	26.75	3.76	221.33	3.33	195.81	1.12	1.13
D2*	33.24	3.64	200.0	3.71	198.40	0.97	1.01
D3*	30.0	4.16	245.33	4.16	244.23	1.001	1.004
D4*	30.82	3.64	312.0	3.37	288.25	1.07	1.08
D5*	28.82	5.03	298.0	4.82	283.28	1.04	1.05
D6*	29.93	3.7	218.0	3.58	210.48	1.03	1.03
D7*	30.68	3.78	222.66	3.83	225.23	0.98	0.98
D8*	31.51	4.02	236.66	3.38	198.44	1.19	1.19
D9*	30.20	3.9	230.0	3.24	190.41	1.20	1.20
D10*	30.13	4.60	172.66	4.14	154.69	1.11	1.11
D11*	31.24	-	315.33	6.86	331.78	-	0.95
D12*	31.24	3.50	301.33	3.58	306.03	0.97	0.98
D13*	33.24	6.07	334.66	6.80	399.49	0.89	0.83
D14*	51.58	3.64	215.33	3.24	190.46	1.12	1.13
D15*	29.58	4.88	288.0	4.53	266.01	1.07	1.08
D16*	29.58	2.52	324.66	2.78	356.64	0.90	0.91
D17*	24.68	3.05	260	3.43	293.29	0.89	0.88
D18*	24.68	-	-	2.96	253.45	-	-
D19*	29.17	4.76	408.66	4.36	372.26	1.09	1.09
D20*	29.17	5.06	177.33	4.62	172.90	1.09	1.02
D21*	30.89	5.37	296.0	4.91	288.23	1.09	1.03
D22*	30.89	4.2	157.33	3.84	143.54	1.09	1.09
D23*	30.68	3.22	258.0	3.72	318.26	0.86	0.81
D24*	30.68	3.42	294.66	3.88	331.32	0.88	0.88
D25*	35.17	3.21	384.66	3.65	468.37	0.87	0.82
D26*	35.17	2.86	369.33	2.86	367.04	1.0	1.01
D27*	31.37	3.83	226.66	3.40	199.93	1.12	1.13
D28*	30.13	3.14	270.0	3.33	285.0	0.94	0.94
D29*	51.58	5.04	298.0	5.23	307.49	0.96	0.96
D30*	51.58	4.11	353.33	4.48	383.31	0.91	0.92
D31*	32.41	7.22	424.66	5.93	389.20	1.21	1.09
D32*	32.41	6.15	314.66	6.82	400.52	0.90	0.78
D33*	33.31	0.32	178.66	4.08	233.21	0.079	0.76
D34*	26.20	3.60	241.33	3.09	206.63	1.16	1.16
D35*	26.20	2.79	360.0	3.03	388.94	0.91	0.92
D36*	30.41	5.84	344.0	5.06	312.63	1.15	1.10
D37*	30.41	5.94	336.66	6.83	401.07	0.86	0.83
D38*	21.79	3.14	186.0	2.86	168.20	1.09	1.10
D39*	21.79	3.05	180.0	2.91	171.28	1.04	1.05
D40*	36.41	4.22	346.66	3.89	332.25	1.08	1.04
Mean (μ) for (exp)/(cal)						1.002	1.006
Standard Deviation (σ) for (exp)/(cal)						0.181	0.115
Coefficient of Variance (σ/μ) for (exp)/(cal) %						18.03	11.44

*Experimental Investigation Conducted by Chinn et al., 1955 [98]

Table 6.2- Comparison between the Experimental and predicted values of u_{sp}, and f_s (High Strength Concrete Specimens)

Specimen No.	f_c', MPa	$\tau_{sp(exp)}$, MPa	$f_{s(exp)}$, MPa	$\tau_{sp(cal)}$, MPa	$f_{s(tho)}$, MPa	$\tau_{sp(exp)}/\tau_{sp(cal)}$	$f_{s(ex)}/f_{s(cal)}$
PC-00-B-SP2*	65.6	8.22	401.08	9.07	434.57	0.91	0.92
SC-05-B-SP2*	76.7	8.06	393.47	7.35	352.30	1.09	1.11
SC-10-B-SP2*	76.7	7.36	358.25	7.35	352.30	1.01	1.02
SC-15-B-SP2*	67.1	7.85	383.25	6.88	329.52	1.14	1.16
SC-20-B-SP2*	73.5	8.17	398.53	7.20	344.87	1.13	1.16
PC-00-T-SP2*	63.7	8.28	404.15	6.70	321.06	1.23	1.25
SC-05-T-SP2*	76	7.7	375.82	7.32	350.69	1.05	1.07
SC-10-T-SP2*	84.9	7.23	352.8	7.74	370.66	0.93	0.95
SC-15-T-SP2*	83.4	7.07	345.15	7.67	367.37	0.92	0.94
SC-20-T-SP2*	84.3	7.2	351.37	7.71	369.34	0.93	0.95
PC-00-B-SP4*	52.3	7.85	382.89	6.07	290.92	1.29	1.32
SC-10-B-SP4*	70.7	7.28	355.07	7.06	338.24	1.03	1.05
SC-20-B-SP4*	76.4	5.52	269.57	7.34	351.61	0.75	0.77
PC-00-T-SP4*	54.7	8.36	407.85	8.28	396.83	1.01	1.03
SC-10-T-SP4*	74.8	7.52	367.05	7.26	347.91	1.04	1.05
SC-20-T-SP4*	79.5	7.09	346.22	7.49	358.68	0.95	0.96
Mean (μ) for (exp)/(cal)						1.026	1.046
Standard Deviation (σ) for (exp)/(cal)						0.134	0.1367
Coefficient of Variance (σ/μ) for (exp)/(cal) %						13.07	13.06

* Experimental Investigation Conducted by Hamad and Itani, 1988 [102]

Table 6.3- Comparison of expressions for Splitting bond and steel stresses

Reference	$\tau_{sp(exp)}/\tau_{sp(cal)}$			$f_{s(ex)}/f_{s(cal)}$		
	Mean, μ	Standard Deviation (σ)	Coefficient of Variance (σ/μ) %	Mean, μ	Standard Deviation (σ)	Coefficient of Variance (σ/μ)%
Chamberlin, 1956 [99]*	1.029	0.065	6.35	0.996	0.064	6.38
Azizinamini et al., 1999 [103]**	0.975	0.156	16.03	0.971	0.134	13.91

* Normal Strength Concrete Specimens
** High Strength Concrete Specimens

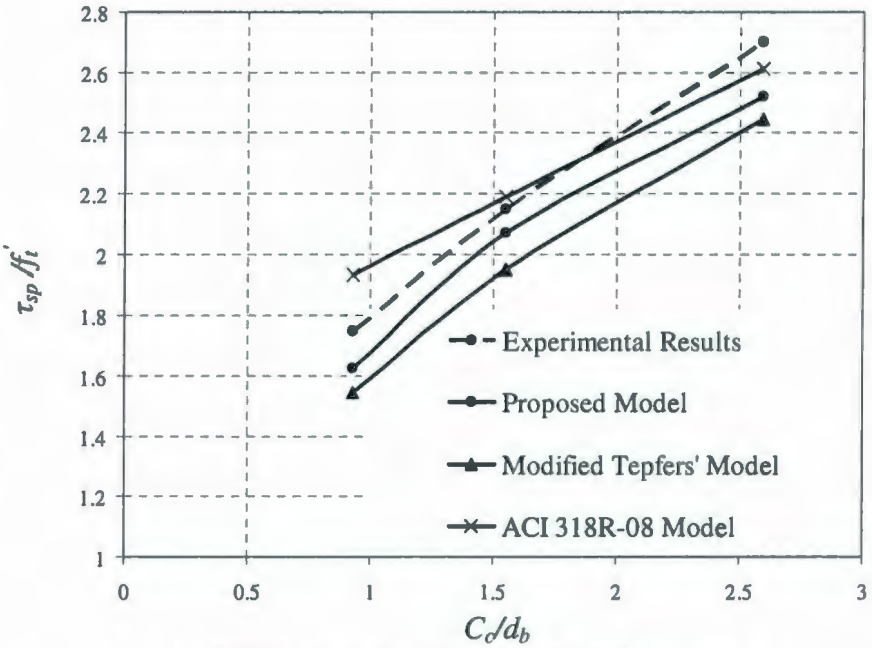

(a) Normal Strength Concrete member (26Y20) [104]

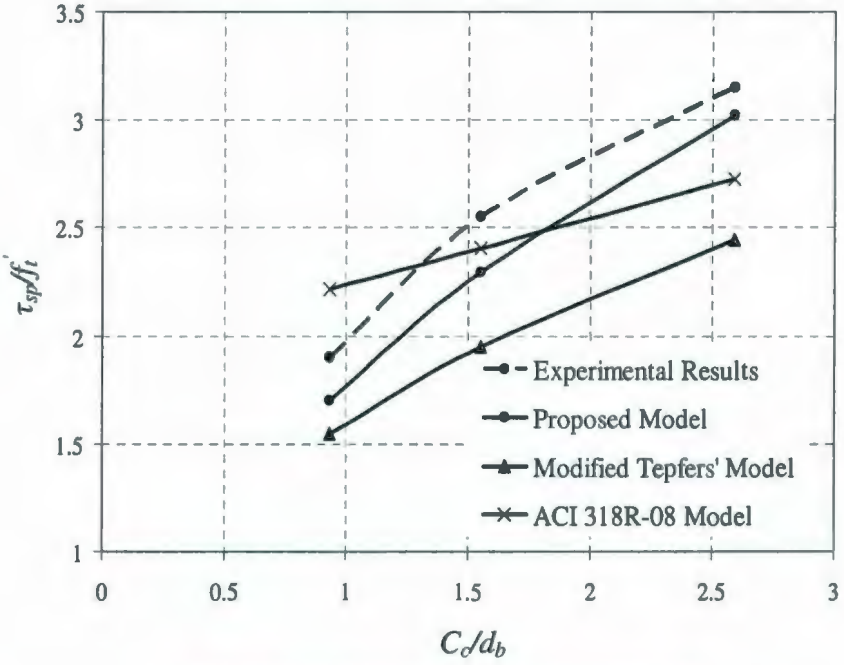

(b) High Strength Concrete member (75Y20) [104]

Fig.6.8 τ_{sp}/f_t' - C/d_b Relationship for Axially Loaded Reinforced Concrete Member [104]

6.5 Confinement Effect Provided by Transverse Reinforcement

It is important for reinforced concrete members to resist splitting failure along longitudinal bars, as the bond stress drops dramatically once the splitting crack appears, unless a sufficient confinement is provided. Little evaluation for the confinement provided by the concrete cover and lateral reinforcement has been reported. Thus, it is desirable to investigate the confinement effect provided by both concrete cover and transverse reinforcing bars against the splitting cracks, to establish a clear understanding for the bond characteristics and cracking behavior. As the transverse reinforcement extends perpendicular to the direction of the splitting cracks, it restrains the opening of these cracks, thus increases the bond stress between the reinforcement and concrete, as illustrated in Fig. 6.9.

The effect of transverse reinforcing bars on the splitting behavior can be incorporated through the addition of the forces induced in the transverse reinforcing bars due to the splitting action into Eq. 6.2, as illustrated in Fig. 6.9.

These forces can be calculated by multiplying the total area of the transverse bars crossing the splitting cracks plane by the average transverse bars stress.

$$F_{trans} = \Sigma A_{trans}\, \sigma_{trans} \tag{6.20}$$

where ΣA_{trans} represents the total area of the of transverse reinforcement normal to the splitting cracks and contributes in resisting the splitting forces; σ_{trans} = average stress induced in the transverse reinforcement due to splitting stresses. Thus, to calculate the forces developed in the transverse reinforcing bars due to applying the forces in the

longitudinal direction, the average stresses in the transverse bar should be measured at the occurrence of splitting.

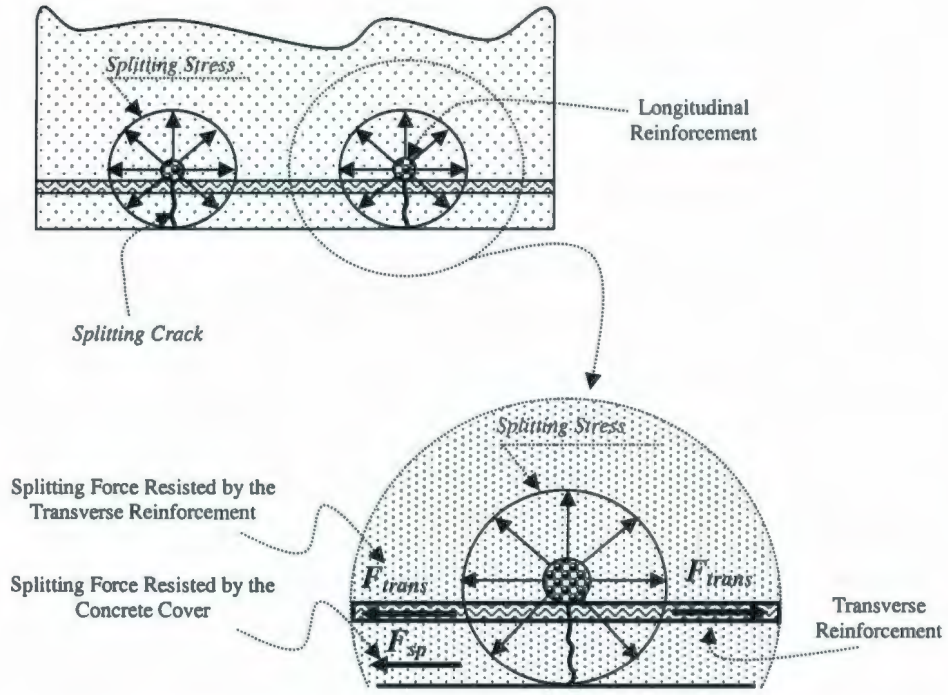

Fig. 6.9 Confinement Provided by the Transverse Reinforcing Bars

The manner in which the splitting stress resistance is shared between the concrete cover and the transverse reinforcement along the length of a member can be expected considering the equilibrium of forces shown in Fig. 6.9.

$$F_{spT} = F_{sp} + F_{trans} \tag{6.21}$$

where F_{spT} is total splitting force, F_{sp} and F_{trans} are the forces induced in the concrete section and the transverse reinforcing bars passing through the splitting crack, respectively. Substituting by the values of F_{sp} and F_{trans} in Equations 6.4 and 6.20, respectively, into Eq. 6.21:

$$F_{spT} = \int_{0}^{l_b} \int_{-\pi/2}^{\pi/2} f_{sp} \frac{d_b}{2} \cos\theta . d\theta . dl + \Sigma A_{trans}\, \sigma_{trans} \tag{6.22}$$

$$F_{spT} = f_{sp}\, d_b\, l + \Sigma A_{trans}\, \sigma_{trans} = F_{sp} + F_{trans} \tag{6.23}$$

Substituting by the value of the splitting force in Eq. (6.23) into Eq. (6.1), the value of the oblique angle (tan α) can be expressed as:

$$\tan\alpha = \frac{F_{sp} + F_{trans}}{F_l} \tag{6.24}$$

For the sake of simplicity, the experimental measurements are performed in the present experimental program to determine the average tensile stress induced in the transverse due to the splitting stress influences. Some strain gages are affixed to the transverse reinforcement to measure the value of the tensile strain induced in the transverse reinforcement due to the load application in the longitudinal direction for the various loading stages. These measured stresses induced in the transverse reinforcement at the splitting crack occurrence are found to be approximately (5-15) % of the yield stress of the reinforcing bars f_y. Thus, on average σ_{trans} can be assumed as 10% f_y.

To verify the confinement effect provided by the transverse reinforcement, the experimental program conducted by Hamad and Machaka, 1999 [105] is used in the present study. Table 6.4 presents a comparison between the experimental and predicted values of the bond splitting and steel stress at the splitting crack occurrence. It is quit clear that the transverse reinforcement enhance the splitting bond resistance of concrete; also there is a good agreement between the experimental and the predicted values for the bond strength and the steel stress at the splitting crack failure.

Table 6.4 Transverse Reinforcement confinement effect on the Splitting bond resistance

Specimen No.	f_c', MPa	$\tau_{sp(exp)}$, MPa	$f_{s(exp)}$, MPa	$\tau_{sp(cal)}$, MPa	$f_{s(tho)}$, MPa	$\tau_{sp(exp)}/\tau_{sp(cal)}$	$f_{s(ex)}/f_{s(cal)}$
C0S0*	46.7	7.14	348.6	6.40	312.45	1.12	1.12
C1S0*	51.4	7.87	384.2	7.06	344.71	1.12	1.11
C2S0*	65	8.98	438.1	8.06	393.72	1.15	1.11
C3S0*	65.1	10.11	493.2	9.08	443.52	1.12	1.12
C0S8*	92.8	6.44	314.3	5.78	282.25	1.12	1.13
C1S8*	75.9	7.48	365	6.71	327.85	1.14	1.13
C2S8*	80.2	8.16	398.3	7.33	358.01	1.11	1.12
C3S8*	75.6	8.98	438	8.07	393.83	1.13	1.12
C0S16*	85.6	5.16	252	4.62	225.84	1.11	1.13
C1S16*	98.4	8.84	285.2	7.21	352.21	1.22	0.81
C2S16*	96.2	8	390.6	8.30	405.07	0.96	0.97
C3S16*	81.3	8.99	438.5	8.93	436.11	1.01	1.05
Mean (μ) for (exp)/(cal)						1.102	1.067
Standard Deviation (σ) for (exp)/(cal)						0.064	0.0957
Coefficient of Variance (σ/μ) for (exp)/(cal) %						5.78	8.94

*Experimental Investigation Conducted by Hamad and Machaka, 1999 [105]

6.6 Tensile Strength of Reinforced Concrete Panels under Biaxial Loading

Most of the existing research work and design equations for estimating the tensile strength of concrete consider only the applied load in uniaxial direction and tend to ignore the influence of biaxial loading that is the case in some structures such as offshore oil platforms, liquefied natural gas structures and containment structures for nuclear power plants.

In attempts to understand how the cracking behavior will be influenced by applying the tension loads into two perpendicular directions, an extensive experimental program was conducted in the present study to investigate the cracking behavior of reinforced concrete

panels with different concrete strength under axial tension (uniaxial and/or biaxial) to provide a clear understanding of the response of cracked concrete. One of the main goals of the present study is to develop a design equation for the tensile strength of concrete subjected to biaxial loading condition, to be more robust and practical for such structures subjected to biaxial tension stresses. Fig. 6.10 shows the normal and splitting stresses distribution, as it is assumed that splitting stresses are uniformly distributed along the reinforcing bars.

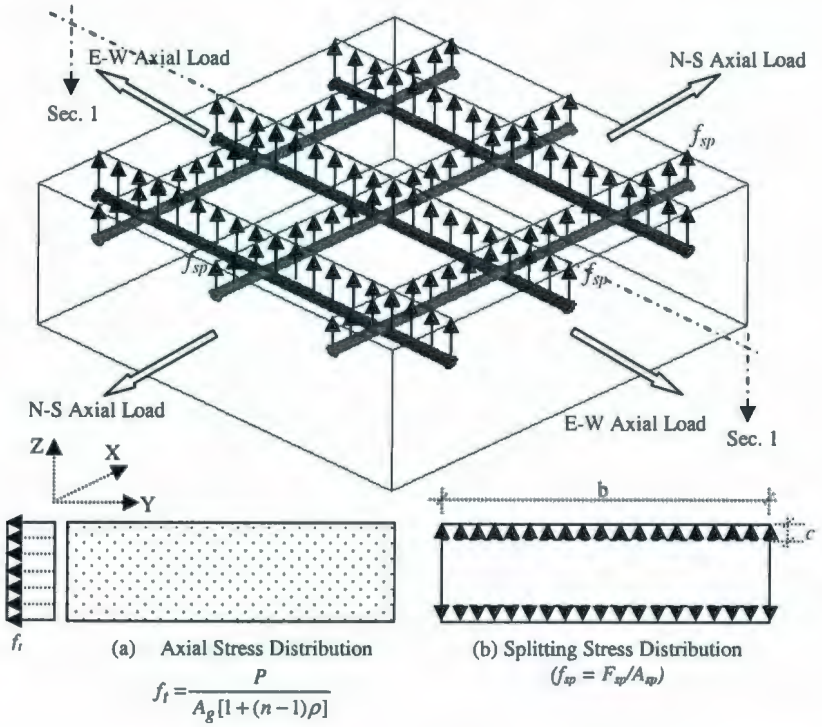

Fig. 6.10 Stress Distribution for a Specimen under Biaxial Loading

For the normal strength concrete specimens (Eq. 4.9), the average of the cracking stress is found to be related to the square root of the cylinder compression strength as:

$$f_t' = 0.34\sqrt{f_c'} \tag{6.25}$$

The cubic root of the compressive stress ($f_c^{1/3}$) provides a good representation of the tensile strength for the high strength concrete as shown in the following equation (Eq. 4.10):

$$f_t' = \beta \sqrt[3]{f_c'} \tag{6.26}$$

where, β is a coefficient ranging from (0.6 - 0.7).

However, for panels subjected to biaxial loading, beside the primary effect of axial stresses form the applied load in the longitudinal direction, there is an additional stress component effect due to the influence of the splitting forces radiating from the reinforcing bars running in the perpendicular direction, as shown in Fig. 6.10.

Based on the experimental results, it can be observed that applying the load in biaxial direction reduced the concrete cracking strength and cracking load. The tensile strength of concrete panel subjected to biaxial loading is found to be (95% – 85 %) of the tensile strength of the identical panel subjected to uniaxial loading condition, this effect is mainly due to the influence of splitting stress, as presented in Table 6.5.

The variation of the factor α_{trans}, that reflects the influence of the splitting stresses, is significantly influenced by the ratio of d_b/ρ_{eff}. The higher the value of d_b/ρ_{eff} ratio, the more influence for the splitting stresses is observed. For panel HS-B-20-2.5-6 subjected to biaxial loading with d_b/ρ_{eff}=100 cm, the splitting stresses causes a small reduction in the concrete cracking strength f_t', compared with the identical panel (H-U-20-2.5-6) under uniaxial loading, and hence the value of the factor α_{trans} is found to be equal to 0.955. However, panel HS-B-30-2.5-6 with d_b/ρ_{eff} ratio equal to 250 cm shows an obvious reduction in the cracking load and the cracking strength of concrete thanks to the splitting

stresses effect, and the value of α_{trans} is found to be equal to 0.86. Assuming a linear relationship between the factor α_{trans} and d_b/ρ_{eff} ratio, see Fig. 6.11, this relationship can be expressed as follows:

$$\alpha_{trans} = \begin{cases} -0.009\dfrac{d_b}{\rho_{eff}} + 1.09 & \dfrac{d_b}{\rho_{eff}} \geq 100 \ cm \\ 1.0 & \dfrac{d_b}{\rho_{eff}} < 100 \ cm \end{cases} \tag{27}$$

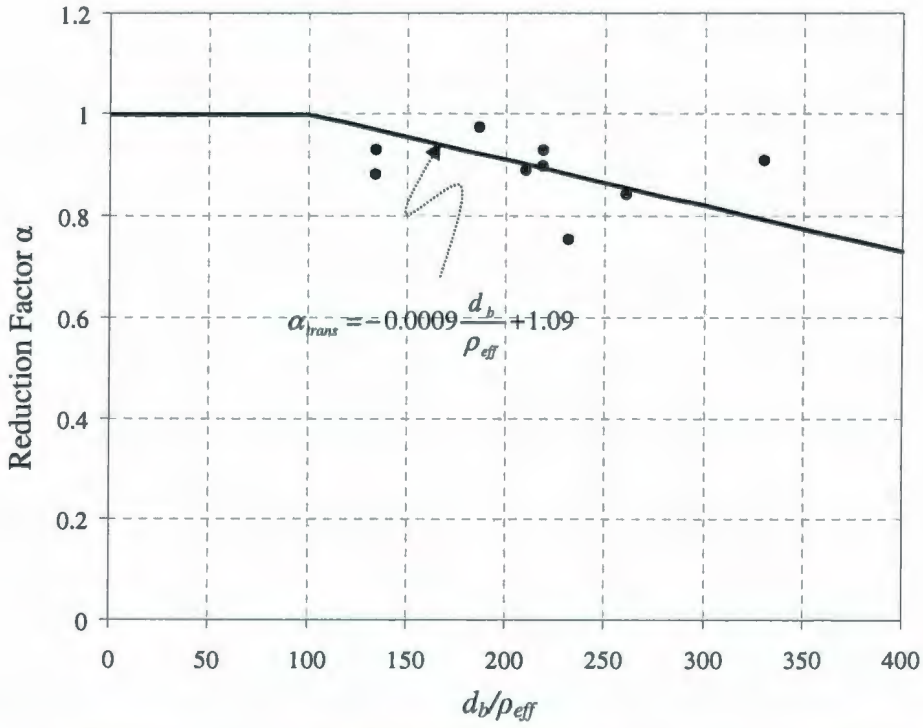

Fig.6.11 Relation between the Reduction factor α and the Bar Diameter d_b/ρ_{eff}

Thus, to account for the influence of splitting cracks on the tensile strength of the reinforced concrete panels, an additional factor α_{trans} is introduced into Eqs. (6.25) and (6.26), giving the following equations to calculate the value tensile strength for reinforced concrete members subjected to biaxial loading:

$$f_t' = 0.3397\,\alpha_{trans}\sqrt{f_c'} \quad \text{For normal strength concrete} \tag{6.28}$$

$$f_t' = \beta\,\alpha_{trans}\sqrt[3]{f_c'} \quad \text{For high strength concrete} \tag{6.29}$$

Validation of the model is based on data that is collected during the test program conducted in the present study, as well as the test data available in the literature [81], as presented in Table 6.5.

Table 6.5: Comparison of Tensile Strength between the Proposed Design Equations and the Experimental Results

S	Specimens Symbol	Specimens Dimensions (mm)	f_c', MPa	d_b/ρ_{eff} (cm)	Tensile Strength $f_{t(ex)}'$ (MP)	$f_{t(cal)}'$ Eq.28, 29 MPa	Tensile Strength Reduction %	$[f_{t(ex)}'-f_{t(cal)}']/f_{t(cal)}'$ %
1	NS-U-15-2.5-6*	600×600×190	40	125	2.1	2.15	8.5	2.4
2	NS-B-15-2.5-6*		35		1.92	1.96		2.3
3	HS-U-15-2.5-6*		90	125	3.2	3.15	15	2
4	HS-B-15-2.5-6*		75		2.72	2.88		5.5
5	HS-U-20-2.5-6*		75	166	3.1	2.95	4.5	4.5
6	HS-B-20-2.5-6*		75		2.96	2.78		6
7	HS-U-20-2.5-4*		80	200	3	3.01	10	0.6
8	HS-B-20-2.5-4*		70		2.7	2.78		2.8
9	HS-U-25-2.5-6*	900×900×260	75	210	2.71	2.74	12	1.2
10	HS-B-25-2.5-6*		65		2.36	2.35		0.2
11	HS-U-25-1.5-6*		75	210	2.7	2.74	9	1.5
12	HS-B-25-1.5-6*		70		2.46	2.41		2
13	HS-U-30-2.5-6*	900×900×380	65	250	2.45	2.61	14	6
14	HS-B-30-2.5-6*		65		2.1	2.26		7.6
15	CL-U-R1-1 **	1500×1500×380	44	330	1.98	1.96	8	1.5
16	CL-B-R1-1 **		44		1.65	1.78		7.8
17	CL-U-R2-1 **		46.2	230	1.9	2.05	25	8.5
18	CL-B-R2-1 **		43.4		1.4	1.8		28

* Current Experimental Program, ** Experimental Program Conducted by Cho et al., 2004 [81].

6.7 Numerical Example

Sample calculations using the proposed model for the bond stress are presented for the experimental program conducted by Abrishami and Mitchell, 1992 [26]. In this

experimental study, the bond stress versus slip response was studied, as well as, the investigation of both pull out and splitting failures.

The following numerical example shows the estimated and the measured value for the bond strength for specimen 35A.

Concrete compressive Strength $f_c^{'}$ = 25 MPa,

Bar diameter d_b = 35 mm

Specimen diameter = 150 mm

Specimen length = 300 mm

Based on the proposed model, the value of the bond stress for normal strength concrete can be estimated according to Eq. (6.21) as follows:

$$\tau_{sp} = 18.3 \frac{A_{sp}}{A_b}\left(\frac{C}{d_b} - \frac{1}{2}\right) f_t^{'} e^{-1.81\sqrt{\frac{C_c}{d_b}}}$$

$$\tau_{sp} = 18.3 \frac{57.5\times 300}{\pi\times 35\times 300}\left(\frac{75}{35} - \frac{1}{2}\right)\times 1.73\times e^{-1.81\sqrt{\frac{57.5}{35}}} = 2.67\,MPa$$

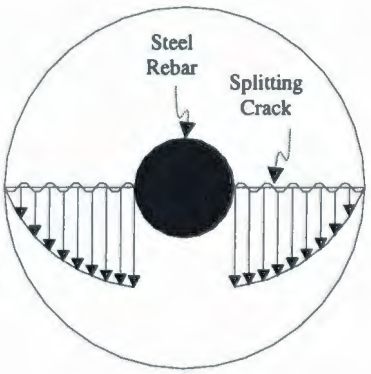

The value of the measured bond stress according to the experimental results was found equal to 3.0 MPa. Thus, the proposed model can be used as a simple and practical design equation to predict the expected value of splitting bond stress.

Using the same manner, the value of the bond stress for different specimens in that experimental program, can be estimated, considering the expected value for the bond stress f_b in Eq. (6.21), as shown in Table A-1.

Table 6.6 Experimental and Theoretical Values for Tensile Strength of Concrete

S	Specimen Symbol	Cylinder Diameter/Length mm/mm	d_b	Bond Stress $\tau_{sp(ex)}$ (MP)	$\tau_{sp(cal)}$ Eq.16 MPa	$[f'_{t(ex)}-f'_{t(cal)}]/f'_{t(cal)}$ %
1	35A	150/300	35	3.0	2.67	15
2	35B	200/300	35	3.6	3.46	7.7
3	30B	200/300	30	4.0	3.83	10.7
4	20A	150/300	20	4.2	4.10	5.1
5	20B	200/300	20	5.6	4.85	7.1
6	15C	200/100	16	5.3	4.70	8.1
		Mean (μ) for (exp)/(tho.)				1.09
		Standard Deviation (σ) for (exp)/(tho)				0.054
		Coefficient of Variance (σ/μ) for (exp)/(tho) %				4.93

6.8 Summary

A model to predict the effect of the splitting stresses, caused by bond action between the uncracked concrete and deformed bars, on the cracking behavior of orthogonally reinforced concrete panels subjected to in-plane axial stresses, is developed. This model considers the influence of confinement provided by the tensile strength of concrete cover and the transverse reinforcing bars perpendicular to the direction of splitting cracks propagation. Furthermore, this study is extended to provide design equations for evaluating the tensile strength of normal and high strength reinforced concrete thick plates subjected to biaxial tension loading condition, considering the secondary effect of the splitting stress on the cracking behavior of these members. The comparison between the predicated results of the concrete tensile strength and the corresponding measured data obtained experimentally reveals a favorable agreement.

Chapter 7

Estimate of Crack Spacing and Width

7.1 General Remarks

Cracking in reinforced concrete structures is unavoidable due to the low tensile strength of concrete. To provide a reasonable crack control, the concrete structures are designed based on the available equations and guidelines prescribed in various building codes. Most of the available expressions for crack spacing and width were developed for building structures of normal-strength concrete and normal concrete cover. However, most of the offshore structures are built using high-strength concrete with thick concrete cover as these structures are constantly exposed to harsh environmental conditions.

In the first part of this chapter, a practical and new analytical model that is capable of predicting the crack spacing of orthogonally reinforced concrete plate elements is developed. The major parameters influencing the cracking behavior of reinforced concrete members, such as the tensile strength of concrete, reinforcement ratio, bar diameter and spacing in both longitudinal and transverse directions, are also considered. A reinforced concrete plate element is studied using equilibrium and compatibility equations to formulate the average stresses of steel and concrete. A series of verification comparisons with the experimental investigation conducted in this study, as well as the previous experimental work that involved various types of structural elements and loading conditions, are performed to measure the validity and reliability of the model.

The second part of this chapter investigates the cracking behavior of several thick high strength reinforced concrete plates. The experimental results raise questions about the variations in the crack widths that propagate in the transverse direction. An analytical model is proposed for estimating the variations in the primary crack opening along the length of the crack that occurs in thick high strength reinforced concrete panels subjected to axial loading. The main objective of this investigation is to provide a theoretical estimate for the crack width due to axial loading, and also ways to ensure the control of crack openings in designing thick high strength reinforced concrete structures subjected to in-plane axial stresses. The main objective is then extended to investigate the effects of factors that primarily have a profound influence on the expected value of crack widths, such as spacing between the reinforcing bars, and the concrete cover.

7.2 Analytical Model Formulation for the Crack Spacing

For a reinforced concrete member that is subjected to axial force or a bending moment; the member is free from cracks as long as the stress in the concrete never exceeds its tensile strength. When the tensile strength in concrete is exceeded, primary cracks are formed in a region of maximum tensile stresses when the external loads reach the cracking load. At the location of a crack, the tensile stress is assumed to be resisted completely by the reinforcement, where the concrete stress is zero at the crack location.

When a segment of reinforced concrete panel is subjected to axial tension loading that is greater than the cracking load P_{cr}, as illustrated in Fig. 7.1(a), the idealized cracked panel is assumed to consist of the effective tensile area of concrete A_{ct}, and reinforcing steel

area A_{st}. In a section situated between two cracks, the bond between the concrete and reinforcing bars restrains the elongation of the steel and the compatibility between the reinforcing bars and the surrounding concrete is assumed, thus, a part of the tensile force in the reinforcement at the crack is transmitted to the concrete situated between the cracks.

The equilibrium of a segment of the longitudinal chord representing the tensile zone between two consecutive cracks subjected to an axial tensile force P is studied; the length of the segment S represents the crack spacing.

The free body diagrams of the steel reinforcement and concrete elements are shown in Fig. 7.1(b). The equilibrium for the free body of differential steel of length dx is:

$$F_s + \tau_b (\pi \phi_1 \, dx) = F_s + dF_s \tag{7.1}$$

$$\frac{dF_s}{dx} = \pi \phi_1 \tau_b$$

$$\frac{d\sigma_s}{dx} = \frac{\pi \phi_1 \tau_b}{\pi \phi_1^2 / 4} = \frac{4\tau_b}{\phi_1} \tag{7.2}$$

Fig. 7(c) shows a part of the concrete panel and the layout of the reinforcement in the directions X and Y. As a result of presence of the reinforcement in two perpendicular directions, and considering the a firm connection between the longitudinal and transverse reinforcements, when the load is applied in the longitudinal direction, the bars in the longitudinal bars are stretched and concrete bond mechanism in the longitudinal direction is considered plus the contribution of the transverse bars in the perpendicular direction through the assumed bearing against the surrounding concrete (Desayi and Kulkarni, 1976) [106].

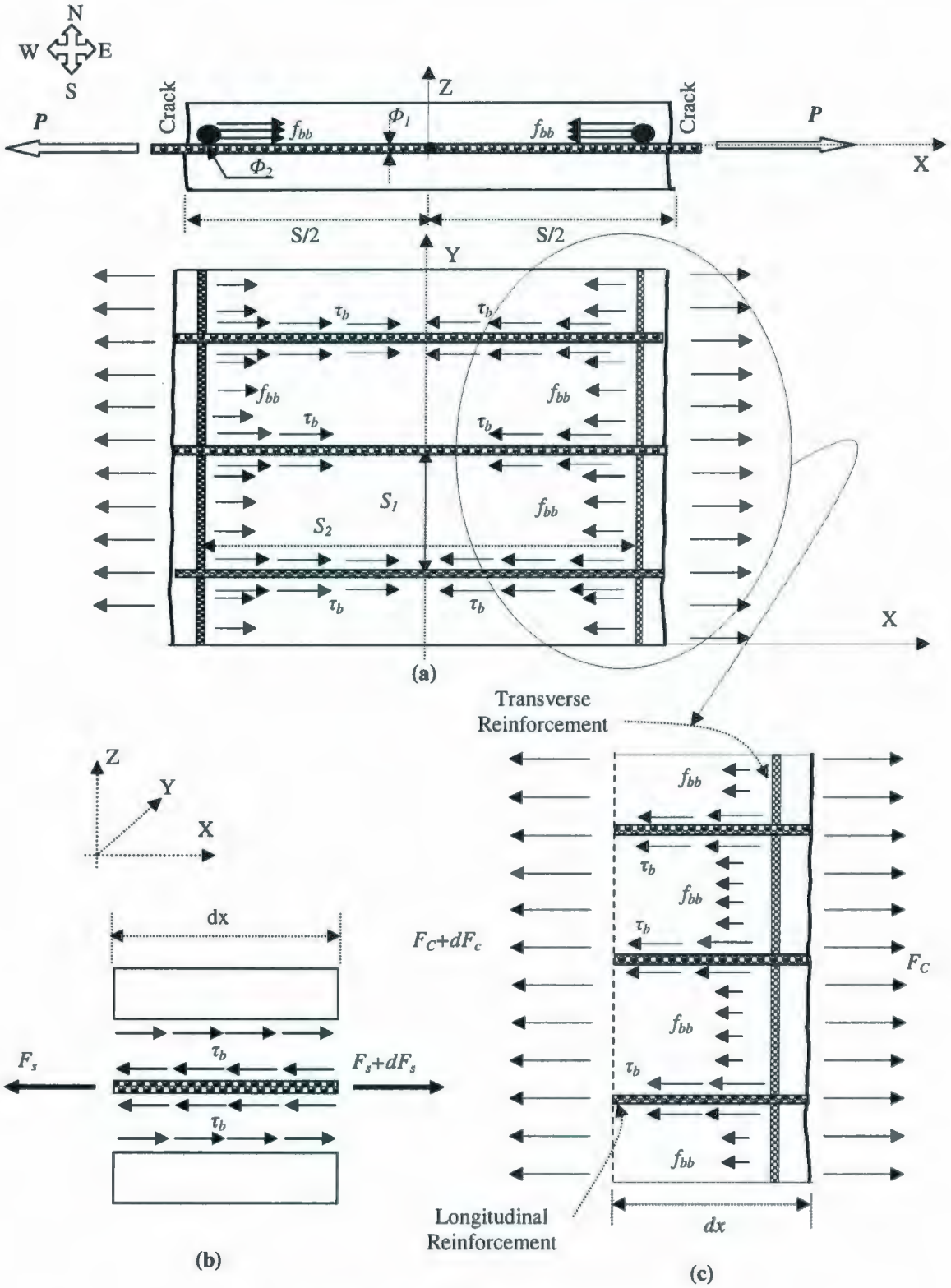

Fig.7.1 Free Body Diagram for a Cracked Member

The crack will form over in the transverse direction, when both of the bond force and the bearing force of the transverse bars exceeds the maximum tensile capacity of concrete. The crack is located at a distance $X=S$ (the spacing between cracks). Considering uniform stress distribution along the concrete cross section (Desayi and Kulkarni, 1976) [106], the equilibrium of forces acting on the concrete segment can be written as follows:

$$F_c = F_c + dF_c + (\pi \phi_1 \, dx)\tau_b + f_{bb}\,\phi_2 \frac{S_1}{S_2} dx \tag{7.3}$$

$$\frac{dF_c}{dx} = -[(\pi \phi_1 \, dx)\tau_b + \phi_2 \frac{S_1}{S_2} f_{bb}] \tag{7.4}$$

$$\frac{d\sigma_c}{dx} = -[\frac{(\pi \phi_1)}{A_{ct}}\tau_b + \frac{S_1 \phi_2}{S_2 A_{ct}} f_{bb}]$$

$$\frac{d\sigma_c}{dx} = -[\frac{4\rho_{eff}}{\phi_1}\tau_b + \frac{S_1 \phi_2}{S_2 A_{ct}} f_{bb}] \tag{7.5}$$

$$d\sigma_c = -[\frac{4\rho_{eff}}{\phi_1}\tau_b .dx + \frac{S_1 \phi_2}{S_2 A_{ct}} f_{bb} .dx] \tag{7.6}$$

where f_{bb} is the bearing stress due to the presence of the transverse reinforcement extended in Y-direction, τ_b is the bond stress at steel-concrete interface, ρ_{eff} is the effective reinforcement ratio (ratio of the tensile reinforcement area to the area of the effective concrete in tension), $\emptyset_1$ is the longitudinal bar diameter, $\emptyset_2$ is the transverse bar diameter, S_1 is the longitudinal bar spacing, and S_2 is the transverse bar spacing. For simplicity, it is assumed that on average, this bearing stress f_{bb} on all bars placed in both directions X and Y is half of the tensile strength concrete (Desayi and Kulkarni, 1976) [106].

Gilbert, 2006; 2008 [70, 71] proposed that $\tau_b = \alpha_1 \alpha_2 f_t'$, where α_1 depends on the steel stress at the crack (and varies from 3.0 at low stress levels to 1.0 at high stress levels); and where $\alpha_2 = 1.0$ for short-term calculations and $\alpha_2 = 0.5$ for long-term calculations. Short-term calculations are considered is the present investigation to study the cracking response of the concrete plates. For short-term calculations, the bond stress $\tau_b = (2.2\sim2.5)$ f_t'. Concrete tensile stresses σ_c in Eq. 7.6 cannot be greater than the direct tensile strength f_t', so the requirement should be satisfied for the maximum crack spacing $S = S_{max}$, which will occur when the concrete stress $\sigma_c = f_t'$ as presented in the following equations:

$$\begin{aligned}\sigma_c &= -[\int_{x=S/2}^{x=0} \frac{4\tau_b \rho_{eff}}{\phi_1} dx + \int_{x=S/2}^{x=0} \frac{f_{bb} \phi_2 S_1}{A_{ct} S_2} dx] \le f_t' \\ &= [\frac{4\tau_b \rho_{eff}}{\phi_1}(\frac{S}{2}) + \frac{f_{bb} \phi_2 S_1}{A_{ct} S_2}(\frac{S}{2})] \le f_t'\end{aligned} \tag{7.7}$$

Therefore, the maximum crack spacing in a fully developed pattern may be expressed as:

$$S_{max} = f_t' / [\frac{2\tau_b \rho_{eff}}{\phi_1} + \frac{f_{bb} \phi_2 S_1}{2 A_{ct} S_2}] \tag{7.8}$$

As loading is increased, additional cracks will form and the number of cracks will be stabilized when the stress in the concrete no longer exceeds its tensile strength at further locations regardless of load increase. This condition basically produces the absolute minimum crack spacing that can occur at high steel stresses; termed here as stabilized crack spacing Gilbert, 2006 [70]. In this research, the stabilized crack spacing is assumed to be expressed as:

$$S_m = \lambda S_{max} = \lambda f_t' / [\frac{2\tau_b \rho_{eff}}{\phi_1} + \frac{f_{bb} \phi_2 S_1}{2 A_{ct} S_2}] \tag{7.9}$$

where λ is a factor that represents the ratio between the stabilized crack spacing at high steel stress value and the maximum crack spacing at the primary crack formation stage and it is assumed to be equal to 0.67 (Marti et al., 1997) [107, 108].

The proposed model presented in Eq. (7.9) takes the effect of transverse steel reinforcement bar diameter, and the bar spacing in both perpendicular directions into account.

7.3 Comparison with Experimental Results

A series of verification tests, involving various types of structural elements and loading conditions, is conducted to measure the reliability of the model. The selection of the test series was based so that the test must allow the verification of the model in various loading conditions for thick normal and high strength concrete structures that is the case for offshore and nuclear power plants structures. The selected tests involve direct tension tests conducted in the present research as well as the previous experimental work conducted by Rizkalla et al., 1984 [61, 62]. Also, the accuracy of the model is verified using laterally loaded thick slabs experimental data conducted by Hossin and Marzouk, 2006 [109].

7.3.1 Direct Tension Tests

Table 7.1 shows a comparison of the average crack spacing of thick plates tested in the present study, between the results of the experimental work and the analytical model proposed in Eq. (7.9) next to the previously proposed equations in Eq.(2.7); (2.9); and

(2.10) proposed by Leonhardt, 1977 [67]; Beeby, 1972 [68]; and Rizkalla et al., 1984 [61], respectively. Statistical comparison study is presented in Table 7.1 between the proposed model in Eq. (7.9) and the previously developed model by Beeby, Leonhard, and Rizkalla, at the stabilized crack pattern.

Furthermore, the proposed Eq. (7.9) is used to predict the value of the crack spacing for previous experimental work on uniaxially loaded slabs conducted by Rizkalla et al., 1983; 1984 [61, 62], as presented in Table 7.2.

Table 7.1: Measured and Calculated Average Crack Spacing of Reinforced Concrete Plates under Axial Loading, (Current Experimental Investigation)

Specimen Serial	Specimen Number	Measured Average Crack spacing (mm)	Beeby S_b Equation (mm)	Leonhard S_L Equation (mm)	Rizkalla Equation (mm)	Proposed Model S (mm)
1	NS-U-15-2.5-6	151	139.9	203.3	178.9	155.9
2	NS-B1-15-2.5-6	144	139.9	186.1	178.9	148.5
3	HS-U-15-2.5-6	152	139.9	238.9	178.9	166.9
4	HS-B1-15-2.5-6	151	139.9	211.9	178.9	157
5	HS-U-20-2.5-6	150	133.2	172	197.2	156.6
6	HS-B1-20-2.5-6	148	133.2	159.5	197.2	147.2
7	HS-U-20-2.5-4	240	186.5	268.3	261.2	250
8	HS-B1-20-2.5-4	275	186.3	245.3	261.2	265
9	HS-U-25-2.5-6	270	233.2	318.8	322.2	310
10	HS-B1-25-2.5-6	290	233.2	288.5	322.2	320
11	HS-U-25-1.5-6	240	200	304.8	289	260
12	HS-B1-25-1.5-6	285	200	293.8	289	275
13	HS-U-30-2.5-6	290	279.8	369.2	393.8	340
14	HS-B1-30-2.5-6	305	279.8	339.6	393.8	310
15	HS-U-30-1.5-6	230	239.9	357.5	353.9	300
16	HS-B2-25-2.5-6	290	233.2	277.5	322.2	286.9
17	HS-B3-25-2.5-6	295	233.2	270.4	322.2	286.9
18	HS-B4-25-2.5-6	300	233.2	270	322.2	286.9
Mean (μ) for $S_{m(ex)}/S_{m(tho.)}$			1.176	0.881	0.849	0.967
Standard Deviation (σ^2) for $S_{m(ex)}/S_{m(tho)}$			0.138	0.154	0.097	0.07
Coefficient of Variance (σ^2/μ) for $S_{m(ex)}/S_{m(tho)}$			11.7%	17.5%	11.4%	7.2%

Table 7.2: Measured and Calculated Average Crack Spacing of Reinforced Concrete Plates under Axial Loading (Rizkalla et al., 1984 [61])

Specimen Serial	Specimen Number	Measured Average Crack spacing (mm)	Beeby S_b Equation (mm)	Leonhard S_L Equation (mm)	Rizkalla Equation (mm)	Proposed Model S (mm)
1**	Slab #1	96.01	86.9	142.8	102.36	96.91
2**	Slab #2	103.89	86.9	139.2	99.31	123.3
3**	Slab #3	137.16	112.3	163.6	131.32	121.2
4**	Slab #4	101.85	112.3	162.1	129.54	111
5**	Slab #5	155.7	112.3	162.6	126.24	112.5
6**	Slab #6	129.79	112.3	162.1	126.49	116.8
7**	Slab #7	123.7	112.3	162.1	123.19	133.3
Mean (μ) for $S_{m(ex)}/S_{m(tho.)}$			1.153	0.772	1.011	1.00
Standard Deviation (σ^2) for $S_{m(ex)}/S_{m(tho)}$			0.145	0.109	0.134	0.11
Coefficient of Variance (σ^2/μ) for $S_{m(ex)}/S_{m(tho)}$ %			12.6	14.1	13.3	11.0

** Experimental Program Conducted by Rizkalla et al, 1984 [61].

This is to ensure the suitability of the proposed model for evaluating the value of the average crack spacing for both thick and thin reinforced concrete members under axial loading conditions.

7.3.2 Reinforced Thick Reinforced Concrete Members under Punching Load [109]

A series of two-way reinforced thick concrete slabs were tested under punching load by Hossin and Marzouk, 2006 [109]. This experimental testing program was designed to examine the influence of the concrete cover and bar spacing of normal and high strength concrete on the cracking behavior. A total of eight concrete slabs were tested. Five high strength concrete slabs (HSC) and three normal strength concrete slabs (NSC) were

selected for the experimental investigation of the cracking behavior study as presented by slabs 1 through 8 as shown in Table 7.3. The variables considered in that experimental investigation were the concrete cover, slab thickness, and bar spacing for normal- and high-strength concrete. The selected dimensions for the experimental testing were typical of those for possible use in Canadian offshore applications.

Table 7.3: Measured and Calculated Average Crack Spacing of Reinforced Concrete Members Loaded laterally (Hossin and Marzouk, 2006 [109]).

Specimen Serial	Specimen Number	Measured Average Crack spacing (mm)	Beeby S_b Equation (mm)	Leonhard S_L Equation (mm)	Rizkalla Equation (mm)	Proposed Model S (mm)
1*	Slab NSC1	134	99.52	161.56	188.52	121
2*	Slab NSC2	223	173.82	218.42	212.82	235.3
3*	Slab NSC3	239	221.2	275.48	235.2	252.2
4*	Slab HSC1	171	126.12	172.7	215.12	142.1
5*	Slab HSC2	185	139.42	174.19	228.42	154.2
6*	Slab HSC3	163	119.47	204.71	208.47	161.4
7*	Slab HSC4	172	139.26	243.18	228.26	165.5
8*	Slab HSC5	120	96.15	184.12	135.15	112.3
Mean (μ) for $S_{m(ex)}/S_{m(tho.)}$			1.28	0.86	0.85	1.02
Standard Deviation (σ^2) for $S_{m(ex)}/S_{m(tho)}$			0.094	0.149	0.123	0.06
Coefficient of Variance (σ^2/μ) for $S_{m(ex)}/S_{m(tho)}$			0.073	0.172	0.145	0.059

*Experimental Program Conducted by Hossin and Marzouk, 2006 [105]

Tables 7.1 through 7.3 show a comparison between the proposed model in Eq. (7.9) versus different approaches for calculating crack spacing of reinforced concrete structures. This is to check the suitability of such expressions for evaluating the crack spacing of offshore structures that require using high strength concrete sections and thick concrete covers.

Based on the comparisons presented in Tables 7.1 through 7.3, the model proposed by Leonhardt in Eq. (2.6) overestimates the value of the crack spacing. However, the approach suggested by Beeby in Eq. (2.8) underestimates the value of the crack spacing when it is compared with the experimental results. Thus, it might be concluded that neither of these two expressions is accurate enough to predict the value of the crack spacing of the offshore structures that include the presence of transverse reinforcement and a thick concrete cover. The model recommended by Rizkalla et al., 1984 [61] in Eq. (2.10) offers reasonable results as the reinforced structures have a small bar diameter, such as 10 mm and 15 mm. However, when a higher bar diameter, such as 20, 25, 30 mm is used, the model starts to overestimate the value of the crack spacing, since the first part in Eq. (2.10) $[5(d_b - 7.2)]$ is sensitive to the effect of increasing the bar diameter. The equation is very sensitive to the effect of the bar diameter. Thus, when a higher bar diameter is used, the final value of the crack spacing is relatively high in comparison to the experimental value. For all of the studied cases, the proposed model in Eq. (7.9) in this study has a satisfactory performance as it is compared with the measured crack spacing.

7.3.3 Comparison of Experimental versus Different Codes Approach for Crack Spacing

One of the main objectives for this investigation is to check the applicability of the various approaches in the different code provisions for calculating the value of crack spacing, by comparing the calculated value of the crack spacing according to different

code equations and the proposed model with the experimental results for various concrete members. The test results will be evaluated with regards to available codes, such as: Canadian offshore CSA code S474 (CSA-04) [74], Norwegian Code 3473E (NS-92) [75], European Committee for Standardization Eurocode 2 (EC2-2004) [76], ACI Committee 318-01 [73] and the European CEB-FIP model code (CEB- 90) [44]. The average crack spacing measured at each experiment is considered and presented in Tables 7.4 through 7.6 along with numerical estimations of other international codes.

Table 7.4: Measured and Calculated Average Crack Spacing, (Current Experimental Investigation)

Specimen Serial	Specimen Number	Measured Average Crack spacing (mm)	CSA (mm)	NS (mm)	EC2 (mm)	CEB-FIP (mm)	ACI (mm)	Proposed Model S (mm)
1	NS-U-15-2.5-6	151	230	230	285	230	212	155.9
2	NS-B1-15-2.5-6	144	230	230	285	230	212	148.5
3	HS-U-15-2.5-6	152	230	230	285	230	212	166.9
4	HS-B1-15-2.5-6	151	230	230	285	230	212	157
5	HS-U-20-2.5-6	150	230	230	280	185	250	156.6
6	HS-B1-20-2.5-6	148	230	230	280	185	250	147.2
7	HS-U-20-2.5-4	240	325	325	480	305	360	250
8	HS-B1-20-2.5-4	275	325	325	480	305	360	265
9	HS-U-25-2.5-6	270	390	390	515	385	390	310
10	HS-B1-25-2.5-6	290	390	390	515	385	390	320
11	HS-U-25-1.5-6	240	340	340	450	345	335	260
12	HS-B1-25-1.5-6	285	340	340	450	345	335	275
13	HS-U-30-2.5-6	290	460	460	635	460	424	340
14	HS-B1-30-2.5-6	305	460	460	635	460	424	310
15	HS-U-30-1.5-6	230	400	400	475	355	350	300
16	HS-B2-25-2.5-6	290	400	400	475	355	350	286.9
17	HS-B3-25-2.5-6	295	400	400	475	355	350	286.9
18	HS-B4-25-2.5-6	300	400	400	475	355	350	286.9

Table 7.5: Measured and Calculated Average Crack Spacing, (Rizkalla et al., 1984 [61])

Specimen Serial	Specimen Number	Measured Average Crack spacing (mm)	CSA (mm)	NS (mm)	EC2 (mm)	CEB-FIP (mm)	ACI (mm)	Proposed Model S (mm)
1	Slab #1	96.01	92.26	89.39	119	88.9	122.7	96.91
2	Slab #2	103.89	92.62	89.39	119	88.9	122.7	123.3
3	Slab #3	137.16	130.4	127.5	211.7	125.9	188.5	121.2
4	Slab #4	101.85	130.4	127.5	211.7	125.9	188.5	111
5	Slab #5	155.7	130.4	127.5	211.7	125.9	188.5	112.5
6	Slab #6	129.79	130.6	127.5	211.7	125.9	188.5	116.8
7	Slab #7	123.7	130.6	127.5	211.7	125.9	188.5	133.3

Table 7.6: Measured and Calculated Average Crack Spacing, (Hossin and Marzouk, 2006 [109])

Specimen Serial	Specimen Number	Measured Average Crack spacing (mm)	CSA (mm)	NS (mm)	EC2 (mm)	CEB-FIP (mm)	ACI (mm)	Proposed Model S (mm)
1	Slab NSC1	134	127	127	93	78.2	192	121
2	Slab NSC2	223	203	203	163	189.8	268.3	235.3
3	Slab NSC3	239	223	223	195	143.3	264	252.2
4	Slab HSC1	171	167	167	137	69.3	250	142.1
5	Slab HSC2	185	187	187	118	67.6	283	154.2
6	Slab HSC3	163	148	148	109	109.5	233.2	161.4
7	Slab HSC4	172	170	170	123	130.9	277.3	165.5
8	Slab HSC5	120	139	139	111	83.3	156.2	112.3

Tables 7.4 through 7.6 show that both CSA and NS code approaches for calculating the crack spacing fail to take the effect of the transverse reinforcement into consideration, and that is the reason for giving the same value for crack spacing for some slabs with different transverse bar spacing.

With regards to the EC2 code, in spite of its simplicity in calculating the value of the crack spacing, it is obvious in Table 7.4 that this code equation overestimates the calculated value for the crack spacing when using a thick concrete cover of 50~60 mm for offshore structures.

The CEB-FIP code equation gives reasonable values for both pure tension and flexural specimens with a normal concrete cover of 20~35 mm. However, for specimens with thick concrete covers, the CEB-FIP equation overestimates the value of the crack spacing where the effect of the concrete thick cover is not taken into consideration, as shown in Tables 7.4 and 7.5.

In general, the calculated average crack spacing is higher than the actual test results for the HSC plates with thick concrete cover, and as both the concrete cover and bar spacing increase, the crack spacing increases theoretically and experimentally. All of the previous code equations ignore the effect of the transverse reinforcement on the cracking behavior of the reinforced concrete structures.

7.4 Crack Width Model for Thick Reinforced Concrete Plates

The use of thicker concrete covers has been increasing due to durability concerns, where the durability of reinforced concrete is of prime interest in the designing of offshore structures and containment structures for nuclear power plants. The question arises whether current design provisions for evaluating the crack width applicable for thick concrete structures subjected to in plane axial stresses. This study develops a model for evaluating crack widths for thick reinforced concrete plates subjected to axial loading.

The calculation procedure is supported by an evaluation of existing test data. Based on this procedure, analyses that investigate the primary crack width variation along its length are conducted, as well as parameters necessary to control the primary crack opening under the serviceability limit. Meanwhile, the available codes such as the Canadian Standards Association (CSA) offshore code CSA-S474-04 (CSA-2004) [74], Norwegian Council for Building Standardization code 3473E (NS-1992) [75], the European committee for standardization Eurocode 2 (EC2-2004) [76], ACI Committee 224R-01 [73], and the Comité Euro-Internationale du Béton et Fédération Internationale de la Précontrainte model code MC 90 (CEB-FIP 1990) [44], are used to evaluate the average crack width for thick concrete plates compared with the measured experimental results.

7.4.1 Crack Width Variations

Most of the existing design equations for predicting crack width evaluate the average or maximum value as a function of the average crack width, ignoring the variations in the crack opening along the length of the crack. Crack width variations reflect the need to adjust the spacing between the longitudinal reinforcing bars and concrete cover thickness, so as to provide proper cracking control of reinforced concrete structures.

Based on the experimental results conducted in the present research, the minimum value of the crack opening for a primary crack is obtained over the location of the longitudinal bars. The width of the crack that propagates perpendicular to the principal stress direction increases with increasing the distance from the longitudinal reinforcing bars until it reaches its maximum value at the mid-distance between the longitudinal bars, as shown

in Fig. 7.2. The measured maximum and minimum crack widths, as illustrated in Fig. 7.2 for a typical panel, are compared to the average crack width for each panel in the experimental program conducted in this study for the various levels of steel stresses. The ratios of w_{max}/w_{ave} and w_{min}/w_{ave} are found to be approximately 0.7 and 1.3, respectively, as shown in Fig. 7.3. These values emphasize the nature of the variation of the crack opening along the primary cracks and introduce the range within which the prediction of the crack width could be acceptable for reinforced concrete thick plates subjected to axial loading. Thus, the measured maximum value of the crack opening at the mid-distance between the longitudinal bars reaches approximately 1.3 of the average crack width, however, the minimum value of the crack width over the bar location is approximately 0.7 of the average crack width.

Expressing the variation of the crack opening along the length of the crack, factor ξ_x is introduced into the equation for calculating the value of the average crack width. Thus, a relevant crack model that allows the calculating of the crack width at any location along the length of the crack of reinforced concrete panels subjected to axial loading is provided, so that it is possible to construct a profile for the primary crack. Measuring the value of the crack opening at different locations reveals that the exponential equation is the best function for simulating crack width variations at different locations from the longitudinal bar reinforcement, as shown in Fig. 7.2. Thus, the value of ξ_x can be expressed as shown in the following equation:

$$\xi_x = Ae^{-Bx^2} \tag{7.10}$$

Figure 7.2 shows that can be expressed as follows:

$$\tan\theta = \frac{S_b - 2x}{2C}, \text{ then } x = \frac{S_b}{2} - C\tan\theta \tag{7.11}$$

Substituting by the value of x in Eqs (7.11) into Eq. (7.10), the value of ξ_x can be expressed as:

$$\xi_x = Ae^{-B\left(C\tan\theta - \frac{S_b}{2}\right)^2} \tag{7.12}$$

where C is the concrete cover; and S_b is the spacing between the reinforcing bars.

Calibrated experimentally, consider that the boundary conditions control the primary crack width profile, as follows:

At x = 0, tan ϴ = S_b/2C and ξ_x = 1.3 (7.13)

At x = S_b/2, tan ϴ = 0 and ξ_x = 0. 7 (7.14)

Substituting the boundary conditions presented in Eqs. (7.13) and (7.14) into Eq. (7.12), the values of A and B can be expressed as:

$$A = 1.3,\ B = \frac{2.5}{S_b^2} \tag{7.15}$$

Thus,

$$\xi_x = 1.3e^{-\frac{2.5}{S_b^2}\left(C\tan\theta - \frac{S_b}{2}\right)^2} \tag{7.16}$$

Fig. 7.4 presents the variations in the value of ξ_x by changing the distance from the longitudinal bar. It also shows the expected variations in the crack width along its length, where the crack width reaches its maximum and minimum values at mid-distance between the adjacent reinforcing bars, and over the center line of the longitudinal reinforcement, respectively.

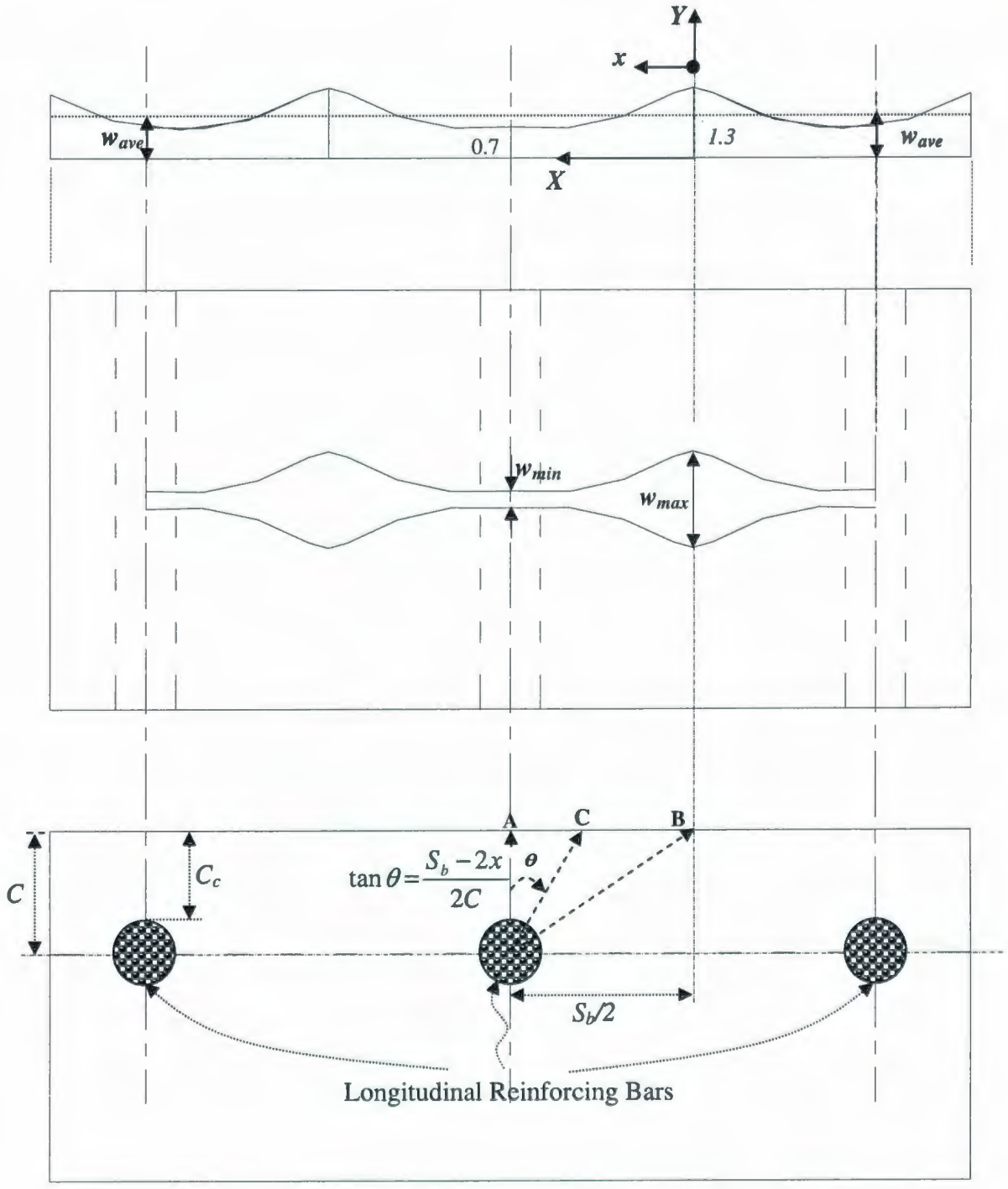

Fig. 7.2 Crack Width Variation between Adjacent Reinforcing Bars

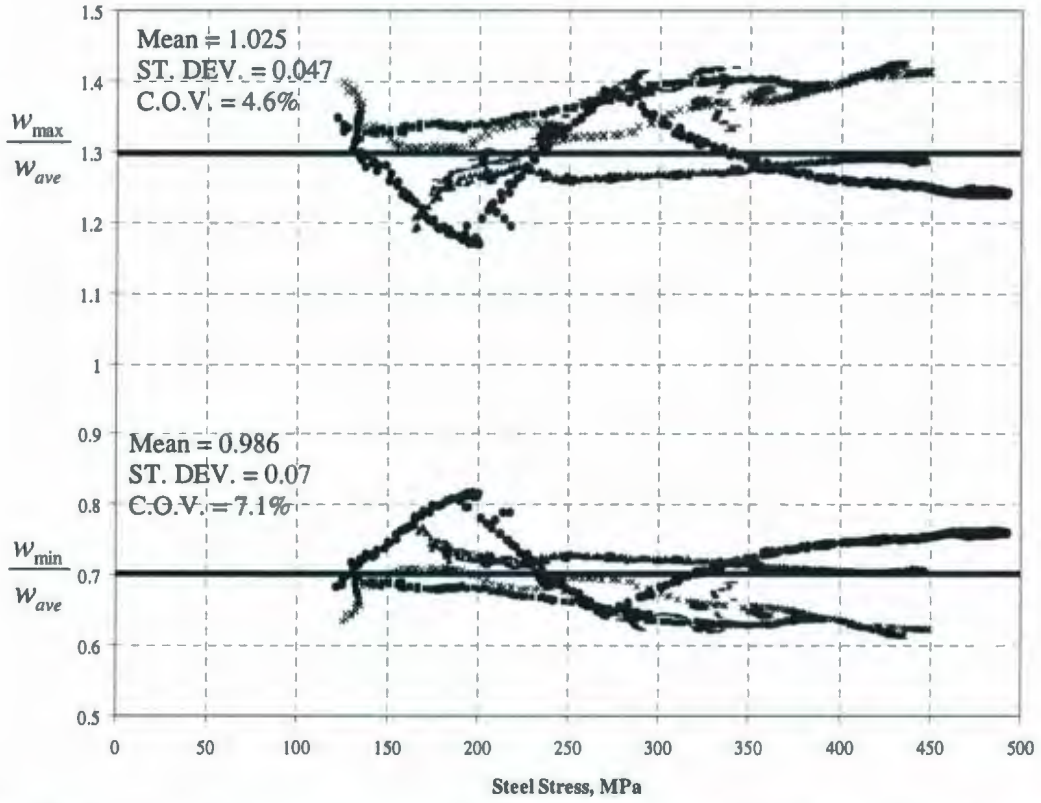

Fig. 7.3 Comparison between Maximum, Minimum, and Average Measured Crack Width

The average crack width can be estimated by the following expression in Eq. (7.17) for the crack runs in a direction that is perpendicular to the main reinforcement in members subjected to an axial force. In this equation, it is assumed that the elongation of the concrete between two adjacent cracks is small enough to be neglected as it is compared with the elongation of the reinforcing bars. Then, the average crack width can be evaluated by the following equation:

$$w_m = S_m \varepsilon_{sm} \tag{7.17}$$

where S_m is the average spacing between cracks; ε_{sm} is the average increase in the strain of the reinforcement relative to the adjacent concrete.

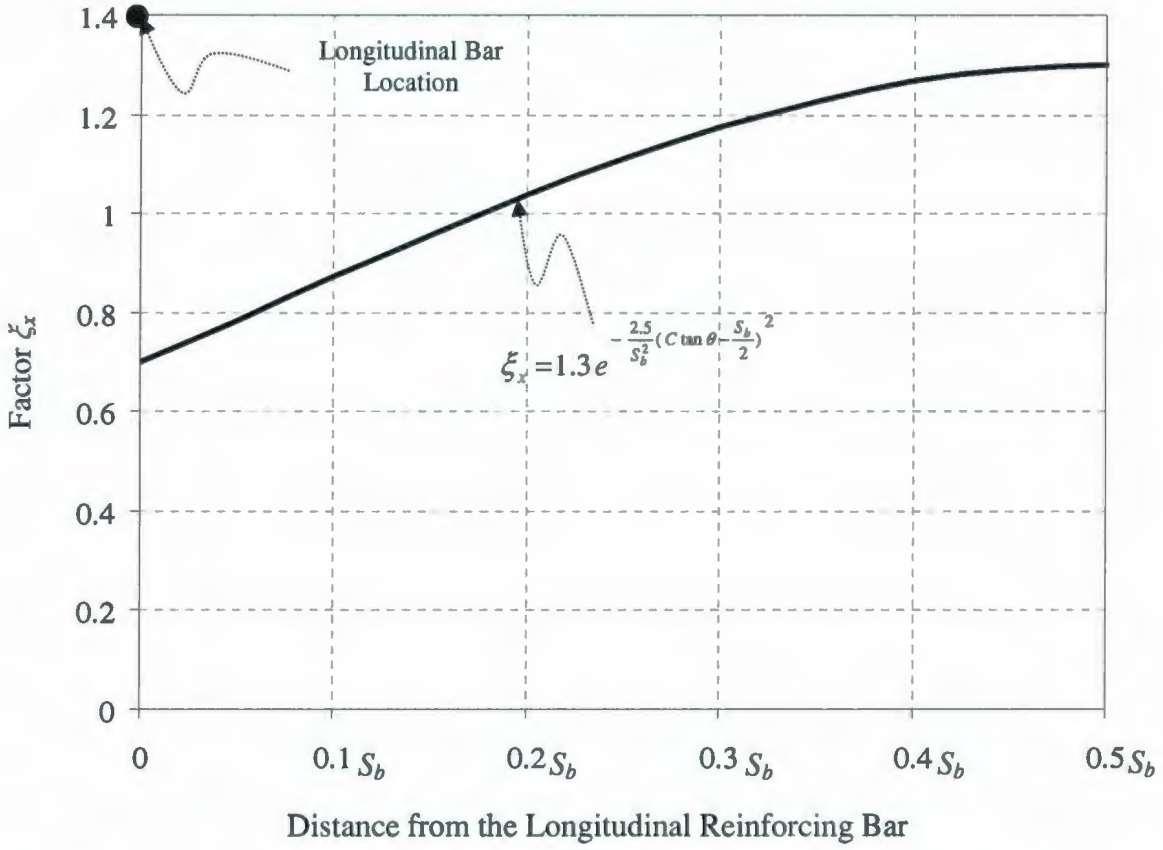

Fig. 7.4 Values of ξ_x at Varies Distance from the Longitudinal Reinforcing Bar

To determine the local value of the crack opening over the length of the crack between the longitudinal reinforcing bars in a concrete member subjected to axial loading conditions, it is necessary to consider the factor ξ_x, as it reflects the effect of the longitudinal reinforcing bar on the values of the crack width. Thus, the value of the local crack width at any location along the length of the crack can be expressed as:

$$w_x = \xi_x S_m \varepsilon_{sm} \tag{7.18}$$

The average crack width w_m is equal to the average crack spacing S_m, which can be evaluated based on Eq. (7.9), times the average increase in strain of reinforcement

relative to the adjacent concrete (ε_{sm}). The average strain increase in steel can be estimated as follows:

$$\varepsilon_{sm} = \zeta \, \varepsilon_{s2} \tag{7.19}$$

$$\zeta = [1 - \beta_1 \beta_2 (\frac{\sigma_{sr}}{\sigma_{s2}})^2] \tag{7.20}$$

where ε_{s2} is the calculated strain in the steel calculated for a transformed section in which the concrete in tension is ignored (state 2) and neglecting the contribution of concrete tension stiffening. Variable ζ is a strain reduction factor to allow for the tension stiffening effect of the concrete. Variables σ_{s2} and σ_{sr} are the steel stresses in a cracked section under the applied load and at initial crack formation, respectively. Variable β_1 is a factor characterizing the bond quality of the steel (β_1 is 0.5 for smooth bars, otherwise is 1.0). Variable β_2 is a factor representing the effect of load type (β_2 is 0.5 for cyclic load or long term, otherwise is 1.0).

As illustrated in Fig. 7.2, the value of the crack width at any location on the cross section can be calculated using Eq. (7.18). To evaluate the value of the crack width at point A (the point on the surface located closest to the center of the reinforcing bar), the value of the average crack width presented in Eq. (7.17) should be multiplied by the calibrated value of the factor $\xi_{x(A)}$ at this location, as explained in the aforementioned Eq. (7.16).

In the same manner, the value of the crack width at a point located at any distance between two adjacent reinforcing bars can be estimated, if it is taken into consideration that the expected value for ξ_x at that point based on Eq. (7.16).

7.4.1.1 Experimental Validation of the Model

a) Current Experimental Investigation

The proposed model for calculating the crack width variation of the reinforced concrete member subjected to axial loading presented in Eq. (7.18) enables the estimation of the crack width at any section along the crack length. Figs 7.5 and 7.6 illustrate the variation of crack width for panels tested under uniaxial loading (HS-U-25-2.5-6); and biaxial loading (HS-B1-25-2.5-6), respectively, at different steel stress levels.

Figs. 7.5 and 7.6 show that the model performs satisfactorily for thick HSC plates subjected to uniaxial and biaxial loading conditions, respectively, as it compared with the measured values of the crack width.

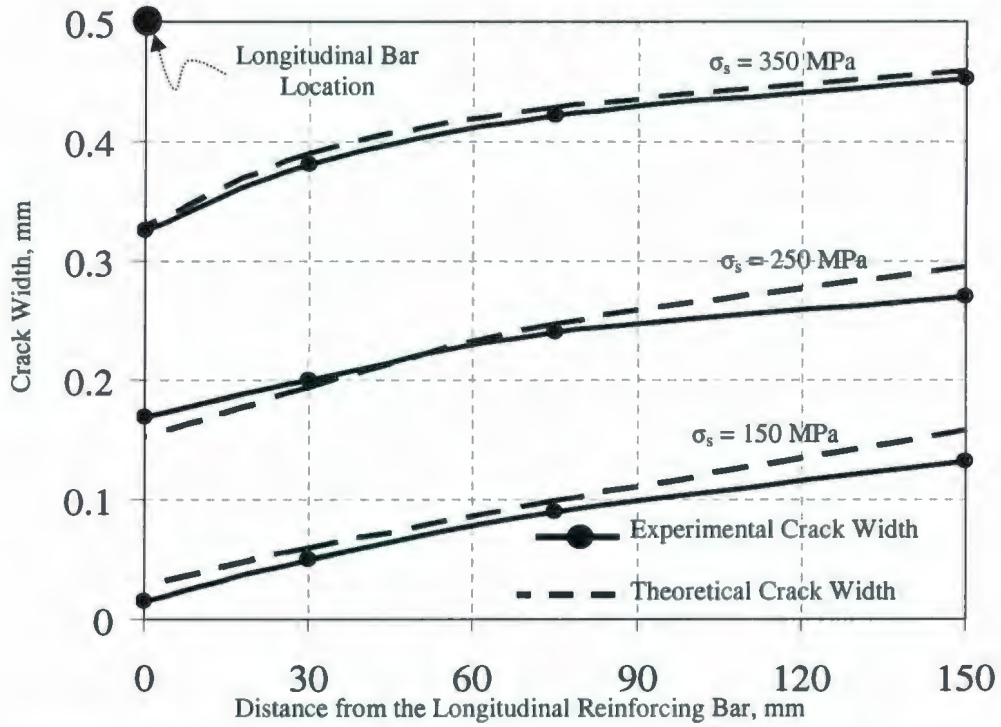

Fig. 7.5 Crack Width Profile for Panel HS-U-25-2.5-6 at Different Steel Stress Levels

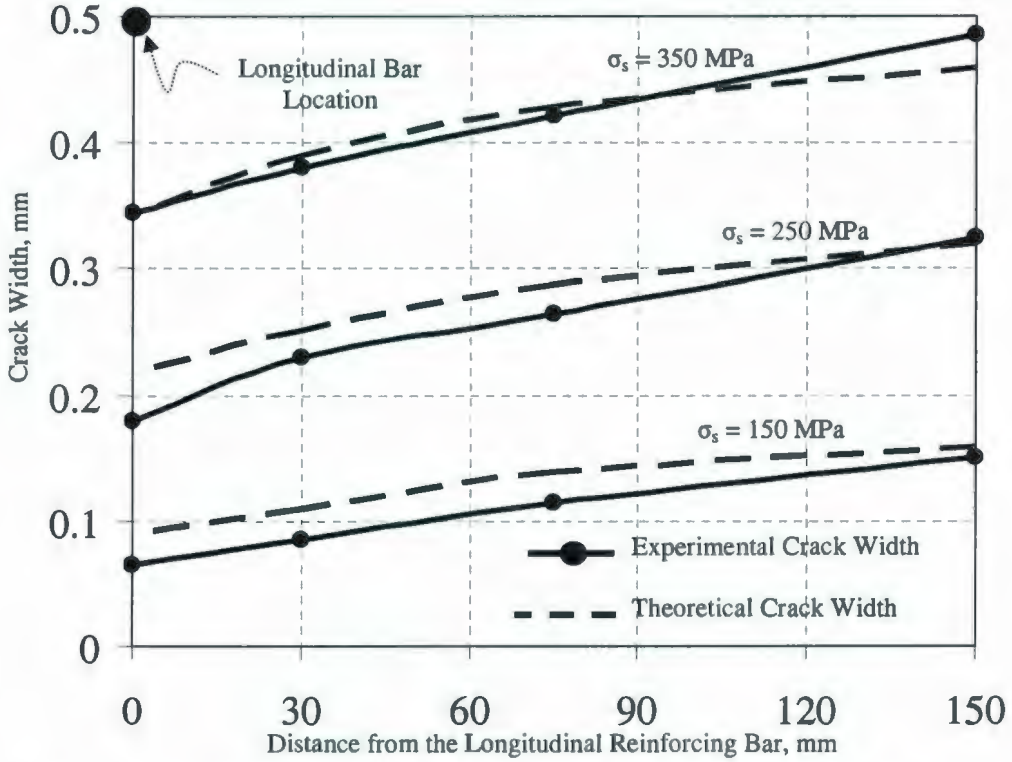

Fig. 7.6 Crack Width Profile for Panel HS-B1-25-2.5-6 at Different Steel Stress Levels

b) Williams' Test Results

Direct tension tests on large reinforced NSC panels with a typical cross section of 1500×250 mm, and a test length of 2500 mm, was conducted by Williams, 1986 [63]. The variations in the crack width for the cracks that propagated perpendicular to the longitudinal bars were investigated. Fig. 7.7 shows a comparison between Williams' experimental test results of the crack width at different locations between the longitudinal reinforcing bars, and the predicted values of the crack width using the proposed model in Eq. (7.18), for two specimens of Group (1) that was designed to investigate the effects of varying the bar size and spacing while maintaining a constant reinforcement ratio (ρ = 1.0%). Meanwhile, Fig. 7.8 shows a comparison for the variations in the value of the crack opening between Williams' experimental results of the panels in Group (3) in which the effects of the bar spacing for the same bar diameter was investigated, and the predicted values of the crack width according to the proposed model in Eq. (7.18).

In understanding the general crack width profile as well as specifying the location where the maximum crack width can be expected, it is possible to investigate the influence of major factors that affect the value of the crack width, and ways that ensure cracking control for structures subjected to in-plane axial stress.

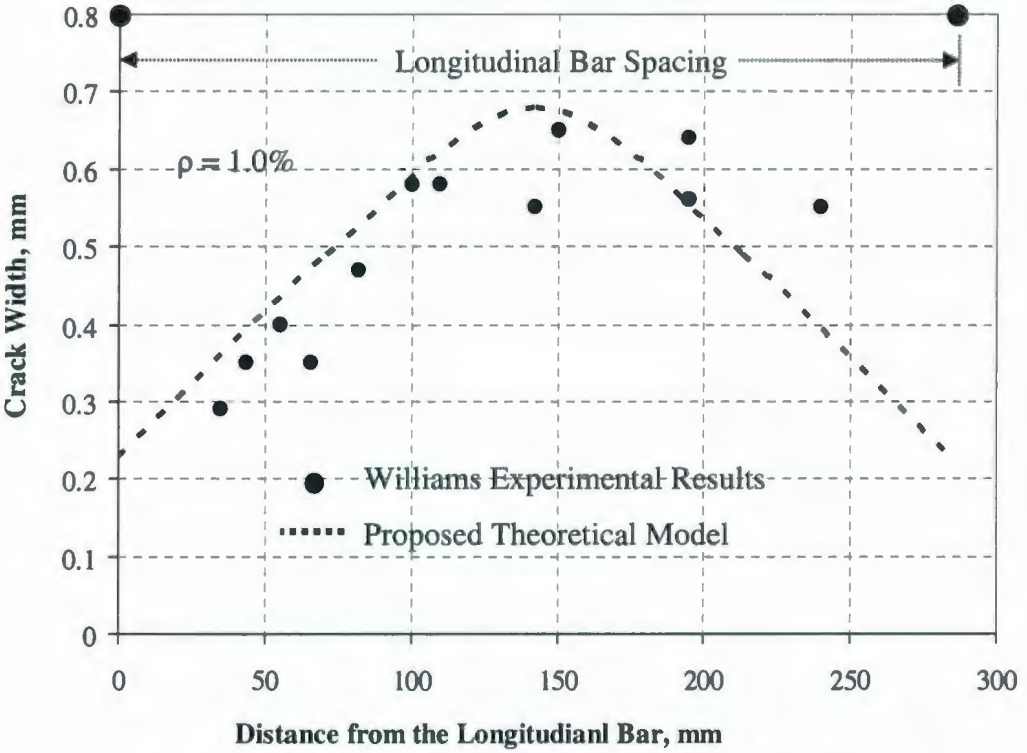

(a) Specimen No. 5 (Bar Spacing S_b = 284 mm, Φ = 20 mm)

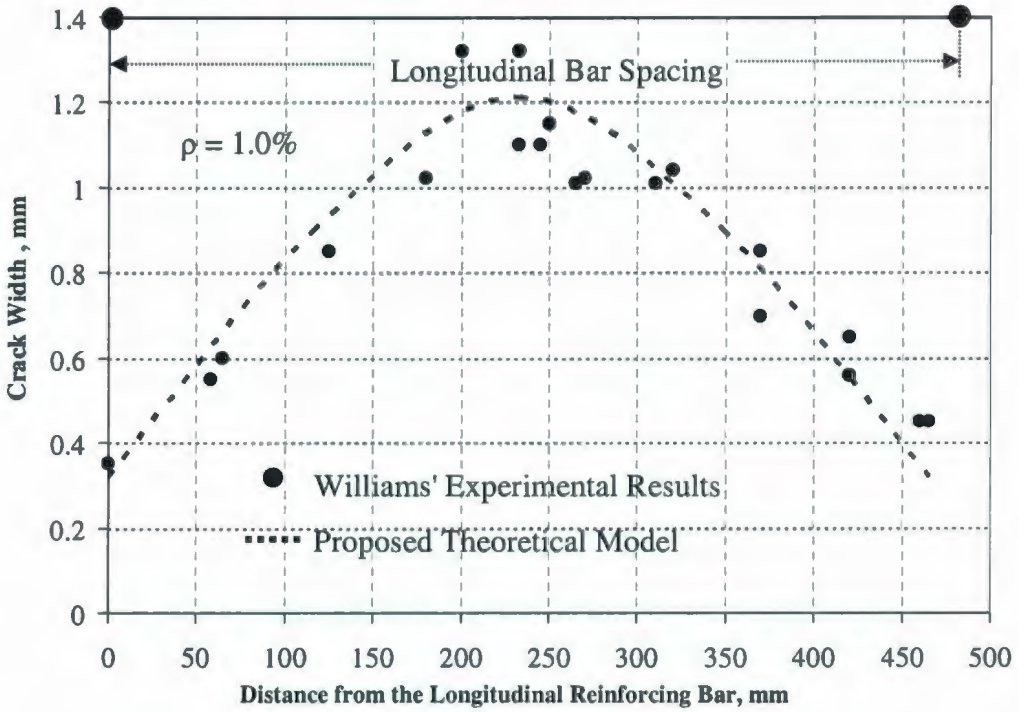

(b) Specimen No. 6 (Bar Spacing S_b = 472 mm, Φ = 25 mm)

Fig. 7.7 Typical Crack Widths for Specimens in Group 1, at Stress Level = 280 MPa

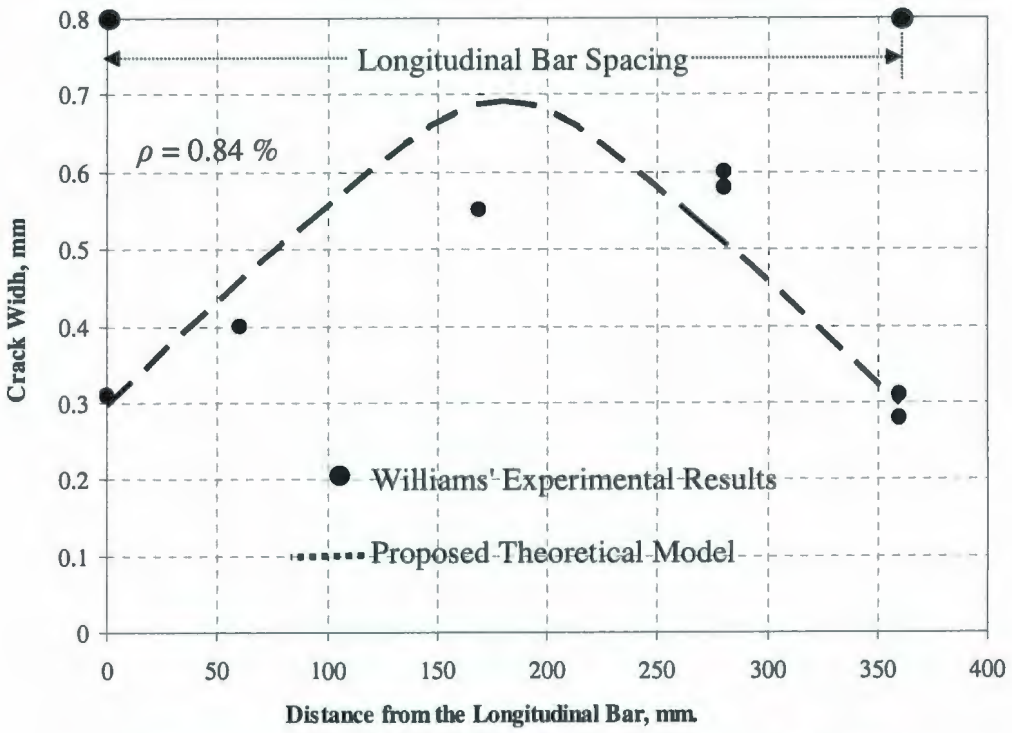

(a) Specimen No. 4 (Bar Spacing S_b = 355 mm, Φ = 20 mm)

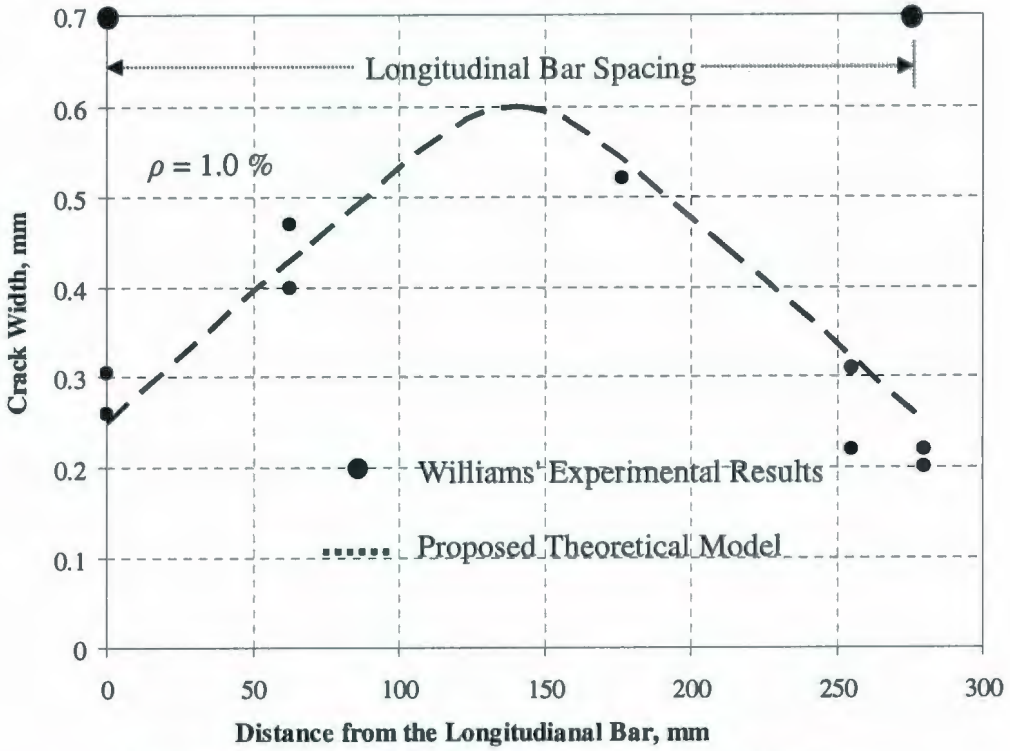

(b) Specimen No. 5 (Bar Spacing S_b = 284 mm, Φ = 20 mm)

Fig. 7.8 Typical Crack Widths for Specimens in Group 3, at Stress Level = 270 MPa

7.4.2 Estimate of Crack Width

Reinforced concrete structures can crack easily due to their low tensile strength, where the tensile strength of concrete is less than 10 percent of its compressive strength. Hence, the cracking of reinforced concrete is expected and can not economically be eliminated. Control of cracks then becomes one of the crucial concerns in designing reinforced concrete structures, especially for certain types of structures, such as containment structures, nuclear reactors, offshore structures, and water tanks, where tensile cracks can cause very serious problems. One of the main targets of this study is to develop a model that considers the effects of reinforcement distribution and thickness of the concrete cover on the cracking behavior of thick reinforced concrete plates subjected to in-plane axial stress conditions.

a) Effect of Transverse Reinforcement

The crack spacing model in Eq. (7.8) is utilized to predict the value of crack width considering the influence of the thickness of the concrete cover and the spacing between the longitudinal bars.

The second term in the parentheses in Eq. (7.8) represents the effect of the transverse reinforcement on the cracking behavior, and it is found that the influence of the transverse bar represents approximately 10% of the first term of the denominator between the parentheses. Therefore, for simplicity, the maximum crack spacing can be determined by:

$$S_{max} = f_t' / [\frac{2.2\ \tau_b\ \rho_{eff}}{\phi_1}] \qquad (7.21)$$

where τ_b is the bond stress at the steel-concrete interface, ρ_{eff} is the effective reinforcement ratio, and $\emptyset_1$ is the longitudinal bar diameter. The proposed Eq. (7.21) relates the value of the maximum crack spacing to the concrete characteristics represented by tensile and bond strength and also depends on the geometric properties of the cross section represented by the reinforcement ratio of the member.

b) Effects of Bar Spacing

Fig. 7.9 illustrates the effective tension area of the concrete surrounding the tension reinforcement, and thus the effective reinforcement ratio can be defined as:

$$\rho_{eff} = \frac{A_s}{A_{ct}} = \frac{\pi \phi_1^2}{4 h_{eff} S_b} \tag{7.22}$$

where S_b is the spacing between the longitudinal reinforcing bars, h_{eff} is the effective concrete height around the reinforcing bar, as illustrated in Fig. 7.9.

Substituting the value of the effective reinforcement ratio in Eq. (7.22) into Eq. (7.21),

$$S_{\max} = f_t^{'} / [\frac{2.2 \pi \tau_b \phi_1^{\,2}}{4 \phi_1 h_{eff} S_b}] \tag{7.23}$$

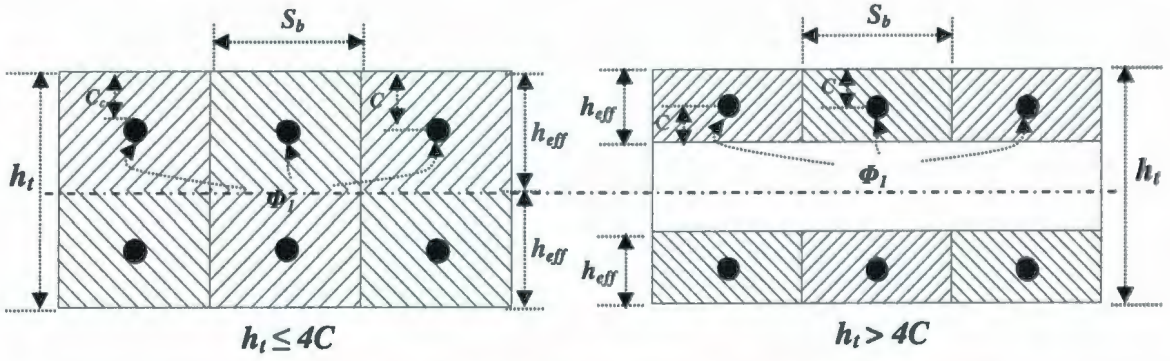

Fig. 7.9 Effective Tension Area around the Steel Reinforcement

Gilbert, 2006 [70] proposed that $\tau_b = \alpha_1 \alpha_2 f_t^{'}$, where α_1 depends on the steel stress at the crack (and varies from 3.0 at low stress levels to 1.0 at high stress levels); and $\alpha_2 = 1.0$ for short-term calculations and $\alpha_2 = 0.5$ for long-term calculations.

For short-term calculations, the bond stress at the serviceability limit can be estimated based on the developed design equations (6.17, 6.18) or using the proposed model by Gilbert [70]:

$$\tau_b = (2.2 \sim 2.5) f_t^{'} \tag{7.24}$$

Substituting the above relationship for the bond stress into Eq. (7.24), the relationship between the maximum crack spacing and the spacing between the reinforcing bars is derived in Eq. (7.25):

$$S_{max} = 0.22 \frac{h_{eff}\, S_b}{\phi_1} \tag{7.25}$$

c) Effects of Concrete Cover

Assuming that $h_{eff} = \alpha\, C$, where the value of α has a range between 1 and 2 ($1.0 < \alpha \leq 2.0$), as shown in Fig. 7.9:

$$S_{max} = 0.22\, \alpha \frac{C\, S_b}{\phi_1} = 0.22\, \alpha \frac{C}{\phi_1} S_b \tag{7.26}$$

Based on the experimental observations reported by Gillbert, 2006; 2008 [70, 71], and Rizkalla et al., 1984 [61], the ratio of S_{max}/S_m is taken to be (1.34 ~ 1.5). Thus, the value of the average crack spacing can be expressed as:

$$S_m = 0.17\, \alpha \frac{C}{\phi_1} S_b \tag{7.27}$$

Inserting the average crack spacing value from Eq. (7.27) into Eq. (7.18) that represents the value of the crack width as a function of the crack spacing at any level of steel strain, the following expression is given for the crack width:

$$w_x = 0.17\,\xi_x\,\alpha\frac{C}{\phi_1}S_b\,\varepsilon_{sm} \tag{7.28}$$

Eq. (7.28) shows that, the crack width along the cross section of reinforced concrete panels subjected to axial loading is a function of the geometric properties of the cross section, spacing between the longitudinal reinforcing bars, thickness of the concrete cover, and the strain level of the reinforcing bars.

7.4.2.1 Comparison with Experimental Results of Axially Loaded Members

Eq. (7.28) presents a developed model that can be used to predict the cracking behavior of thick reinforced concrete panels subjected to axial loading. Validation of the model is based on data that was collected during the test program conducted in the present study, as well as the test data available in the literature (Lorrain et al., 1998) [110]. Also, the expected values for the average crack width are evaluated with regard to the available codes such as the Canadaian Standards Association (CSA) offshore code CSA-S474-04 (CSA-2004) [75], Norwegian Council for Building Standardization code 3473E (NS 1992) [74], European Committee for Standardization Eurocode 2 (EC2-2004) [76], ACI Committee 224R-01 [73], and the Comité Euro-Internationale du Béton et Fédération Internationale de la Précontrainte model code MC 90 (CEB-FIP 1990) [44]. The measured crack width from the experimental program conducted in the present study is

compared with the computed crack width based on Eq. (7.28) along with the different code provisions, at different levels of steel stress.

Fig. 7.10 shows the cracking response of panel HS-U-20-6-2.5. The concrete cover of this panel is 50 mm, and the spacing between the reinforcing bars is 150 mm, as shown in Table 2.1. At the serviceability limit ($\frac{2}{3} f_y$) (ACI 318-08) [78], the measured value for the crack width is 0.089 mm, and the corresponding calculated values are 0.096, 0.109, 0.173, 0.124, 0.181, and 0.092 mm according to CSA 2004, NS 1992, EC2 2004, CEB-FIP 1990, ACI 318-01, and the proposed model in Eq. (7.28), respectively.

Also, Figs. 7.11, 7.12 present the average crack width for panels HS-B1-25-2.5-6 with a concrete cover of 62.5 mm, and HS-U-25-1.5-6 with a concrete cover of 37.5 mm, respectively. Generally, the codes approaches show a good agreement with the experimental results for the panel with normal concrete cover, as shown in Fig. 7.12. However, the code equations are sensitive to increasing the thickness of the concrete cover. EC2-2004 and CEB-FIP code equations overestimate the predicted value of the crack width; but the ACI-01 expression underestimates the calculated value of the crack width, as shown in Fig. 7.12. Figures 7.10 through 7.12 show the model's ability to replicate the experimental results with favorable agreement, substantiating it as a valuable analytical tool for research and design applications related to the cracking response of thick reinforced concrete panels subjected to axial loading conditions.

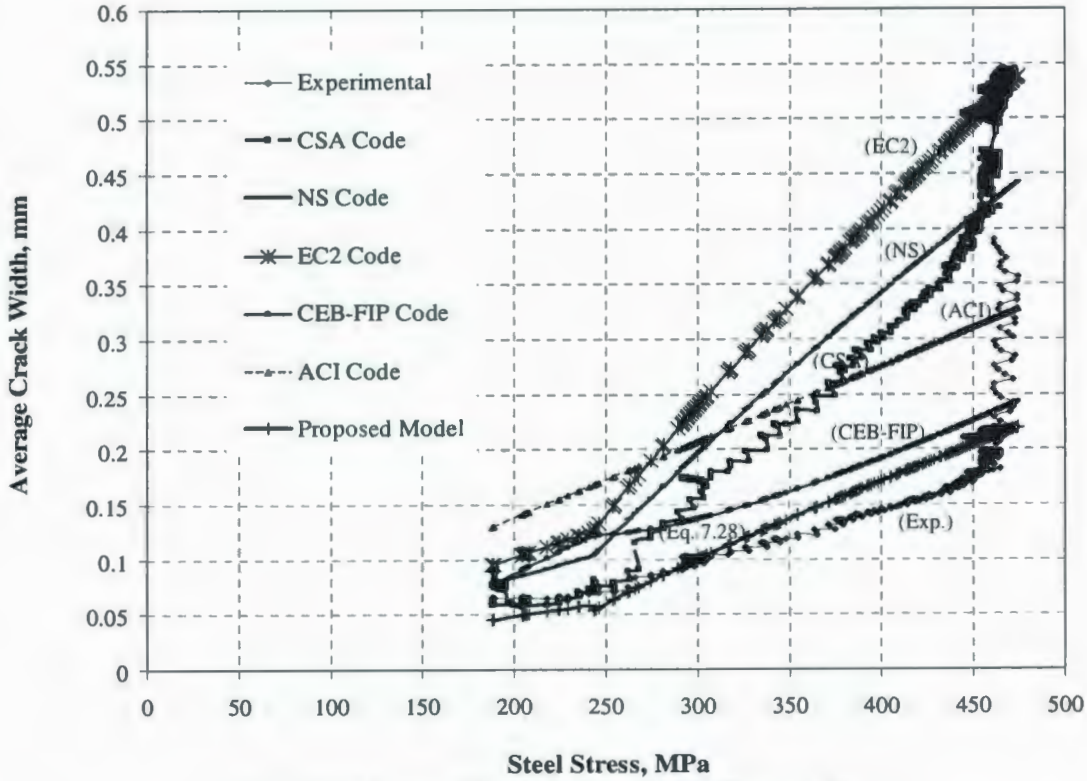

Fig. 7.10 Crack Width for Panel HS-U-20-2.5-6

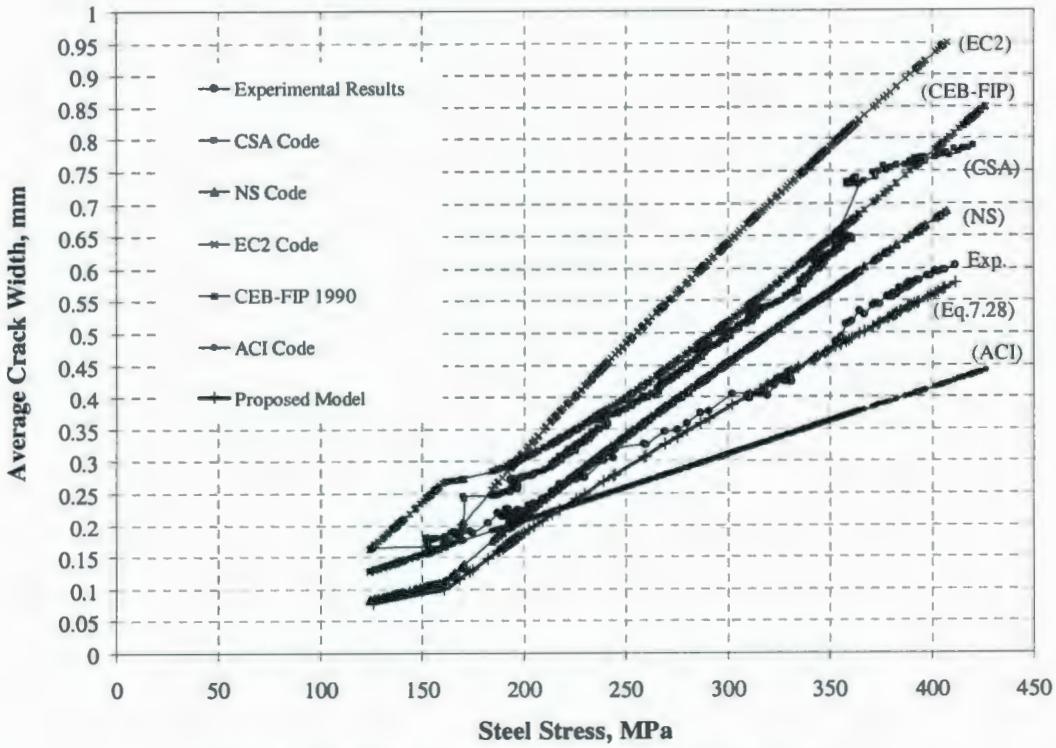

Fig. 7.11 Crack Width for Panel HS-B1-25-2.5-6

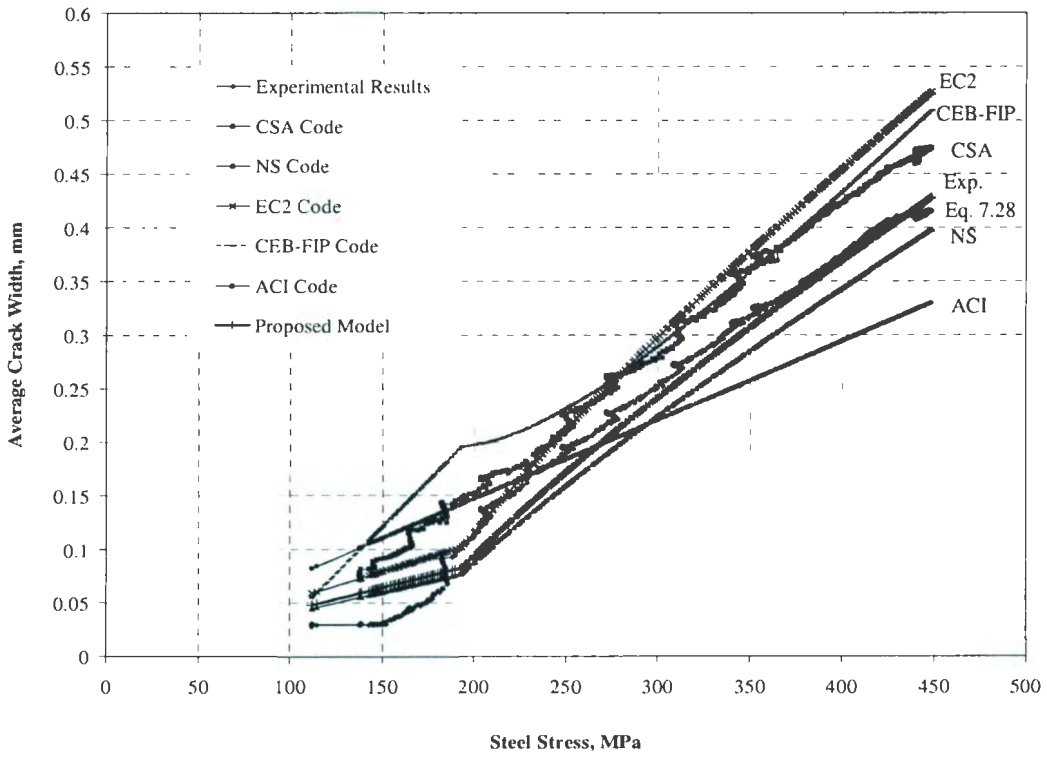

Fig. 7.12 Crack Width for Panel HS-U-25-1.5-6

Additionally, the experimental results provided by Lorrain et al., 1998 [110] are used to add a further verification for the reliability of the proposed model in Eq. (7.28). Experimental values and model predictions agreed satisfactorily, as presented in Fig. 7.13.

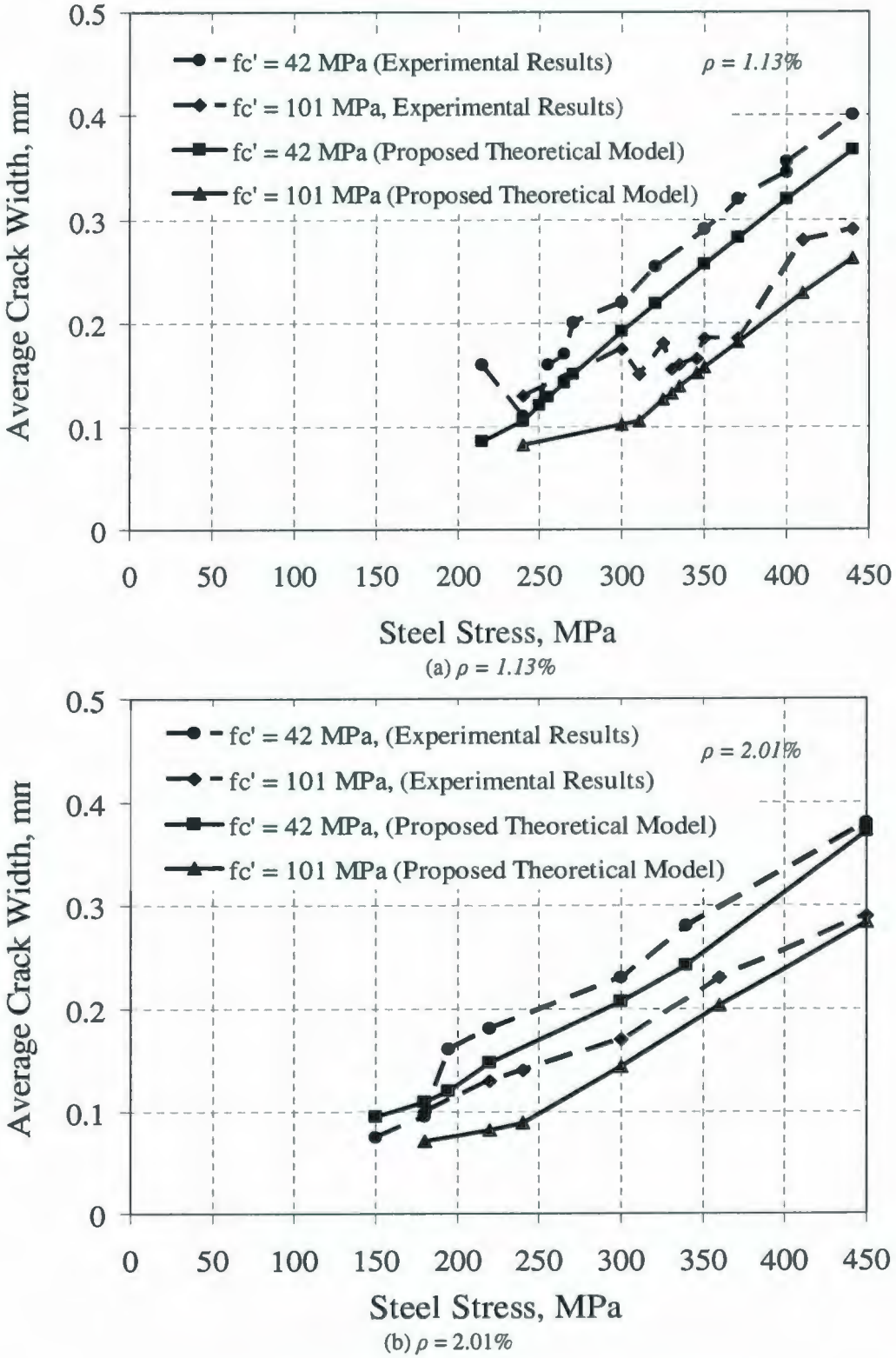

Fig. 7.13 Mean Crack Width-Steel Stress Relation [110]

7.5 Effects of the Bar Size and Reinforcement Ratio on the Crack Width and Crack Control

The bar diameter-reinforcement ratio (d_b/ρ_{eff}) is found to be the one of the most influential parameters on the cracking behavior of the thick reinforced concrete plates. Results of the experimental program conducted in the present investigation reveal that using HSC panels with well distributed reinforcing bars has a positive influence on crack control and durability concerns.

In the absence of specific requirements, such as water tightness or specific exposure classes, a limiting value of w_{lim} equal to 0.30 mm (0.012 in.) is satisfactory with respect to appearance and safety, according to crack-control recommendations proposed in the ACI 224R- 01 [73], as well as the European Model Code for Concrete Structures (CEB-FIP 1990 [44]; and Euro EC2 2004 [76]) applied to reinforced concrete structures. At this crack opening value, the steel stress reaches 0.72 f_y, and 0.83 f_y for panels HS-U-20-2.5-4, and HS-U-15-2.5-6, respectively, as illustrated in Fig. 7.14. The significant effect of the d_b/ρ_{eff} ratio on the cracking behavior and the stress level of steel reinforcing bars required to keep the crack opening value within a range guide to reasonable crack width values, is calibrated based on the conducted experimental investigation in this study, and the available experimental results conducted by Williams, 1986 [63]. Fig. 7.15 shows the relationship between the measured average value of the steel stress versus the various values of the d_b/ρ_{eff} ratio. It was observed that to control the crack width value, the average value of the steel stress should be kept in the range of (0.55 ~ 0.70) of the yield stress of the reinforcing bars (f_y) according to the corresponding value of the d_b/ρ_{eff} ratio.

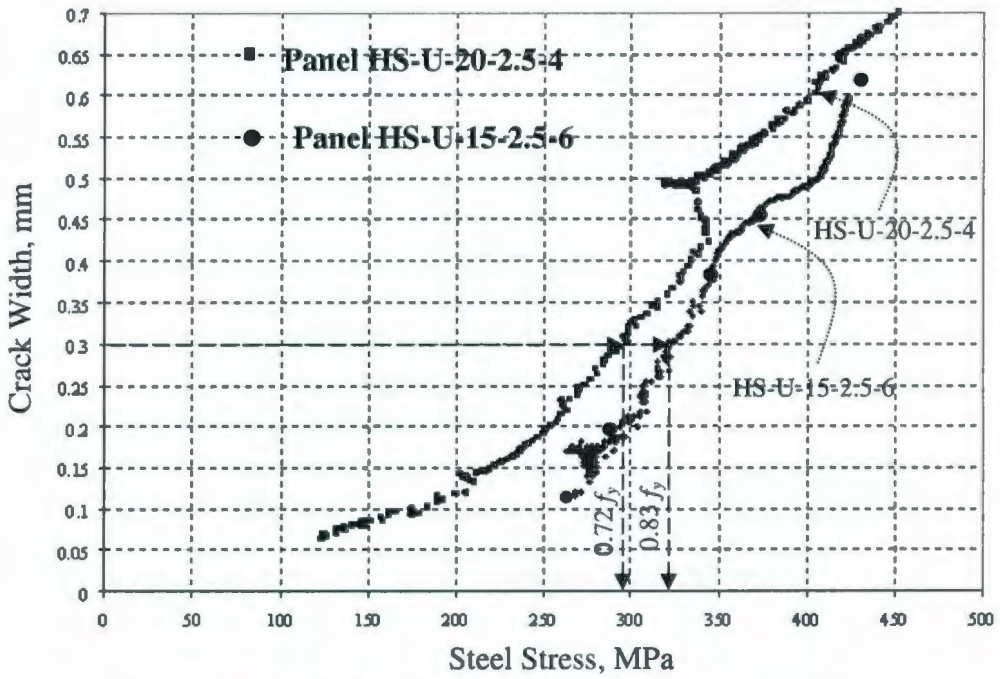

Fig. 7.14 Crack Width-Steel Stress Relationship for Panels HS-U-20-2.5-4 and HS-U-15-2.5-6

This relationship between the allowable steel stress for crack control and d_b/ρ_{eff} can be expressed as follows:

$$\sigma_{sm} = 1.395\left(\frac{d_b}{\rho_{eff}}\right)^{-0.24} f_y \tag{7.27}$$

The CEB-FIP 1990 [44], EC2-2004 [76], and AS3600-2001 [111] codes also stipulate that for cracks dominantly caused principally by flexure, their widths will not usually exceed the standard 0.30 mm if the size of the reinforcing bars and the steel stress are within the range of values as presented in Fig. 7.16. The predicted values of the steel stress based on the aforementioned model show the same trend in comparison with the values of the steel stress recommended by the EC2 [76], CEB-FIP 1990 Code [44], and AS3600-2001 [111].

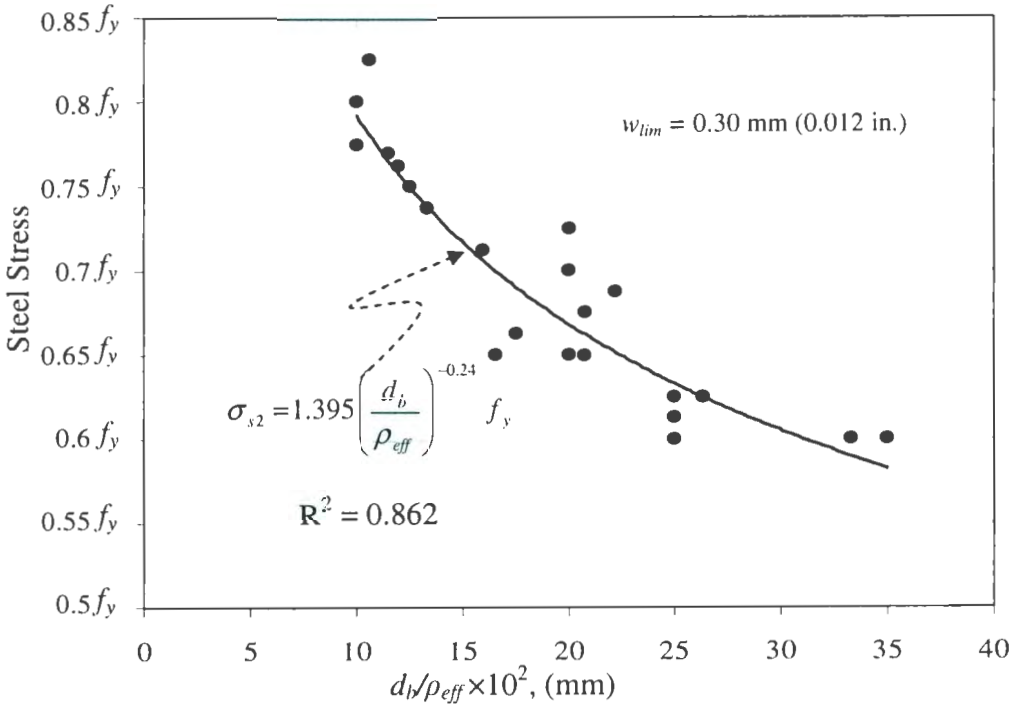

Fig. 7.15 Influence of (d_b/ρ_{eff}) on the Recommended Values of the Steel Stress

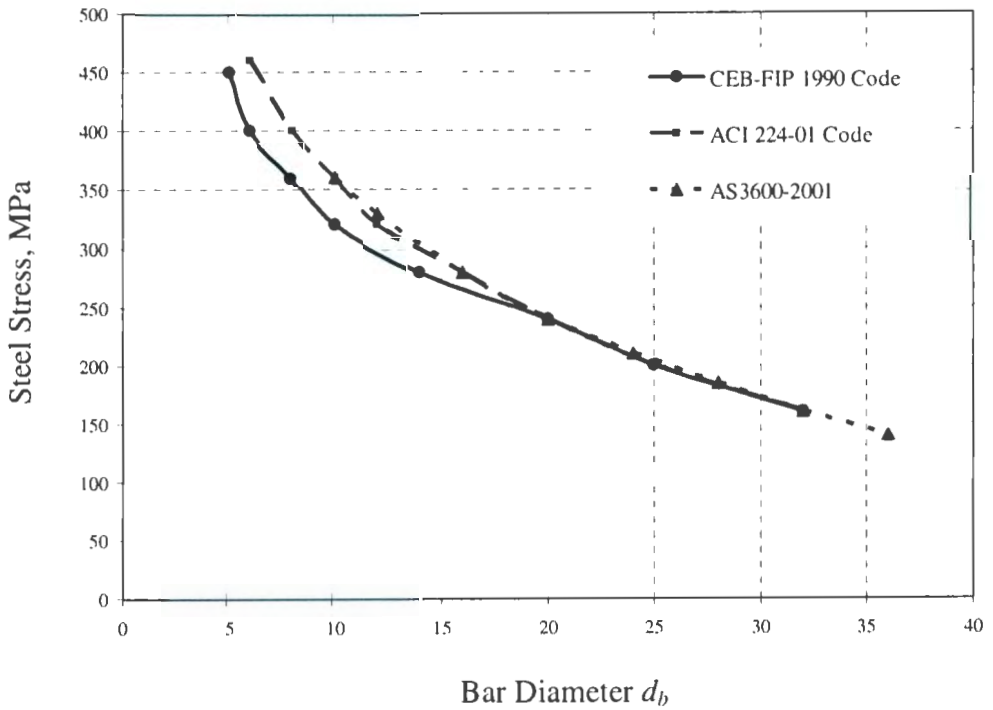

Fig. 7.16 Recommended Values for the Maximum Value of Steel Stress for Crack Control (ACI224-01, CEB-FIP 1990, and AS3600-2001)

7.6 Summary

In this chapter, a rational crack spacing model is developed by considering the equilibrium and compatibility equations of reinforced concrete elements. The influence of the main parameters affecting the cracking behavior of reinforced concrete structures, such as the tensile strength of concrete, reinforcement ratio, and longitudinal bar diameter $Ø_1$ and spacing S_1 are taken into consideration. Moreover, the effect of transverse reinforcement is incorporated into this model in terms of the transverse bar diameter $Ø_2$ and spacing S_2.

To validate the proposed model, the predicted value of the crack spacing based on the proposed model is compared to the results of various experimental investigations conducted on thick reinforced concrete panels loaded axially in tension, thick reinforced concrete slabs subjected to lateral loads. In all of the studied cases in this research, the model predicts the value of crack spacing satisfactorily. This new approach shows a favorable performance in predicting the values of the crack spacing for thick reinforced concrete members under different loading conditions. Therefore, this model can be used as a practical aid for calculating an accurate value for the crack spacing in designing thick heavy reinforced concrete structures, such as offshore oil platforms, and containment structures for nuclear power plants.

This theoretical investigation is extended to develop a model for calculating the crack width for thick reinforced concrete plates subjected to in-plane axial loading. This model enables the estimation of the variations in crack width at any section along the crack length. As well, a crack width model is developed that considers the significant effect of

the reinforcement distribution, concrete cover, and the level of the strain of the reinforcement. Recommendations for control of cracking for thick reinforced concrete panels are achieved based on the measured data from the experimental results.

Chapter 8

Nonlinear Finite Element Analysis of NSC and HSC Plates

8.1 Introduction

Nonlinear analysis of reinforced concrete structures has become increasingly important in recent years. This type of analysis is particularly desirable for certain type of structures such as concrete reactor vessels, nuclear containment structures, and parts of offshore platforms, to assess all safety aspects of a structure and find its deformational characteristics. The nonlinear response is caused by two major effects, namely; cracking of concrete in tension, and yielding of the reinforcement or crushing of concrete in compression. Nonlinearities also arise from the interaction of the constituents of reinforced concrete, such as bond-slip between reinforcing steel and surrounding concrete, aggregate interlock at a crack and dowel action of the reinforcing steel crossing a crack. Cracking in concrete takes place at low load levels due to its low tensile strength, where the tensile strength of concrete is less than 10 percent of its compressive strength. The mechanical response of concrete is weakened by the development of micro-cracks and is mainly characterized by strain softening, progressive deterioration, volumetric dilatancy, and induced anisotropy.

The nonlinear behavior of concrete can be presented using the plastic-damage model proposed by (Lubliner et al., 1989 [111]; Lee and Fenves, 1998 [112]). An adequate yield function is defined for taking into account the different responses of concrete under

tension and compression states. Therefore, cracking can be interpreted as a local damage effect, defined by the evolution of know material parameters and by a single yield function that controls the onset and evolution of damage.

The model takes into account all the important aspects under tension and compression, the effect of stiffness degradation and the problem of the results with respect to finite element mesh (Oller et al., 1990 [113]; Lee and Fenves, 1998[112]; Grassl and Jirásek, 2006 [114]). This model was developed for quasi-brittle materials like concrete, rock and ceramics. It captures the material behavior using both classical plasticity and continuum damage mechanics. Therefore, this model is supposed to have a wide range of applicability and can serve as an appropriate material model for the present material.

Also, one of the advantages of such a model is the independence of the analysis with respect to the crack directions that can be simply identified from the converged values of the nonlinear solution. This allows to overcome the problems associated to most elastic-brittle smeared cracking models such as the need for an uncoupled constitutive equation along each cracking direction (Borst and Nauta, 1984 [115]); the use of arbitrary defined shear retention (Gálvez et al., 2002 [116]; Rots et al., 1985 [117]); and the lack of equilibrium in the damage points when more than one crack is formed.

In the plastic damage approach, the stiffness degradation is implemented in a plasticity model by introducing the effective stress concept in continuum damage mechanics (Simo and Ju, 1987 [118]; Ju, 1989 [119]; Lubliner et al., 1989 [111]) to represent stiffness degradation occurring in to the cracked concrete section. The essential elements of

simulation of the material behavior under static loading based on damaged plasticity model are depend on yield criterion, the flow rule and hardening rule.

The modeling of the material behavior is performed with the finite element software ABAQUS 6.7-1, where an implementation of the plastic-damage model is available (ABAQUS/Standard User's Manual, 2007 [120]). The plasticity damage model provides a general capability for modeling concrete in all types of structures (beams, trusses, shells, and solids); uses concepts of isotropic damaged elasticity in combination with isotropic tensile and compressive plasticity to represent the inelastic behavior of concrete. This model can be used for plain concrete, even though it is intended primarily for the analysis of reinforced concrete structures; can be used with rebar to model concrete reinforcement; is primarily intended to provide a general capability for the analysis of concrete structures subjected to monotonic, cyclic, and/or dynamic loading under low confining pressures.

In section 2 of this chapter, mechanical behaviors of concrete under tension and compression are discussed that serve as the source of the material parameters. The proposed tension stiffening model is described to simulate the actual tensile capacity of the intact concrete between cracks. The finite element modeling, material properties determination process, and the simulation of the finite element meshing are discussed in sections 3. The model predictions were compared with the experimental results and these comparisons are presented in section 4. The experimental data include the results of tests of thick reinforced concrete plates in axial tension (uniaxial and biaxial) conducted in the present research; as well as the available experimental data from the previously

conducted tests, to verify the proposed model for the tension stiffening. The conclusions and the outlook of the present work are mentioned in section 5.

8.2 Mechanical Behavior of Concrete

In the plasticity-based damage model for concrete, it is assumed that the two main failure mechanisms are tensile cracking and compressive crushing of the concrete material. The evolution of the yield (or failure) surface is controlled by two hardening variables, $\tilde{\varepsilon}_t^{pl}$ and $\tilde{\varepsilon}_c^{pl}$, linked to failure mechanisms under tension and compression loading, respectively. $\tilde{\varepsilon}_t^{pl}$ and $\tilde{\varepsilon}_c^{pl}$ are referred to the tensile and compressive equivalent plastic strains, respectively. The following sections discuss the main characteristics of the mechanical behavior of concrete.

8.2.1 Defining Tension Stiffening

Tension stiffening is a global property of reinforced concrete, because of the presence of the steel within the concrete. Tension stiffening phenomenon can be defined as the increase in stiffness in a cracked reinforced concrete member due to the interaction between cracked concrete and reinforcement. As a member cracks, concrete between cracks rebound to its original state but is restrained by the reinforcement. The concrete between cracks is still able to develop tensile stresses away from the crack as load is transferred from the reinforcing steel back into the surrounding concrete, resulting in some tensile stresses in the concrete.

The inclusion of a realistic tension stiffening model is very important when analyzing reinforcing concrete sections using the finite element modeling, as the tension stiffening phenomenon in reinforced or prestressed concrete members is related to crack distribution and the tensile capacity of the intact concrete between the cracks. Different models for tension stiffening were developed to express the tensile response of concrete between cracks (Hawng and Rizkalla, 1983 [48]; Shima et al., 1987 [84]; Marzouk and Chen, 1993 [36]; Fields and Bischoff, 2004 [47]).

Based on the experimental study conducted in the present experimental progam, a new approach for the post cracking stress strain of reinforced concrete member in tension is defined. The best mathematical form to fit the descending branch of the experimental stress-strain curve can be expressed as:

$$\frac{f_t}{f_t'} = e^{\frac{-0.0008}{\alpha}(\varepsilon_t - \varepsilon_t')} \tag{8.1}$$

where f_t/f_t' represents the normalized tensile stress, ε_t is the measured member strain, ε_t' represents the concrete cracking strain, and the factor α in Eq. (8.1) reflects the influence of the transverse reinforcement bars on the constitutive laws for the stress-strain relationship of concrete in tension. The value of α is found to be equal to approximately between 0.92 – 0.95.

In reinforced concrete, the specification of post-failure behavior generally means giving the post-failure stress as a function of cracking strain ($\tilde{\varepsilon}_t^{ck}$). The cracking strain is defined

as the total strain minus the elastic strain corresponding to the undamaged material; that is, $\tilde{\varepsilon}_t^{ck} = \varepsilon_t - \varepsilon_{0t}^{el}$, where $\varepsilon_{0t}^{el} = f_t / E_0$, as illustrated in Fig. 8.1.

Based on Eq. (8.1), the relationship between the average concrete strain after the cracking stage and average stress is derived as:

$$\varepsilon_t = \varepsilon_t^{'} - 1100 Ln(\frac{f_t}{f_t^{'}}) \tag{8.2}$$

$$\tilde{\varepsilon}_t^{ck} = \varepsilon_t^{'} - 1100 Ln(\frac{f_t}{f_t^{'}}) - \varepsilon_{0t}^{el} = \varepsilon_t^{'} - 1100 Ln(\frac{f_t}{f_t^{'}}) - \frac{f_t}{E_0} \tag{8.3}$$

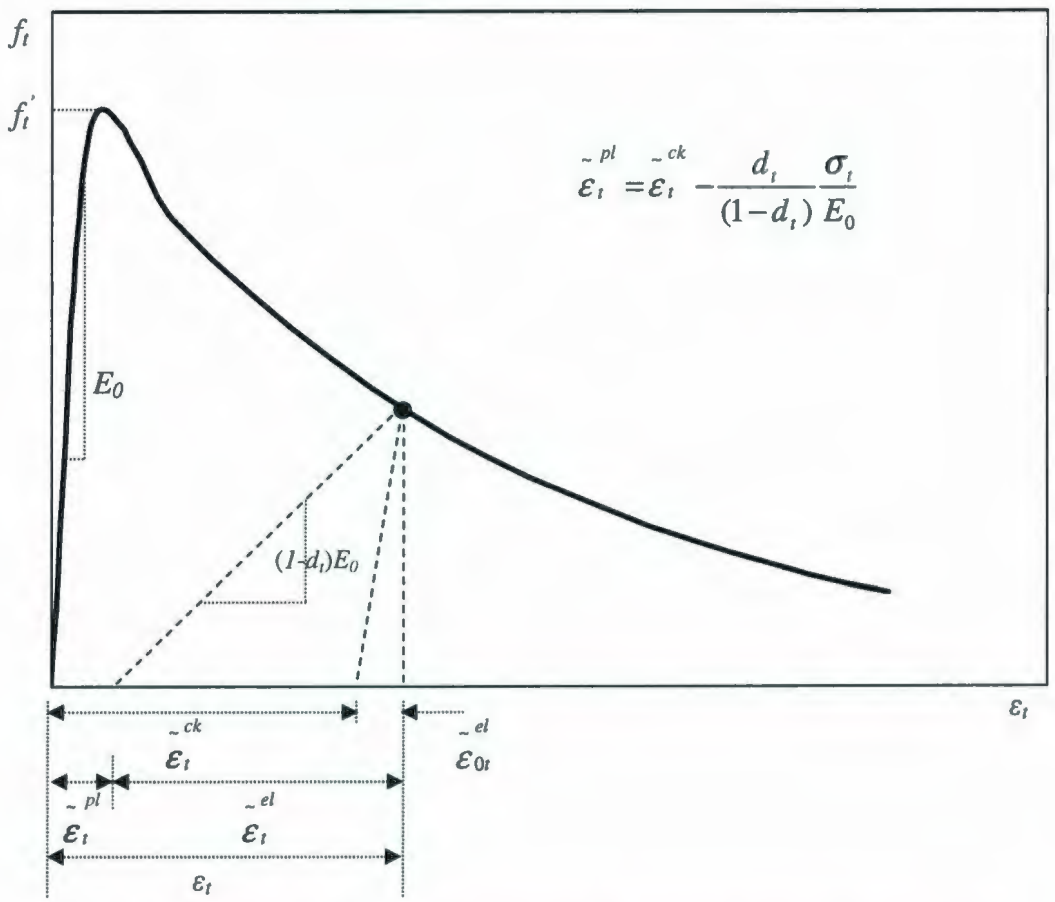

Fig. 8.1 Response of Reinforced Concrete to Tension Axial Loading [120]

The implementation of the tension stiffening model is relatively simple, since the formulae is derived based on stress-strain relationship and the descending portion of this relationship is considered. The tension stiffening model developed in the present study has been implemented in 3D concrete model that combines features from Drucker-Prager, 1952 [121] hyperbolic function for the nonassociated potential plastic flow, and the yield function of Lubliner et al., 1989 [111] with the modifications proposed by Lee and Fenves, 1998 [112].

8.2.2 Defining Compressive Behavior

The stress-strain behavior of plain concrete in uniaxial compression can be defined outside the elastic range, as the compressive stress data are provided as a tabular function of inelastic (or crushing strain), $\tilde{\varepsilon}_c^{in}$. The stress-strain curve can be defined beyond the ultimate stress, into the strain-softening regime.

Hardening data are given in terms of an inelastic strain, $\tilde{\varepsilon}_c^{in}$, instead of plastic strain, $\tilde{\varepsilon}_c^{pl}$. The compressive inelastic strain is defined as the total strain minus the elastic strain corresponding to the undamaged material, $\tilde{\varepsilon}_c^{in} = \varepsilon_c - \varepsilon_{0c}^{el}$, where $\tilde{\varepsilon}_{0c}^{el} = \sigma_c / E_0$, as illustrated in Fig. 8.2.

Thus, based on experimental σ–ε curves for both axial tension and compression, it is possible to definite the dependence between stress–cracking strain ($\tilde{\varepsilon}_t^{ck}$) in axial tension,

and stress–crushing strain ($\tilde{\varepsilon}_c^{in}$) in axial compression, as presented in Figs 8.1 and 8.2, respectively.

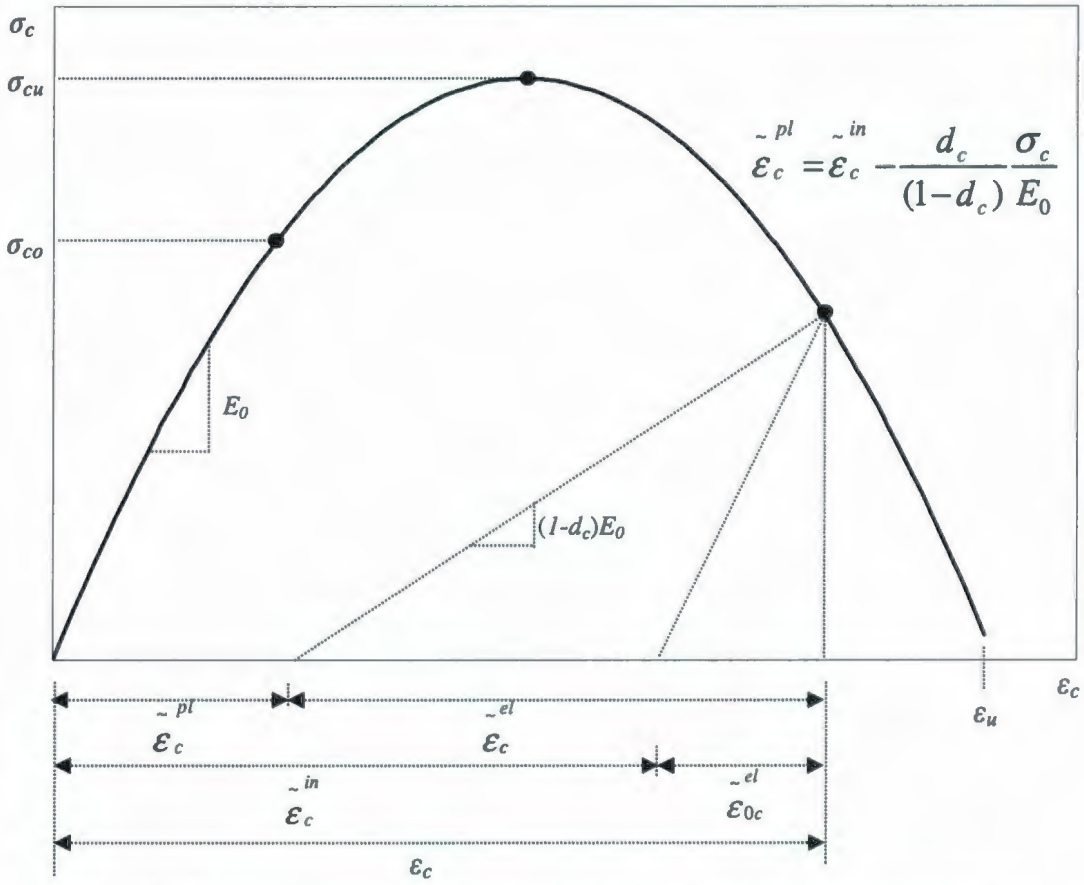

Fig. 8.2 Response of Concrete to Uniaxial Loading in Compression [120]

8.3 The Finite Element Model

8.3.1 General

A non-linear finite element analysis (F.E.A.) was carried out to predict the tensile response of the tested panels under uniaxial and/or biaxial loading conditions. The computer code ABAQUS version 6.7-1 was used to perform the numerical analysis for the tested reinforced concrete panels. The concrete damaged plasticity model in

ABAQUS/Standard provides a general capability for modeling concrete and other quasi-brittle materials in all types of structures (beams, trusses, shells, and solids). This model uses concepts of isotropic damaged elasticity in combination with isotropic tensile and compressive plasticity to represent the inelastic behavior of concrete. The model takes into consideration the degradation of the elastic stiffness induced by plastic straining both in tension and compression. Also, this model assumes that the main two failure mechanisms are tensile cracking and compressive crushing of the concrete material.

In this study, one quarter of the panel was modeled, as two symmetry plans in the test set-up was utilized when building the FE models. The symmetry plans are the apparent symmetry plans along the middle of the concrete panels in X and Z directions. In the latter case, the symmetry is certainly present during elastic deformations but can be questionable in the nonlinear region. It was assumed that this irregularity does not have a significant influence on the results.

The concrete and the steel rebars in the reinforced concrete panels were adapted by eight-node linear brick elements C3D8 with full Gaussian integration rule over the element face. The embedded element technique was used to model rebar reinforcement. Full transfer of load between the reinforcement and concrete, was assumed. The boundary conditions for the model were set along the middle of the panel in X and Z plans of symmetry, and at the four corner points of the bottom surface in Y directions.

There are very close similarities between the predicted results and the experimental results such as the pre and post cracking stress strain relationship, and the tensile strength of the reinforced concrete panels tested under in-plane axial stresses.

8.3.2 Material Properties

8.3.2.1 Concrete

Two levels of compressive strength were used to cast specimens in the present investigation. The average concrete compressive strength $f_c^{'}$ was found equal to 35 MPa for normal strength concrete specimens, and 75 MPa for high strength concrete specimens. The concrete average cracking strength and the modulus of elasticity are estimated according to the proposed equations 4.9 through 4.12 for both normal and high strength concrete in chapter 4.

The yield function is formulated in terms of effective hydrostatic pressure and the Mises equivalent effective stress and depends on two hardening variables. The two hardening variables are the integrated plastic strain rates separated into tension and compression. The shape of the yield surface can be governed by the two parameters K_c, and σ_{b0}/σ_{c0}. The first describes the shape of the deviatoric plane; the latter defines the ratio of initial equibiaxial to uniaxial compressive yield stress. The model uses a non-associated plastic flow rule to describe the plastic strain increments, and the flow potential follows the Drucker-Prager, 1952 [121] hyperbolic function. The dilation angle for concrete defines the plastic strain direction with respect to the deviatoric stress axis. In this study, a value of 45° was used for the dilation angle of concrete (Rahman et al., 2007) [122]. Damage characterizes the stiffness degradation for the unloading response.

The proposed tension stiffening model in Eq. 8.1 was used to define pre- and post-cracking properties for the concrete. The model assumed that the direct stress across a crack gradually reduced to zero as the crack opened. Tension stiffening was defined in

the present study using stress-strain data, as expressed in Eq. (8.3), and as shown Fig. (8.1). The hardening and softening rule and the evolution of the scalar damage variable for compression $\tilde{\varepsilon}_c^{in}$ and tension $\tilde{\varepsilon}_t^{ck}$ are presented in Tables 8.1 and 8.2, for Normal and high strength, respectively.

Table 8.1 The material parameters of Damaged Plasticity model for NSC

Material's Parameters	NSC	The Parameters of Damaged Plasticity Model	
		dilation angle Ψ	45°
Potential Eccentricity		ε	0.1
E (MPa)	19500	σ_{b0}/σ_{c0}	1.16
ν	0.2	K_c	⅔
Concrete Compression Hardening		Concrete Compression Damage	
Stress, MPa	Crushing Strain $\tilde{\varepsilon}_c^{in}$	Compressive damage variable d_c	
22.98	0	0	
30.85	0.0004	0	
35.0	0.0007	0	
32.43	0.0025	0.086	
27.22	0.0028	0.229	
22.98	0.003	0.371	
18.14	0.0032	0.486	
12.70	0.0034	0.657	
6.65	0.0036	0.81	
3.40	0.0037	0.903	
Concrete Tension Stiffening		Concrete Tension Damage	
Stress, MPa	Cracking Strain $\tilde{\varepsilon}_t^{ck}$	Tensile damage variable d_t	
2.2	0	0	
2	0.000121	0.091	
1.8	0.000237	0.182	
1.6	0.000366	0.273	
1.4	0.000513	0.364	
1.2	0.000683	0.455	
1	0.000883	0.545	
0.8	0.001129	0.636	
0.6	0.00144	0.727	
0.4	0.00189	0.818	

Table 8.2 The material parameters of Damaged Plasticity model for HSC

Material's Parameters	HSC	The Parameters of Damaged Plasticity Model	
		dilation angle Ψ	45°
Potential Eccentricity		ε	0.1
E (MPa)	27000	σ_{b0}/σ_{c0}	1.16
ν	0.2	K_c	⅔
Concrete Compression Hardening		Concrete Compression Damage	
Stress, MPa	Crushing Strain $\tilde{\varepsilon}_c^{in}$	Compressive damage variable d_c	
57.6	0	0	
63.47	0.0002	0	
75.0	0.0008	0	
68.76	0.0038	0.093	
63.47	0.004	0.16	
57.6	0.0042	0.232	
44.08	0.0046	0.413	
28.21	0.005	0.624	
19.39	0.0052	0.747	
9.99	0.0054	0.868	
Concrete Tension Stiffening		Concrete Tension Damage	
Stress, MPa	Cracking Strain $\tilde{\varepsilon}_t^{ck}$	Tensile damage variable d_t	
2.7	0	0	
2.3	0.000345	0.148	
2.1	0.000464	0.222	
1.9	0.000594	0.296	
1.7	0.000738	0.37	
1.5	0.000901	0.444	
1.3	0.00108	0.519	
0.9	0.00156	0.667	
0.5	0.00232	0.815	
0.3	0.00299	0.889	

8.3.2.2 Steel

The modeling of the reinforcing bar in concrete must be based on the properties of the bare bar and the effect of the bonding between the bar and the concrete. For simplicity, an elastic-plastic model was used to describe the constitutive behavior of steel bars. The

Tensile stress-strain curve of the steel was modeled by two straight lines. The first straight line represents the elastic range with slope of E_s, the second straight line model the post-yield average bar behavior with E_p. The plastic modulus E_p is taken as the slope of strain hardening region of the steel reinforcement with a value ranging from 1.8% to 2.5% of the elastic modulus E_s (Shima et al., 1987 [84]; Maekawa et al., 2003 [92]; Belarbi and Hsu, 1994 [46]), see Fig. 8.3. Material properties of steel reinforcement, such as the Young's modulus and Poisson's ratio were taken as E_s=200000 MPa and $\nu = 0.3$, respectively.

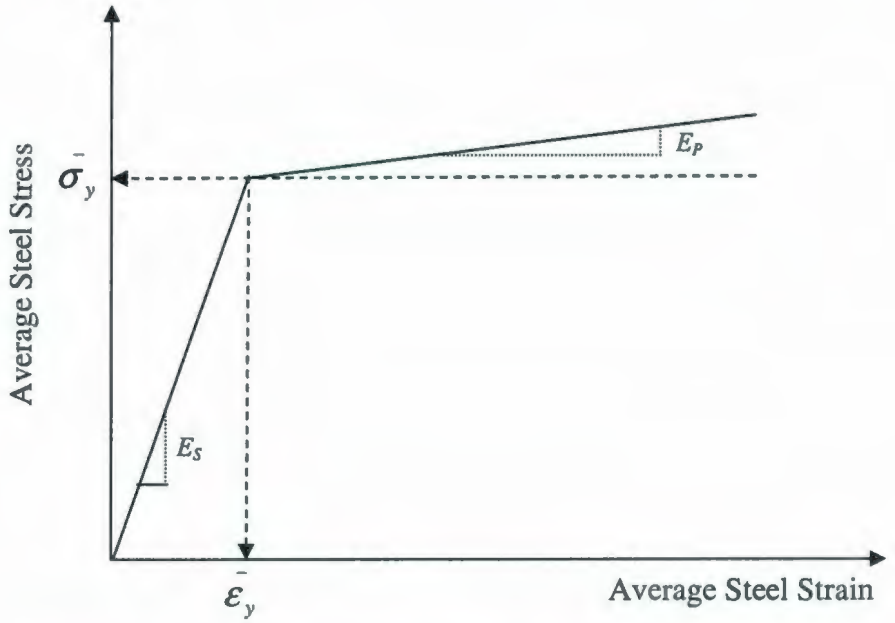

Fig. 8.3 Idealized Stress-Strain Relationship of Reinforcing Steel Using the Elastic-Plastic Model

8.4 Finite Element Mesh

8.4.1 General

It has been recommended earlier (Bazant and oh, 1983 [123, 124]), that for the finite element approximation to accurately represent the cracking behavior close to the crack

tip; it is necessary that the size of the finite elements be smaller than the actual size of the crack band zone. The approximation length of the crack band zone for plane stress Mode I could be approximated on the basis of optimum fitting of numerous test data (Bazant and Oh, 1983) [123]. The width of the crack band front was found to be approximately $3d_a$ (d_a is the maximum aggregate size). As well, it was recommended (Hillerborg et al., 1964 [125]) that, the distance between nodes point in finite elements should not be chosen greater than 0.2 l_{ch}. The material characteristic length is defined by the following Eq. (8.4):

$$l_{ch} = \frac{E G_f}{f_t^2} \approx \frac{K_{Ic}^2}{f_t^2} \tag{8.4}$$

where G_f is the fracture energy of the concrete, and K_{Ic} is the fracture toughness for mode I cracking. The fracture energy value for normal strength concrete (35 MPa) is around 110 N/m, while for high-strength concrete (75 MPa) its value is in the range of 160 N/m reported by Marzouk and Chen, 1995 [5, 36].

In the modeling of the concrete panel and steel rebar a three-dimensional eight-node element C3D8 (3D 8-node solid elements) with three degree of freedom at each node was used as shown in Fig. 8.4. C3D8 is a general purpose linear brick element, with fully integration points, and with translations in the nodal x, y, and z directions. The element is capable of plastic deformation, cracking in three orthogonal directions, and crushing. The node and the integration point numbering follow the convention of Fig. 8.4. This latter information is important since element variables printed with the EL PRINT keyword are

given in the integration points. For purposes of analysis, it is convenient to replace each round bar with an equivalent square bar having the same area.

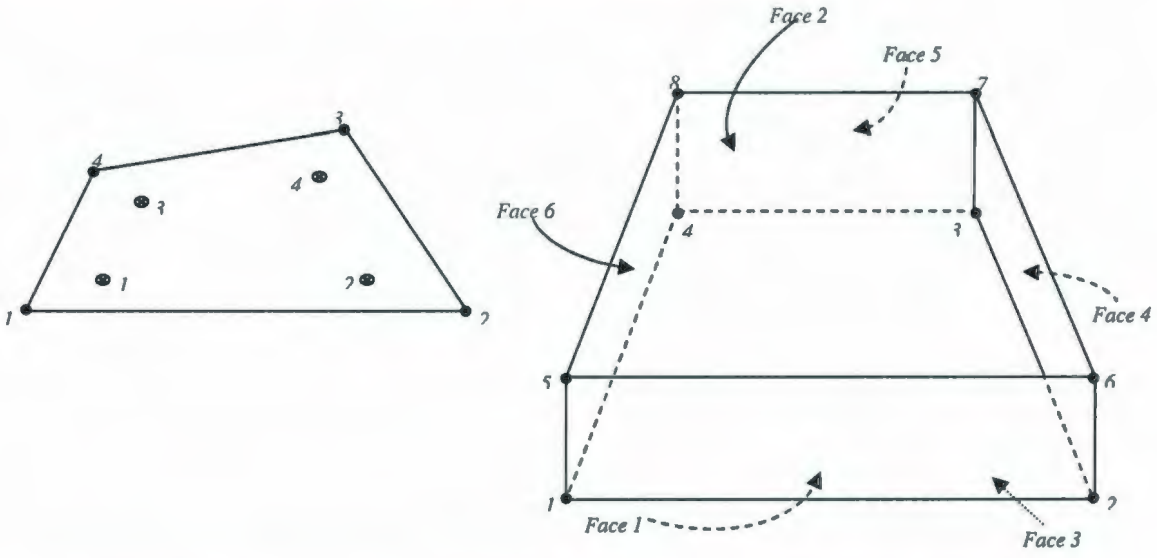

Fig. 8.4 Node Ordering, Face Numbering, and Elements Numbering of Integration Points for Brick C3D8 [120]

Over the past decade, a number of embedded representations for reinforcement have been published. Phillips and Zienkiewicz, 1975 [126]; and Elwi and Murray, 1980 [127] separately developed embedded representations in which the virtual work integration is performed along the reinforcing layer and the reinforcement is aligned with one of the local isoperimetric element coordinate axes. Fig. 8.5 shows typical F.E. models for the reinforced concrete panel.

The embedded element technique was used to specify that an element or group of elements was embedded in "host" elements. The embedded element technique can be used to model rebar reinforcement. ABAQUS searches for the geometric relationships between nodes of the embedded elements and the host elements. If a node of an

embedded element lies within a host element, the translational degrees of freedom at the node are eliminated and the node becomes an "embedded node". The translational degrees of freedom of the embedded node are constrained to the interpolated values of the corresponding degrees of freedom of the host element.

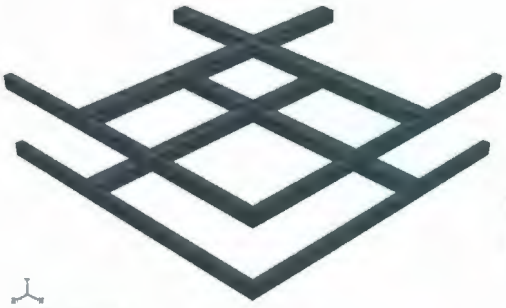

(a) Steel

(b) Concrete Block

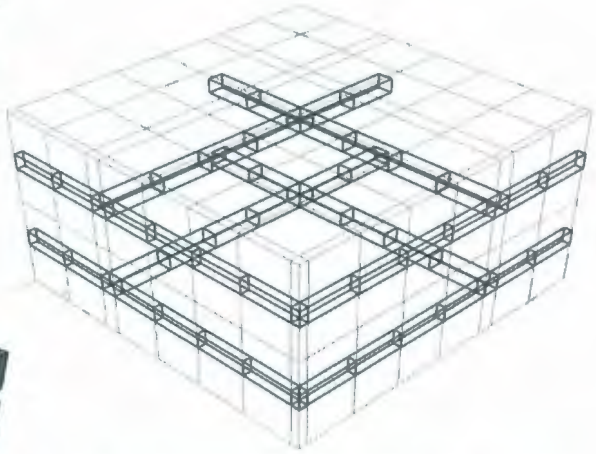

(c) Reinforcement Embedded in Concrete

Fig. 8.5 Typical FEM Discretization for a Quarter of the Reinforced Concrete Panel

Embedded elements are allowed to have rotational degrees of freedom, but these rotations are not constrained by the embedding. Multiple embedded element definitions are allowed. With this modeling approach, the embedded element technique can be used to model a set of rebar-reinforced elements that lie embedded in a set of three-dimensional solid (continuum) concrete elements.

8.4.2 Loading and Boundary Conditions

The reinforced concrete panels were tested under axial load, as shown in Fig. 8.6. Because a quarter of the entire panel was used for the model, planes of symmetry were required at the internal faces. At a plane of symmetry, the displacement in the direction perpendicular to the plane was held at zero. Fig. 8.6 shows loading and boundary conditions for a typical finite element model.

Fig. 8.6 Loading and Boundary Conditions

8.5 Comparison with Experimental Results

Realization of the full potential of the damaged plasticity model with the developed tension stiffening model in Eq. (8.3) to study the nonlinear behavior of structural concrete elements requires an extensive verification to establish the accuracy of the responses of a variety of structural members, by comparing their computed responses under a variety of loadings with the available experimental results. This comparative study includes stress strain relationship, and tensile strength of concrete.

8.5.1 Direct Tension Tests (Current Experimental Program)

Several tests were performed in the current investigation on thick normal and high strength concrete panels subjected to uniaxial and biaxial loadings, to study the cracking behavior of reinforced concrete thick plates under tension. The details of tested panels are given in Chapter 3 in Table 3.1, and shown in Fig. 3.1.

The main purpose of the finite element modeling is to simulate the pre- and post-cracking behavior of the thick reinforced concrete panels subjected to axial loading (uniaxial and biaxial), and also to predicted the tensile strength of normal and high strength concrete. These numerical results were compared with the experimental results to check the suitability of the damaged plasticity model to simulate the tensile response of thick plates, and to verify the reliability of the proposed tension stiffening model implemented in the damaged plasticity model.

Figs. 8.7 (a) and (b) illustrate a comparison between the numerical and experimental results for NSC panels tested under uniaxial (panel NS-U-15-2.5-6) and biaxial (panel NS-B1-15-2.5-6), respectively. Meanwhile, Figs. 8.7 (a) and (b) show the numerical results using the proposed tension stiffening model in Eq. (8.3), and the bilinear model proposed by Bazant and Oh, 1984 [128] to simulate the complete response of the reinforced concrete.

Furthermore, Figs. 8.8 and 8.9 illustrate a comparison between the numerical and experimental results under uniaxial and biaxial tension for the different tested HSC panels, parallel with the predicted response of the panels using the bilinear model for simulating the tension stiffening effect proposed by Bazant and Oh, 1984 [128].

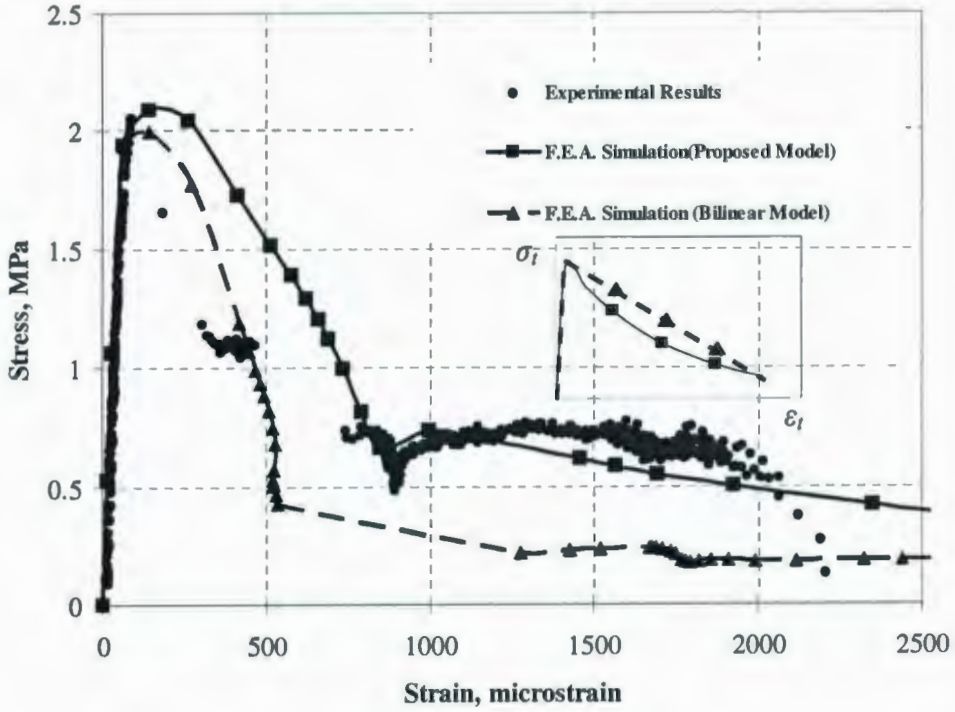

(a) Panel NS-U-15-2.5-6

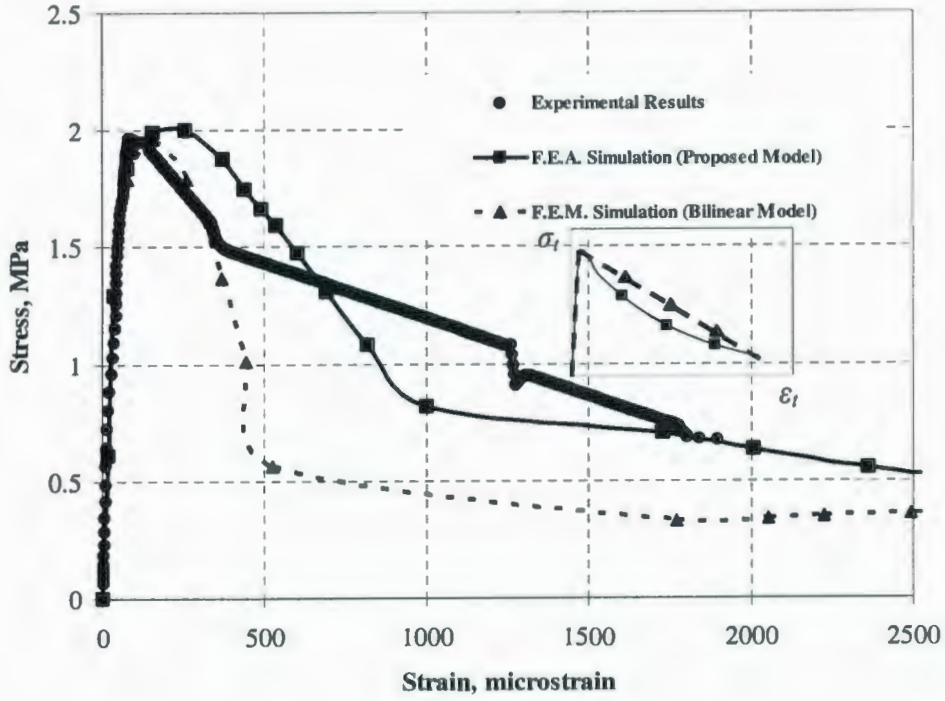

(b) Panel NS-B1-15-2.5-6

Fig. 8.7 Comparison of Numerical Solutions against Experimental Results for NSC Panels: (a) Uniaxial tension (NS-U-15-2.5-6); and (b) Biaxial Tension (NS-B1-15-2.5-6)

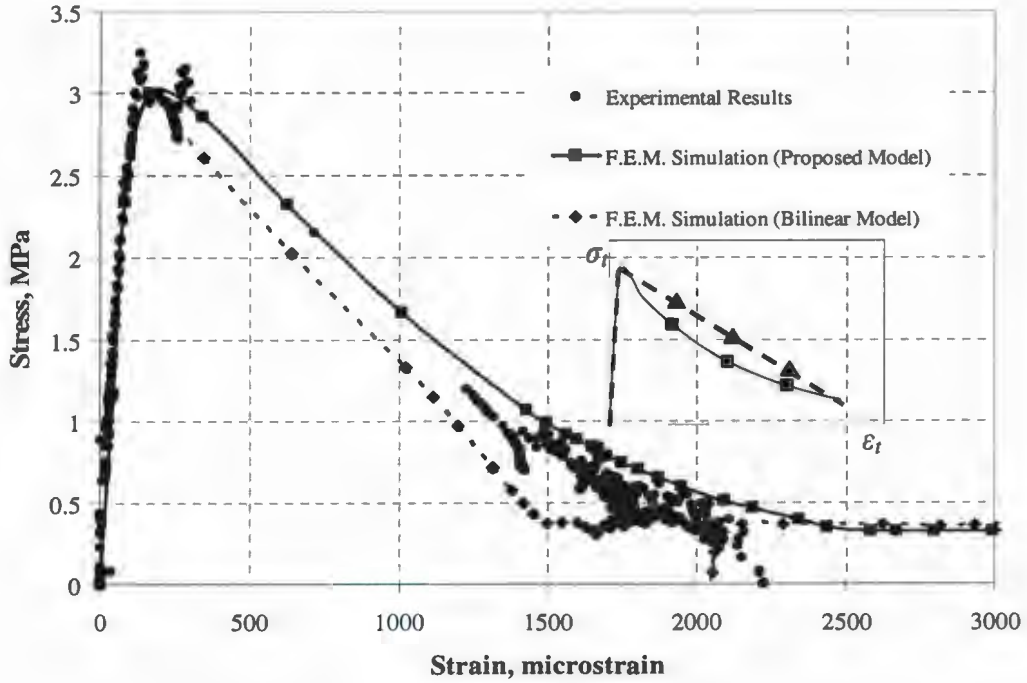

a) Panel HS-U-15-2.5-6

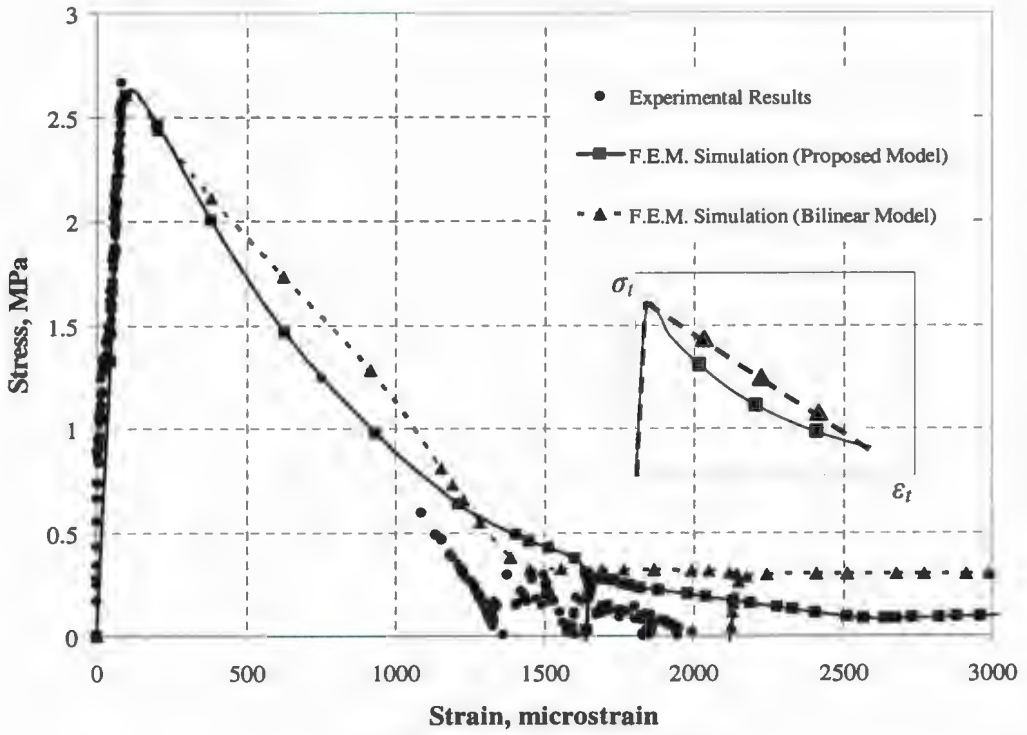

b) Panel HS-B1-15-2.5-6

Fig. 8.8 Comparison of Numerical Solutions against Experimental Results for HSC Panels:(a) Uniaxial tension (HS-U-15-2.5-6) ; and (b) Biaxial Tension (HS-B1-15-2.5-6)

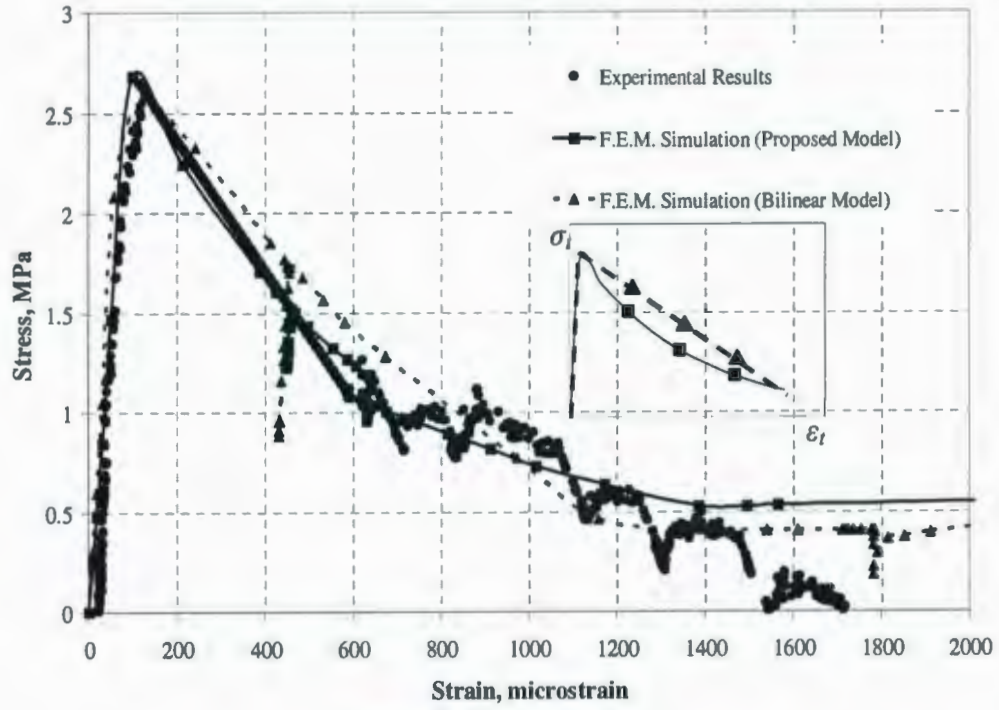

a) Panel HS-U-25-1.5-6

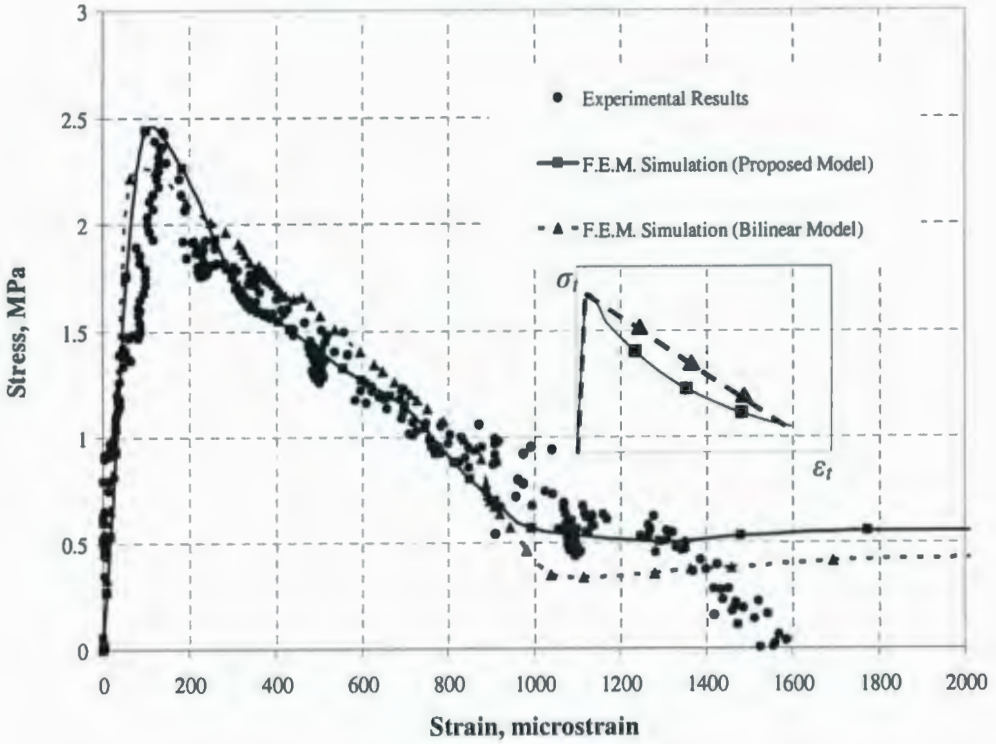

a) Panel HS-B1-25-1.5-6

Fig. 8.9 Comparison of Numerical Solutions against Experimental Results for HSC Panels: (a) Uniaxial tension (HS-U-25-1.5-6); and (b) Biaxial Tension (HS-B1-25-1.5-6)

Based on the comparative study in Figs. 8.7 through 8.9, it is clear that the numerical results are sensitive to the concrete tensile strength and the shape of the descending response for the concrete, where a slight variance in these parameters can significantly reduce the accuracy of the solution. Accurate methods of determining these material parameters are essential for the finite element analysis. Results of the nonlinear analyses using the proposed tension stiffening model, and brick elements to model the response of reinforced concrete panels show a good agreement with the experimental test result.

Table 8.3 shows the tensile strength measured experimentally and the predicted values from the numerical analysis, for the different concrete panels. Finite element analysis shows good agreement with the experimental results.

Table 8.3 Summary of the Measured Test Result and Predicted Numerical Data

S	Specimens Symbol	Specimens Dimensions (mm) (a × b × h)	Concrete Strength f_c' (MPa)	Experimental Tensile Strength $f_{t(ex)}'$	Numerical Tensile Strength $f_{t(F.E.A.)}'$	Absolute Difference in f_t'(%) $(f_{t(ex)}' - f_{t(F.E.A.)}')/f_{t(ex)}'$
1	NS-U-15-2.5-6	600×600×190	40	2.10	2.15	2.3
2	NS-B1-15-2.5-6		35	1.92	2.08	8.4
3	HS-U-15-2.5-6		90	3.2	3.08	3.7
4	HS-B1-15-2.5-6		75	2.72	2.70	0.75
5	HS-U-20-2.5-6		75	3.10	3.08	0.65
6	HS-B1-20-2.5-6		75	2.96	3.01	1.7
7	HS-U-20-2.5-4		80	3.0	3.02	0.67
8	HS-B1-20-2.5-4		75	2.70	2.91	7.8
9	HS-U-25-2.5-6	900×900×260	75	2.71	2.69	0.75
10	HS-B1-25-2.5-6		65	2.36	2.32	1.5
11	HS-U-25-1.5-6		75	2.7	2.73	1.1
12	HS-B1-25-1.5-6		70	2.46	2.48	0.8
13	HS-U-30-2.5-6	900×900×380	65	2.45	2.51	2.5
14	HS-B1-30-2.5-6		65	2.1	2.02	3.8
15	HS-B1-30-1.5-6		65	2.32	2.37	2.2

8.5.2 Verification with the Previous Experimental Results

In the present study, the proposed tension stiffening model is based on experimental investigation conducted in this study, as a result the prediction will undoubtedly be acceptable as the model parameters are obtained from the set of data used for verification. Thus, the verification should be extended to verify the proposed model based on data not directly used for obtaining model parameters. The selection of the test series was based that the test must allow the verification of the model in various loading conditions for normal and high strength concrete structures. The selected tests involve direct tension tests, laterally loaded slabs.

8.5.2.1 Direct Tension Tests

The Damaged plasticity model was used to predict the tensile stress-strain response for previous experimental work on uniaxially loaded members conducted by Fields and Bischoff, 2004 [47]. This is to ensure the suitability of the proposed tension stiffening model in Eq. 8.3 to simulate the tensile response of the reinforced concrete members under axial loading conditions.

Fig. 8.10 shows a comparison between the predicted tensile stress-strain responses based on the numerical simulation using the damaged plasticity and proposed tensing stiffening models, and results of experimental program conducted on RC members with different levels of concrete strength. Fig. 8.10 shows that, the model preformed satisfactorily as compared with the experimental data on the reinforced concrete members.

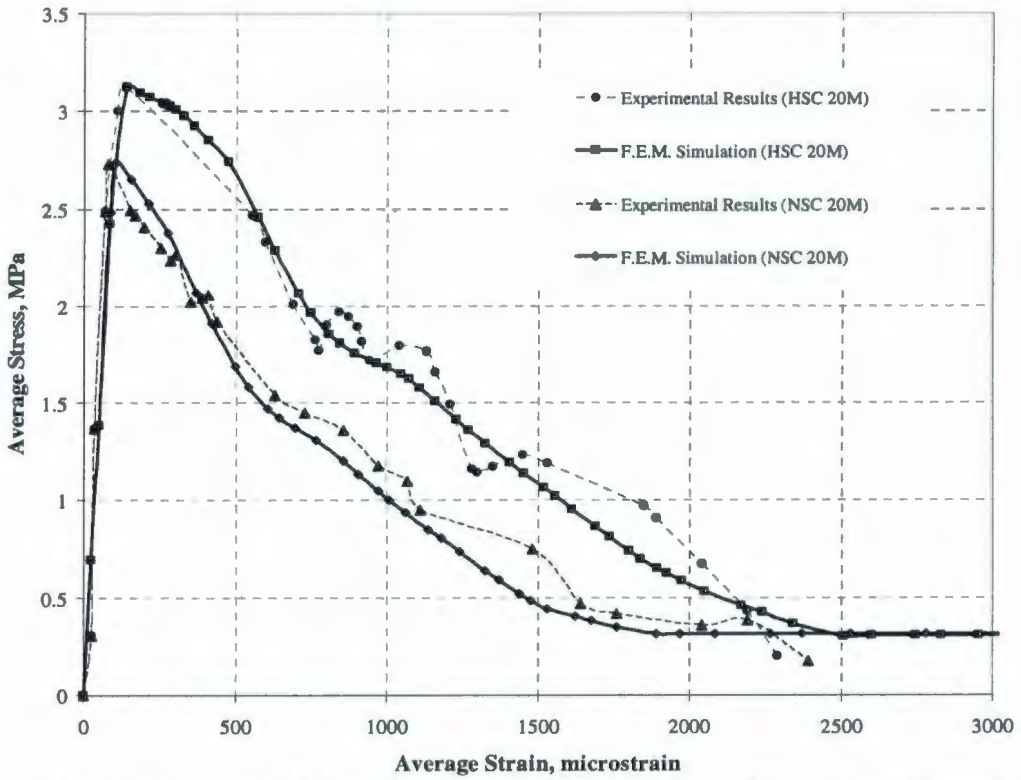

Fig. 8.10 Comparison of Numerical Solutions against Experimental Results [47] of Tensile Stress-Strain Response of RC Concrete members under axial Loading

8.5.2.2 Reinforced Thick Concrete Members under Punching Load

A series of two-way reinforced thick concrete slabs were tested under punching load by Hossin and Marzouk, 2008 [109]. This experimental testing program was designed to examine the influence of the concrete cover and bar spacing of normal and high strength concrete on the cracking behavior.

Fig. 8.11 plots the measured values of the deflection at the center of the slabs versus the value of the applied load, for experimental program conducted on RC slabs with different levels of concrete strength. It also shows the predicted load-deflection curves based on the numerical simulation using the damaged plasticity and proposed tensing stiffening models. For both normal and high thick concrete slabs, experimental values and model

predictions agreed satisfactorily in terms of load-deflection behavior and the failure load, as shown in Fig. 8.11.

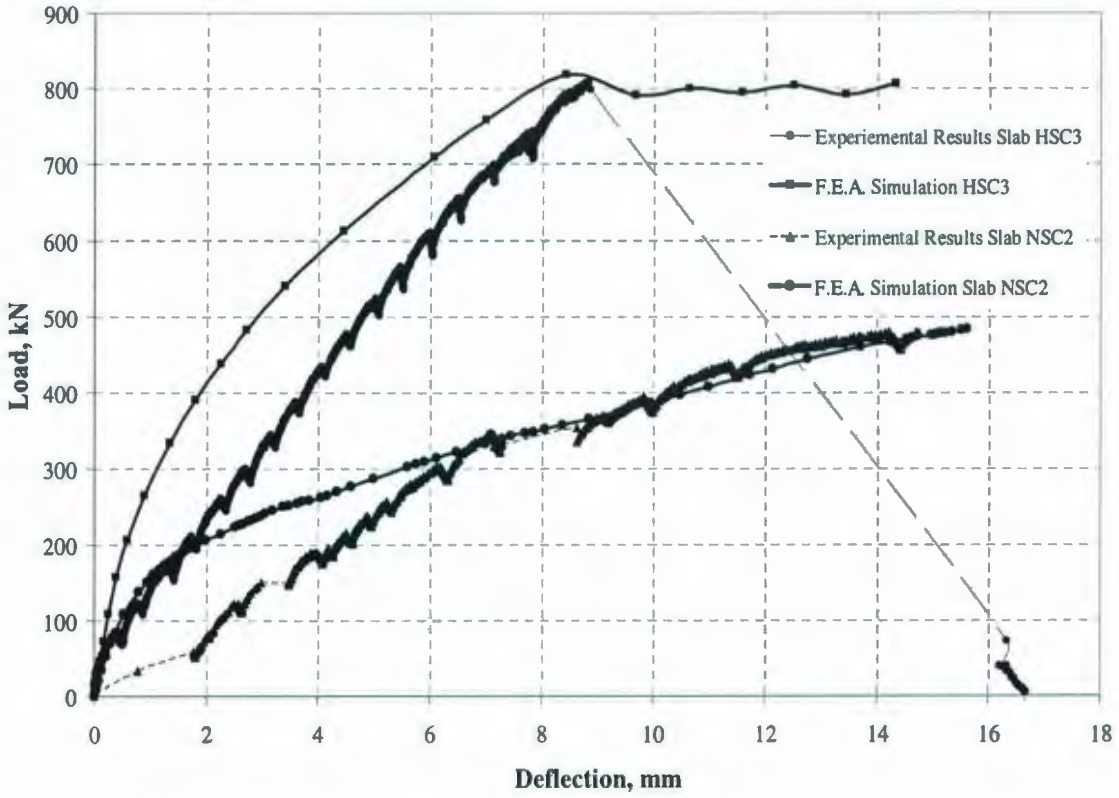

Fig. 8.11 Comparison of Numerical Solutions against Experimental Results [109] of Load Deflection Curves at Center Span of Test Slabs

8.6 Summary

The present study suggest that using the damaged plasticity model for the finite element analysis is considered a helpful tool at the establishment of rational numerical bases for providing a clear understanding for the tensile response of the reinforced concrete structures. One of the essential contributions of the present investigation is the development of a theoretical model for the tension stiffening behavior based on the experimental results in the current study, and implementation of that model into the

damaged based plasticity model to reflect the actual behavior of various reinforced concrete structures subjected to different loading conditions.

To validate the proposed model, the predicted value of the concrete tensile strength and tensile stress-strain relationship of concrete are compared to the experimental results conducted in the present investigation. As well, the comparative study is extended to verify the proposed model based on data not directly used for obtaining model parameters. In all of the studied cases in this research, the model predicts the cracking response (tensile strength and stress-strain relationship) satisfactorily.

Chapter 9

Summary and Conclusions

9.1 Summary

In the current research, the cracking behavior of normal- and high-strength reinforced concrete panels under uniaxial and biaxial states of loading was studied carefully. In order to do that, an extensive experimental program was carried out. A special test set-up was used to perform the experimental program. For panels tested under biaxial loading condition, proportional loading was used for all the tests. The ratio of the two applied load into the perpendicular directions was kept constant throughout the test. The experimental data was continuously recorded from the hydraulic pressure transducer, LPDTs, and the strain gauges. Afterwards, the data was collected and processed automatically using a data acquisition system. Influences of the main parameters that affect cracking behavior and the tension stiffening response of the reinforced concrete panels were critically investigated, Constitutive models for pre- and post cracking stress-strain behaviors of the concrete panels were developed.

In the second phase of the current research, an analytical study was conducted to study the bond characteristics between concrete and steel reinforcing bars. Analytical models for predicting the complete distribution of the slip, bond stress, concrete and steel stress, are developed.

A reinforced concrete plate element was studied using equilibrium and compatibility equations to formulate the average stresses of steel and concrete. A practical and new

analytical model that is capable of predicting the crack spacing of orthogonally reinforced concrete plate elements was developed. Afterwards, this study developed a model for evaluating crack widths for thick reinforced concrete plates subjected to axial loading. The calculation procedure was supported by an evaluation of existing test data. Based on this procedure, analyses that investigate the primary crack width variation along its length were conducted, as well as, parameters necessary to control the primary crack opening under the serviceability limit.

Finally, the nonlinear analysis of reinforced concrete plates using the damage plasticity model was preformed. The tension stiffening model developed in this study was implemented to simulate the cracking response of the concrete. The comparison between the predicted value of the concrete tensile strength and tensile stress-strain relationship of concrete and the corresponding experimental results conducted in the present investigation shows a favorable agreement.

9.2 Experimental Findings

The cracking behavior of two types of reinforced concrete panels was studied in this experimental program: a normal strength concrete (35 MPa), and high strength concrete (75 MPa). The main findings of the experimental program can be briefly summarized as follows:

1. Compared with NSC panels, HSC panels showed lower strains and greater tension stiffening response at a given load level thanks to the corresponding improvement

of the bond between the reinforcing steel bars and the high strength concrete matrix.

2. Once the concrete strength increased from 40 to 90 MPa (125%), the concrete tensile stress at the cracking stage also increased by 52% for panels subjected to uniaxial loading. However, for panels tested under biaxial loading, as the concrete strength was increased from 35 to 75 MPa (115%), the concrete stress at the cracking stage increased by 42%.
3. High strength concrete cracked at a higher steel stress level as compared with panel casted with NSC. At the first cracking load, the measured steel stress was found to be 0.48 f_y, and 0.8f_y for panels NS-U-15-2.5-6 and HS-U-15-2.5-6, respectively, tested under uniaxial loading condition. Also, the steel stress reached approximately 0.4f_y, 0.63f_y for panels NS-B1-15-2.5-6 and HS-B1-15-2.5-6, respectively.
4. The concrete tension stiffening contribution between cracks decayed at higher rate with the bar spacing, for various loading stages. This effect was more obvious in case of applying the axial load into biaxial direction.
5. The panels tested under biaxial loading conditions showed lower concrete tensile strength and tension stiffening response, compared with the panels subjected to uniaxial loading conditions. This reduction in the tensile strength of concrete panels subjected to biaxial loading was found to be equal to 5% – 15%. The reduction of the tension stiffening contribution of concrete between cracks due to

applying the axial into biaxial direction became more significant as the reinforcing bar diameter was increased.

6. The transverse reinforcing bars acted as crack initiators as long as the spacing between these bars didn't exceed the length required to develop the cracking stress in concrete, forcing the cracks to propagate at certain locations across the panel.
7. The increase in concrete cover to the main reinforcement led to higher tension stiffening response for different level of the steel stress.
8. The steel stress at cracking stage was sensitive to the value of d_b/ρ_{eff}, where the lower the value of d_b/ρ_{eff}, the higher the measured value of the steel stress at cracking stage, for both panels tested under uniaxial and biaxial loading.
9. Based on the experimental results, a good fit for the ascending and descending branches of the stress-strain curves for HSC plates subjected to axial loading conditions were recommended.
10. Concrete strength has insignificant effect on the average crack spacing for the panels under uniaxial or biaxial loading conditions. However, the value of the average crack width was influenced by the level of compressive strength of concrete, where at the serviceability limit, as the concrete strength increased by 115% the average crack width becomes smaller by 20%, as the test results of panels NS-B1-15-2-5-6 and HS-B1-15-2-5-6 were compared.
11. For panels tested under biaxial loading, most of the cracks propagated approximately along the location of the reinforcing bars in both directions. Thus, the measured values for the crack spacing were found to be very close to the

spacing between the reinforcing bars in both directions. However, for the panels subjected to uniaxial loading, the cracks propagated not only along the transverse bars location but also between theses bars, as long as the spacing between the transverse bars was higher than the required distance to develop the tensile strength of the concrete.

12. The experimental data indicated that, as the bar spacing increased by 50%, the crack spacing at the stabilized cracking stage is also increased by 37% and 46% for the panels tested under uniaxial and biaxial loading. Also, increasing the bar spacing by 50%, the average crack width increased by 47% and 46% at the serviceability load limit for the panels tested under uniaxial and biaxial loading, respectively.
13. Increasing the concrete cover thickness by 40% led to a corresponding increase in the average crack spacing by 14%, 2% for the panels subjected to uniaxial and biaxial loading conditions, respectively. Furthermore, the test results for the measured crack width showed that as the concrete cover increased by 40%, the recorded average crack width At service load ($\frac{2}{3} f_y$) became higher by 20% and 12% for panels subjected to uniaxial and biaxial loading, respectively.
14. This investigation examined five types of tension loads, 1:0, 1:1, 1:2, 1:3, and 1:4. Tensile strength of the concrete panels decreased as the loading ratio was changed from 1:4 to 1:1. The tensile strength of the concrete was found to be 2.71, 2.36, 2.42, 2.55, and 2.61 for panels HS-U-25-2.5-6 (1:0), HS-B1-25-2.5-6 (1:1), HS-B2-25-2.5-6 (1:2), HS-B3-25-2.5-6 (1:3), HS-B4-25-2.5-6 (1:4), respectively.

15. The tension stiffening contribution for the concrete between cracks was decreased as the loading ratio (P_1/P_2) is changed from 1:4 to 1:1. At steel stress level of approximately 300 MPa, the tension stiffening of the concrete between cracks for panels HS-B1-25-2.5-6 (1:1) and HS-B2-25-2.5-6 (1:2) diminished and these panels show a response similar to the bare bar. However, at the same steel stress level, panels HS-B3-25-2.5-6 (1:3) and HS-B4-25-2.5-6 (1:4) showed some tension stiffening response for the concrete between cracks.
16. There was a general tendency whereby the measured average crack width increased as the loading ratio changed from 1:4 to 1:1. At the service load level ($\frac{2}{3} f_y$), the measured average crack width was found to be 0.282, 0.358, 0.354, 0.317, and 0.308 for panels HS-U-25-2.5-6, HS-B1-25-2.5-6, HS-B2-25-2.5-6, HS-B3-25-2.5-6, HS-B4-25-2.5-6, respectively. This effect is maily due to the reduction in the tension stiffening concrete contribution between the successive cracks as the loading ratio changed from 1:4 to 1:1.

9.3 Analytical Investigation Conclusions

The following conclusion can be drawn from the analytical study carried out in Chapters 5, 6, and 7:

1- Theoretical Model was developed for predicting the bond characteristics and concrete behavior of reinforced concrete member under tension stresses. The model enables the determination of the complete distribution of the slip, bond stress, concrete stress, and steel stress at different loading stages. The model

preformed satisfactorily as compared with the experimental data for the different levels of the steel stress.

2- A mechanical model was developed to predict the effect of the splitting stresses, caused by bond action between the uncracked concrete and deformed bars, on the cracking behavior of orthogonally reinforced concrete panels subjected to in-plane axial stresses. Furthermore, this study was extended to provide design equations for evaluating the tensile strength of normal and high strength reinforced concrete thick plates subjected to biaxial tension loading condition, considering the secondary effect of the splitting stress on the cracking behavior of these members.

3- A rational crack spacing model was developed by considering the equilibrium and compatibility equations of reinforced concrete elements. The influence of the main parameters affecting the cracking behavior of reinforced concrete structures, such as the tensile strength of concrete, reinforcement ratio, and longitudinal bar diameter $\emptyset_1$ and spacing S_1 were taken into consideration. Moreover, the effect of transverse reinforcement was incorporated into this model in terms of the transverse bar diameter $\emptyset_2$ and spacing S_2.

4- The theoretical study was extended to develop a model for calculating the crack width for thick reinforced concrete plates subjected to in-plane axial loading. This model enables the estimation of the variations in crack width at any section along the crack length.

5- Recommendations for control of cracking for thick reinforced concrete panels were achieved based on the measured data from the experimental results and proposed models.

6- The Canadian Offshore code CSA-04, Norwegian Code NS-92, and the American Code ACI 224R-01 provided good results for the crack width value compared with the experimental results of the specimens with normal concrete cover (≈ 40 mm). However, these codes showed a conservative estimation for the value of the average crack width and spacing of the reinforced concrete panels with thick concrete cover.

9.4 Finite Element Model

A damaged plasticity model based was adopted. This model was used in the general purpose finite element program ABAQUS. The numerical implementation of the calibrated tension stiffening model using the data obtained from the experiments was carried out. The numerical results were then compared to the experimental data. Results of the verification indicated that the damaged plasticity model with the implemented tension stiffening model revealed a favorable agreement with the experimental results.

9.5 Contribution

1. This thesis contains comprehensive experimental study to investigate the cracking response of thick high strength reinforced concrete panels subjected to uniaxial and /or biaxial loading conditions used for offshore platforms, containment structures for

nuclear power plants. The previous studies in the literature were quite limited to specimens subjected to uniaxial loading state. The influence of various actual test parameters that have profound effect on the tension stiffening response and cracking behavior of thick HSC plates such as concrete strength, reinforcing bar distribution, concrete cover thickness, and applying the axial load in biaxial direction were critically investigated. This type of study can further our understanding of cracking response and cracking control of such structures.

2. To the author's knowledge, this is the first model developed to simulate the cracking behavior (crack spacing and width) of thick high strength concrete panels considering the effects of factors that have a profound influence on the value of crack widths, such as the tensile strength of concrete, reinforcement ratio, and longitudinal bar diameter $Ø_1$ and spacing S_1. Moreover, the effect of transverse reinforcement is incorporated into this model in terms of the transverse bar diameter $Ø_2$ and spacing S_2, and the concrete cover. Most of the available expressions for crack spacing and width were developed for building structures of normal-strength concrete and normal concrete cover. However, most of the offshore structures are built using high-strength concrete with thick concrete cover as these structures are constantly exposed to harsh environmental conditions.
3. The calibrated tension stiffening model based on the experimental data was implemented in nonlinear damaged plasticity model to investigate the cracking response of the concrete plates subjected to axial loading. It is a powerful tool that can be used to provide insight into the behavior of reinforced concrete structures.

9.6 Recommendations for Further Research

1. Studying the behavior of thick high strength concrete plates subjected to in plane shear condition.
2. Investigating the cracking response of thick high strength concrete plates using steel fiber in the concrete mix.
3. Using the fiber optic sensor technology to monitor cracking response and provide assessment of damage, such as the locations of cracks and their corresponding depth, width, and spacing, as fiber optic sensor is thought to be the most promising alternative to conventional sensors.
4. Using of FEA to study the various effects of the factors that affect the cracking response of thick high strength concrete panels.

REFERENCES

[1] Hillerborg, A. 1983. Concrete fracture energy tests performed by laboratories according to a draft RILEM recommendation. Report TVBM-3015, Division of Building Materials, Lund Institute of Technology.

[2] Bazant, Z. P., and Oh, B. H. 1983. Crack band theory for fracture of concrete. RILEM Material and Structural, 16(93):155-177.

[3] Phillips, D. V., and Zhang, B. 1993. Direct tension tests on notched and un-notched plain concrete specimens. Magazine of Concrete Research, 45(162): 25-35.

[4] Etse, G., and Willam, K. 1994. Fracture energy formulation for inelastic behavior of plain concrete. Journal of Engineering Mechanics ASCE, 120(9): 1983-2011.

[5] Marzouk, H., and Chen, Z. W. 1995. Fracture energy and tension properties of high-strength concrete. Journal of Material in Civil Engineering, 7(2): 108-116.

[6] Gopalaratnam, V. S., and Shah, S. P. 1985. Softening response of plain concrete in direct tension. ACI Structural Journal, 82(3): 310–323.

[7] Guo, Z. H., and Zhang, X. Q. 1987. Investigation of complete stress-deformation curves for concrete in tension. ACI Material Journal, 84(4): 278-285.

[8] Welch, G. B. 1966. Tensile strains in unreinforced concrete beams. Magazine of Concrete Research, 18(54): 9-18.

[9] Evans, R. H., and Marath, M. S. 1968. Microcracking and stress-strain curves for concrete in tension. Materials and Structures Journal, 1(1): 61-64.

[10] Kupfer, H., Hilsdorf, H. K., and Rusch, H. 1969. Behavior of concrete under biaxial stresses. ACI Material Journal, 66(8): 656-666.

[11] Oral, B., Nilson, A. H., and Salte F. O. 1971. Stress-strain response and fracture of concrete model in biaxial loading. ACI Material Journal, 68(8): 590-599

[12] Liu, T., Nilson, A., and Slate, F. 1972. Stress-strain response and fracture of concrete in uniaxial and biaxial compression. ACI Material Journal, 69(5): 291-295.

[13] Tasuji E. M., Nilson, A. H., and Slate F. O. 1979. Biaxial stress-strain relationships for concrete. Magazine of Concrete Research, 31(109): 1025-1034.

[14] Bresler, B., and Pister, K. 1958. Strength of concrete under combined stresses. ACI Material Journal, 55(3): 321-345.

[15] Bellamy, C. J. 1961. Strength of concrete under combined Stress. ACI Material Journal, 58(4): 367-381.

[16] McHenry, D., and Karni, J. 1958. Strength of concrete under combined tensile and compressive stress. ACI Material Journal, 54(10): 829-840.

[17] Su, E. C., and Hsu, T. T. 1988. Biaxial compression fatigue and discontinuity of concrete. ACI Material Journal, 85(3):178-188.

[18] Yin, W.S., Su, E. C., Mansur, M. A., and Hsu, T. T. 1989. Biaxial tests of plain and fiber concrete. ACI Material Journal, 86(3): 236-243.

[19] Hussein, A., and Marzouk, H. 2000. Behavior of high-strength concrete under biaxial stresses. ACI Material Journal, 97(1): 27-36.

[20] Ren, X., Yang, W., Zhou, Y., and Li, J. 2008. Behavior of high-performance concrete under uniaxial and biaxial loading. ACI Material Journal, 105(6): 548-558.

[21] Lutz, L. A., Gergely, P., and Winter, G. 1966. The mechanics of bond and slip of deformed reinforcing bars in concrete. Structural Engineering report no. 324, Cornell University, Ithaca, New York

[22] Lutz, L. A., and Gergely, P. 1967. Mechanics of bond and slip of deformed bars in concrete. ACI Structural Journal, 64(11): 548-558.

[23] Goto, Y. 1971. Cracks formed in concrete around deformed tension bars. ACI Material Journal, 68(4): 244-251.

[24] Somayaji, S., and Shah, S. P. 1981. Bond stress versus slip relationship and cracking Response of tension members. ACI Structural Journal, 85(4): 217-225.

[25] Jiang, D. H., Shah, S. P., and Andonian, A. T. 1984. Study of the transfer of tensile forces by bond. ACI Structural Journal, 85(4): 251-259.

[26] Abrishama, H. H., and Mitchell, D. 1992. Simulation of uniform bond stress. ACI Materials Journal, 89(2): 161-168.

[27] Alavi-Fard, M., and Marzouk, H. 2004. Bond of high-strength concrete under monotonic pull-out loading. Magazine of Concrete Research, 56(9): 545-557.

[28] Alavi-Fard, M., and Marzouk, H. 2002. Bond strength of high strength concrete pull out Cyclic Loading. Canadian Journal of Civil Engineering, 29: 191-200.

[29] Yang, S., and Chen, J. 1988. Bond slip and crack width calculations of tension Members. ACI Structural Journal, 85(4): 414-422.

[30] MacGregor, J. G. (1992). Reinforced concrete mechanics and design. Second Edition, Prentice Hall, New Jersey: 844.

[31] Sezen, H., and Moehle, J. P. 2003. Bond-slip behavior of reinforced concrete members. Proceedings, FIB symposium, Concrete Structures in Seismic Regions, Athens, Greece.

[32] FIB-2000. Bond of reinforcement in concrete. State-of-art Report, Bulletin 10, CEB-FIP, Lausanne, Switzerland: 366-379.

[33] Rheinhard, H. W., and Cornelissen, H. A. 1984. Post–peak cyclic behavior of concrete in uniaxial tensile and alternating tensile and compressive loading. Cement and Concrete Research. 14(2): 263-270.

[34] Goto, Y. 1971. Cracks formed in concrete around deformed tension bars. ACI Material Journal, 68(4):244-251.

[35] Clacrk, L. A., and Cranston, W. B. 1979. The Influence of bar spacing on tension stiffening in reinforced concrete slabs. Proceeding Internal Conference on Concrete Slabs, Dundee: 118-128.

[36] Marzouk, H., and Chen, Z. W. 1993. Nonlinear analysis of normal- and high-strength concrete slabs. Canadian Journal of Civil Engineering, 20(4): 696-707.

[37] Abrishami, H. H., and Mitchell, D. 1996. Influence of spilitting cracks on tension Stiffening. ACI Structural Journal, 93(6):703-710.

[38] Stevens, N. J., Uzumeri, S. M., Collins, M. P., and Will, G. T. 1991. Constitutive model for reinforced concrete finite element analysis. ACI Structural Journal, 88(1): 49-59.

[39] Bischoff, P. H. 1995. Influence of shrinkage on tension stiffening. Proceeding of Canadian Society for Civil Engineering, Annual Conference, Ottawa, 2: 433-442.

[40] Bischoff, P. H. 2001. Effect of shrinkage on tension stiffening and cracking in reinforced concrete. Canadian Journal of Civil Engineering, 28: 363-374.

[41] Johnson, A. I. 1951. Deformations of reinforced concrete. International Association for Bridge and Structural Engineering (IABSE) Publications, 11: 253-290.

[42] Rostasy, F. S., Koch, R., and Leonhardt, F. 1976. Minimum reinforcement for restrained external light weight reinforced concrete walls. DAFSTB, Ernst & Sohn, Berlin, Heft, 267: 83

[43] CEB-FIP-1978. CEB-FIP Model Code for Concrete Structures (MC 78). 3rd Edition, Comité Euro-International du Béton (CEB), Paris : 348

[44] Comite Euro-International Du Beton, CEB-FIP model Code 1990, Comité Euro-Internationale du Beton et Federation Internationale de la Procontrainte. Lausanne, Switzerland.

[45] Collins, M. P., and Mitchell, D. 1991. Prestressed concrete structures. Prentice-Hall, Inc., Englewood Cliffs, N.J.:766.

[46] [46] Belarbi, A., and Hsu, T. T. 1994. Constitutive laws of concrete in tension and reinforcing bars stiffened by concrete. ACI Structural Journal, 91(4): 465-474.

[47] Fields, K., and Bischoff, P. H. 2004. Tension stiffening and cracking of high-strength reinforced concrete tension members. ACI Structural Journal, 101(4): 447-456.

[48] Hwang, L. S., and Rizkalla, S. 1983. Effective tensile stress-strain characteristics for reinforced concrete. Proceedings of the Canadian Society of Civil Engineering, Annual Conference, Ottawa: 129-147.

[49] Link, R. A., Elwi, A. E., and Scalon, A. 1989. Biaxial tension stiffening due to generally oriented reinforcing layers. Journal of Engineering Mechanics, ASCE, 115(8):1647-1662.

[50] Massicotte, B., Elwi, A. E., and MacGregor, J. G. 1990. Tension-stiffening model for planner reinforced concrete members. Journal of Structure Engineering, ASCE, 116(11): 3039-3058.

[51] Lin, C. S., and Scordelis, A. C. 1975. Nonlinear analysis of RC shells of general form. Journal of Structural Division, ASCE, 101(3): 523-538.

[52] Gilebert, R. I., and Warner, R. F. 1978. Tension stiffening in reinforced concrete slabs. Journal of the Structural Division, ASCE, 104(12): 1885-.1900

[53] Cervenka, V. 1985. Constitutive model for cracked reinforced concrete. ACI Structural Journal, 82(6): 877-882.

[54] Cervenka, V., Eligehausen, R., and Pukl, R. 1990. SBETA-computer program for nonlinear finite element analysis of reinforced concrete structures. Report 90/1, Institute of Building Materials, University of Stuttgart.

[55] Scanlon, A., and Murray, D. W. 1974. Time dependent reinforced concrete slab deflections. Journal of the Structural Division, ASCE, 100(9):1911-1924.

[56] Base, G. D., Read, J. B., Beeby, A. W., and Taylor, H. P. 1966. An investigation of crack cotrol characteristics of various types of bar in reinforced concrete beams. Research Report No. 41.018, Part 1, Cement and Concrete Association, Wexham Springs: 44.

[57] Broms, B. B., and Lutz, L. A. 1965. Effects of arrangement of reinforcement on crack width and spacing of reinforced concrete members. ACI Structural Journal, 62(11):1395-1420.

[58] Beeby, A. W. 1979. The prediction of crack widths in hardened concrete. Structural Engieer (London), 57(1): 9-17.

[59] Hognestad, E. 1962. High strength bar as concrete, Part 2 control of flexural cracking. PCA Journal Research and Development Laboratories, 4(1): 46-63

[60] Lenhardt, F. 1988. Crack and crack control in concrete structures. PCA Journal, 22(4): 124-145.

[61] Rizkalla, S. H., Hwang, L. S., and EL Shahwi, M. 1984. Transverse reinforcement effect on cracking behavior of R.C. members. Canadian Journal of Civil Engineering, 10(4): 556-581.

[62] Riakalla, S. H., and Hwang, L. S. 1984. Crack predition for members in uniaxial tension. ACI Structural Journal, 81(4): 572-579.

[63] Williams, A. 1986. Tests on large reinforced concrete elements subjected to direct tension. Cement and Concrete Association, Technical Report 562: 1-56

[64] Simmonds, S. H., Rizkalla, S. H., and MacGeregor, J. G. 1979. Tests of wall segments from reactor containments. Structural Engineering Report No.81, Department of Civil Engineering, University of Alberta, Edmonton, Canada: 1-72.

[65] MacGeregor, J. G., Rizkalla, S. H., and Simmonds S. H. 1980. Cracking of reinforced and prestressed concrete wall segments. Structural Engineering Report No.82, Department of Civil Engineering, University of Alberta, Edmonton, Canada: 1-78.

[66] Oesterle, R. G., and Russell, H. G. 1980. Shear transfer in large scale reinforced concrete containment elements. Report No.1, Nuclear Regulatory Commission Report No. NUREG/CR- 1374: 1-64.

[67] Leonhardt, F. 1977. Crack control in concrete structures. IABSE Surveys, No.S-4/77, IABE Periodical 3/1977, International Association for Bridge and structural Engineering Zurich, Switzerland: 26.

[68] Beeby, A. W. 1972. Study of cracking in reinforced concrete members subjected to pure tension. Technical Report 42.468, Cement and Concrete Association, London.

[69] Marti, P., Alvarez, M., Kaufmann, W., and Sigrist, V. 1998. Tension chord model for structural concrete. Structural Engineering International: 287-298.

[70] Gilbert, R. I. 2006. Design for flexural crack control-recent amendments to the Australian Standard AS3600. 1st International Structural Specially Conference, Calgary, Alberta, Canada: ST-048-1- ST-048-10.

[71] Gilbert, R. I. 2008. Control of flexural cracking in reinforced concrete. ACI Structural Journal, 105(3): 301-307.

[72] Park, R. and Paulay, T. 1975. Reinforced concrete structures. John Wiley and Sons, New York.

[73] ACI Committee 224-2001. Causes, Mechanism, and Control of Cracking in Concrete. ACI Bibliography No. 9, American Concrete Institute Farmingtion Hills, Mich.:92.

[74] Canadian Standard Associations, S474 Concrete Structures, Canadian Standard Associations, Mississauga, Ontario, Canada, 2004.

[75] NS 3473E, Norwegain Council for Building Standardization, Norway Concretes Structures Design rules. Prepared by NBR Norges Byggst and Ardiseringsrad, 4th Edition, November 1992: 34.

[76] EC2, Eurocode 2. Design of concrete structures- Part I: General rules and rules for buildings, "European Committee for Standardization, Paris, 2004.

[77] Gergely, P., and Lutz, L. A. 1968. Maximum crack width in reinforced concrete flexural members. Causes, Mechanism, and Control of Cracking in Concrete, SP-20, ACI Farmington Hills, Mich.:87-117.

[78] ACI Committee 318. Building Code Requirements for Structural Concrete (ACI 318-08) and Commentary (ACI 318R-08). Reported by ACI Committee 318, American Concrete Institute, Farmington Hills, Mich., 2008.

[79] MacGregor, J. G., Rizkalla, S. H., Simmonds, S. H. 1980. Cracking of reinforced and prestressed concrete wall segments. Structural Engineering Report No. 82, Department of Civil Engineering, University of Alberta, Edmonton, Alberta.

[80] Hsu, T. T., Belarbi, A., and Pang, X. 1995. A universal panel tester. Journal of Testing and Evaluuation, JTEVA, 23(1): 41-49.

[81] Cho, J. Y., Kim, N. S., Cho, N. S., and Choun Y. S. 2004. Stress-strain relationship of reinforced concrete subjected to biaxial tension. ACI Structural Journal, 101(2): 202-208.

[82] Sabrah, T. B., Marzouk H., and Hussein, A. 2009. Development of a new test facility to examine Reinforced concrete panels under uniaxial and biaxial direct tension. Journal of Test Evaluation ASTM, 37(6).

[83] ACI Committee-ACI 224.2R-1992 (Reapproved 2004). Cracking of concrete members in direct tension. ACI Structural Journal: 1-12.

[84] Shima, H., Chou, L., and Okamura, H. 1987. Micro and macro models for bond behavior in reinforced concrete. J. Faculty of Engineering, University of Tokyo (B), 39(2): 178-186.

[85] ACI Committee 408. 1966. Bond Stress the State of the Art. ACI Journal, 63(11):1161-1190.

[86] Jaing, D. H. 1983. Bond and slip between steel and concrete. No. 8312, Information center of Tongji University: 1-77.

[87] Teng, M. Z., and Zhang, H. G. 1985. Bond slip calculations in reinforced concrete. Research Bulletin No. 85-09, Qinghua University: 1-28.

[88] Duff, A. A. 1913. Test of bond between concrete and steel. University of Illinois, Engineering Experiment Station, Bulletin No. 71.

[89] Losberg, A., and Olsson, P. 1979. Bond failure of deformed reinforcing bars based on the longitudinal splitting effect of the bars. ACI Structural Journal, 76(1): 5-18.

[90] Azizinamini, A., Stark, M., Roller, J. H., and Ghosh, S. K. 1993. Bond performance of reinforcing bars embedded in high-strength concrete. ACI Structural Journal, 90(5): 554-561.

[91] Azizinamini, A., Chisala, M., Roller, J. H., and Ghosh, S. K. 1995. Tension development Length of Reinforcing Bars Embedded in High-Strength Concrete. Engineering Structures, 17(7): 512-522.

[92] Maekawa, K., Pimanmas, A., and Okamura, H. 2003. Nonlinear Mechanics of Reinforced Concrete. London; New York: Spon Press, Taylor & Francis Group: 27-30.

[93] Canbay, E., and Frosch, R. J. 2005. Bond strength of lap-spliced bars. ACI Structural Journal, 102(4): 605-614.

[94] Tepfers, R. 1973. A Theory of bond applied to overlapped tensile reinforcement splices for deformed bars. Division of Concrete structures, Chalmers University of Technology, Goteborg, Sweden, Publication 73(2):328.

[95] MacGregor, J. G., and Bartlett, M. F. 2000. Reinforced concrete mechanics and design. First Canadian Edition, Prentice Hall Canada Inc., Toronto, Ontario: 301-309.

[96] Harajli, M. H. 1994. Development/splice strength of reinforcing bars embedded in plain and fiber reinforced concrete. ACI Structural Journal: 91(5): 511-520.

[97] Kemp, E. L. 1986. Bond in reinforced concrete: behavior and design criteria. ACI Structural Journal, 83(1): 50-57.

[98] Chinn, J., Ferguson, P. M., and Thompson, J. N. 1955. Lapped splices in reinforced concrete beams. ACI Structural Journal, 52(10): 201-213.

[99] Chamberlin, S. J. 1958. Spacing of spliced bars in beams. ACI Structural Journal, 54(2): 201-213.

[100] Ferguson, P. M., and Breen, J. E. 1965. Lapped splices for high strength reinforcing bars, Part I & II. ACI Structural Journal, 62(9): 1063-1077.

[101] Tepfers, R., and Olsson P. A. 1992. Ring test for evaluation of bond properties of reinforcing bars. International Conference on Bond in Concrete, Riga, Latvia, 1: 89-99.

[102] Hamad, B. S., and Itani, M. S. 1998. Bond strength of reinforcement in high performance concrete: role of silica fume, casting position, and superplasticizer dosage. ACI Materials Journal, 95(5): 499-511.

[103] Azizinamini, A., Pavel, R., Hatfield, E., and Ghosh, S. K. 1999. Behavior of lap-spliced reinforcing bars embedded in high-strength concrete. ACI Structure Journal, 96(5): 826-835.

[104] Esfahani R. M., Rangan V. B. 1998. Local bond strength of reinforcing bars in normal strength and high strength concrete (HSC). ACI Structural Journal, 95(2): 96-106.

[105] Hamad, B. S., and Machaka, M. F. 1999. Effect of transverse reinforcement on bond strength of reinforcing bars in silica fume concrete. Materials and Structures Journal, 32: 468-476.

[106] Desayi, P., Kulkarni, A. B. 1976. Determination of maximum crack width in two-way reinforced concrete slabs. Proceedings, Inst. of Civil Engineers (London), Part 2, Research and Theory, 61:343–349.

[107] Marti, P., Sigrist, V., and Alvarez, M. 1997. Mindestbewehrung von Betonbauten (Minimum reinforcement of concrete structures. Bundesamt für Strassenbau, Report Number 529: 55.

[108] Marti, P., Alvarez, M., and Sigrist, V. 1997. Rissbildung und Mindestbewehrung (Cracking and minimum reinforcement). Schweizer Ingenieur und Architekt, Zurich, Switzerland, 115(41): 832-838.

[109] Hossin, M. A., and Marzouk, H. 2006. Offshore concrete crack analysis. 1st International Structural Specially Conference, Calgary, Alberta, Canada, May 23-26, ST-119-1: ST-119-10.

[110] Lorrain, M., Maurel, O., and Seffo, M. 1998. Cracking behavior of reinforced high-strength concrete tension ties. ACI Structural Journal, 95(5): 626-635.

[111] Lubliner, J., Oliver, J., Oller, S., and Oñate, E. 1989. A plastic-damage model for concrete. International Journal of Solids and Structures, 25(3): 299-326

[112] Lee, J., and Fenves, J. L. 1998. Plastic-damage model for cyclic loading of concrete structures. J Eng Mech, 124(8): 892–900.

[113] Oller, S., Onate, E., Oliver, J., and Lubliner, J. 1990. Finite element nonlinear analysis of concrete structures using a plastic-damage model. Eng Fract Mech 35:219-231.

[114] Grassl, P., and Jirásek, M. 2006. Damage-plastic model for concrete failure. International Journal of Solids and Structures, 43:7166-7196.

[115] Borst, D. R., Nauta, P. 1984. Smeared crack analysis of reinforced concrete beams and slabs failing in Shear. Proced. Int. Conf. on Computer-Aided Analysis and Design of Concrete Structures, 1:261-273.

[116] Gálvez , J. C., Červenka, J., Cendón D. A., and Saouma, V. 2002. A discrete crack approach to normal/shear cracking of concrete. Article Cement and Concrete Research, 32(10): 1567-1585.

[117] Rots, J., Nauta, P., Kursters, G., and Blaauwendraad, J. 1985. Smeared crack approach and fracture localization in concrete. Heron, 30:1–48.

[118] Simo, J. C., Ju, J. W. 1987. Stress and strain based continuum damage models. Part I and II. Int. J. Solids Struct. 23:375–400.

[119] Ju, J. W. 1989. On energy-based coupled elasto-plastic damage theories: constitutive modeling and computational aspects. Internat. J. Solids Structures, 25(7): 803–833.

[120] HKS, 2007. ABAQUS/Standard User's Manual. Version 6.7, Hibbit, Karlsson & Sorensen, Inc., Pawtucket; USA.

[121] Drucker, D. C., and Prager, W. 1952. Soil mechanics and plastic analysis or limit design. Quarterly of Applied Mathematics, 10: 157–165,

[122] Rahman, T., Lutz, W., Finn, R., Schmauder, S., and Aicher S. 2007. Simulation of the mechanical behavior and damage in components made of strain softening cellulose fiber reinforced gypsum materials. Comp. Mat. Sci. 39(1): 65-74.

[123] Bažant, Z. P., and Oh, B. H. 1983. Crack band theory for fracture of concrete. Mater. Struct. 16 : 155–177.

[124] Bazant, Z. P. and Oh, B. H. 1983. Spacing of cracks in reinforced concrete. J. of Structural Engineering, ASCE, 109(9):2066-2085.

[125] Hillerborg, A., Modéer M., and Petersson, P. E. 1976. Analysis of crack formation and crack growth in concrete by means of fracture mechanics and finite elements. Cement and Concrete Research 6(6):163–168.

[126] Phillips, D. V., and Zienkiewicz, O. C. 1976. Finite element non-linear analysis of concrete structures. ICE Proceedings, 61(1):59-88.

[127] Elwi, A. E., and Murray, D. W. 1980. Nonlinear analysis of axisymmetric reinforced concrete structures. Structural Engineering Report No. 87, Department of civil Engineering, University of Alberta, Edmonton, Alberta, Canada.

[128] Bazant, Z. P., and Oh, B. H. 1984. Deformation of progressively cracking reinforced concrete beams. ACI Structural Journal, 81(3):268-278.